Light-Controlled Conductance Using Molecular Switches

Kudernác, Tibor

Light-Controlled Conductance Using Molecular Switches

Photochromic Switches Get Wired

Tibor Kudernáč

RIJKSUNIVERSITEIT GRONINGEN

Light-Controlled Conductance Using Molecular Switches

Photochromic Switches Get Wired

Proefschrift

ter verkrijging van het doctoraat in de
Wiskunde en Natuurwetenschappen
aan de Rijksuniversiteit Groningen
op gezag van de
Rector Magnificus, dr. F. Zwarts,
in het openbaar te verdedigen op
vrijdag 5 oktober 2007
om 14.45 uur

door

Tibor Kudernáč

geboren op 19 september 1978
te Košice, Slowakije

Contents

Chapter 6 Intermolecular Repulsion through Interfacial Attraction: Polymorphism in Self-Assembled Monolayers

Chapter 1

Introduction: Light-induced switching of conductance in molecular systems

In the first chapter of this thesis an overview is given of the efforts to control conductance by employing light sensitive molecular switches, so-called photochromic switches. The classification of the four most commonly used types of photochromic compounds is given and their conductive properties in solution and on conductive surfaces, as a function of light-induced transformations are described. The light-induced single molecule switching of conductance is discussed to demonstrate the ability of a single molecule to behave as an addressable electronic device. More robust devices that have been realized, based on photochromic molecules (not single molecule devices), having the capability to control conductance are briefly described. Finally, at the end of the chapter an outline of this thesis will be given.

1.1 Introduction

Perhaps, the most basic element of molecular devices is a molecule that can be switched[1,2] between states of low and high conductivity, i.e., can undergo on/off switching. The recent announcement by Stoddart, Heath and coworkers[3] of a 160-kilobit memory based on 'wired-up' organic molecular switches has demonstrated the viability of the bottom up approach to molecular components into electronic circuitry promulgated by Richard Feynman almost half a century earlier[4] and popularized by Aviram and Ratner by their pioneering work in 1974.[5] In Stoddart's and Heath's system redox stimulation is used to drive changes in molecular states and hence the electronic charge transport properties through the junction.

Photochromic molecular switches are a class of compounds capable of undergoing a reversible photo-induced transformation between two stable states, whose absorption spectra are distinctly different (Scheme 1).[1] The two isomeric forms exhibit different geometries and physical properties such as hydrophobicity, redox chemistry etc. The advantage of photochromic systems are their ease of addressability, reversibility and short response times. Consequently, this offers the possibility of changing local and bulk properties of a molecular based system by irradiation.[6] Indeed the versatile nature of photochromic molecular systems has seen their application in molecular memory devices,[7] molecular electronics,[8] smart surfaces and in the control of supramolecular organization, to name but a few areas.[9]

$$A \underset{\lambda_2}{\overset{\lambda_1}{\rightleftharpoons}} B$$
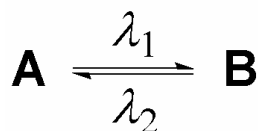
Scheme 1 *Optical molecular switch that can exist in two different forms and each of them can be selectively addressed by light at a different wavelength.*

Photochromic molecules represent many challenges as well as opportunities to their application in functioning devices. In particular, the translation of the changes in molecular structure, which accompany photochromism, to changes in molecular conductivity requires that photochromic systems be held as components in electronic circuits and that their charge transport properties change to a measurable degree when the system is addressed with light.

2

However, to exploit fully the potential of responsive molecular components in electronic devices we need to consider two distinct contributions molecular systems make towards the charge transport across the electrode gap: the effect on tunneling between the metallic contacts, i.e. by modification of the density of states at the surfaces of the metal contacts and the resonant tunneling mediated through the molecular orbitals of the responsive molecule.[10] In the latter case the photochemical changes in the molecule affects either or both the occupied and unoccupied frontier orbitals of the molecule. [11]

1.2 Main Classes of Photochromic Switches

Among all organic photochromic compounds there are four most commonly used types of photochromic switches: azobenzenes (Scheme 2), overcrowded alkenes (Scheme 3), spiropyrans (Scheme 4) and diarylethenes (Scheme 5).

Azobenzenes were among the first photochromic switches used and are still the subject of extensive investigation (Scheme 2). Their *cis-* and *trans*-isomers have a different spatial arrangement of the aromatic moieties, and consequently show significantly different physical and chemical properties.[12] A major advantage of azobenzene switches is that they are easy to synthesize and photoconversion yields are generally high. However, an important drawback is that, depending on the nature of the substituents on the aromatic groups, these switches often undergo thermal *cis* to *trans* isomerization at room temperature.
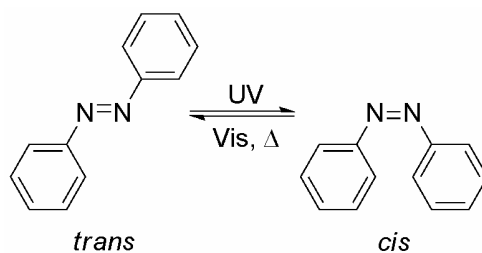
Scheme 2 *Trans-cis isomerization of azobenzene.*

Photochromic interconversions in overcrowded alkenes[13] are based on light-induced isomerization around the central double bond (Scheme 3). The molecular design prevents the notorious photocyclization and other fatigue photochemical pathways common to stilbene-type compounds.[14] The intrinsically chiral structure, based on their helical shape, allows for their use as chiroptical switches *i.e.* the chirality can be controlled by light. This makes them excellent candidates for detection and observation by circular dichroism

3

spectroscopy or other chiroptical techniques. Their helical shape and possibility of dynamic interconversions between stereoisomers allows them to induce light-driven reversible modifications to supramolecular architectures i.e. liquid crystals.[15] Overcrowded alkenes became the basis for the first light-driven unidirectional molecular motor.[16]

(P) helix   *(M)* helix
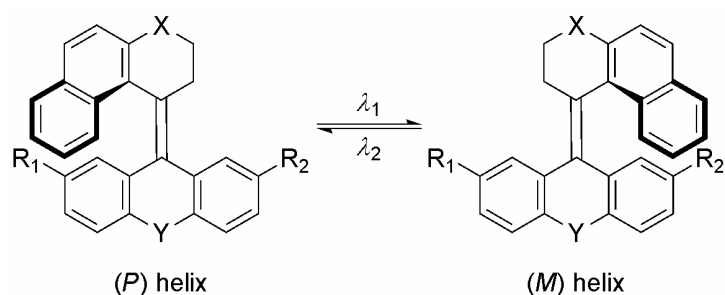
Scheme 3 *Sterically overcrowded alkene undergoing reversible interconversion between a P and M helix upon irradiation.*

Spiropyrans[17] are molecular switches that can undergo reversible photoisomerization between a stable state and a metastable state using UV and/or visible light. They are well suited to control the interactions within the local environment, since the relatively hydrophobic "closed" spirocyclic isomer can be reversibly converted to a highly polar hydrophilic "open" zwitterionic merocyanine isomer that has a much larger dipole moment as shown in Scheme 4. In addition, the flexibility in the molecule changes considerably going from the rigid closed to the open state. The thermal conversion from the merocyanine isomer back to the closed spirocyclic form occurs typically with a half-life at room temperature of tens of minutes in non-polar media, while the photochemical isomerization with visible light occurs on a much faster timescale.[18]

closed   open
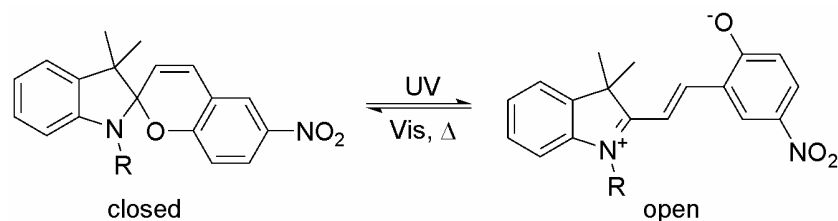
Scheme 4 *Switching of a spiropyran derivative.*

Diarylethenes are reversible molecular switches consisting of conjugated parts connected by a switching element.[19] There are two isomers, i.e., a closed form and an open form of the molecule (Scheme 5). The π-conjugation extends over the entire molecule in the closed

4

form whereas it is restricted to each half of the molecule in its open form. As a consequence, the closed form is expected to exhibit intrinsically better electrical conductance properties than the open form. The transition from closed to open form takes place for wavelengths $500 < \lambda < 700$ nm; for the reverse, one requires $300 < \lambda < 400$ nm. Furthermore, diarylethenes usually exhibit excellent thermal stability and high fatigue resistance.
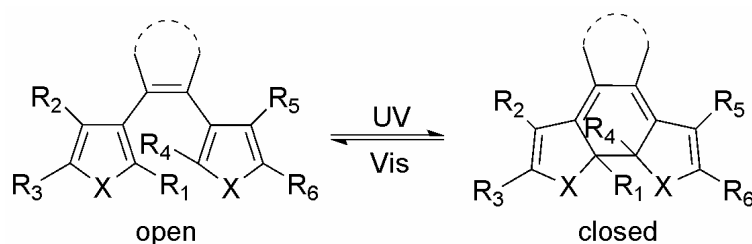
Scheme 5 *Switching cycle of diarylethenes.*

1.3 Electrochemical Read-Out Following Photochemistry in Solution

The simplest approach to measuring changes in electronic structure, and consequently molecular conductivity (in terms of resonant tunneling), is to examine the changes in the electronic absorption that occur upon photo-switching. In general, a blue or red shift in the lowest electronic absorption band would indicate an increase or decrease in the HOMO/LUMO gap of the molecule, respectively, which can be viewed simplistically as a change in the 'band-gap' of the molecule or as a decease or increase, respectively in the conjugation pathlength in the molecule. However, this interpretation must be made with caution as the effect of the change in conjugation on 'molecular conductivity' and specifically the change in terms of resonant tunneling requires more detailed information in the absolute changes in the free energy of the HOMO and LUMO orbitals. Cyclic voltammetry offers a powerful tool towards the non-destructive readout of molecular states during photochemical reactions of photochromic molecules (Figure 1). The open and closed forms of diarylethenes give distinguishably different signals.[20] Cyclic voltammetry is a convenient tool to monitor not only the change in the HOMO-LUMO gap (the origin of the change in electronic absorption upon photoreaction) but also provides detailed information as to whether it is the HOMO or LUMO orbital or both which changes in energy – a factor critical to understanding changes in resonant tunneling via these orbitals. For example, two well-known classes of photochromic molecules, the diarylethenes and the spiropyrans show

5

very similar changes in their electronic absorption spectra upon irradiation, changes which are accompanied by changes in their electrochemical properties.[17,19]
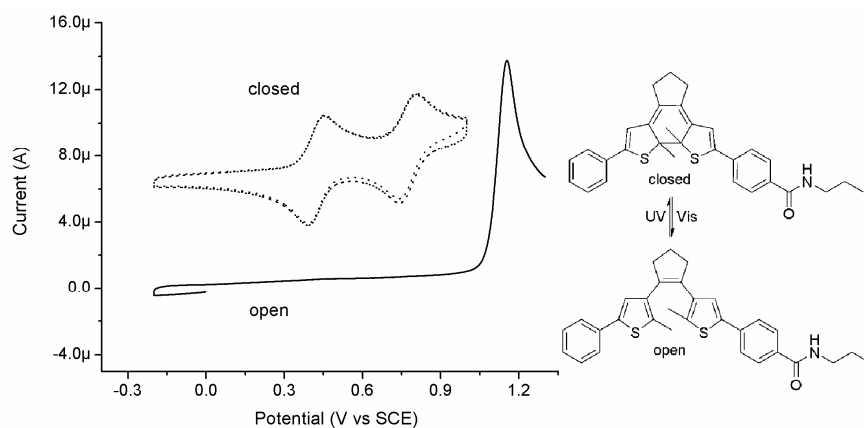
Figure 1 *Cyclic voltammetry and structure of the closed and open diarylethene switch at 0.1 V s^{-1} in CH$_2$Cl$_2$ (0.1 M TBAPF$_6$).*

The change in redox potential between two photochromic states provides a strong indication of the effect of a photochromic change on the electronic and hence conductive properties of a molecular system. As mentioned above, in the case of the diarylethenes and spiroyrans the dramatic change in the HOMO/LUMO gap is manifested as a bathochromic shift in the absorption spectrum upon irradiation. Based on electrochemical measurements, in the case of the spiropyrans[21] the HOMO levels are essential unaffected by the ring opening and closing while the LUMO is shifted. In contrast to spiropyrans, for the diarylethenes the increase in conjugation pathlength upon photochemical ring closure results in a lowering of the bandgap by increasing the HOMO energy and decreasing the LUMO energy.[22]

Photochromic behavior is not limited to changes in molecular structure, as also changes in molecular shape can drive changes in electronic structure. This is exemplified in two recent examples. In the case of bis-thiaxantylidene[23] the steric crowding between the four phenyl rings forces the molecule to adopt one of several conformations (Figure 2). In this case the anti-folded state is most stable and is the only state observed at room temperature. Irradiation of this compound in solution at 263 K results in the change of the geometry and a pronounced hypsochromic shift in the absorption spectrum and a complete loss in fluorescence. However, in contrast to spiropyrans and diarylethenes, this change is not due to a change in bonding, but instead in a change in the conformation of the molecule, i.e. to a

6

syn-folded state. Importantly, the formal conjugation in this system is not affected. However, the electrochemical properties of the molecular change also with a cathodic shift in the first oxidation process upon irradiation (Figure 2). As would be expected, the conversion to a conformationally less stable state implies that the ground state of the molecule is destabilized, i.e. the HOMO rises in energy. The blue shift in the absorption spectrum, however, shows that the destabilization of the LUMO is much more pronounced than that of the HOMO. This is remarkable as there is no simple change in conjugation involved in this transformation but only a change in conformation. Furthermore, the blue shift in the absorption spectrum could be expected to indicate a decrease in conjugation, however, in this case HOMO mediated superexchange process would be enhanced rather than reduced.[24] This is again in stark contrast to the diarylethenes. Hence, a frontier orbital approach i.e. drawing double bonds says little about the charge transport ability of a system. Besides the described photochemical addressing, electrochemical addressing of this compound is also possible. Oxidation of the anti-folded state leads to a dicationic species where the upper and lower halves are oriented perpendicularly to each other. After re-reduction of the dicationic species, the molecule thermally relaxes to the syn-folded state.[23]
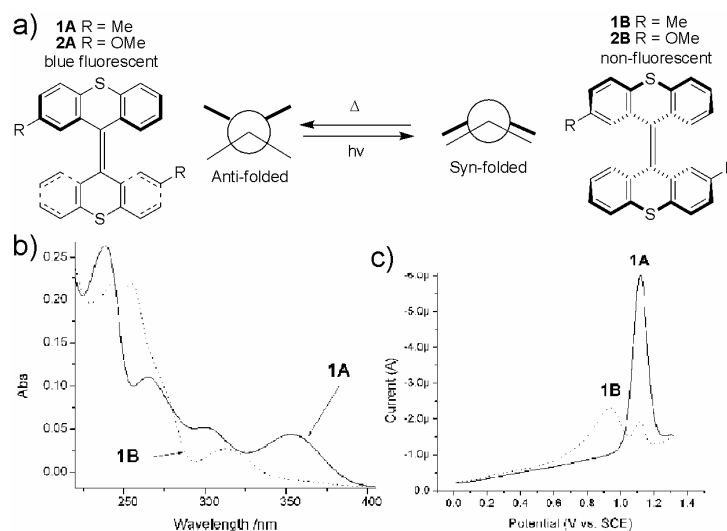
Figure 2 *a) Changes in conformation between the anti-folded and syn-folded states. b) UV/Vis spectrum showing the anti-folded and syn-folded states. c) Differential pulse voltammetry of the anti-folded and syn-folded states.*

In the previous example the change in electronic properties was driven by a change in molecular conformation. However, changes in electronic properties driven by

7

conformational changes can be effected by using photochromic units, which are electronically separated from the unit of interest (Figure 3).[25] The photochromic azobenzene unit in this system is covalently linked to a tetrathiophene moiety. The switching of HOMO level energy is modest but is due to the change in conformation imposed on the tetrathiophene by the photochromic azabenzene unit. The mechanically induced distortion results in the reversible variation of the HOMO/LUMO gap of the tetrathiophene as indicated by cyclic voltammetry (Figure 3a). These effects of mechanical distortions in conductance are known[26] and have important implications for molecular junctions.
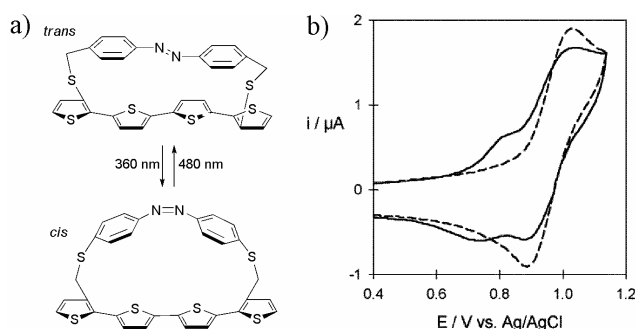
Figure 3 *a) Photomechanical manipulation of the electronic properties of linear π-conjugated system. b) Cyclic voltammogram of the trans form before irradiation (dashed line) and after 2 h of irradiation at 360 nm (solid line).*

1.4 Electrochemical Read-Out Following Photochemistry on Surfaces

Electronics based on molecular systems can be defined as technology exploiting the properties and functionality of molecules as components in electronic devices.[1,27] However, the molecular component must be "wired up" using other functional units (e.g., thiol or thioacetate groups used for anchoring on gold surfaces, etc.) and must be addressable independently of other switch molecules and functional units in its surroundings.

The electrochemical properties of many of photochromic systems on surfaces have been noted for some time, in particular with respect to the change in surface conductivity which accompanies changes in molecular state.[28] Recently, electrochemistry has been applied as

8

both complimentary switching method as well as a read-out method for immobilized photochromic switches.[20,29,30]
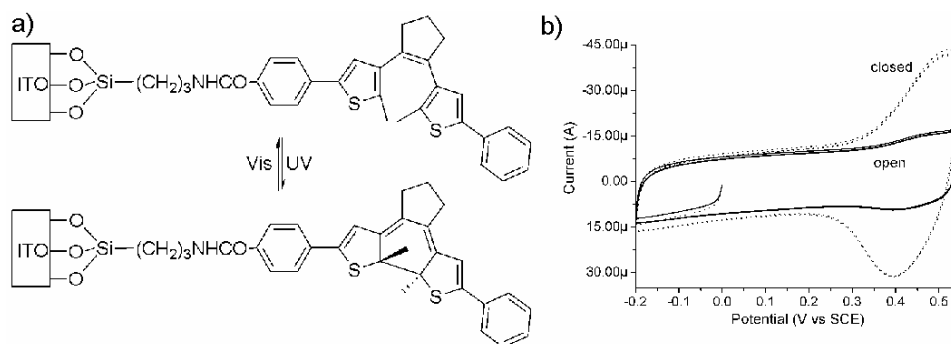
Figure 4 *a) The open (top) and closed (bottom) form-modified ITO electrode. b) Cyclic voltammetry of the open and closed form covalently attached to ITO electrodes.*

However, in immobilizing photochromic switches it is essential to understand that in addition to direct electronic interactions between the surface and the molecule (which can quench photochemistry, change the molecular orbital structure, etc.), other effects can be important, including packing and steric effects, *i.e.* decreases in conformational freedom, intermolecular interactions – changes to rates of intermolecular electron and energy transfer. For example, in the case of dithienylcyclopentenes, in solution the state can be switched in both directions by UV and visible irradiation, but only in one direction by electrochemical stimulation.[22] When immobilized on an ITO surface (Figure 4), no changes in the photochemical properties of the dithienylcyclopentene moiety occur, however it can be switched in both directions electrochemically.[20] The change from solution to surface is not due to changes in intrinsic properties of the molecular species or by orbital interactions with the surface, but rather by a change in observed intermolecular electron transfer rates between the individual molecules, now held closely together on the surface instead of diffusing randomly in solution.

1.5 Photochromism on Metallic Nanoparticles

Metallic nanoparticles offer tremendous opportunities for understanding of molecular surface interactions due to the range of nanoparticle sizes which can be accessed uniformly.[31] As such, they offer a convenient model system for mimicking properties of bulk solids, with the additional benefit of being able to tune size-dependent properties, in particular surface plasmon energies.[32] Of particular interest are SAMs of photoactive

9

molecules formed on the surface of gold nanoparticles. Due to the high surface-to-volume ratio, the concentration of photoactive compounds compared to the number of gold atoms allows for standard characterization techniques such as UV/Vis or FTIR spectroscopy to be employed to detect photochromic switching. Metallic nanoparticles can be easily synthesized from cheap starting materials and thus might serve as a fast screening technique for evaluation of photochromic properties of organic molecules grafted on metallic surfaces.

The effect of self-assembly of photoswitches on metallic nanoparticulate surfaces can be seen in two major contributions. Firstly, a direct electronic coupling of a nanoparticle core with a chromophore due to their proximity,[31b] which might results in complete quenching of the photoreaction (see Chapter 4). Secondly, effects of steric constraints, which limit conformational freedom of the molecular entities.

Trans-cis isomerization of azobenzenes and stilbenes chemisorbed on gold nanoparticles via alkylthiol linkers with a range of spacer lengths has been reported.[33] The quantum yields for the photoisomerization from *trans* to *cis* isomers were found to be dependent on the length of the alkyl chain and were attributed to distance-dependent quenching of the excited state by the metallic core. By contrast, *trans* to *cis* isomerization of an analogous stilbene monolayer on planar gold was not observed because of high crystallinity and dense packing of the monolayer.[34] These observations demonstrate the importance of conformational restrictions on the photoreactivity of photochromic molecules. More recently, unsymmetrical azobenzene disulfides were employed in an attempt to realize highly efficient isomerization on colloidal gold surfaces.[35] In the SAMs formed, the free volume for photoreaction of azobenzenes was guaranteed by a 50% dilution due to the presence of the second alkyl unit used for surface assembly of the disulfide (Figure 5). As a result of this dilution effect both *trans* to *cis* and the *cis* to *trans* isomerizations occur as they were relatively free of steric restrictions in contrast to that obtained on the planar gold surface.[36]
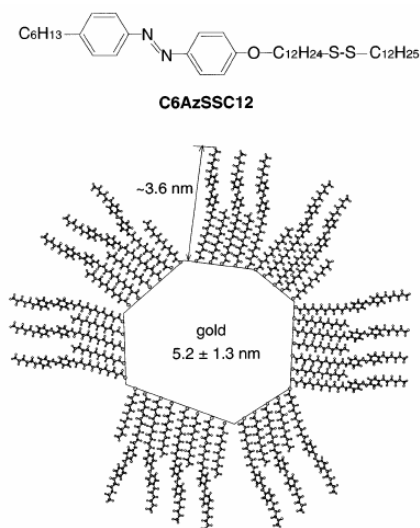
Figure 5 *Molecular structure of the azobenzene disulfide and schematic drawing of the azobenzene-capped gold nanoparticle (adopted from reference 34).*

The *cis-trans* isomerization on gold nanoparticles has been studied recently in the so-called light-driven unidirectional molecular motors[37] (Figure 6). A sequence of two energetically uphill photochemical isomerization steps each followed by an energetically downhill irreversible thermal helix inversion step result in a full 360° rotation of a rotor part with respect to a stator part around the central double bond (axis of rotation). Separation of the motor molecules from the gold surface by two eight- methylene-unit linkers was chosen to ensure that the function of the motor observed in solution is retained upon grafting to the gold surface. The barrier for thermal isomerization of molecules grafted on gold nanoparticles was found to be slightly higher than for the molecules in solution, a change which was attributed to the decrease in the molecules' degrees of freedom.
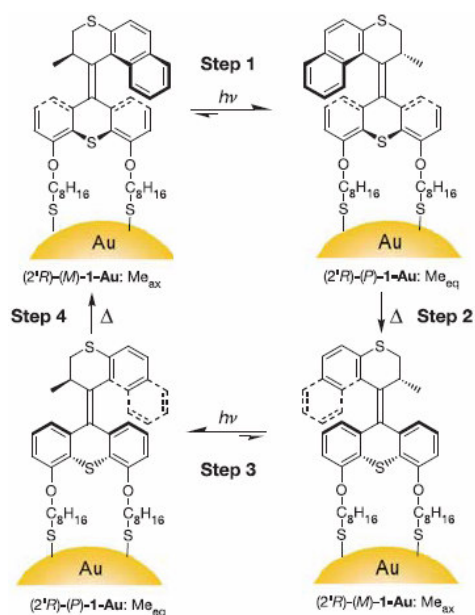
Figure 6 *The four-state unidirectional rotation of a motor-functionalized nanoparticle is shown (h*ν*, photochemical step; Δ, thermal step). The photoisomerizations were induced by irradiation at λ ≥ 280 nm or λ = 365 nm. Me$_{ax}$ indicates the pseudo-axial orientation of the methyl substituent, Me$_{eq}$ indicates the unstable pseudo-equatorial orientation of the methyl substituent.*

In the previous examples, direct electronic coupling and steric restrictions contributed to the change in photochemistry observed upon immobilization. For diarylethenes, however, steric effects arising from close packing in SAMs should not significantly alter photochemistry, since the photoswitching is not accompanied by dramatic geometrical changes and photochemistry is preserved even in crystalline states.[38] An early attempt to investigate photoswitching of diarylethenes self-assembled on a surface of gold nanoparticles showed that when the switching unit is isolated from the surface by a linker based on pentamethylene alkyl chain (Figure 7), the photochromic behavior stays intact.[39] Both ring closure and ring opening processes of molecules grafted on gold nanoparticles resembled those of free molecules in solution.
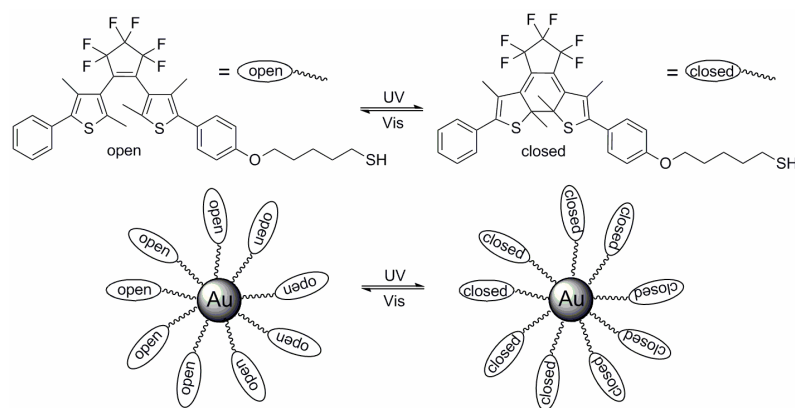
Figure 7 *Photochromic interconversions of unbound (top) and bound to gold nanoparticles (bottom) thiol-terminated diarylethene derivative.*

As discussed above an easy way to preserve photochemistry upon grafting on metallic surfaces is to isolate the switching unit by non-conjugated linker. However, this might have negative implications on charge transport properties, since a certain level of communication between switching unit and metallic surface is essential in order to make molecular switching devices feasible. Hence, it is of great interest to study photochromic behavior of diarylethenes with their switching unit connected to the surface of gold nanoparticles directly *via* conjugated spacers (see Chapter 4).

1.6 Light Switching of Conductance of Individual Molecules and Monolayers

In the frame of development of optoelectronic molecular devices a crucial milestone would be a direct observation of photo-induced conductance switching under the conditions similar to those that molecules will be confronted with in real devices, i.e. molecules assembled on nanoscopic metallic electrodes at ambient pressures in air. Fundamental questions related to charge transport in molecules (i.e. stability of molecule-electrode contact versus conductance, random conformational changes versus conductance changes, random switching versus controlled switching) can be addressed in setups allowing measurements of individual molecules (scanning tunneling microscopy[40] (STM), mechanically controlled break-junction[41] (MCBJ)). Understanding of these issues will help to design future suitable molecular candidates for switchable devices.

13

In one of the first reported experiments correlating photochromic switching and changes of conductance for individual molecules, the azobenzene derivatives were embedded in n-dodecanethiol SAMs formed on Au(111).[42] The STM tip was used as a nanoscale probe for the charge transport properties of the switch. Direct evidence of light-induced switching for individual azobenzene molecules was achieved by comparing unequal apparent STM heights for *trans* respectively *cis* isomers during irradiation. When azobenzenes undergo a *cis-trans* isomerization, the physical height of the molecules is altered (Figure 8). This does not significantly change the conductance of the molecule itself but does significantly change its height. The apparent changes in conductivity observed by STM thus can be attributed to the switching of height of the molecules rather than to an internal structural modification leading to a modification of resistance. Additionally, it was shown that even in the absence of light, conductance switching was observed and attributed to the reversible *trans-cis* isomerization driven by external electric field and current flow. By varying potentials this voltage-induced switching could be suppressed.
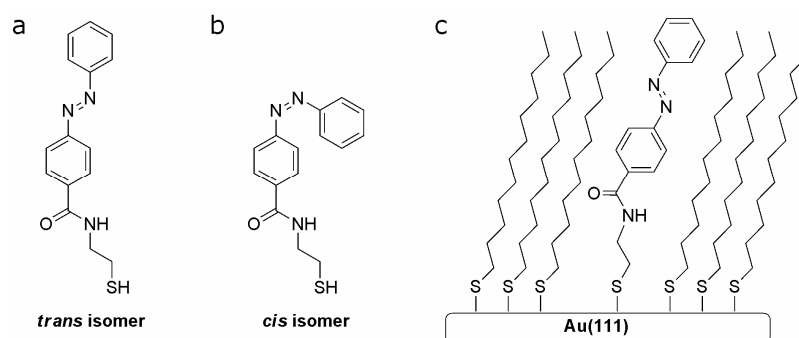
Figure 8 Schematic structrures of an azobenzene derivative which can be grafted on a surface through a S–Au bond. (a) trans isomer, (b) cis isomer. (c) The trans isomer was inserted in a SAM of n-dodecanethiol, forming a mixed azobenzene/n-dodecanethiol monolayer. The state of the embedded azobenzenes was characterized by their apparent height as seen by STM, which measures a convolution of real physical height and of local density of states.

In the aforementioned case the photoactive unit was isolated form Au(111) surface by the linker composed of two non-conjugated sp^3 carbon atoms terminated by a thiol group providing chemical bonding to the Au(111) surface. More recently, light-induced switching of individual azobenzenes physisorbed on Au(111) was investigated under ultra-high vacuum conditions.[43] *Tert*-butyl groups lift the switching unit away from the substrate (Figure 9), thereby increasing molecular photomechanical activity by decreasing molecule-surface coupling. If the molecule contained zero or two *tert*-butyl legs no isomerization

14

could be observed, due to the stronger electronic coupling of the switching unit with the substrate. The "transition" that was observed from quenched to active photomechanical behavior reveals the importance of electro-mechanical coupling between a molecule and substrate in determining single molecule photoswitching capability.
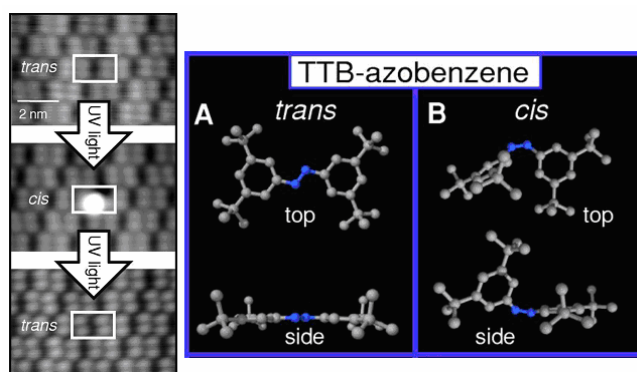
Figure 9 *(left) Reversible photo-induced switching is observed for a single azobenzene molecule. The same individual azobenzene molecule (identified by white boxes in three successive panels) is shown before and after two successive exposures to UV light. The molecule starts out in the trans state (top panel), is then switched to the cis state after the first exposure to UV light (middle panel), and is then switched back to the trans state after a second exposure to UV light (bottom panel). (right) Simulated trans- and cis- azobenzene structures compared to experiment. (A) Calculated trans geometry. (B) Calculated cis geometry.*

Both examples of conductance switching of azobenzene derivatives relied inherently on switching of height rather than direct switching of intrinsic conductance of the molecules. This means that a setup, sensitive to height switching (as is STM) would have to be employed if azobenzenes are to be used for switching devices. On the other hand, in case of diarylethene photochromic switches rearrangement of double and single bonds after photoswitching should be accompanied by significant modification of conductance, while their physical height is not dramatically altered. Confirmation of the tremendous potential of 1,2-dithienylethenes for molecular electronics was obtained by studying the conductivity of a dithienylethene switch with thiophene groups as spacers and functionalized by two thiol functions chemisorbing on each side of a MCBJ electrode (for the detailed results see Chapter 2).[44] These experiments revealed that switching a molecule from the closed to the open form results in a significant resistance increase of three orders of magnitude. This constitutes an additional indication that closed and open forms are characterized by

15

intrinsically different charge transport properties. However, once the switch is connected to gold via the Au–S bond, it could only be switched from the closed to the open form. These results were subsequently corroborated by measuring a monothiol analogue of the switch in a STM setup (Chapter 2).[45] Additionally to one-way photoswitching, an extensive analysis of random (stochastic) switching was carried out exhibiting a voltage-dependent behavior. An important consequence of such studies is immediately obvious since both effects, light-induced or stochastic switching, are of the same order of magnitude. The lack of reversibility in those systems (the same behavior was observed for the monothiol derivative on gold nanoparticles) was theoretically investigated and attributed to the quenching of the excited state of the open form by gold.[46] More specifically, density functional theory (DFT) calculations suggested that the observed quenching may result from the alignment of the Fermi-level of gold with the open isomers. The deep-lying HOMO level at a high metal density of states offers the opportunity for many possible electron transfer events, thus reducing the lifetime of the hole created after an excitation. In contrast, the HOMO of the closed isomer is higher in energy within the low density of states of gold and the ring opening can take place (for more details see Chapter 2).

More recently, a new diarylethene derivative with one CH_2 group separating the aromatic part of the switch from the gold surface was investigated using a repetitive break junction method based on a STM setup (Figure 10).[47] Extensive statistical analysis of conductance properties of the single switch is possible as repeatedly a gold probe is pushed into a gold surface and pulled out again to form a thin gold filament in the solution of switch. Markedly different resistances of 526 MΩ in the open form and 4 MΩ in the closed form were found. The isolation of the switching unit by a not fully conjugated linker allowed for the perseverance of reversible photoisomerizations.

16

a)

b)

tip

substrate
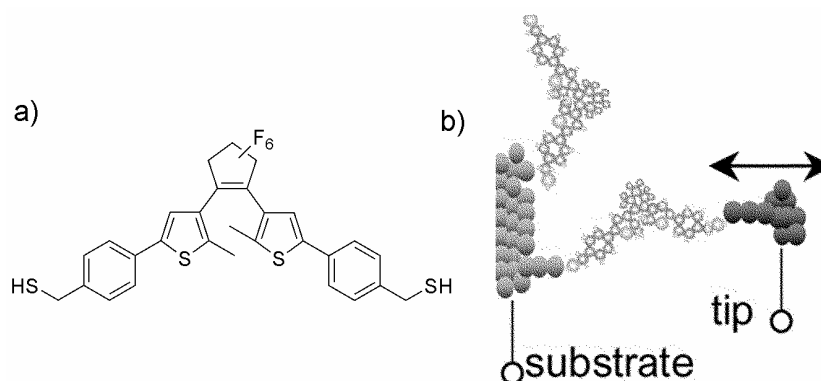
Figure 10 *a) Dithiolated diarylethene switch. b) Schematic representation of the apparatus for conductance measurements. A break junction is formed by pushing a gold probe tip into a gold surface covered with dithiolated switches and retracting it. Molecules become transiently trapped in the gap.*

1.7 Switching Devices Based on Photochromic Molecules

The most obvious objective of molecular electronics is to create fully functioning devices based on molecules. The first "macroscopic" switching device based on diarylethene photochromic molecules has been previously realized.[48] A conductive polymer based on diarylethenes (Figure 11) was sandwiched between metallic (Al and Au) and ITO electrodes. The sets of experiments with different metals as an electrode showed dramatic changes in conductance. If an Al electrode was used devices containing the open form showed rectifying behavior due to the significant junction barrier at the Al/polymer interface, in contrast to the ohmic Au/polymer interface, which in combination with the ohmic polymer/ITO interface results in symmetric IV characteristics of the device. The lower workfunction of Al was responsible for this difference in the junction properties. After ring closure, induced by UV light irradiation, larger currents were observed and IV curves became symmetric. This was attributed to the loss of the junction barrier at the Al/polymer interface because of new electronic states at the previously forbidden area in the original polymer. This highlights the importance of the material that is used as an electrode. The overall reversibility of current switching was found to be poor. However, this was not a direct consequence of a loss of reversibility in photochemical switching judging from the reversible changes in the fluorescence emission intensity. Instead, it was attributed to the instability of the junction or interface structure upon the photochromic reaction. This is not surprising since the surface morphology for a single crystal of

17

diarylethenes can be changed following photoreactions.[49] The problems with the instability of the interface in the sandwiched photoswitching polymer devices can be overcome by using a non-photochromic polystyrene polymer doped with diarylethene molecules.[50] The domination of photochromic dopants in charge transport in non-conductive polymers was emphasized by the fact that the switch molecule with a donor-acceptor structure exhibited the highest conductance profile (the conductance increases by factor of two changing from the closed to the open form).
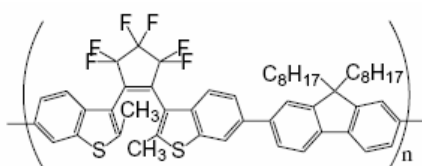
Figure 11 *Chemical structure of the diarylethene based polymer from ref. 48.*

More recently, a µm-sized device based on a network of nanoparticles deposited in between interdigitated nanogapped Au electrodes (Figure 12) was reported.[51] Nanoparticles were encapsulated by switchable diarylethene molecules connecting pairs of nanoparticle cores. Fully reversible conductance switching was achieved by a sequence of UV and visible irradiation cycles. Switching times were, however rather long (10 h for the maximum ON/OFF ratio).
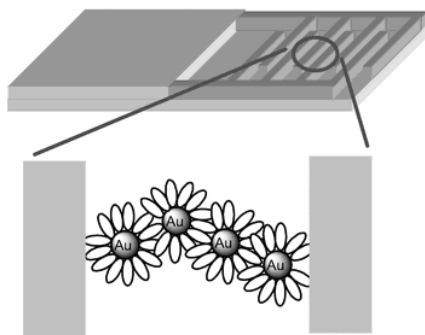
Figure 12 *Schematic drawing of the diarylethene-Au nanoparticle network on an interdigitated nano-gap Au electrode.*

A field effect transistor (FET) based on isolated single-walled carbon nanotubes (SWCNTs) functionalized with spiropyran photochromic molecules was also constructed (Figure 13).[52] Pyrene- or alkane-tethered spiropyrane molecules were self-assembled on a SWCNT. The single nanotube was contacted on each side to Au electrodes (Figure 13b).

18

Using alternating UV and visible light as an external trigger the observed low and high conductance of the devices could be switched back-and-forth. The reversible switching in the functionalized SWCNT FETs was attributed to the photoswitching of the tethered molecules. Two explanations of the phenomenon were provided. One possibility is that the charge-separated state of the merocyanine (Figure 13a) introduces scattering sites for the carriers by creating localized dipole fields around the tubes. These sites then scatter charge when it flows in the nearby SWNT channel and thereby lower the mobility in the devices. Another possibility is that the nearby phenoxide ion quenches the p-type carriers in the tubes and behaves like a charge trap.
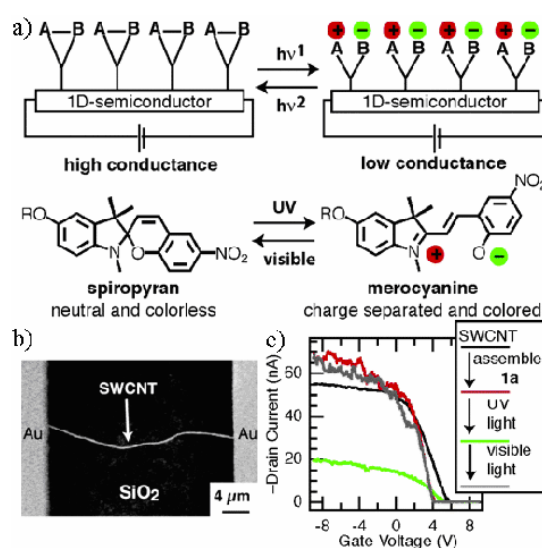
Figure 13 *a) Schematic of a carbon nanotube based semiconductor that has spiropyran molecules assembled on its surface (adapted from reference 52). b) Scanning electron micrograph image of a gold-contacted single carbon nanotube. c) Change in drain current of an individual SWCNT device as a function of V_g. Black curve is device before assembly; red curve is device after assembly of the spiropyrans; green curve after irradiation with UV light for ~10 min; blue curve after irradiation with visible light.*

1.8 Conclusions and Contents of this Thesis

The future of molecular electronic systems based on photoswitchable components looks increasingly bright. However, many challenges remain in achieving the goal of making the leap from fundamental science to applied technologies. The demonstration of a working

19

redox based device based on assemblies of switchable molecules by Stoddart, Heath and coworkers[3] and the demonstration of single molecule photoswitching of conductance[47] (see also Chapter 2 and Chapter 5) have paved the way for this transition. However, to realize the full potential of photochromic systems key issues in device assembly, in particular interfacing molecular systems with the macroscopic world, stability, and the understanding of the relative contributions of photochromic responses to changes in tunneling and resonant tunneling contributions to charge transport over the gap bridged by these systems remain to be resolved.

The progress towards the development of light switchable electronic devices based on diarylethene photochromic molecular switches is described in this thesis. The main focus is on fundamental aspects that have to be solved before a fully operational device can be constructed. The central questions of the research are: synthetic availabilities and costs of the molecules of interest, fundamental aspects of the photochemical switching (reversibility, fatigue efficiency), influence of the surface anchoring on the reversibility of the switching processes, effects of different surfaces on the organization of molecules, charge transport properties, scaling down to nanoscale as small as single molecule and finally, can conductivity switching be realized with a single molecule? The investigation on several of these aspects is described in the following chapters.

In Chapter 2 the first attempt towards single molecule light-induced switching of the conductance is described. Two independent techniques (MCBJ and STM) were used to follow changes of conductance of individual molecules upon irradiation. Important limits in light switching were found for molecules chemisorbed on gold surfaces.

Chapter 3 deals with the synthesis of new diarylethene derivatives capable of chemisorption on gold surfaces. Subsequently, their photochromic properties in solution are studied. Suppression of the photochemical reaction at low temperatures is discussed in detail, indicating the existence of a thermal activation barrier involved in the photochemical ring opening.

Chapter 4 focuses on photochromic properties of SAMs of diarylethenes on the surface of gold nanoparticles and bulk gold electrodes. Both approaches seem to provide key methods to rapidly assess switching behavior of photochromic compounds on surfaces. The main finding is that the switching behavior of diarylethenes is strongly influenced by a spacer unit which connects the central switching unit with the gold surface. Equally important is the investigation of redox properties of the SAMs with implications on non-destructive read-out.

Reversible light induced single molecule switching of conductance is described in Chapter 5. The molecule which was found to preserve its photochromic behavior upon chemisorption on gold (Chapter 4) is investigated using STM. Irradiation of photochromic molecules inserted in an insulating matrix of alkanethiols results in modulations of their conductivity.

Finally, Chapter 6 focuses on molecular monolayers formed spontaneously at the interface between a series of atomically flat surfaces and a solution containing N-salicylideneaniline based photochromic molecules. The effect of a systematic variation of substrates on the geometry of SAMs is discussed. The polymorphism observed on Au(111), is rationalized by a consideration of the substrate-induced intermolecular interactions, suggesting that a simplified view on separated effects of molecule/molecule interactions and molecule/substrate interactions is not always sufficient enough to explain the self-assembly properties of organic molecules.

1.9 References and Notes

[1] a) B.L. Feringa (Ed.), Molecular Switches, Wiley-VCH, Weinheim, **2001**. b) J. C. Crano, R. Guglielmeti, Organic Photochromic and Thermochromic Compounds Vol. 1, Plenum Press, New York, **1999**

[2] R. L. Carroll, C. B. Gorman, *Angew. Chem. Int. Ed*. **2002**, *41*, 4378-4400; b) C. Joachim, J. K. Gimzewski, A. Aviram, *Nature* **2000**, *408*, 541-548.

[3] J. E. Green, J. W. Choi, A. Boukai, Y. Bunimovich, E. Johnston-Halperin, E. DeIonno, Y. Luo, B. A. Sheriff, K. Xu, Y. S. Shin, H. –R. Tseng, J. F. Stoddart, J. R. Heath, *Nature* **2007**, *445*, 414-417.

[4] R. P. Feynman, *The Pleasure of Finding Things Out*; Perseus Books: Cambridge, MA, **1999**; Chapter 5. Richards Feynman's original lecture "There's plenty of room at the bottom" can read at www.its.caltech.edu/~feynman.

[5] A. Aviram, M. Ratner, *Chem. Phys. Lett*. **1974**, *29*, 277-283.

[6] a) W. R. Browne, B. L. Feringa, *Nature Nanotechnology* **2006**, *1*, 25-35; b) M. Irie (guest editor), Photochromism: Memories and Switches, *Chem. Rev*. **2000**, *100*, 1683-1890 and references therein.

[7] K. Uchida, M. Saito, A. Murakami, T. Kobayashi, S. Nakamura, M. Irie, *Chem. Eur. J*. **2005**, *11*, 534-542, b) M. Irie, Applied Photochromic Polymer Systems (Ed.: C. B. McArdle), Blackie, Glasgow, **1991**, pp. 174-206; c) T. Ikeda, O. Tsutsumi, *Science* **1995**, *268*, 1873-1875; d) S. Shinkai, *Pure Appl. Chem*. **1987**, *59*, 425-430.

[8] S. L. Gilat, S. H. Kawai, J. -M. Lehn, *Chem. Eur. J*. **1995**, *1*, 275-284.

⁹ a) J. J. D. de Jong, L. N. Lucas, R. M. Kellogg, J. H. van Esch, B. L. Feringa, *Science* **2004**, *304*, 278-281; b) R. Eelkema, M. M. Pollard, J. Vicario, N. Katsonis, B. S. Ramon, C. W. M. Bastiaansen, D. J. Broer, B. L. Feringa, *Nature* **2006**, *440*, 163-163.

¹⁰ X.-Y. Zhu, *Surf. Science Reports* **2004**, *56*, 1–83.

¹¹ T. Albrecht, A. Guckian,.A. M. Kuznetsov, J. G. Vos,. J. Ulstrup, *J. Am. Chem. Soc*. **2006**, *128*, 17132-17138.

¹² H. Rau, Photoisomerization of azobenzenes, in: J.F. Rebek (Ed.), Photochemistry and Photophysics, CRC Press, Boca Raton, **1990**.

¹³ B. L. Feringa, R. A. van Delden, N. Koumura, E. M. Geertsema, *Chem. Rev*. **2000**, *100*, 1789-1816.

¹⁴ H. Meier, *Angew. Chem. Int. Ed. Engl*. **1992**, *31*, 1399-1420.

¹⁵ B. L. Feringa, N. P. M. Huck, H. A. van Doren, *J. Am. Chem. Soc*. **1995**, *117*, 9929-9930.

¹⁶ a) N. Koumura, R. W. J. Zijlstra, R. A. van Delden, N. Harada, B. L. Feringa, *Nature* **1999**, *401*, 152-155; b) E. R. Kay,D. A. Leigh, F. Zerbetto, *Angew. Chem. Int. Ed.* 2007, *46*, 72-191; c) R. Eelkema, M. M. Pollard, J. Vicario, N. Katsonis, B. S. Ramon, C. W. M. Bastiaansen, D. J. Broer, B. L. Feringa, *Nature* **2006**, *440*, 163-163.

¹⁷ G. Berkovic, V. Krongauz, V. Weiss, *Chem. Rev*. **2000**, *100*, 1741-1753.

¹⁸ R. Rosario, D. Gust, M. Hayes, J. Springer, A. Garcia, *Langmuir* **2003**, *19*, 8801-8806.

¹⁹ a) M. Irie, *Chem. Rev*. **2000**, *100*, 1683-1684; b) H. Tian, S. Yang, *Chem. Soc. Rev*. **2004**, *33*, 85-97.

²⁰ J. Areephong, W. R. Browne, N. H. Katsonis, B. L. Feringa, *Chem. Commun.,* 2006, 3930-3932.

²¹ a) M. Campredon, G. Giusti, R. Guglielmetti, A. Samat, G. Gronchi, A. Alberti, M. Benaglia, *J. Chem. Soc. Perkin. Trans. 2* **1993**, 2089-2094; b) A. S. Saraç, B. Ustamehmetoglu; A. Leiminer; B. Stephan; A. Mannschreck, *Electrochimica Acta* **1997**, *42*, 3629-3635; c) J. F. Zhi,R. Baba, K. Hashimoto, A. Fujishima, *Ber. Bunsenges. Phys. Chem*. **1995**, *99*, 32-39.

²² a) W. R. Browne, J. J. D. de Jong, T. Kudernac, M. Walko, L. N. Lucas, K. Uchida, J. H. van Esch, B. L. Feringa, *Chem. Eur. J*. **2005**, *11*, 6414-6429 and references therein; b) W. R. Browne, J. J. D. de Jong, T. Kudernac, M. Walko, L. N. Lucas, K. Uchida, J. H. van Esch, B. L. Feringa, *Chem. Eur. J*. **2005**, *11*, 6430-6441 and references cited therein.

²³ W. R. Browne, M. M. Pollard, B. de Lange, A. Meetsma, . B. L. Feringa, *J. Am. Chem. Soc*. **2006**, *128*, 12412-12413.

²⁴ W. R. Browne, N. M. O'Boyle, J. J. McGarveyc, J. G. Vos, *Chem. Soc. Rev*. **2005**, *34*, 641-663.

[25] a) B. Jousselme, P. Blanchard, N. Gallego-Planas, J. Delaunay, M. Allain, P. Richomme, E. Levillain, J. Roncali, *J. Am. Chem. Soc*. **2003**, *125*, 2888-2889; b) B. Jousselme, P. Blanchard, M. Allain, E. Levillain, M. Dias, J. Roncali, *J. Phys. Chem. A* **2006**, *110*, 3488-3494; c) B. Jousselme, P. Blanchard, N. Gallego-Planas, E. Levillain, J. Delaunay, M. Allain, P. Richomme, J. Roncali, *Chem. Eur. J*. **2003**, *9*, 5297-5306.

[26] C. Joachim, J. K. Gimzewski, R. R. Schlittler, C. Chavy, *Phys. Rev. Lett*. **1995**, *74*, 2102-2105.

[27] Y. Wada, *Pure Appl. Chem*. **1999**, *71*, 2055-2066.

[28] a) I. Willner, A. Doron and E. Katz, *J. Phys. Org. Chem.* **1998**, *11*, 546-560; b) I. Willner, V. Prado-Yissar, E. Katz, K. T. Ranjit, *J. Electroanal. Chem.* **2001**, *497*, 172-177.

[29] R. Baron, A. Onopriyenko, E. Katz, O. Lioubashevski, I. Willner, S. Wang and H. Tian, *Chem Commun*., **2006**, 2147-2148.

[30] I. Willner, B. Basnar, B. Willner, *Adv. Funct. Mater*. **2007**, *17*, 702-717.

[31] a) M.-C. Daniel, D. Astruc, *Chem. Rev*. **2004**, *104*, 293-346; b) K. G. Thomas, P. V. Kamat, *Acc. Chem. Res*. **2003**, *36*, 888-898.

[32] M. Brust, C.J. Kiely, *Colloids Surf. A: Physicochem. Eng. Asp*. **2002**, *202*, 175-186.

[33] a) J. Hu, J. Zhang, F. Liu, K. Kittredge, J. K. Whitesell, M. A. Fox, *J. Am. Chem. Soc*. **2001**, *123*, 1464-1470. b) J. Zhang, J. K. Whitesell, M. A. Fox, *Chem. Mater*. **2001**, *13*, 2323-2331.

[34] M. O. Wolf, M. A. Fox, *Langmuir* **1996**, *12*, 955-962.

[35] A. Manna, P. -L. Chen, H. Akiyama, T. -X. Wei, K. Tamada, W. Knoll, *Chem. Mater*. **2003**, *15*, 20-28.

[36] K. Tamada, H. Akiyama, T. X. Wei, *Langmuir* **2002**, *18*, 5339.

[37] R. A. van Delden, M. K. J. ter Wiel, M. M. Pollard, J. Vicario, N. Koumura, B. L. Feringa, *Nature* **2005**, *437*, 1337-1340.

[38] a) S. Kobatake, S. Takami, H. Muto, T. Ishikawa, M. Irie, *Nature* **2007**, *446*, 778-781; b) M. Irie, S. Kobatake, M. Horichi, *Science* **2001**, *291*, 1769-1772.

[39] K. Matsuda, M. Ikeda, M. Irie, *Chem. Lett*. **2004**, *33*, 456-457.

[40] a) P. Jiang, G. M. Morales, W. You, L. Yu, *Angew. Chem. Int. Ed*. **2004**, *43*, 4471-4475; b) J. He, Q. Fu, S. M. Lindsay, J. W. Ciszek, J. M. Tour, *J. Am. Chem. Soc*. **2006**, *128*, 14828-14835; c) L. A. Bumm, J. J. Arnold, T. D. Dunbar, D. L. Allara, P. S. Weiss, J. *Phys. Chem. B* **1999**, *103*, 8122-8127; d) B. Xu, N. J. Tao, *Science* **2003**, *301*, 1221-1223.

[41] a) C. Kergueris, J.-P. Bourgoin, S. Palacin, D. Esteve, C. Urbina, M. Magoga and C. Joachim, *Phys. Rev. B* **1999**, *59*, 12505-12513; b) M. Mayor, H. B. Weber, J. Reichert, M.

23

Elbing, C. von Hänisch, d. Beckmann and M. Fisher, *Angew. Chem. Int. Ed.* **2003**, *42*, 5834-5838; c) J. Reichert, R. Ochs, D. Beckmann, H. B. Weber, M. Mayor, H. von Lohneysen, *Phys. Rev. Lett.* **2002**, *88*, 176804.

[42] S. Yasuda, T. Nakamura, M. Matsumoto, H. Shigekawa, *J. Am. Chem. Soc.* **2003**, *125*, 16430–16433.

[43] M. J. Comstock, N. Levy, A. Kirakosian, J. Cho, F. Lauterwasser, J. H. Harvey, D. A. Strubbe, J. M. J. Fréchet, D. Trauner, S. G. Louie, M. F. Crommie, arXiv: *cond-mat*/0612201v2 [*cond-mat.mtrl-sci*] (last revised 8 May **2007**).

[44] a) D. Dulic, S. J. van der Molen, T. Kudernac, H. T. Jonkman, J. J. D. de Jong, T. N. Bowden, J. van Esch, B. L. Feringa, B. J. van Wees, *Phys. Rev. Lett.* **2003**, *91*, 207402.

[45] S. J. van der Molen, H. van der Vegte, T. Kudernac, I. Amin, B. L. Feringa, B. J. van Wees, *Nanotechnology* **2006**, *17*, 310.

[46] a) J. Li, G. Speyer, O. F. Sankey, *Phys. Rev. Lett.* **2004**, *93*, 248302; b) M. Zhuang, M. Ernzerhof, *Phys. Rev. B: Condens. Matter Mater. Phys.* **2005**, *72*, 073 104.

[47] J. He, F. Chen, P.A. Liddell, J. Andreasoon, S.D. Straight, D. Gust, T.A. Moore, A.L. Moore, J. Li, O.F. Sankey, S.M. Lindsay, *Nanotechnology* **2005**, *16*, 695-702.

[48] T. Kawai, Y. Nakashima, T. Kunitake, M. Irie, *Curr. Appl. Phys.* **2005**, *5*, 139-142.

[49] a) M. Irie, S. Kobatake, M. Hirichi, *Science* **2001**, *291*, 1769-1772; b) S. Kobatake, S. Takami, H. Muto, T. Ishikawa, M. Irie, *Nature* **2007**, *446*, 778-781.

[50] E. Kim. M. Kim, K. Kim, *Tetrahedron* **2006**, *62*, 6814-6821.

[51] M. Ikeda, N. Tanifuji, H. Yamaguchi, M. Irie, K. Matsuda, *Chem. Commun.* **2007**, 1355-1357.

[52] X. Guo, L. Huang, S. O'Brien, P. Kim, C. Nuckolls, *J. Am. Chem. Soc.* **2005**, *127*, 15045-15047.

Chapter 2

One –Way Conductance Switching of Single Photochromic Molecules connected to Gold Electrodes

In this chapter the light-induced conductance switching of single photochromic molecules connected to gold electrodes is described. Photochromic properties of two newly synthesized diarylethenes have been studied in solution showing reversible behavior. Two experimental techniques, namely, the Mechanically Controllable Break-Junction technique and Scanning Tunneling Microscopy are used to investigate electrical properties of the open and closed states of the molecules. Switching from a conductive to an insulating state is observed upon illumination with visible light. However, upon illumination with UV light the reverse process is not observed for molecules covalently attached to gold electrodes. We have attributed this to quenching of the excited state of the molecules in the open form by the presence of metallic gold. Additionally, reversible and irreversible stochastic switching, independent of the use of light, is observed in Scanning Tunneling Microscopy experiments showing dependence on the used bias voltage.[*]

2.1 Introduction

A major challenge of molecular electronics is to design useful devices based on addressable molecular structures and to incorporate these into integrated circuits[1]. As a result of decades of research in this area substitutes for conventional switches,[2] rectifiers,[3] wires[4] and transistors[5] have been introduced, although still considerable effort is needed to realize practical and robust molecular based electronic devices.[6] The necessity to respond to external stimuli places molecular switches amongst the most challenging of systems.[7] Photochromic molecular switches[7] meet this requirement and specifically 1,2-dithienylethenes (Figure 1) hold a prominent position among others because of their reversible photo-induced transformations that modulate electrical conductivity and their exceptional thermal stability and fatigue resistance.[8] Despite the noticeable progress in designing new molecular electronic components, including molecular switches, their incorporation into integrated circuits remains a challenge. A common approach is based on anchoring molecules to metal electrodes.[3,9] However, in the case of photochromic molecules, the situation is more complicated, since the presence of a metal surface may influence optical processes in photoactive molecules.[10]

Another important question, which has to be addressed, is the nature of electron transport through these hybrid metal-molecular systems. Investigation of the electron transport properties of a single or a limited number of molecules connected to metallic electrodes is therefore presently the subject of intense research activity. Besides the fundamental interest in electron transport phenomena operating at the nanoscale, it also represents an important milestone for the development of molecular electronics. Part of the problem lies in the fact that if we want to perform reliable electronic transport measurements on a molecular system, we have to make a well controlled electrical contact between the molecule and the nanometer-scale electrodes used in the measurements. This connection can influence intrinsic properties of the molecules. Several techniques have been recently employed to explore conductive properties of individual or small numbers of molecules chemically connected to one or two electrodes. All the techniques involve at least one electrode of nanometer size. Mechanically Controlled Break-Junction (MCBJ),[9,11] electromigration-induced tunnel devices,[12] Scanning Tunneling Microscopy (STM)[13] or conductive-probe Atomic Force Microscopy (cAFM)[14] are all techniques measuring one or at most a few molecules. For MCBJ and electromigration, molecules are chemically connected to two electrodes, which are freshly formed in a controlled manner. In the case of MCBJ, a thin metallic wire is mechanically stretched until it breaks into two nano-dimensional electrodes. Electromigration-induced nanogaps are produced by applying large current

26

densities to gold wires. At high current densities j (typically 108 A/cm^2) momentum transfer from the electrons to the gold atoms leads to drift of the atoms, in the direction of the electron flow. This mass flux can lead to the growth of voids in the wire, finally leading to the formation of gaps.[15] Typical STM and cAFM setups are used to study conductance of molecules that are incorporated into a self-assembled monolayer (SAM) formed on a planar substrate. Molecules are covalently linked to a planar substrate, serving as one electrode and a conductive atomically sharp tip, positioned on top of SAMs, acts as a second electrode while scanning. In addition to the aforementioned techniques, which focus primarily on single molecules, there are other experimental setups that involve greater but nevertheless small number of molecules that are inserted between two nanometer size contact electrodes. The tunneling junction, here consisting of two metal plates separated by molecules, can be assembled using several approaches, among them: crossed wires,[16] mercury-drop junction[17] and metal-capped nanopores with[18] or without[19] a conducting polymer interlayer between the SAM and the metal top electrode to prevent formation of electrical short circuits.

The main goal of our work was to study and control the conductive properties of diarylethene photochromic molecular switches connected to metallic electrodes. Figure 1 shows a schematic of the incorporation of thiol terminated diarylethene switch between two
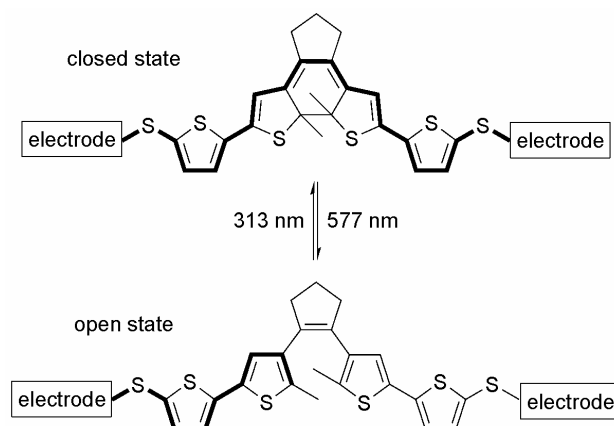
Figure 1 *A photochromic molecular switch between two electrode contacts in the closed state and the open state. By exposing the molecule to light of wavelength 577 nm, the molecule will switch from the closed to open form. The molecule can be switched back to the closed state by exposing it to UV light at 313 nm.*

electrodes. The molecule consists of conducting conjugated units, separated by switching units, which allow electron transport to be turned on-and-off reversibly by exposure to light

27

with specific frequencies. DFT calculations predict that the energies of diarylethene's LUMO and HOMO levels are in the range of 1.0 – 3.0 eV and 4.5 – 6.0 eV respectively.[†] In order to study the electronic transport through individual switches directly we attach them to metallic electrodes with controlled spacing in the nanometer range. In order to obtain complementary information we use two different experimental techniques: MCBJ and STM.

2.2 Synthesis and Photochromic Properties of Novel Thiol Terminated Diarylethene Compounds

Diarylethene photochromic switches **3** (Scheme 1) and **6** (Scheme 2) have been designed specifically for our electronic transport experiments. They consist of a central switching unit, two thiophene rings on both sides of the switching unit, and one (in case of **6**) or two (in case of **3**) thiol groups, protected with acetyl groups, at the ends of the molecules. The synthetic strategy has been based on Suzuki couplings and a subsequent introduction of thiol groups (Scheme 1 and 2). Compound **1** is known to be easily accessible and suitable for further functionalizations.[20] Its treatment with *n*-butyl lithium followed by tri-*n*-butyl borate gives a reactive boronic acid intermediate, which can react with a heteroaromatic bromide leading to compounds **2** or **4**. In case of **4**, subsequent Suzuki coupling with bromothiophene gives compound **5**. Compounds **2** and **5** were first lithiated and then treatment with sulfur and acetyl chloride which leads to formation of **3** and **6** in reasonable yields.
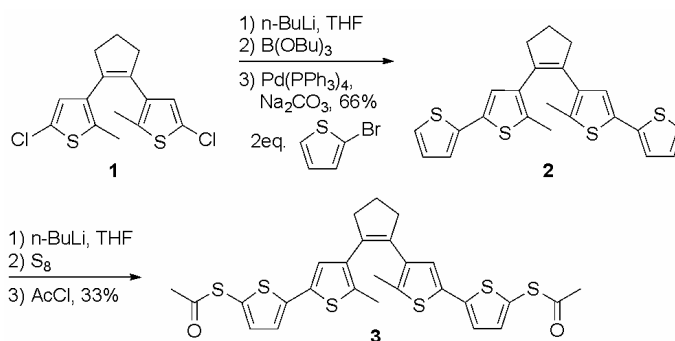
***Scheme 1** Synthetic route to compound **3**.*

28
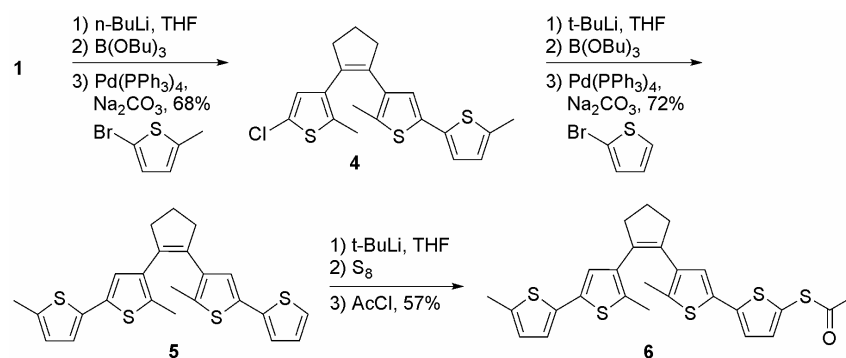
Scheme 2 *Synthetic route to compound* **6**.

Compounds **3** and **6**, like other dithienylethene-based molecular switches, can exist in two different forms, the so-called open and closed state (Figure 2). Upon irradiation with UV light the open form (dissolved in toluene) transform into the closed form with a high photoconversion (99%). When visible light is used the closed form returns quantitatively to the open form. In the open form, electronic interactions between two halves of the molecules are weak due to the lack of direct conjugation over both halves of the molecule. By contrast, the closed form allows π electrons to be delocalized over the whole linearly conjugated molecular backbone. As a consequence of the difference in π electron delocalization, the open form is colorless and the closed form is colored (Figure 2). The UV/Vis absorption spectra indicate that the HOMO-LUMO gaps of **3** and **6** are considerably reduced in their closed forms. Therefore, one can anticipate a major increase in conductance for the closed forms compared to the open forms.
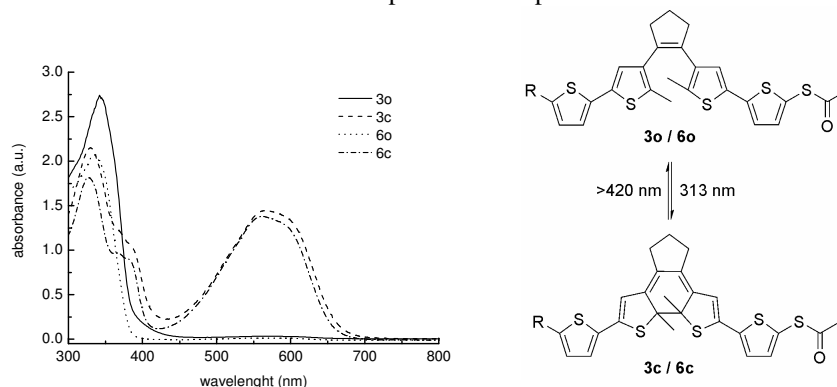
Figure 2 *UV/Vis absorption spectra of compounds* **3** *and* **6** *and photochemical interconversion of the open and closed forms. For* **3** *R is SAc and for* **6** *R is Me.*

2.3 Mechanically Controlled Break-Junction Experiment

In order to measure single molecule transport we use the mechanically controllable break-junction (MCBJ) technique.[9,11] A schematic illustration of the set-up for the technique is displayed in Figure 3. For MCBJ experiments, the molecular switches **3o** (open state) were first dissolved in tetrahydrofuran (THF). Upon irradiation with UV light (λ = 313 nm) switching to the closed form **3c** occurs. To prevent the molecules from switching back, all subsequent experiments were performed in the dark. A droplet of solution was introduced onto the break junction with a microsyringe. Once the molecules reach the gold, the protective acetyl groups split off and a self-assembled monolayer (SAM) is formed.[21] In principle, there are two approaches to achieve a molecular bridge. The first is to break the junction, open the electrodes far apart, and then form a SAM.[11] In this situation the system is in the tunneling regime and the resistance has an exponential dependence on the distance between the electrodes. Now we decrease the distance, applying a bias voltage of V = 1 V to assist a molecule to align between the electrodes, until we observe stable behavior. In the employed device, this always occurred at resistances of the order of MΩ, and it corresponds to the establishment of a Au-molecule-Au bridge.[11] The second approach is to first apply the solution and then open the wetted junction to form a molecular bridge.[9] Both methods were tested and the same results were observed.
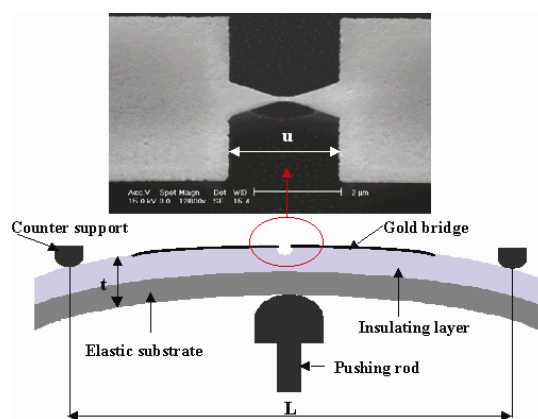
Figure 3 *The mechanically controllable break-junction (MCBJ) technique. Top: Scanning electron micrograph of the free standing gold bridge. Bottom: layout of the technique (not to scale). The whole device is 2 x 2 mm²*.

Once the resistance is stabilized by molecular bridge formation, current-potential (IV) characteristics were measured (Figure 4a). The room temperature IV's (Figure 4a) do not show sharp features (see also Reichert et al.[11] and Heurich et al.[22]). After waiting for about half an hour, irradiation of the junction with $\lambda = 546$ nm light was begun, while monitoring the resistance as a function of time. In Figure 4b a typical result is shown. After a short time a sharp increase in the resistance is observed, attributed to switching of the molecule from the closed to the open form. The resistances we find after switching are in the GΩ range, about 3 orders of magnitude larger than the initial value. Such a ratio between the resistances of the open and closed form is in reasonable agreement with the work by Fraysse et al.,[23] who both calculated and measured the coupling through the switching unit in a similar molecule. In Figure 4c a typical IV curve obtained after switching is displayed. Also shown in Figure 4c is a fit to Stratton's tunneling formula (a schematic representation of electron tunneling in a polarized tunnel junction is shown in Chapter 6) $I = I_0$ sin$h(eVd\sqrt{(m/2\hbar^2\varphi)})$ in which we put I_0 and φ as free parameters (m is the electron mass[24]). For d the calculated length of the open molecule (1.81 nm) was used. From the fit $\varphi = 1.5$ eV and $I_0 = 4 \times 10^{-11}$ A was found.

31
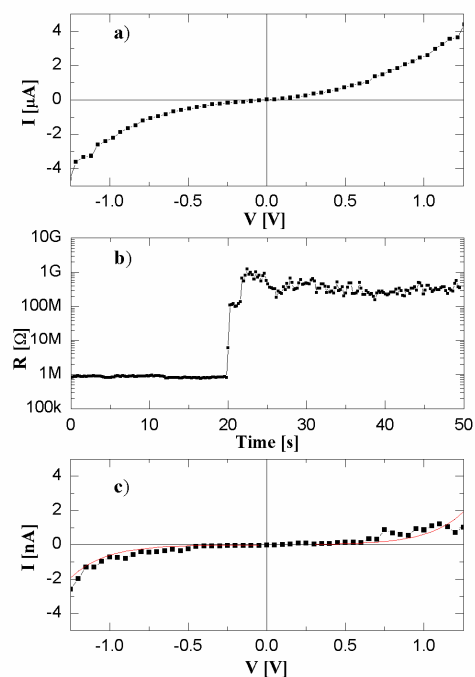
Figure 4 *MCBJ results. (a) Typical IV curve of the connected molecule in the closed form and (b) resistance versus time. At t = 0 a lamp is turned on (λ = 546 nm). After approximately 20 s a clear jump is observed (1 V bias). (c) Typical IV curve of the molecule after switching. The line is a fit to the Stratton formula (for details, see text).*

We observed the switching process ten times out of 12 attempts. The two times that were not successful a much lower concentration of the molecules in THF (0.15 mM) was used. In the other ten experiments we used a concentration of 1 to 2 mM. Switching times ranging from 10 s to 6 min, were observed.[25] After switching to the open state we attempted to switch the molecule back to the closed state by illuminating it with UV light (313 nm). However, this was unsuccessful. Since in solution the switching process from the open to closed state has a very high quantum yield (typically for similar compounds ~0.4 which is two orders of magnitude higher than from closed to open[26]) the absence of the reverse process seems to be related to the influence of the gold electrodes on the molecular system (see below).

One also has to consider other possibilities for a sharp jump in the resistance, such as migration of gold atoms or breaking of the gold thiol bonds. In order to exclude these possibilities additional experiments were performed: (a) illumination of the open junction without molecules and (b) illumination of molecular bridges formed by conjugated T3 molecules (three thiophene rings with two thiol end groups).[9] In these experiments such jumps in the resistance were not observed after the lamp was turned on (for at least 1 h).

2.4 STM Experiments

The break junction experiments on the dithiol thiophene-substituted diarylethene switch **3** described above yielded two main conclusions:

i)   switching a molecule from the closed to the open state results in a significant resistance increase of over two orders of magnitude;

ii) once thiophene-based diarylethenes are connected to gold via the Au-S bond, they were found only be switching from the closed to the open form.

The nature of the break-junction experiment does not allow for direct determination of the number of molecules that are connecting two electrodes (if repetitive break-junction experiments are not performed with a subsequent statistical analysis). The conformation of the molecules and their binding position on break-junction electrodes, with unknown geometry, cannot be established precisely as well as the nature of environment that is surrounding them. It is known that "small" variations in the microscopic geometry of the contact may lead to significant variation in the measured conductance.[27] In order to understand charge transport through a molecule attached to electrodes the aforementioned issues have to be investigated. Many of these difficulties can be addressed when a molecule of interest is inserted into a self assembled alkanethiol monolayer with a relatively well-defined geometry.[28] A combination of STM and Scanning Tunneling Spectroscopy[13] present themselves techniques of choice to investigate the conductive properties of molecules and their surroundings.

To study individual thiophene-substituted switches **6**, a mixed self-assembled monolayer (SAM) of dodecanethiol (DT) and closed form switches **6c** was formed on atomically flat gold.[29] In Figure 5a, a constant current STM image of a mixed self-assembled monolayer is shown. In accordance with the literature,[30] a set of domains is observed, each consisting of an ordered alkanethiol lattice. The domains are separated by domain boundaries and by several lower areas. The latter 'islands' are one atomic gold step lower than their surroundings, but are also covered with alkanethiols. The key features, however, are the

small peaks (bright spots) that occur within the alkanethiol lattice. Since these spots are lacking when a sample has only been in a dodecanethiol solution, we associate them with the conjugated switches (single molecules or small aggregates of diarylethenes). An STM signal is a convolution of topography (real height) and local conductance.[30] Hence the apparent height difference (typically 0.25 nm) between **6c** and DT (molecular lengths 1.70 and 1.62 nm, respectively) is largely determined by the conductance properties of **6c** and DT. Since the conductance of the diarylethenes decreases considerably upon switching from closed to open forms, STM observes photochromic switching as a sudden decrease in the molecule's apparent height. This is associated with the disappearance of the bright spots upon irradiation (Figure 5c). To demonstrate such light induced switching, however, it is essential to separate light-induced switching from other switching effects. In recent years, several studies of statistical 'on–off' switching effects or 'blinking' during STM scanning have appeared, the origin of which is heavily debated.[30e-k]
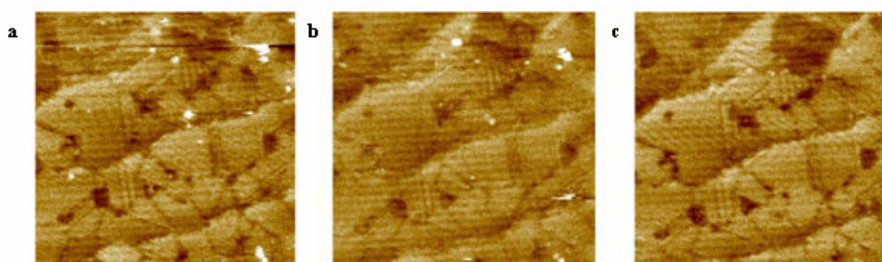
Figure 5 *Three STM images (77 x 74 nm^2, height scale: 1 nm; I$_s$=2 pA, V=0.75 V, taken in air, unfiltered zoomed images) of a DT SAM containing photochromic switches **6c**. Scanning in the dark begins at t=0, whereas at t=52 min illumination is started (300 W Xe lamp with high pass filter, δ>450 nm). Image a is taken at t=11.8 min. (dark), b at t=32 min. (dark) and c at t=77.7 min. (illuminated). Both stochastic switching (a to b) and photochromic switching (b to c) are observed. In c, after 25.7 min of illumination, almost all molecules have been converted to the open state.*

The following experiments (see Figure 5) were performed in order to study and separate stochastic and light-induced switching effects. First, a mixed DT-**6c** monolayer was scanned in the dark for typically 30 min (see Figures 5a and 5b). Detailed inspection of all images taken without illumination indeed revealed random "ON"-"OFF" switching. After scanning in the dark for a certain period (defined below), we turn on a 300 W Xe lamp with appropriate filtering. Scanning continued and increased switching to the "OFF" state was observed. This indicates photochromic switching from the conjugated to the non-

34

conjugated isomer. Finally, after 25.7 min of illumination, almost all photochromic switches have switched to the open form (see Figure 5(c)).

2.4.1 Stochastic switching

Since both stochastic and photochromic switching phenomena are present in our measurements, we choose to separate the data on the individual contributions using statistics. For each image taken, the number of molecules in the "ON" and "OFF" states was counted. Two different counting schemes were introduced to obtain additional information (see Figures 6a and 6b). In 'method A', all molecules that are "ON" within an STM image are counted (regardless of their position) and this number (N) was plotted versus time. Note that a molecule that was "OFF" at $t = 0$, but turns "ON" at a time t, is counted. In 'method B', we only focus on molecules that were 'on' at $t = 0$ and note their x, y-coordinates. For each later image we check if at these coordinates (within a few nm^2) there still is an "ON"-state molecule. If not (e.g., the molecule is "OFF", or has moved substantially) it is not counted. Note also that a molecule that is "OFF" initially, but 'on' at $t = \tau$, is not counted. We first focus on stochastic switching, i.e., exclusively on STM scanning in the dark. In Figure 6c, the normalized counting results for the sample in Figure 5 are displayed (diamonds, method A; squares, method B). For both methods, we recognize the 'blinking' effect in the statistical fluctuation of N on smaller timescales ('noise'). Furthermore, an initial decrease in N was observed until, after around 20 min, the number stabilizes. This decrease and stabilization is typical for experiments in the dark. There is quite a difference in final plateau values between methods A ($N/N_0 \rightarrow 0.78$) and B ($N/N_0 \rightarrow 0.26$). In fact, this is observed more generally. Figure 6d displays the normalized plateau values for all data sets as a function of STM bias voltage. At all biases, the plateau values for method A exceed those for method B, while both sets decrease with increasing bias voltages. To interpret this, both methods were associated with three possible effects: reversible stochastic switching (blinking), irreversible "ON"-to-"OFF" switching and diffusion.
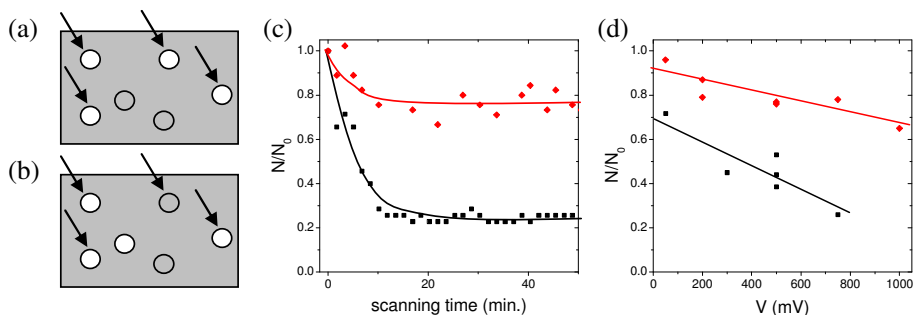
Figure 6 *Stochastic switching effects. Two methods of counting are used as illustrated in (a) and (b). In both (a) (at t=0) and (b) (at t=t) two molecules are "OFF" and four are "ON", but they are not the same ones. With method A, all "ON"-state molecules are counted regardless of history, giving N=4 for both (a) and (b), so that $N_{(t)}/N_0=1$. With method B, only the molecules that are 'on' at t=0 are followed, marked with an arrow, giving N=4 for (a) and N=3 for (b), so that $N_{(t)}/N_0=3/4$. (c) Normalized number of molecules in the "ON" state, $N_{(t)}/N_0$, vsersus time for the sample in Figure 5 (measured at 0.75 V). Diamonds: method A; squares: method B. After 20 min, a plateau in the number of counts is found, giving us two 'equilibrium values' for methods A (0.78) and B (0.26) (d) Equilibrium values versus bias for method A (diamonds) and method B (squares), determined for various samples. The "ON"-"OFF" ratio shifts to the "OFF"-state molecule side, if we scan at higher voltages. Lines are guides to the eye.*

First, let us suppose that reversible switching takes place only, and that its typical timescale is small ($\tau < 10$ min). When the first image is recorded, we expect some of the conjugated molecules to be "ON" (N_{on}), and some to be "OFF" (N_{off}). Both in method A and B, we have $N_0 = N_{on}$ ($t = 0$). After a substantial period of scanning ($>\tau$), some of the molecules that were first 'on' will have turned "OFF" and vice versa. However, N_{on} (which is the number counted in method A) and N_{off} are not expected to change. Hence, for method A, one expects $N_{(t)}/N_0 \approx 1$, i.e., no change except for statistical variations. (Interestingly, these fluctuations are found to increase with bias voltage themselves.) For method B, however, one follows a particular set of molecules (i.e. 'on' at $t = 0$). If some of these turn "OFF", the number counted decreases (regardless of others going from "OFF" to "ON"). At a time $t > \tau$, the spatial distribution of 'on' and 'off' states is randomized (though the numbers N_{on} and N_{off} have not changed). Hence $N_{(t)}/N_0$ approaches $N_{on}/(N_{on} + N_{off})$ for $t > \tau$, so that method B gives information about the dynamic equilibrium between "ON" and "OFF" states. Inspecting the images, we infer that this is the major contribution to the difference between

36

methods A and B (see below). Thus, Figure 6d implies that upon increasing the voltage bias ($V > 0$) the dynamic equilibrium between molecules in the "ON" and "OFF" states shifts to the "OFF" side. Although we have chosen a somewhat different method, our results can be compared to those of Lewis et al,[30h] who study conjugated molecules ('NPPB') in a functionalized alkanethiol SAM. They find the equilibrium to shift to the "OFF" state when the bias voltage is decreased from +1 to −1 V. However, since Lewis et al use functionalized conjugated molecules and alkanethiols, which interact via hydrogen bonding, the mechanism behind their results might be different.

Second, we look at the effect of irreversible "ON"-to-"OFF" switching. This would influence the results for both method A and B significantly: molecules that go to "OFF" and stay "OFF" are effectively taken out of the ensemble. Hence a decrease in the number of counts is now expected, especially for method A. This is indeed seen in Figure 6, though the effect is relatively small at low bias. Various origins for this irreversible switching can be thought of. One reason could be that due to the local environment the blinking time constant τ of some individual molecules exceeds the total scanning time, i.e., returning just takes too long.[30f-h] Furthermore, 'real' irreversible phenomena may occur. For diarylethenes, voltage and current-induced switching cannot be excluded. It has been shown that these molecules can switch due to a redox potential[31] or a current (provided excitons can be formed, which is unlikely in STM experiments).[32] In any case, N as counted by method A, appears to decrease rather smoothly with voltage. This is quite different from the work of Blum et al, who find a well defined switching voltage (from "OFF" to "ON") for 'BPDN' molecules.[30k]

Third, we consider the influence of diffusion. If a molecule moves away from its original spot by more than a few nanometres, it is no longer counted in method B (but still in method A). We note that spontaneous random walking will be quite limited. It is likely for a **6c** molecule to hop only if there is a vacancy or defect in the dense DT lattice. Indeed, at biases up to 0.5 V, we do not observe significant random walk. For experiments at higher bias, however, it appears that some molecules do shift position leading to a lower plateau value within method B. Possibly the large fields around the tip are able to help the **6** molecules overcome the diffusion barrier.

There is still no consensus on the origin of stochastic switching.[30f-k] The Weiss group has provided evidence for conformational switching in particular molecules, e.g. by looking at the influence of the alkanethiol matrix density on blinking.[30f-h] Nevertheless, stochastic switching appears in almost any system consisting of individual molecules inserted in an alkanethiol SAM. Hence, there must also be an additional, more general origin. Since STM measures a convolution of conductance and real height, either could be important here.

Ramachandran *et al*. relate the phenomenon to instabilities of the Au–S bond.[30i] A drawback of the latter explanation is that the energy scales do not seem to match. As noticed, the Au–S bond has a strength of 1.6 eV, whereas the typical energy scale for stochastic switching is found to be ~0.1 eV. As a possible way out, one could consider temporary disulfide formation (between the alkanethiol and the inserted molecule). This would loosen the Au–S bond with an energy barrier much lower than 1.6 eV. It should be noted, however, that the data of Donhauser *et al*. do not support such a model: instead of increased switching to a denser SAM (as expected for the disulfide picture), they see the opposite.[30f,g] In our opinion, the most general and hence most probable explanation for stochastic switching is that it is due to orientational changes, in particular changes in the tilt angle of the molecule.[30j] These can either be spontaneous or the result of the strong electric field between tip and substrate (~GV m^{-1}). The fact that we see a shift in the dynamic equilibrium (as well as increased fluctuations for increasing voltages) hints in this direction. Unfortunately, it appears difficult to find conclusive evidence for any of the mechanisms above. It is important to note, however, that stochastic switching has an origin different from photochromic switching. In the latter case, light-induced ring opening results in loss of the conjugation within the molecule, leading to a significant increase of resistance.

2.4.2 Photochromic switching

Having characterized stochastic switching in our samples, we turn to light-induced conductance switching. After scanning in the dark until a stable number N (method A) is reached, illumination was started to switch the closed switchable molecules to the open form. In Figure 7, the number of "ON"- state molecules **6** as a function of time for two series of STM experiments is displayed. It is observed that the number of "ON" molecules starts decreasing as soon as illumination starts. We relate this to photochromic switching from the closed to the open state, leading to a lower conductance and, consequently, a lower apparent height. The decrease in N is smooth and goes, roughly, exponentially with time. This is indeed what one expects for photochromic switching since each event is independent. We find decay half times of typically 30 min for the switches in the mixed SAM. This number is rather large compared to the conversion time measured for free closed switches in THF. For the same lamp and filtering, the half time in solution is a few minutes.[33] However, the half times for switching in a mixed SAM do compare well with those obtained for solutions of gold colloids covered by a monolayer of closed switches. For the latter we find a decay half time of around 40 min.[33] Coupling to gold appears to reduce the switching efficiency (from the closed to the open state), but, importantly, it does not completely hamper the conversion.

38

(a) (b)
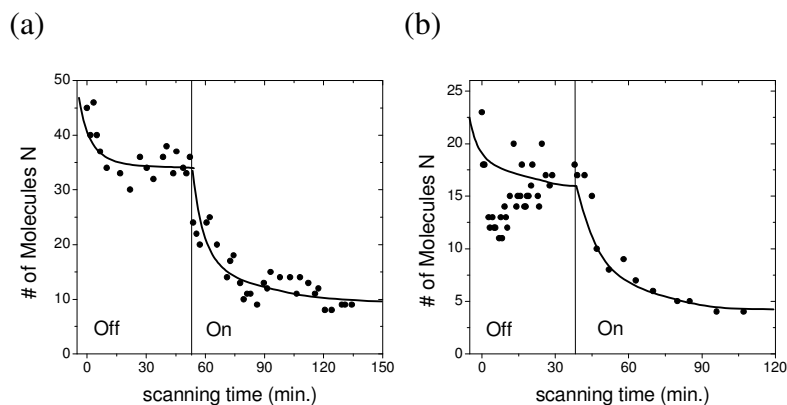
Figure 7 *Number of molecules in the 'on' state versus time (min), determined from two series of STM-images taken in air, both in the dark and during illumination (300 W Xe lamp). Counting is done using Method A. In (a) (same sample as in Figure 5), the lamp is turned on after 52 min (high pass filter, δ > 450 nm). (I_s = 2 pA, V = 0.75 V). In (b), the lamp (band pass filter around 550 nm) is turned on after 38 min (I_s = 30 pA, V = 1.0 V). Lines are guides to the eye.*

Since illumination of our sample may lead to spurious effects, the experiment will be discussed in more detail. First, heating may take place, leading to expansion effects. Although this could instantaneously change the tip–surface distance, the feedback loop will immediately correct for this. Furthermore, a temperature increase could lead to faster stochastic switching (lower τ).[30i] However, this would not lead to different counting statistics and, hence, it cannot explain the decrease observed in Figure 7. Second, light-induced Au–S bond breaking might occur, removing both alkanethiols and switches from the surface. For visible light, however, this is not expected and we do not see any evidence for it in our STM scans. After photochromic switching the molecules are still present.

We find that molecules in the open form (**6o**) have an apparent height that is approximately 0.2 nm lower than that of the closed form. Since the open conformer is in average slightly longer (by 0.1 nm) than its closed counter part, we have an apparent height change of 0.3 nm. It is instructive to compare this number to the conductance change measured in the break junction experiments.[33] For constant current STM, we can do this by setting G_c exp($-2\kappa d_c$) = G_o exp($-2\kappa d_o$).[30c,34] Here G_c (G_o) denotes the conductance of the closed (open) form, d is the distance between tip and molecule, and κ is the tunnel decay constant between tip and molecule. Taking G_c/G_o ~ 200, we obtain the right apparent height

39

difference, i.e. $d_c - d_o = 0.3$ nm, if we use $\kappa = 8.8$ nm^{-1}. The latter number corresponds to a tunnel barrier height of 3 eV, which is reasonable. We note however that it is difficult to quantify the exact conductance change associated with switching, since we have no independent information regarding the molecular tilt angles.

Unfortunately, the thiophene-based diarylethenes used in this study as well as in reference 33 have an important drawback. Whereas switching is reversible in solution, the situation changes once these molecules are connected to gold via a thiol bond. In the latter case, switching from the closed to the open form is still possible, but from open to closed is not.

2.5 The Origin of Irreversibility

To rationalize these findings regarding irreversibility of the switching process for the switches covalently attached to gold electrodes, the switching process of compound **3** was investigated theoretically and the influence of gold on the switching discussed qualitatively. For this, potential curves were calculated using a selection of semiempirical quantum chemical computational methods implemented in the HYPERCHEM 6.0 program package. The ground state and excited state potential curves were generated in a procedure in which the switching coordinate q (the distance between the carbon atoms which are responsible for the ring closure process) was changed in a systematic way between 0.13 and 0.4 nm (calculated distances for the closed and open form are 0.15 and 3.5 nm). In Figure 8 we plot, as a function of q, the ground state and excited state energy of the molecule **3** with respect to the vacuum level. The ground state and excited state profiles shown here are very similar to the results obtained by Ern et al.[35] using a different method. In Figure 8 the paths for ring opening and closure are drawn for the isolated molecule upon optical excitation in the UV and visible spectral region. Clearly the ring opening process is expected to have a lower quantum yield than the reverse process, due to the presence of a barrier.[26] To consider the influence of gold on the molecular system, we have also plotted the Fermi level of polycrystalline gold (5.3 eV with respect to the vacuum level) in Figure 8.[36] We relate the failure of the closing process to the proximity of the gold Fermi level and the excited state molecular energy for $0.22 < q < 0.25$ nm. As a consequence, an efficient mixing of the gold states and the first excited molecular electronic state is expected, taking place at the right side of the ground state maximum. This results in quenching of the excited open state inhibiting the ring closure process. The electronic excited state involved in the ring opening process, on the other hand, is separated by more than 1 eV from the gold Fermi level. Hence, the ring opening process is not inhibited.

40
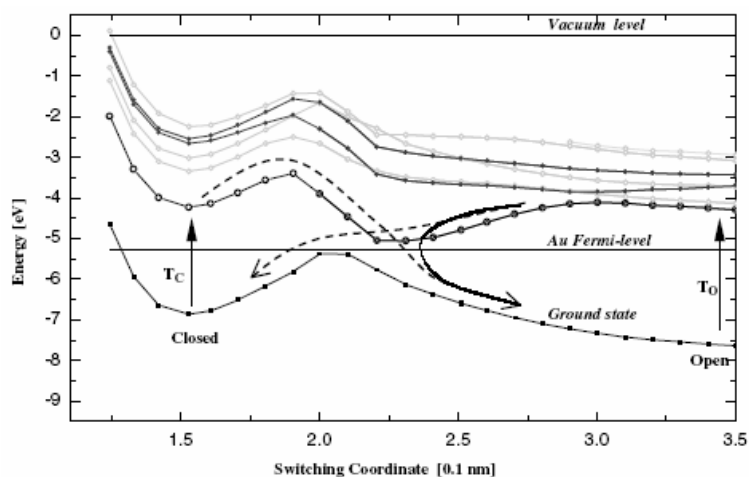
Figure 8 *Potential energy curves of the molecular switch **3** along the switching coordinate q (black lines: optically allowed states; gray lines: optically forbidden excited states). The vacuum level is set at 0 eV. The switching process is initiated by an excitation to the first excited state (T_c; T_o). For a molecule in solution, the evolution of the switching process is indicated with dashed arrows. For a molecule connected to gold, however, the potential curve of the first excited state comes very close to the Au Fermi level (at 0.22<q<0.25 nm), resulting in an efficient mixing of these respective states. When the open molecule goes to the first excited state (T_o), the closing process sets in, i.e., the excited state potential curve is followed towards lower q (solid arrow). However, when 0.22<q<0.25 nm, the interaction with the gold makes the excited molecule relax back to the ground state (at the right side of the local maximum), and hence back to the open form. As a consequence there is no switching from the open to the closed form.*

An intention of the presented *ad hoc* calculations[37] was to explain the behavior observed by focusing on potential energy curves of the switching and the role of the gold Fermi level. Major drawbacks of these calculations are that the semiempirical approach has been used and an effect of a gold anchoring on molecular energy levels has been neglected. Based on our break-junction experiment results also other groups tried to explain the lack of reversibility for the molecule **3** connected to gold. Li *et al.*[38] calculated HOMO and LUMO levels of model diarylethene molecules connected to small gold clusters using a density functional theory (DFT) based method. Comparing alignments of the metal Fermi level and the HOMO and LUMO orbitals of the open and closed isomers they found that the HOMO of the open isomer is buried more than 1 eV beneath the metal Fermi level near to the fast increasing edge of the 3D bands of Au (where the Au density of states is high). In contrast,

41

the HOMO of the closed isomer is within the low density of states *s* band near the Au Fermi level. Li *et al*. speculate that the observed quenching of the ring closure reaction may result from the Fermi-level alignment in the open isomer. The deep lying HOMO level at a high metal density of states offers the opportunity for many possible electron transfer events, thus reducing the lifetime of the hole created after an excitation. Using DFT calculations Zhuang *et al*.[39] came to the similar conclusions investigating how strongly the HOMO orbitals of the open and closed isomers are mixed with orbitals of a contact electrode. They show that orbitals of the open form are strongly mixed with contact orbitals. As a consequence, it is not possible to empty the molecular HOMO by photoexcitation; it will simply be refilled with contact electrons. The HOMO stabilizes the open isomer compared to the closed one. On the other hand, the HOMO of the isolated closed isomer keeps its identity when attached to the gold contacts and a mixing of orbitals is low. These two theoretical approaches[38,39] offered an alternative explanation for the observed experimental results.

2.6 Conclusions

Based on the presented results it has been demonstrated that diarylethenes are promising candidates for molecular electronics. An ease of synthetic accessibility and addressability makes this an ideal system for many studies. UV/Vis measurements performed in toluene show that the open and closed forms can be addressed selectively resulting in the interconversion between both forms. Using MCBJ and STM diarylethene molecules have been incorporated between metallic nanoelectrodes and thus single molecule switching devices have been realized although so far only in one direction. Both methods confirm the dramatic decrease in conductance of the molecules when the closed form transforms to the open form upon an irradiation with visible light. Both sets of measurements show that for the molecules covalently connected to gold the switching occurs only in one direction, from the closed to the open form. The latter is attributed to quenching of the first excited state of the open form under the influence of gold. In the following chapters (4 and 5) an effect of spacer unit, connecting the central switching unit with anchoring groups, on the switching reversibility will be discussed.

2.7 Experimental Section

General Remarks

42

Reagents and starting materials were used as obtained from Aldrich and Acros Chimica, Fluka or Merck. ^{1}H NMR spectra were recorded on a Varian VXR-300 spectrometer (at 300 MHz) at ambient temperature. ^{13}C NMR spectra were recorded on a Varian VXR-300 (at 75.4 MHz). Chemical shifts are denoted in δ (ppm) referenced to the residual $CHCl_3$ peaks. Coupling constants *J*, are denoted in Hz. The splitting patterns are designated as following: s (singlet), d (doublet), t (triplet), q (quartet), m (multiplet) and b (broad). Mass spectra were recorded with a Joel JMS-600 mass spectrometer by Mr. A. Kiewiet with ionisation according to CI^+, DEI, EI^+ procedures. UV measurements were performed on a Hewlett-Packard HP 8453 FT spectrophotometer using UVASOL grade solvents (Merck). Aldrich, silica gel, Merck grade 9385, (230-400 mesh) was used for column chromatography. If necessary, solvents were distilled and dried before use by standard methods. Irradiations were performed with a 180 W Oriel Hg-lamp adapted with a suitable Mercury line filter for 313 nm and 546 nm irradiations (typical bandwidth 10 nm) and a cut-off (420 nm) filter for visible irradiation. Photostationary states are ensured by monitoring composition changes in time by taking UV spectra at distinct intervals until no further changes were observed.

Mechanically Controlled Break-Junction Experiments

The break-junction experiments were performed by Dr. D. Dulić and Dr. S. J. van der Molen. The device was patterned on an elastic phosphor bronze substrate covered with a thin insulating layer of polyimide by electron beam lithography. The device is made of gold and has a narrow neck in the middle (see Figure 3). After the gold deposition the polyimide below the bridge is removed, leaving behind a freestanding gold bridge. The bridge was broken by bending with a three-point bending mechanism. We obtain a mechanical ''attenuation factor'' [40] $r = 6tu/L^2 = 1{:}7 \times 10^{-5}$, for our device, where $t = 0.42$ mm is the substrate thickness, $u = 2.4$ μm the suspended length of the bridge, and $L = 18.8$ mm the distance between the counter supports. This provides control of the spacing between the electrodes with a precision of 10 pm. The two open ends form point contacts to which the molecules will be attached via the thiol groups that form a strong chemical bond with gold. Prior to the experiments with the molecules a number of devices were calibrated in ambient and argon atmosphere. We obtained an exponential increase of the resistance upon increase of the distance between the electrodes which is characteristic of the tunneling regime for the metal-air-metal junction. The $R(d)$ data were used, where the distance d was taken from the geometrical formula, to obtain an average value of the work function of gold $\langle \varphi \rangle = 6 \pm 2$ eV. This is in reasonable agreement with the experimental work function for gold which is 5.3 eV. Furthermore, IV characteristics were measured which can be satisfactorily fitted to the Simmons[41] and Stratton[42] formulas.

43

STM Experiments

The STM experiments were performed by Dr. S. J. van der Molen. For monolayer formation, *n*-dodecanethiol was purchased from Aldrich. Flat gold layers are created using the procedure described in reference 29. Within atomically flat plateaus, the herringbone structure was observed.[43] Two SAM preparation methods are chosen. For the first ('exchange reaction method'), a gold sample was put in a solution of dodecanethiol in ethanol (concentrations ranging from 1 to 100 mM) for 4 to 24 h (at 295 K). Next, the solution was heated to 351K for 2 h. Finally, the sample was put in ethanol containing closed switches (concentration 1 mM) for 4 h. For the second method, we directly prepare the SAM from a mixture of DT (95–99 molecular %) and **6** in ethanol ('co-adsorption method'). STM measurements were performed in air with a Digital Instruments Multimode scanner with a Nanoscope IV controller, purchased from Veeco. Illumination of the SAMs was performed with a 300 W Xe lamp (purchased from LOT-Oriel), with appropriate filtering and fiber optics.

Details on Semiempirical Calculations

The potential curves were calculated by Dr. H. T. Jonkman using a selection of semiempirical quantum chemical computational methods implemented in the HYPERCHEM 6.0 program package (provided by Hypercube, Inc). The total energy was calculated with the AM1 quantum chemical semiempirical method. For each q, the geometry of the molecule was fully optimized using a conjugate gradient procedure (Polak-Ribiere). The singlet excited state manifold was calculated with the Zerner intermediate neglect of differential overlap/spectroscopy method in which ten occupied and ten unoccupied orbitals were incorporated in the single excited state configuration interaction procedure. The vacuum level is here defined as the total energy of the molecule with one electron removed; i.e., it is equal to the ionization potential of the molecule. Within Koopman's theorem, this ionization potential is representative for the position of the highest occupied molecular orbital (HOMO) of the molecule. In the same approximation the energy of the electron addition state (electron affinity) is the energy of the lowest unoccupied molecular orbital (LUMO). In that description the optical and conduction gap coincide and the first excited state mimics the HOMO-LUMO gap.

1,2-Bis[2-methyl-5-(thien-2-yl)thien-3-yl]cyclopentene (2)

To a solution of compound **1**[20] (240 mg, 0.729 mmol) in THF (7 mL), kept under an inert N_2 atmosphere, *n*-BuLi (1.2 mL of 1.6 M solution in *n*-hexane, 1.92 mmol) was added. After 1h, $B(OBu)_3$ (0.05 mL, 2.19 mmol) was added and the mixture was stirred for 1h to produce a boronic ester intermediate. In a separate flask 2-bromo-5-methylthiophene (0.287

44

mL, 2.96 mmol), Pd(PPh$_3$)$_4$ (0.096 mg, 0.083 mmol), THF (5 mL), 2M Na$_2$CO$_3$(aq.) (4 mL) and ethylene glycol (5 drops) were preheated to 80 ^{o}C and the boronic ester solution was added slowly. The reaction mixture was heated under reflux overnight, diluted with diethyl ether (50 mL) and washed with water (50 mL). The aqueous layer was washed with an additional volume of ether (50 mL) and the combined organic phases were dried over Na$_2$SO$_4$ and concentrated. Subsequent chromatography on silica gel (*n*-hexane) afforded compound **2** (203 mg, 66 %). mp. 204-208°C (dec.) ^{1}H NMR (300MHz, CDCl$_3$) δ 1.94 (s, 6H), 2.04 (m, 2H), 2.79 (t, *J* = 12.5 Hz, 4H), 6.87 (s, 2H), 6.95 (t, *J* = 6.5 Hz, 2H), 7.03 (d, *J* = 4.5 Hz, 2H), 7.13 (d, *J* = 8.5 Hz, 2H) ppm. ^{13}C NMR (75.4 MHz, CDCl$_3$): δ 14.3 (q), 22.9 (t), 38.5 (t), 122.9 (d), 123.7 (d), 124.5 (d), 127.6 (d), 133.0 (s), 134.0 (s), 134.5 (s), 136.3 (s) ppm. HRMS calcd. for C$_{23}$H$_{20}$0S$_4$ 424.045, found 424.045.

1,2-Bis[5-(5-acetylsulfanylthien-2-yl)-2-methylthien-3-yl]cyclopentene (3)

Compound **2** (100 mg, 0.236 mmol) was dissolved in THF (5 ml) and the solution was cooled to -80 ^{o}C. To this solution was added dropwise *n*-BuLi (0.4 ml of 1.6 M solution in hexane, 0.64 mmol). After 2h S$_8$ (15 mg, 0.469 mmol) dissolved in THF (1 ml) was added and the mixture was allowed to reach slowly room temperature. After 2h the reaction mixture was cooled to 0 ^{o}C and acetyl chloride (0.068 ml, 0.952 mmol) was added. After 3h the mixture was diluted with dichloromethane, washed with water and the organic phase dried (Na$_2$SO$_4$) and concentrated. Subsequent chromatography (*n*-hexane / dichloromethane 7:2) afforded compound **3** (41 mg, 33 %). mp. 204-208°C (dec.) ^{1}H NMR (500MHz, CDCl$_3$) δ 1.93 (s, 6H), 2.04 (m, 2H), 2.40 (s, 6H), 2.78 (t, *J* = 7.5 Hz, 4H), 6.88 (s, 2H), 7.00 (d, 2H), 7.34 (d, 2H) ppm. ^{13}C NMR (75.4 MHz, CDCl$_3$): δ 14.5 (q), 23.0 (t), 29.6 (q), 38.6 (t), 122.7 (d), 123.2 (s), 123.3 (s), 125.1 (s), 125.2 (s), 132.2 (d), 134.4 (d), 136.4 (s), 136.5 (s), 136.6 (s) ppm. MS (EI): 572 [M+]; HRMS calcd. for C$_{27}$H$_{24}$O$_2$S$_6$ 572.010, found 572.010.

1-(5-Chloro-2-methylthien-3-yl)-2-[5-(5-methylthien-2-yl)-2-methylthien-3-yl]cyclopentene (4)

To a solution of compound **1** (2.25 g, 6.83 mmol) in THF (100 mL), kept under an inert N$_2$ atmosphere, *t*-BuLi (4,70 mL of 1.6 M solution in *n*-hexane, 7.51 mmol) was added. After 1h, B(OBu)$_3$ (2.77 mL, 10.3 mmol) was added and the mixture was stirred for 1h to produce a boronic ester intermediate. In a separate flask 2-bromo-5-methylthiophene (1.56 mL, 13.66 mmol), Pd(PPh$_3$)$_4$ (0.237 g, 0.21 mmol), THF (23 mL), 2M Na$_2$CO$_3$(aq.) (18 mL) and ethylene glycol (20 drops) were preheated to 80 ^{o}C and the boronic ester solution was added slowly. The reaction mixture was heated under reflux overnight, diluted with diethyl ether (200 mL) and washed with water (200 mL). The aqueous layer was washed with an additional volume of ether (200 mL) and the combined organic phases were dried

45

over Na_2SO_4 and concentrated. Subsequent chromatography on silica gel (*n*-hexane) afforded compound **4** as a sticky oil (1.82 g, 68 %). ^{1}H NMR (300 MHz, CDCl_3): δH 1.88 (s, 3H), 1.93 (s, 3H), 1.98-2.08 (m, 2H), 2.46 (s, 3H), 2.71-2.80 (m, 4H), 6.61-6.62 (m, 2H), 6.76 (s, 1H), 6.48 (d, *J*=3.7 Hz, 1H) ppm. ^{13}C NMR (75.4 MHz, CDCl_3): δC 14.1 (q), 14.2 (q), 15.3 (q), 22.8 (t), 38.3 (t), 38.4 (t), 122.8 (d), 123.6 (d), 125.0 (s), 125.7 (d), 126.8 (d), 133.2 (s), 133.4 (s), 133.5 (s), 133.8 (s), 135.0 (s), 135.3 (s), 135.9 (s), 138.5 (s), ppm. HRMS: calcd. for $C_{21}H_{19}S_2Cl$ 370.062, found 370.063.

1-[2-Methyl-5-(5-methylthien-2-yl)thien-3-yl]-2-[2-methyl-5-(thien-2-yl)thien-3-yl]cyclopentene (5)

To a solution of compound **4** (1.34 g, 3.43 mmol) in THF (50 ml), kept under an inert N_2 atmosphere, *t*-BuLi (2.74 ml of 1.5 M solution in *n*-pentane, 4.11 mmol) was added. After 1h, $B(OBu)_3$ (1.39 ml, 5.15 mmol) was added and the mixture was stirred for 1h to produce a boronic ester intermediate. In a separate flask 2-bromothiophene (0.66 ml, 6.86 mmol), $Pd(PPh_3)_4$ (0.119 g, 0.10 mmol), THF (19 ml), (aq.) 2M Na_2CO_3 (13 ml) and ethylene glycol (18 drops) were preheated to 80 ^{o}C and the boronic ester solution was added slowly. The reaction mixture was heated under reflux overnight, diluted with diethyl ether (200 ml) and washed with water (200 ml). The aqueous layer was washed with an additional volume of ether (200 ml) and the combined organic phases were dried over Na_2SO_4 and concentrated. Subsequent chromatography on silica gel (*n*-hexane) afforded compound **5** as a sticky oil (1.08 g, 72 %). ^{1}H NMR (300 MHz, CDCl_3): δ = 1.96 (s, 3H),1.97 (s, 3H), 2.05-2.10 (m, 2H), 2.47 (s, 3H), 2.82 (t, *J*=7.7 Hz, 4H), 6.63 (d, *J*=3.7 Hz, 1H), 6.82 (s, 1H), 6.85 (d, *J*=3.7 Hz, 1H), 6.91 (s, 1H), 6.98-7.00 (m, Hz, 1H), 7.07 (d, *J*=3.3 Hz, 1H), 7.16 (d, *J*=5.1 Hz, 1H) ppm. ^{13}C NMR (75.4, CDCl_3): δ = 13.8 (q), 14.9 (q), 22.5 (t), 38.0 (t), 122.3 (d), 122.4 (d), 123.1 (d), 123.2 (d), 124.0 (d), 125.3 (d), 127.1 (d), 132.5 (s), 134.9 (s), 133.0 (s), 133.5 (s), 133.9 (s), 134.1 (s), 134.9 (s), 135.7 (s), 135.9 (s), 137.3 (s), 138.0 (s) ppm. HRMS: calcd. for $C_{24}H_{22}S_4$ 438.060, found 438.062.

1-[5-(5-Acetylsulfanylthien-2-yl)-2-methylthien-3-yl]-2-[2-methyl-5-(5-methylthien-2-yl)thien-3-yl]cyclopentene (6)

Compound **5** (1 g, 2.28 mmol) was dissolved in THF (50 ml) and the solution was cooled to -80 ^{o}C. To this solution was added dropwise *t*-BuLi (1.82 ml of 1.5 M solution in *n*-pentane, 2.74 mmol). After 2h S_8 (0.073 g, 2.28 mmol) dissolved in THF (4 ml) was added and the mixture was allowed to reach slowly room temperature. After 2h the reaction mixture was cooled to 0 ^{o}C and acetyl chloride (0.32 ml, 4.56 mmol) was added. After 3h the mixture was diluted with dichloromethane, washed with water and the organic phase dried (Na_2SO_4) and concentrated. Subsequent chromatography (*n*-hexane / dichloromethane 7:2) afforded compound **6** (0.67 g, 57 %) as a sticky oil. ^{1}H NMR (300 MHz, CDCl_3): δ =

46

1.95 (s, 3H), 1.97 (s, 3H), 2.07-2.10 (m, 2H), 2.42 (s, 3H), 2.47 (s, 3H), 2.81 (t, *J*=7.3 Hz, 4H), 6.63 (d, *J*=3.3 Hz, 1H), 6.81 (s, 1H), 6.85 (d, *J*=3.3 Hz, 5H), 6.93 (s, 1H), 7.03 (s, 2H) ppm. ^{13}C NMR (75.4, CDCl$_3$): δ = 14.2 (q), 14.3 (q), 15.3 (q), 22.9 (t), 29.4 (q), 38.4 (t), 122.7 (s), 122.8 (d), 123.2 (d), 123.7 (d), 125.3 (d), 125.7 (d), 132.1 (s), 133.3 (s), 133.5 (s), 134.1 (s), 134.9 (s), 135.0 (s), 135.3 (s), 136.0 (s), 136.5 (s), 136.6 (d), 138.4 (s), 144.1 (s), 194.3 (s) ppm. HRMS: calcd. for C$_{26}$H$_{24}$OS$_5$ 512.125, found 512.124.

2.8 References and Notes

[1] a) C. Joachim, J. K. Gmizewski and A. Aviram, *Nature* **2000**, *408*, 541-548; b) R. L. Carroll and C. B. Gorman, *Angew. Chem. Int. Ed*. **2002**, *41*, 4378-4400.

[2] S. Fraysse, Ch. Coudret and J.-P. Launay, *Eur. J. Inorg. Chem*. **2000**, 1581-1590; B. Jousselme, P. Blanchard, N. Gallego-Planas, E. Levillain, J. Delaunay, M. Allain, P. Richomme and J. Roncali, *Chem. Eur. J.* **2003**, *9*, 5297-5306.

[3] M.-K. Ng and L. Yu, *Angew. Chem. Int. Ed.* **2002**, *41*, 3598-3601.

[4] N. Robertson and C. A. McGowan, *Chem. Soc. Rev*. **2003**, *32*, 96-103.

[5] H. Yu, Y. Luo, K. Beverly, J. F. Stoddart, H.-R. Tseng and J. R. Heath, *Angew. Chem. Int. Ed.* **2003**, *42*, 5706-5711; A. Babel, S. A. Jenekhe, *J. Am. Chem. Soc*. **2003**, *125*, 13656-13657.

[6] J. E. Green, J. W. Choi, A. Boukai, Y. Bunimovich, E. Johnston-Halperin, E. DeIonno, Y. Luo, B. A. Sheriff, K. Xu, Y. S. Shin, H. –R. Tseng, J. F. Stoddart, J. R. Heath, *Nature* **2007**, *445*, 414-417.

[7] B. L. Feringa, *Molecular switches*, Wiley, Weinheim, Germany, **2001**.

[8] a) M. Irie, in *Molecular switches*, B. L. Feringa, Wiley, Weinheim, Germany, **2001**, pp. 37-62; b) M. Irie, *Chem. Rev*. **2000**, *100*, 1685; c) H. Tian and S. Yang, *Chem. Soc. Rev.* **2004**, *33*, 85.

[9] C. Kergueris, J.-P. Bourgoin, S. Palacin, D. Esteve, C. Urbina, M. Magoga and C. Joachim, *Phys. Rev. B* **1999**, *59*, 12505-12513; M. Mayor, H. B. Weber, J. Reichert, M. Elbing, C. von Hänisch, D. Beckmann, M. Fisher, *Angew. Chem. Int. Ed.* **2003**, *42*, 5834-5838.

[10] K. W. Kittredge, M. A. Fox and J. K. Whitesell, *J. Phys. Chem. B* **2001**, *105*, 10594; A. Ishida, Y. Sakata and T. Majima, *Chem. Commun.* **1998**, 57.

[11] J. Reichert, R. Ochs, D. Beckmann, H. B. Weber, M. Mayor, H. von Lohneysen, *Phys. Rev. Lett.* **2002**, *88*, 176804.

[12] H. Park, J. Park, A. K. L. Lim, E. H. Anderson, A. P. Alivisatos, P. L. McEuen, *Nature* **2000**, *407*, 57-60.

[13] a) P. Jiang, G. M. Morales, W. You, L. Yu, *Angew. Chem. Int. Ed.* **2004**, *43*, 4471-4475; b) J. He, Q. Fu, S. M. Lindsay, J. W. Ciszek, J. M. Tour, *J. Am. Chem. Soc.* **2006**, *128*, 14828-14835; c) L. A. Bumm, J. J. Arnold, T. D. Dunbar, D. L. Allara, P. S. Weiss, *J. Phys. Chem. B* **1999**, *103*, 8122-8127; d) B. Xu, N. J. Tao, *Science* **2003**, *301*, 1221-1223.

[14] D. J. Wold, C. D. Frisbie, *J. Am. Chem. Soc.* **2001**, *123*, 5549-5556; D. J. Wold, R. Haag, M. A. Rampi, C. D. Frisbie, *J. Phys. Chem. B* **2002**, *106*, 2813-2816; X. D. Cui, X. Zarate, J. Tomfohr, O. F. Sankey, A. Primak, A. L. Moore, T. A. Moore, D. Gust, G. Harris, S. M. Lindsay, *Nanotechnology* **2002**, *13*, 5-14; X. D. Cui, A. Primak, X. Zarate, J. Tomfohr,O. F. Sankey, A. L. Moore, T. A. Moore, D. Gust, L. A. Nagahara, S. M. Lindsay, *J. Phys. Chem. B* **2002**, *106*, 8609-8614.

[15] M. Mahadevan, R. M. Bradley, *Phys. Rev. B* **1999**, *59*, 11037-11046.

[16] J. G. Kushmerick, D. B. Holt, S. K. Pollack, M. A. Ratner, J. C. Yang, T. L. Schull, J. Naciri, M. H. Moore, R. Shashidhar, *J. Am. Chem. Soc.* **2002**, *124*, 10654-10655.

[17] R. Holmlin, R. Haag, M. L. Chabinyc, R. F. Ismagilov, A. E. Cohen, A. Terfort, M. A. Rampi, G. M. Whitesides, *J. Am. Chem. Soc.* **2001**, *123*, 5075-5085; M. A. Rampi, G. M. Whitesides, *Chem. Phys.* **2002**, *281*, 373-391; K. Slowinski, H. K. Y. Fong, M. Majda, *J. Am. Chem. Soc.* **1999**, *121*, 7257-7261; R. L. York, P. T. Nguyen, K. Slowinski, *J. Am. Chem. Soc.* **2003**, *125*, 5948-5953.

[18] H. B. Akkerman, P. W. M. Blom, D. M. de Leeuw, B. de Boer, *Nature* **2006**, *441*, 69-72.

[19] C. Zhou, M. R. Deshpande, M. A. Reed, L. Jones II, J. M. Tour, *Appl. Phys. Lett.* **1997**, *71*, 611-613; J. Chen, M. A. Reed, A. M. Rawlett, J. M. Tour, *Science* **1999**, *286*, 1550-1552; K. S. Ralls, R. A. Buhrman, R. C. Tiberio, *Appl. Phys. Lett.* **1989**, *55*, 2459-2461.

[20] L. N. Lucas, J. van Esch, R. M. Kellogg, B. L. Feringa, *Chem. Commun.* **1998**, 2313–2314; L. N. Lucas, J. J. D. de Jong, J. H. van Esch, R. M. Kellogg, B. L. Feringa, *Eur. J. Org. Chem.* **2003**, 155-166.

[21] J. M. Tour, L. Jones II, D. L. Pearson, J. J. S. Lamba, T. P. Burgin, G. M. Whitesides, D. L. Allara, A. N. Parikh, S. V. Atre, *J. Am. Chem. Soc.* **1995**, *117*, 9529-9534.

[22] J. Heurich, J. C. Cuevas, W. Wenzel, G. Schon, *Phys. Rev. Lett.* **2002**, *88*, 256803.

[23] S. Fraysse, C. Coudret, J. P. Launay, *Eur. J. Inorg. Chem.* **2000**, *7*, 1581-1590.

[24] Here we assume the effective mass m = 9.1 x 10^{-31} kg, in contrast to W.Wang, T. Lee, M. A. Reed., *Phys. Rev. B* **2003**, *68*, 035416.

[25] The switching times were somewhat dependent on the lamp employed; a 300 W Xe lamp gives lower times than a 200 W Hg lamp.

48

[26] P. R. Hania, R. Telesca, L. N. Lucas, A. Pugzlys, J. van Esch, B. L. Feringa, J. G. Snijders, K. Duppen, *J. Phys. Chem. A* **2002**, *106*, 8498-8507.

[27] S. M. Lindsay, *Faraday Discuss*. **2006**, *131*, 403-409; K. Stokbro, J. L. Mozos, P. Ordejon, M. Brandbyge, J. Taylor, *Comput. Mater. Sci*. **2003**, *27*, 151-156.

[28] X. D. Cui, A. Primak, X. Zarate, J. Tomfohr, O. F. Sankey, A. L. Moore, T. A. Moore, D. Gust, G. Harris, S. M. Lindsay, *Science* **2001**, *294*, 571-574.

[29] M. Hegner, P. Wagner, G. Semenza, *Surf. Sci.* **1993**, *291*, 39-46.

[30] a) L. A. Bumm, J. J. Arnold, M. T. Cygan, T. D. Dunbar, T. P. Burgin, L. Jones II, D. L. Allara, J. M. Tour, P. S. Weiss, *Science* **1996**, *271*, 1705-1707; b) G. E. Poirier, *Chem. Rev*. **1997**, *97*, 1117–1127; c) L. Patrone, S. Palacin, J. P. Bourgoin, *Appl. Surf. Sci*. **2003**, *212-213*, 446–451; d) K. Moth-Poulsen, L. Patrone, N. Stuhr-Hansen, J. B. Christensen, J.-B. Bourgoin, T. Bjørnholm, *Nano Lett*. **2005**, *5*, 783-785; e) S. Yasuda, T. Nakamura, M. Matsumoto, H. Shigekawa, *J. Am. Chem. Soc*. **2003**, *125* 16430-16433; f) Z. J. Donhauser, B. A. Mantooth, K. F. Kelly, L. A. Bumm, J. D. Monnell, J. J. Stapleton, D. W. Price, A. M. Rawlett, D. L. Allara, J. M. Tour, P. S. Weiss, *Science* **2001,** *292*, 2303-2307; g) Z. J. Donhauser, B. A. Mantooth, T. P. Pearl, K. F. Kelly, S. U. Nanayakkara, P. S. Weiss, *Japan. J. Appl. Phys*. **2002**, *41*, 4871-4877; h) P. A. Lewis, C. E. Inman, Y. Yao, J. M. Tour, J. E. Hutchison, P. S. Weiss, *J. Am. Chem. Soc*. **2004**, *126*, 12214-12215; i) G. K. Ramachandran, T. J. Hopson, A. M. Rawlett, L. A. Nagahara, A. Primak, S. M. Lindsay, *Science* **2003**, *300*, 1413-1416; j) R. A. Wassel, R. R. Fuierer, N. Kim, C. B. Gorman, *Nano Lett*. **2003**, *3*, 1617-1621; k) A. S. Blum, J. G. Kushmerik, D. P. Long, C. H. Patterson, J. C. Yang, J. C. Henderson, Y. Yao, J. M. Tour, R. Shashidhar, B. R. Ratna, *Nat. Mater*. **2005**, *4*, 167-172.

[31] W. R. Browne, J. J. D. de Jong, T. Kudernac, M. Walko, L. N. Lucas, K. Uchida, J. H. van Esch, B. L. Feringa, *Chem. Eur. J*. **2005**, *11*, 6414-6429; W. R. Browne, J. J. D. de Jong, T. Kudernac, M. Walko, L. N. Lucas, K. Uchida, J. H. van Esch, B. L. Feringa, *Chem. Eur. J*. **2005**, *11*, 6430-6441; J. Areephong, W. R. Browne, N. Katsonis, B. L. Feringa, *Chem. Commun.*, **2006**, 3930-3932.

[32] T. Tsujioka, H. Kondo, *Appl. Phys. Lett*. **2003**, *83*, 937-941.

[33] D. Dulic, S. J. van der Molen, T. Kudernac, H. T. Jonkman, J. J. D. de Jong, T. N. Bowden, J. van Esch, B. L. Feringa, B. J. van Wees, *Phys. Rev. Lett*. **2003**, *91*, 207402.

[34] L. A. Bumm, J. J. Arnold, T. D. Dunbar, D. L. Allara, P. S. Weiss, *J. Phys. Chem. B* **1999**, *103*, 8122-8127.

[35] J. Ern, A. Bens, H. D. Martin, S. Mukamel, D. Schmid, S. Tretiak, E. Tsiper, C. Kryschi, *J. Lumin*. **2000**, *742*, 87–89; J. Ern, A. Bens, H. D. Martin, S. Mukamel, D. Schmid, S. Tretiak, E. Tsiper, C. Kryschi, *Chem. Phys*. **1999**, *246*, 115-125.

[36] Note that the foregoing considerations on the Koopmans theorem justify plotting molecular energy states and the gold Fermi level together (see experimental section: "Details on Semiempirical Calculations").

[37] Calculations were performed by Dr. H. T. Jonkman.

[38] J. Li, G. Speyer, O. F. Sankey, *Phys. Rev. Lett*. **2004**, *93*, 248302.

[39] M. Zhuang, M. Ernzerhof, *Phys. Rev. B: Condens. Matter Mater. Phys*. **2005**, *72*, 073104.

[40] J. M. van Ruitenbeek, A. Alvarez, I. Piñeyro, C. Grahmann, P. Joyez, M. H. Devoret, D. Esteve, C. Urbina, *Rev. Sci. Instrum*. **1996**, *67*, 108-111.

[41] J.G. Simmons, *J. Appl. Phys*. **1963**, *34*, 1793-1803.

[42] R. Stratton, *J. Phys. Chem. Solids* **1962**, *23*, 1177-1190.

[43] J. V. Barth, H. Brune, G. Gertl, *Phys Rev B* **1990**, *42*, 9307-9318.

Chapter 3

Synthesis and Photochromic Properties of New Thiol-Terminated Diarylethenes; Temperature Dependence of the Switching Process

This chapter deals with the synthesis and photochemical properties of diarylethene photochromic molecular switches. A number of new derivatives are presented bearing one or more acetyl protected thiol groups. The photochromic properties of the newly synthesized diarylethenes in solution were studied. The temperature dependence of the photochemical ring opening in solution between 115K and 290K was investigated. Suppression of the ring opening process, which is complete below a cut-off temperature, is observed with decreasing temperature. For the corresponding ring closing process no temperature dependence was observed. The results confirm the existence of a thermal activation barrier to photochemical ring opening of diarylethene photochromic molecules.[*]

3.1 Introduction

The rapidly growing interest in diarylethene-based molecular switches has stimulated the synthesis of a variety of new derivatives.[1] There are several possibilities of structural modifications of the photoswitching unit while photochemical processes, ring opening and ring closure, are preserved (Scheme 1). The unexpected loss of reversibility upon covalent anchoring of molecules **3**[2] and **6**[3] (Chapter 2, Scheme 1 and 2) to gold electrodes (discussed in Chapter 2) has aroused us to seek better candidates that would imitate the previously achieved high difference in conductance[2,3] of the closed and the open form while restoring the reversibility. The key problem of designing new diarylethene derivatives is to achieve a photochemically reversible and a thermally irreversible molecular system. Thermal back reaction is attributed to the loss of aromatic stabilization energy in the closed form.[1b] Consequently, it was concluded that the thermal stability of diarylethene-type photochromic compounds can be attained by introducing heterocyclic aryl groups, which have low aromatic stabilization energies. Thiophene, which has a relatively low aromatic stabilization energy, has thus become the most frequently used heterocyclic group in these photochromic compounds. Another structurally important element is the central double bond. Usually, cyclic olefins are used to prohibit cis to trans photoisomerization, which may compete with the photocyclization reaction. Several 1,2-bis(thien-3-yl) systems containing maleic anhydride, maleimide, perfluorocyclopentene, and cyclopentene units have been synthesized so far.[1] Both diarylmaleic anhydrides and diarylmaleimides are readily accessible but are sensitive to acidic conditions. Hence perfluorocyclopentene and perhydrocyclopentene bridging units are the most commonly used.
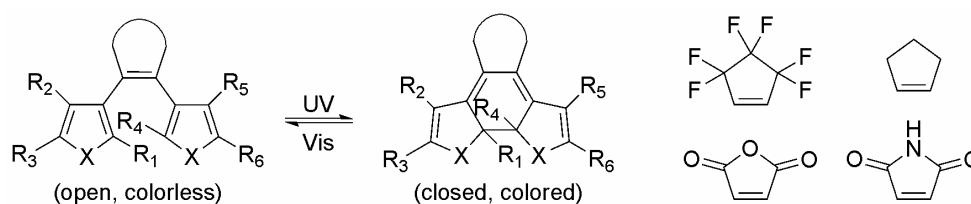
Scheme 1 *Left: general structure and switching cycle for diarylethenes. Right: different bridging units used for diarylethenes (X = S, O, NH).*

Few general synthetic approaches leading to perfluorocyclopentene and perhydrocyclopentene based switches have been developed. Well-established methodology leading to the 1,2-dithienylcyclopentenes based on titanium-mediated carbonyl coupling has been developed in our laboratories (Scheme 2).[4] The synthesis can be performed on a

52

multigram scale from relatively cheap starting materials. Compound **1** is synthesized starting from 2-methylthiophene, which was chlorinated at the 5-position with NCS in AcOH and benzene, followed by a Friedel–Crafts reaction with AlCl$_3$ and glutaryl chloride at 0 °C. The resulting 1,5-bis(5-chloro-2-methyl-3-thienyl)pentadione is used in a McMurry reaction with TiCl$_3$(THF)$_3$ and Zn in THF at 40 °C to provide **1**. The advantage of this approach is that the photochromic switch **1** can be functionalized easily in several ways. Compound **1** can, for instance, readily undergo a chlorine/lithium exchange at ambient temperature thus providing a versatile handle for the introduction of functionality.[4] Consequently, this method may provide both, symmetric or asymmetric dithienylcyclopentenes.
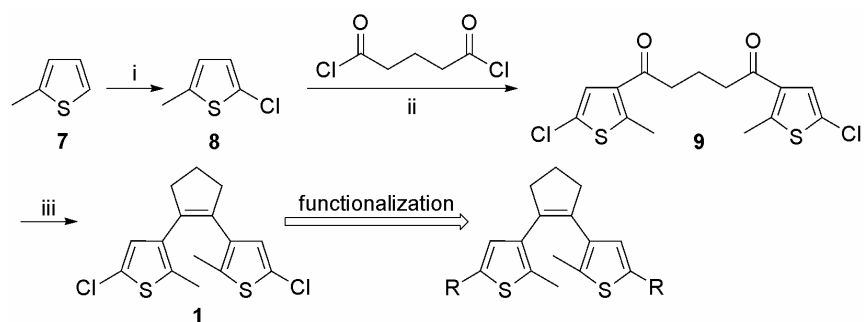
Scheme 2 *Reagents and conditions: i) NCS, AcOH, benzene, reflux, 80%; ii) AlCl$_3$, glutaryl chloride, CS$_2$, 0 °C, 94%; iii) TiCl$_3$(THF)$_3$, Zn, THF, 40 °C, 44%.*

A versatile synthetic route towards hexafluorocyclopentene dithienylethenenes is based on reaction of lithiated thiophenes with octafluorocyclopentene, resulting in switchable products by addition elimination reactions (Scheme 3). Various functionalities can be introduced by using substituted thiophenes. However, those functional groups must tolerate harsh lithiation condition in the final step. The expensive and rather volatile octafluorocyclopentene and the low yields commonly found in double substitution reactions of octafluorocyclopentene with lithiated thiophenes are major disadvantages. An alternative and more economic route leading to hexafluorodithienylethenens has been recently developed.[5] It follows the same synthetic strategy as for perhydrocyclopentene dithienylethenes shown in Scheme 2. The key step is an intramolecular McMurry coupling (Scheme 3) leading to dichloro derivative which can be further functionalized.

53
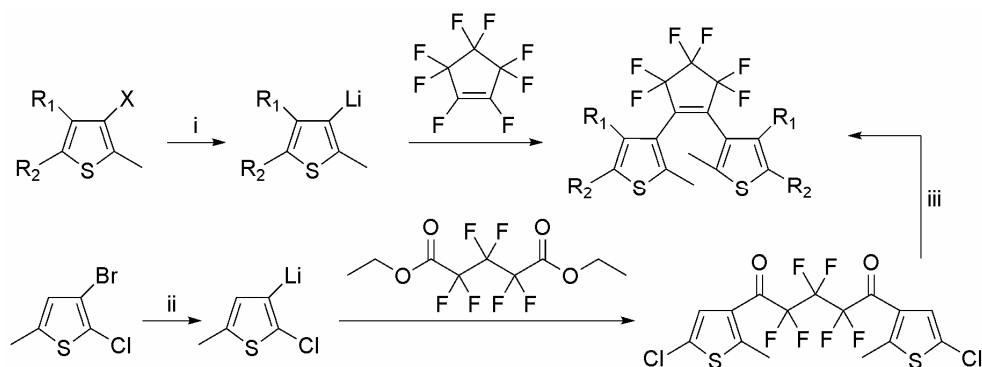
Scheme 3 *Two synthetic routes to perfluoro dithienylethenes. Top: original synthesis using octafluorocyclopentene.[6] Bottom: alternative synthesis forming a versatile dichloro-substituted switch used for further derivatization.[5] i) n-BuLi; ii) n-BuLi; iii) Zn, TiCl$_4$, (R$_1$= H and R$_2$= Cl).*

Photochromism of diarylethenes is the origin of the interest in these molecules. Photoswitching effects of diarylethenes are based on reorganization of the π-conjugated backbone of the molecule, which consequently leads to different physical properties. Knowledge of the key factors governing photochromic processes is essential for future utilization of diarylethenes as smart materials as well as in the fundamental understanding of the photo-processes involved. Hence, temperature dependent studies are necessary to reveal new aspects and limits of the switching process, as previously shown by measurements at elevated temperatures.[7] Additionally, determining possible switching restrictions at low temperatures is particularly important in view of carrying out conductance measurements at the single molecular level, which are restricted at room temperature because of the high mobility of the gold atoms constituting the electrodes in this type of experiments. In order to achieve stability of the metal/molecule/metal system it is often necessary to perform measurements at low temperatures.[8] The goal of the research described in this chapter is to develop fast and convenient synthetic strategies leading to various diarylethene derivatives bearing suitable anchoring groups which can be used for an attachment of these compounds to metallic surfaces and to study in detail the photochemical processes that diarylethene molecular switches undergo. In short, this chapter describes the synthesis of novel diarylethenes and their photochromic properties at ambient conditions as well as temperature-dependent kinetics studies revealing new restrictions to the switching process. Photochromic properties of the selected compounds described in this chapter are subjects of discussion in Chapter 4 and Chapter 5 upon their adsorption on a gold surface.

3.2 Synthesis of Thiol Terminated Diarylethenes

As discussed in Chapter 2, covalent attachment of thiophene-based switches **3** and **6** to a gold surface leads to the complete suppression of ring-closure and retardation of ring-opening. These effects of grafting photoactive molecules on gold have been attributed to the quenching of excited states of the molecules by gold surfaces and several quenching mechanisms have been proposed (see Chapter 2). A simple isolation of the central switching unit from the gold surface by introduction of a saturated aliphatic chain could be sufficient to preserve fully reversible behavior. However, electron transport would be substantially reduced and consequently the on-off ratio between conductance of the closed and open forms would be lowered. On our quest to find the best candidate for a reversible (surface bound) molecular switch we therefore needed to address both aforementioned issues. In order to preserve a fully reversible system after adsorption of a molecule on gold electrodes while keeping the conductance high, one could modify the electronic structure of the switch by careful variation of either the "head" group or the spacer unit (Scheme 4). If the hexahydrocyclopentene head group is exchanged by the electron withdrawing hexafluorocyclopentene group, both HOMO and LUMO levels are lowered, while the gap between them remains almost the same.[9] That would lead to the different alignment of molecular orbitals with the Fermi level of gold resulting in entirely new molecule-metal surface electronic coupling. The new alignment might influence the switching efficiency and due to the unchanged HOMO-LUMO gap the on-off ratio stays high. On the other hand one could choose to decrease the HOMO-LUMO gap *e. g.* by increasing the length of the conjugated system. This can be easily realized by modifying the spacer unit. The original design with a simple thiophene as a spacer can be substituted by two connected thiophene rings (Scheme 4). Another option to achieve full reversibility is to tune the extent of the electronic coupling of the central switching unit with the electrodes. A straightforward way of testing this is to examine an effect of the linearly conjugated spacer on the switching efficiency *versus* a cross conjugated spacer. For that purpose one can use *para* or *meta* di-substituted benzenes. Additionally, it should be possible to partially decouple the central switching unit from the anchoring group using a biphenyl spacer unit where the delocalization of electrons is hampered because of the twisted conformation. The following subsection will focus on the synthesis of the target molecules with the previously mentioned variations of the head group and spacer unit.

55
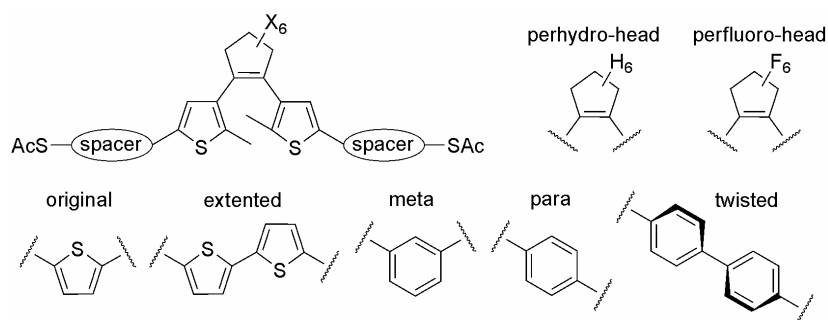
Scheme 4 *General scheme depicting possible variation of the head group or the spacer unit leading to modifications of the electronic structure of the switch.*

Perhydrocyclopentene-based switches **14** and **15** were synthesized following the strategy depicted in Scheme 2, employing compound **1** (Scheme 5). First, intermediate **12** was prepared by palladium catalyzed reaction of the Grignard reagent **10** and dibromide **11**. Treatment of compound **1** with *n*-butyllithium and subsequent reaction with tri-*n*-butylborate results in a boronic acid intermediate, which was reacted with compound **12** in the presence of a palladium catalyst providing **13** in 56% yield. Compound **13** was first lithiated and subsequent treatment with sulfur and acetyl chloride leads to formation of compound **14** as a main product and compound **15** as a side product of the reaction.
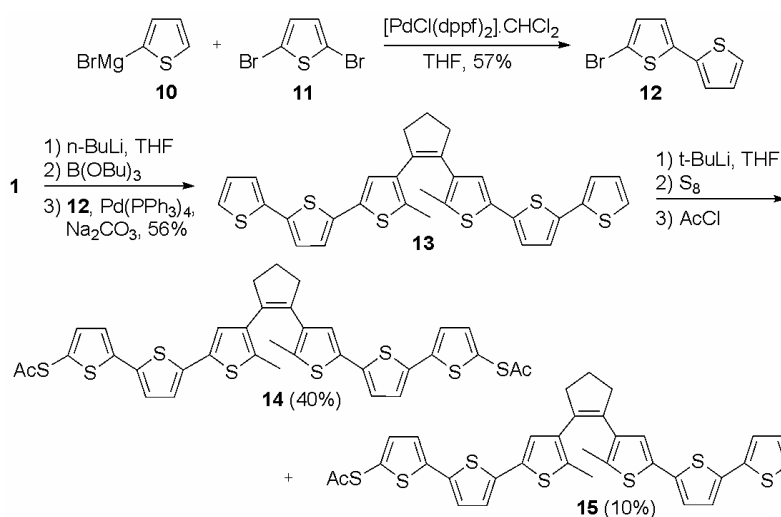
Scheme 5 *Synthetic route to compounds **14** and **15**. The final step gives compound **14** as a main product in 40% yield and compound **15** in 10% yield as a side product.*

56

In order to have access to molecules that differ only in the position of the connection of the central switching unit with terminated thiol groups either in linearly conjugated or cross conjugated manner, compounds **18**, **19**, **23** and **24** were prepared (Scheme 6). In the synthesis of compounds **18**, **19**, **23** and **24,** brominated aryldithienylethenes were prepared as key intermediates. Subsequent lithiations can then be directed to selected sites. The overall strategy was based again on utilization of the versatile intermediate **1**. Two approaches, one towards symmetric and one to asymmetric switches yielded compounds **18**, **19**, **23** and **24**.
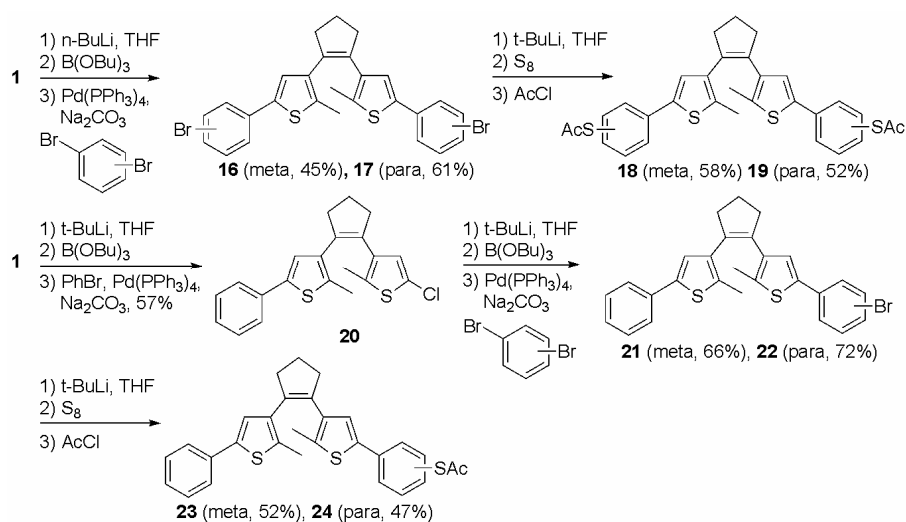
Scheme 6 *Synthetic route to symmetrically substituted compounds **18** and **19** and asymmetrically substituted compounds **23** and **24**. The final steps give yields of 58% of meta substituted **18**, 52% of para substituted **19**, 52% of **23** and 47% of **24**.*

In all so far synthesized diarylethene compounds, sulfur was introduced in the last step. Those reactions give moderated yields and purifications are complicated by the presence of oligomeric sulfur species that are formed. An alternative could be to use intermediates, which already possess protected thiol groups. The protective group must tolerate the basic conditions involved in Suzuki coupling with derivative **1**. An acetyl protective group is not inert under the conditions that are usually employed for derivatization of **1** in a Suzuki coupling. In the course of reaction the acetyl group is being hydrolyzed and the deprotected thiol moiety poisons the palladium catalyst. For the synthesis of compound **29** (Scheme 7) possessing a twisted biphenyl spacer group we decided to test the aforementioned synthetic strategy. A use of a *t*-butyl as a thiol protective group and the conversion to S-acetyl in a synthesis of acetyl protected thiols has been described previously.[10] *t*-butylthiol

57

intermediate **27** was synthesized by reacting dibromobiphenyl **25** with *t*-butylthiol. Palladium catalyzed sulfenylation involves oxidative addition of the aryl halide to Pd, followed by nucleophilic attack of the thiolate anion on the adduct. The resulting compound **27** was then used in Suzuki coupling, without its thiol groups being deprotected. The *t*-butyl protected thiol groups of compound **28** were then deprotected using BBr_3 and re-protected with acetyl chloride in order to prevent any oxidative dimerization of the aromatic thiols. Compound **29** is formed in 33% yield, which is comparable to the results obtained *via* the previous strategy. However, if more complicated side groups are needed this strategy seems to be more favorable since the last step of the previous strategy involves lithiation, which might induce side reactions and is usually less tolerant towards functional groups.
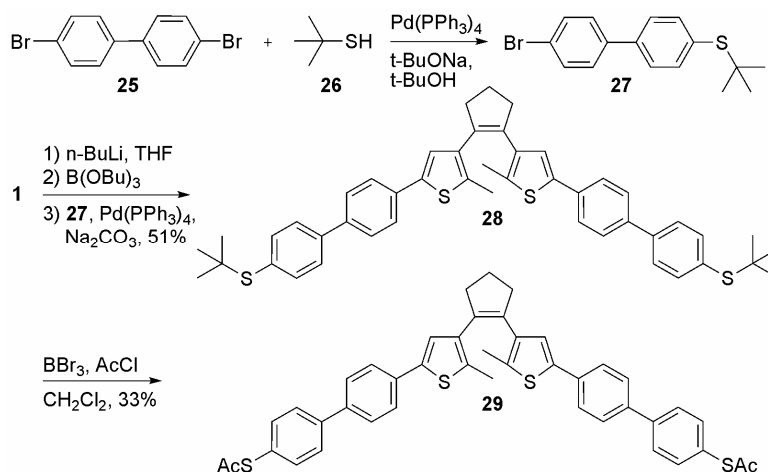
Scheme 7 *Synthetic route to compound 29.*

For the synthesis of perfluorocyclopentene based compounds **35** and **36** (Scheme 8) the original strategy developed by Irie[6] (Scheme 3) was used. The key step is a reaction of lithiated thiophenes with octafluorocyclopentene. In order to prepare the intermediate **32**, palladium catalyzed coupling of boronic acid **30**[11] and bromide **31** was performed. Compound **32** was then reacted with *n*-buthyllithium and the lithiated intermediate reacted with octafluorocyclopentene **33** giving photochromic compound **34** in 43% yield. Compound **34** was next treated with *t*-buthyllithium followed by reaction with sulfur. Thiol groups of the thiol terminated intermediates were subsequently protected *in-situ* by acetyl moieties leading to both disubstituted compound **35**, as a main product, and monosubstituted **36** as a side product.
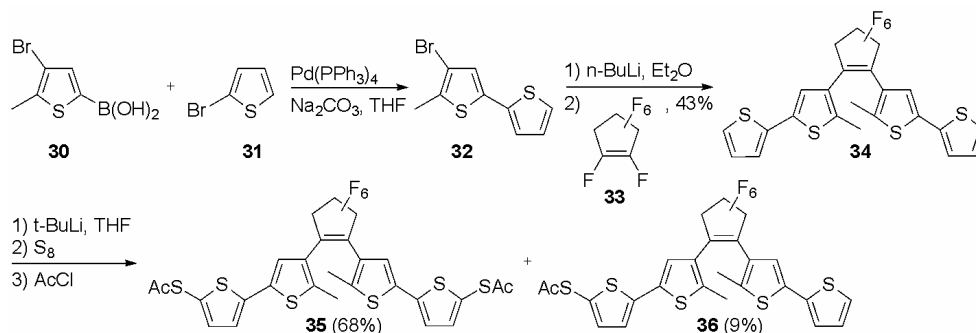
Scheme 8 *Synthetic route to hexafluorocyclopentene compounds **35** and **36**. The final step gives compound **35** as a main product in 68% yield and compound **36** in 9% yield as a side product.*

In addition to the compounds previously discussed, molecule **42** (Scheme 9) was designed as well. It addresses the same problem of the partial isolation of the switching unit from anchoring side groups. π-electrons are not delocalized through the whole molecule due to the presence of both a sp^3 hybridized silicon atom as well as six benzylic sp^3 carbon atoms. Adjacent acetyl protected thiol groups can be deprotected in the course of attachment of the molecule to gold electrodes and create stable "tripodal" anchoring (Scheme 9). This "tripodal" anchoring should have a beneficial effect on the stability of anchored molecules on gold electrodes (Scheme 9, right bottom). The stabile anchoring of molecules to metal surfaces is of great importance in the field of single molecule electronics.[12] For aromatic thiols inserted in *n*-dodecanethiol matrixes so-called stochastic switching has been observed in STM experiments (for more details, see Chapter 2). There is still no consensus on the origin of stochastic switching. However, Ramachandran *et al.* relate the phenomenon to instabilities of the Au–S bond.[13] Compound **42** with its "tripodal" anchoring hence addresses also basic problems of stability in single molecule electronics. The synthetic route to compound **42** is shown in Scheme 9. Tripod base **39** was synthesized as a crucial intermediate starting from *meta*-iodobenzylalcohol. The hydroxy group was first protected using TBDMSCl. Resulting compound **38** was then treated with *n*-butyllithium and the subsequent reaction with tetraethylorthosilicate gave tripod base **39**. Tripod base **39** was reacted with lithiated compound **2** (for the synthesis of compound **2**, see Chapter 2) to give molecular switch **40** in 30% yield. Six protected hydroxyl groups were then deprotected using *tert*-butylammonium fluoride following by Mitsunobu reaction with thioacetic acid as a nucleophile to give the desired compound **42**.
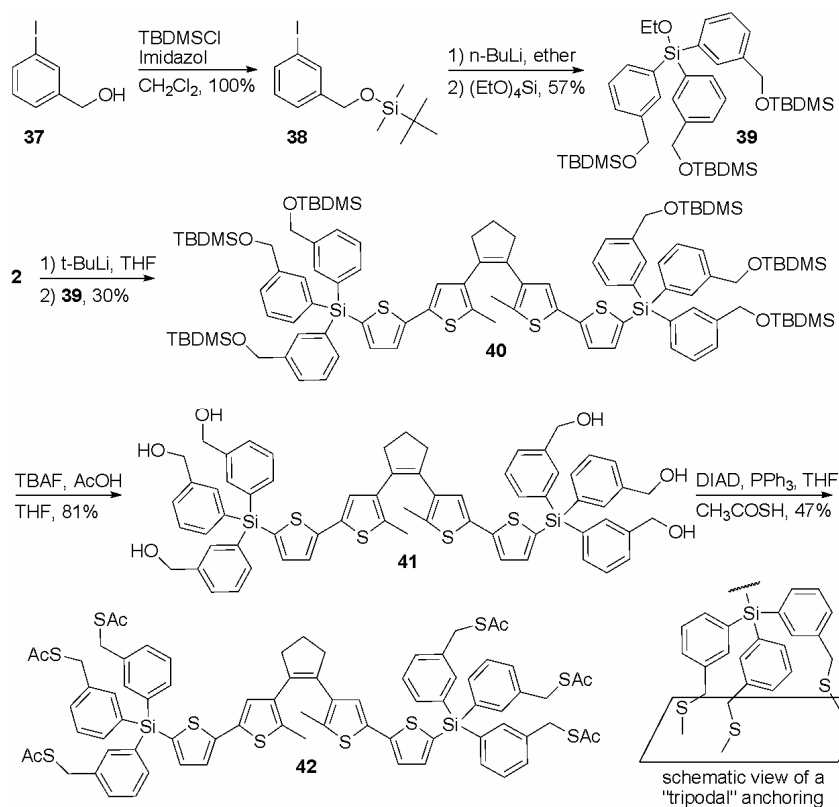
Scheme 9 *Synthetic route to compound **42**.*

3.3   Room Temperature Photochromic Properties of Diarylethenes

3.3.1   Absorption Spectra and Photochemical Interconversion of Open and Closed Forms

In general, the open ring isomers of dithienylethenes have absorption bands at short wavelengths. Upon irradiation with UV light, new absorption bands appear at longer wavelengths, which are ascribed to the closed ring isomers. Most dithienylethenes show large spectral shifts upon photoisomerization from the open to the ring isomers.[1] In the closed ring isomers, π-electrons are delocalized through the whole molecule. The absorption spectra of the closed ring isomers depend on the substituents of the thiophene

60

rings. The absorption spectra of the open ring isomers also depend on the nature of the upper cycloalkene structures.

Figure 1 shows the UV/Vis absorption spectra of the open and closed forms of diarylethene derivatives **3, 6, 14, 15, 18, 23, 24, 29, 35, 36, 42** in toluene. Dynamic interconversion between the open and closed form can be achieved by irradiation at selected wavelengths (λ = 313 nm for the ring closure and $\lambda > 420$ nm for the ring opening). It should be noted that upon irradiation of the open forms with UV light in all cases a photostationary state (PSS) is obtained. Due to nonzero absorption of the closed form in the UV spectral region, both ring closure and ring opening take place after photoexcitation, leading to an equilibrium situation, the so called photostationary state (PSS), determined by the quantum yields of ring closing and ring opening processes. However, quantum yields obtained for diarylethenes showed that the cyclization is more efficient than the ring opening.[1] In the case of the presented compounds the PSSs were determined by ^{1}H NMR spectroscopy. In all cases no traces of the open forms could be detected suggesting that the ring closure process for all compounds reaches essentially full conversions.
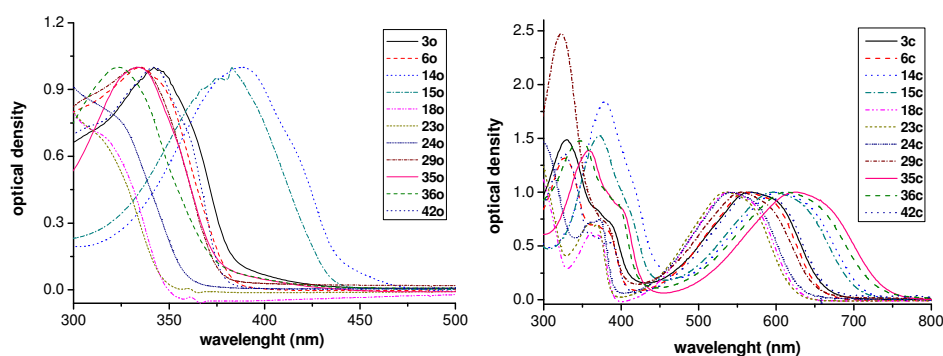
Figure 1 *Normalized absorption spectra of a) open forms and b) closed forms of the photochromic compounds taken in toluene.*

Table 1 shows the absorption maxima for the open and closed forms of the diarylethenes described in this chapter and their corresponding extinction coefficients. The importance of the effect of the substitution of cyclopentene bridging unit is demonstrated by comparing absorption spectra of perhydro compounds **3** and **6** and perfluoro compounds **35** and **36**. The absorption maxima of the open forms of all for compounds appear around a wavelength of 335 nm. However, the closed ring isomers of perfluoro derivatives show significant shifts in the UV/Vis absorption spectra to longer wavelengths in comparison with the perhydro derivatives. The effect of side-group substitution and length of

61

conjugation can be seen on the spectral changes for molecules **14** and **15** with respect to **3** and **6**. Both, the absorption maxima of the open and closed forms of **14** and **15** are shifted to longer wavelengths by 40 to 50 nm compared to **3** and **6**. Thioacetate moieties, if present as substituents on a benzene ring are responsible for small shifts in UV/Vis absorption (~7 nm for the open form and ~12 nm for the closed form) towards longer wavelengths.[9] Additionally the position of substitution on the benzene ring might be important as well. *Para-* substituted derivative **24** exhibits a bathochromic shift compared to *meta-* substituted derivative **23**. This observation suggests that the thioacetate group in the *meta-* position participates to a lesser extent in the delocalization of electrons within the molecular scaffold. Hence it can be anticipated that if molecules **23** and **24** are anchored on a metal electrode the central switching unit of molecule **23** will be partially isolated from the metal surface with respect to **24** and subsequently can be less prone to metal-assisted inhibition of the photoreactions. Compound **29** bearing the biphenyl spacer unit shows a spectral shift to longer wavelengths in comparison with "mono-"phenyl derivatives **18**, **19**. However the effect of one extra benzene ring is approximately four times less significant then for a thiophene ring in compounds **14** and **15**. This is due to the twisted orientation of two adjacent benzene rings. The delocalization of electrons is therefore less effective.

Table 1 *Photophysical properties of open and closed forms in toluene.*

Compound	Open form λ_{max}(abs) [nm] (ε [10^3 cm^{-1}M^{-1}])	Closed form λ_{max}(abs) [nm] (ε [10^3 cm^{-1}M^{-1}])	
3	342	331 (27), 372 (I, 14), 387 (S), 601 (S),	569 (21)
6	335 (32)	328 (28), 365 (I, 14), 369 (14), 386 (S), 602 (S)	562 (22)
14	388 (38)	379 (30), 419 (S), 431 (I, 11)	602 (17)
15	383 (41)	371 (32), 413 (S), 419 (I, 13)	596 (19)
18	323 (S)	340 (I, 10), 361 (17), 370 (17), 578 (S)	538 (28)
23	315 (S)	337 (I, 11), 360 (16), 369 (16), 569 (S)	537 (23)
24	327 (S)	346 (I, 11), 360 (S), 372 (14), 580 (S)	542 (19)
29	333 (55)	323 (52), 365 (I, 19), 385 (S), 606 (S)	555 (21)
35	334 (41)	352 (I, 29), 358 (30), 404 (S)	626 (21)
36	323 (41)	343 (I, 30), 348 (30), 400 (S)	614 (20)
42	342 (110)	327 (94), 369 (S), 370 (I, 40), 614 (S)	567 (69)

I=isosbestic point, S=shoulder

3.3.2 Fatigue Resistance

Photochromic reactions are often accompanied by rearrangement of chemical bonds. During the rearrangement, undesirable side reactions take place to some extent. This limits the number of cycles of photochromic reactions. Eventually, if one wants to use an optical switch for practical applications the performance has to be close to 100%. This need can be

illustrated with the following example: if there is an undesirable reaction which has a quantum yield of 0.001, then after 1000 switching cycles 63% of the initial switch is decomposed. Recently, decomposition products appearing after long irradiation have been shown for both perhydro[14] and perfluoro[15] cyclopentene-based switches.

Fatigue resistance can be measured in the following experiment; a toluene solution containing a diarylethene is irradiated with UV light of a certain wavelength, which can excite the open ring isomer, until the photostationary state is reached, and then the colored closed ring isomer is completely bleached by irradiation with visible light. This operation is repeated several times and the absorbance of the colored closed ring isomer is monitored. Figure 2 shows four repetitive switching cycles for compounds **6**, **23** and **36**. The absorption was monitored at 480 nm. A typical sign of photo-degradation is the decreasing intensity of the closed forms upon repetitive UV irradiation. However, photo-decomposed products might adsorb in the visible region close to the original adsorption peak of the closed forms as well. Therefore, it is also important to monitor the intensity after visible irradiation when the molecule should return to its open state. It can be seen that in all three cases (Figure 2) the intensity of the absorption increases after each visible irradiation, (lower values) suggesting that a photo-inactive side-product adsorbing in the visible region is formed. Judging from Figure 2 it is obvious that compound **6** is the most prone to photo-decomposition and after four switching cycles approximately 20% of the molecule is decomposed. Compounds **23**, bearing a phenyl spacer group, and perhydro derivative **36** show higher fatigue resistance, but photo-decomposition is still observed. Nevertheless, it should be noted that to reach PSS excessive UV irradiation is required due to the exponential nature of the process. It can be concluded that molecules with a phenyl spacer will benefit from higher fatigue resistance. The more electron withdrawing perfluorocyclopentene bridging unit is also responsible for the higher photo-stability of molecule.
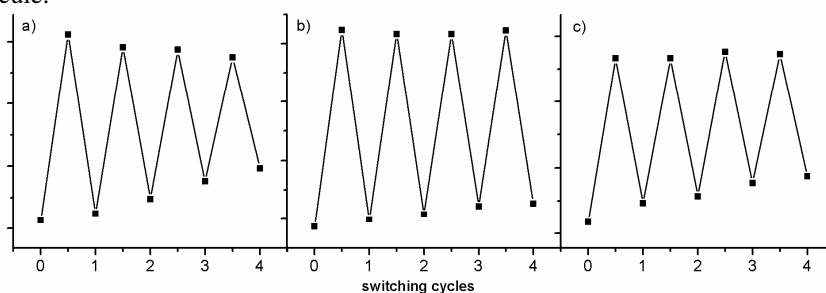
Figure 2 *Four successive switching cycles for compounds a) 6, b) 23 and c) 36 monitored at λ = 480 nm in toluene. Switches are first illuminated with UV light (λ = 313 nm) until the PSS is obtained and subsequently illuminated with visible light (λ > 420 nm).*

63

3.4 Temperature Dependence of Diarylethene Photochromism

Temperature-dependent studies of photochemical processes in diarylethenes are essential for understanding the behavior of these molecular switches before they can be used in advanced technological applications. Furthermore, the observed suppression of the ring opening (*vide infra*) might have important implications for gating of photochromic processes. As for other photoreactions that have a photostationary state with less than 100 % of product, the ring closure process of diarylethenes occurs simultaneously to ring opening, since both forms absorb in the UV region. This phenomenon decreases total conversions.[16] On the other hand, if the ring opening can be blocked, total conversion increases.[17]

In this subsection, the temperature dependence of the photochemical behavior of dithienylcyclopentenes is discussed. The suppression of the ring opening process with decreasing temperature leads to the complete absence of the photoreaction below a cutoff temperature. By contrast, it is demonstrated that the reverse ring closure process shows no significant temperature dependence above 115 K. Two representative examples of dithienylcyclopentene photochromic switches have been investigated, the hexahydro compound **23** and hexafluoro compound **36**.

The UV/Vis absorption spectra at 115 K and 290 K of the switches **23** and **36** in isopentane solution are shown in Figure 3. The broad absorption bands with the maximum at $\lambda = 590$ nm for **36** and $\lambda = 537$ nm for **23** are characteristic of the closed form of the switch. At low temperature the vibrational structure in the absorption spectra becomes more apparent resulting in a sharpening of the absorption band and distinct absorption maxima are observed.
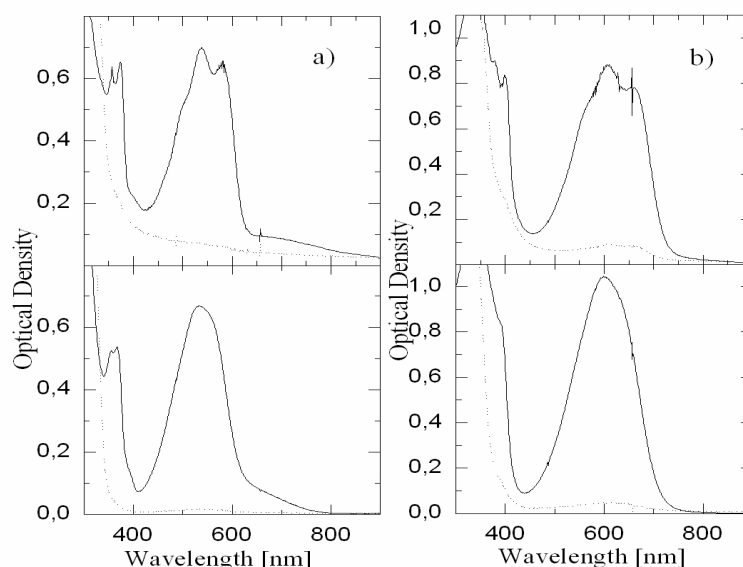
***Figure 3** Absorption spectra of the molecular switches: a) compound **23** in isopentane, concentration of 7.94 x 10⁻⁵ mol/L; solid line (—) closed form, dashed line (---) open form. Upper panel 115 K (isopentane at 115 K was used as a reference), lower panel 290 K (isopentane at 290 K was used as a reference); b) compound **36** in isopentane, concentration of 6.07 x 10⁻⁵ mol/L; solid line (—) closed form, dashed line (---) open form. Upper panel 115 K, lower panel 290 K.*

3.4.1 Ring-Closure Kinetics

In order to explore the effect of temperature on switching efficiency, the kinetics of the switching process was examined (for both ring closure and ring opening). At each temperature a solution containing the switch in the open form was used to obtain a reference spectrum (blank). Therefore, any absorption changes induced by irradiation are related to the evolution of the closed form. The time evolution of the differential absorption of the closed form was monitored to follow the kinetics of the switching reactions. To promote ring closure, UV light with $\lambda = 313$ nm was used until the photostationary state was reached.[18] The kinetics of this process at different temperatures is represented in Figure 4 for compound **23**. For each temperature a fresh solution was used. The data points are plotted for the wavelength corresponding to the maximum absorption of the closed form (λ

65

= 537 nm). The results demonstrate that the ring closure process is effectively temperature independent in the measured temperature range. Similar behavior was observed for compound **36** (monitored at $\lambda = 590$ nm).
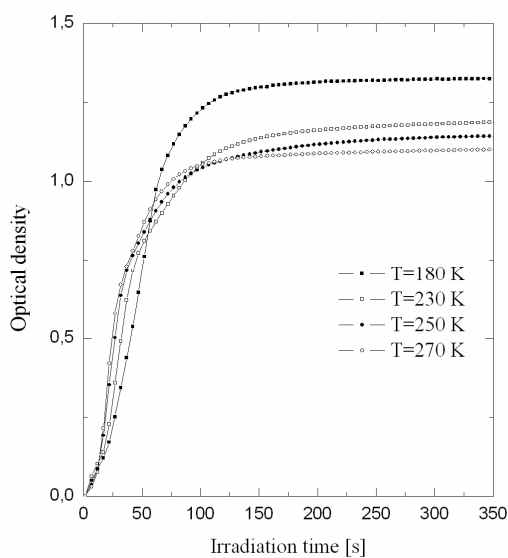
Figure 4 *Kinetics of the ring closure for switch **23** in isopentane obtained at $\lambda = 537$ nm for different temperatures.*

3.4.2 Ring-Opening Kinetics

The kinetics of the ring opening in isopentane were followed at the same wavelengths as ring closing, while irradiating with visible light $\lambda = 546$ nm. In contrast to the ring closure, the ring opening process is strongly temperature dependent, as shown in Figure 5. For both compounds **36** and **23** the ring opening process is suppressed completely at *ca*. 130 K for **36**, and around 120 K for **23**. The observed suppression of the ring opening might have important implications for gating of photochromic processes.

66
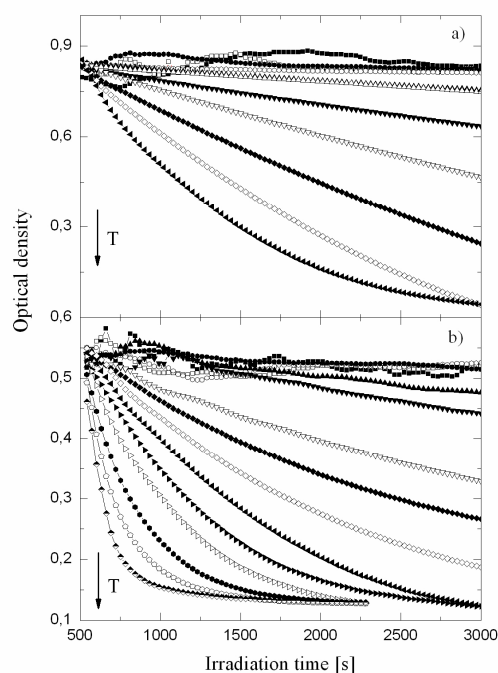
Figure 5 *Temperature-dependent kinetics of the ring opening process in isopentane: a) for compound **36** obtained at λ = 590 nm. Temperatures: 115, 130, 150, 170, 180, 190, 210, 230, 250, 270, 290 K; b) for compound **23** at λ = 537 nm. Temperatures: 115, 120, 125, 130, 140, 150, 170, 180, 190, 200, 210, 220, 230, 250, 270, 290 K. The curves are adjusted to the same value along the y-axis for clarity.*

3.4.3 Activation Energy Barrier

For each temperature the data points were plotted on a logarithmic scale, and the initial portion of the curve was fitted to determine the rate (K(T)) of ring opening. In Figure 6 the logarithm of the rate is plotted versus inverse temperature. The curves show two distinct components, a temperature-dependent region where photochemical ring opening is observed and a temperature independent region where photochemistry is not observed. From the slope of the temperature dependent component of the curve the thermal barrier of the ring opening is obtained. Although the observed rate of ring opening is dependent on the intensity of the light source, the exponential component of the fit is intensity independent. This has an important implication for determination of activation energies.

67

The validity of the approach taken is not immediately obvious. In the following section, it will be demonstrated that this approximation is justified under the low irradiation intensities employed.
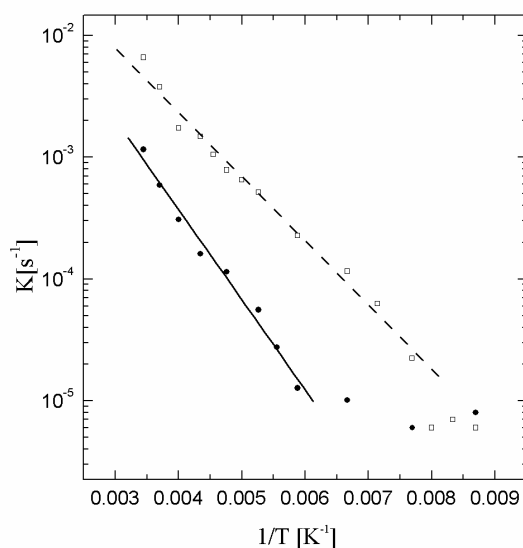
Figure 6 *Arrhenius plots for compound **36** (squares), and **23** (circles) with corresponding linear fits. The activation energies obtained from the Arrhenius plots are 104 meV (10.034 kJmol^{-1}, 838.8 cm^{-1}) for **23** and 147 meV (14.183 kJmol^{-1}, 1185.6 cm^{-1}) for **36**.*

In Figure 7 an illustrative diagram of the energy levels involved in the ring opening process is shown. Ring opening of the closed form requires first that the molecule is promoted to the THEXI state (thermally equilibrated excited state) upon irradiation with visible light, followed by the crossing of a thermal barrier. Semi-empirical quantum chemical computational methods[2] have predicted the existence of this barrier (also see, Chapter 2, Figure 8). So far, experimentally the thermal barrier and its importance in the photochemical processes have not been studied in detail. The only experimental studies describing the temperature dependence of the ring opening so far have been performed at elevated temperatures with very few data points.[19]
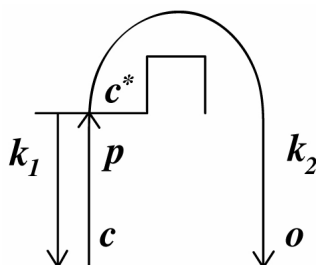
Figure 7 *Sketch of the energy levels of the ring opening process, where c, c* and o represents populations of the ground state and excited state of the closed form and ground state of the open form, respectively: p is the pump rate and k_1, k_2 are rates from excited to closed and excited to open state.*

The full set of differential equations that describes the ring opening dynamics is

$$\frac{dc(t)}{dt} = -p \cdot c(t) + k_1 \cdot c^*(t) \tag{1}$$

$$\frac{dc^*(t)}{dt} = p \cdot c(t) - k_1 \cdot c^*(t) - k_2 \cdot c^*(t) \tag{2}$$

$$\frac{do(t)}{dt} = k_2 \cdot c^*(t) \tag{3}$$

Where $c(t)$, $c^*(t)$ and o(t) represent populations of the ground state and excited state of the closed form and ground state of the open form, respectively. $p = \sigma_0 \cdot I$ is the pump rate, σ_0 is absorption cross section, and I is intensity of light. k_1 and k_2 are rates from excited to closed and excited to open state, respectively, where $k_2 = k_2^0 \exp[(-\Delta E)/(k_B T)]$, with ΔE being the activation energy, k_B Boltzman constant, and T temperature. At steady state conditions when the pump intensity is very weak, the population of the excited state of the molecules in the closed form is proportional to the population of the ground state, $c^*(t) = a \times c(t)$, where $a \ll 1$. With this approximation Eqs.1,2 are reduced to

$$\frac{dc^*(t)}{dt} = -\frac{dc(t)}{dt} - k_2 \cdot c^*(t) \tag{4}$$

$$\frac{dc(t)}{dt} = -c(t) \cdot \frac{a}{a+1} \cdot k_2 \tag{5}$$

69

For $a << 1$ $(1 + a \approx 1)$, Eq. 5 becomes

$$\frac{dc(t)}{dt} = -c(t) \cdot a \cdot k_2 \tag{6}$$

With solution Eq.6

$$c(t) = c_0 \exp(-a \cdot k_2 \cdot t) \tag{7}$$

By fitting our experimental data we obtain $K(t) = k_2$ x a. Since a does not depend on temperature, we can write

$$K(t) = k_2^0 \cdot a \cdot \exp(-\frac{\Delta E}{k_B T}) \tag{8}$$

$$\ln(K(t)) = \ln(k_2^0 \cdot a) - \frac{\Delta E}{k_B T} \tag{9}$$

Therefore, the data presented in Figure 6 can be fitted with a single exponent. The Arrhenius plot allows for determination of activation energies of $\Delta E = 147$ meV (14.183 kJmol^{-1}, 1185.6 cm^{-1}) for **36**, and $\Delta E = 104$ meV (10.034 kJmol^{-1}, 838.8 cm^{-1}). Different values of the activation energies indicate that the thermal barrier is sensitive to changes in molecular structure. It implies that further understanding of the barrier is necessary for optimization of switching properties. In particular, finding a way to reduce the barrier by an order of magnitude would significantly increase the switching rate (by a factor of 1000). On the other hand, the strong temperature dependence of the ring opening can be exploited for a control over the photochemical processes. Low temperatures would effectively block the ring opening while upon heating full reversibility could be restored. Such a gating would be particularly useful for systems where a UV irradiation results in a PSS with a low portion of the closed isomer. This is a result of the UV-induced ring opening reaction. However, if the ring opening is blocked at the particular temperature, UV irradiation would result in a complete conversion to the closed form.

3.5 Conclusions

In conclusion, in this chapter the synthesis of novel thiol terminated diarylethene-based molecular switches is described as well as their photochromic properties. A series of compounds with different spacers connecting the central switching unit with the anchoring groups has been synthesized. Photochemical and conductive properties of some of these compounds, once they are grafted on metal surfaces, will be discussed in detail in the

following chapters. All synthetic routes are straightforward and can be adapted for the synthesis of many different molecular switches with different functional groups. The photochromic behavior of all compounds in solution corresponds with the standard photochemical switching of diarylethenes. Both processes of ring closure and ring opening can be selectively addressed by light of different wavelengths and lead to high yields. The low temperature studies reveal the strong temperature dependence of the ring opening. On the other hand the ring closure is temperature independent within the measured temperature range. The strong temperature dependence of the ring opening implies that variation of temperature might be used for gating of photochromic behavior of diarylethenes.

3.6 Experimental Section

General Remarks

For general remarks see Chapter 2.

Low Temperature Measurements

UV/Vis absorption spectra were measured using a HP 8453 diode array UV/Vis spectrometer. In principle, the light from the spectrometer interacts with the molecules causing a photoreaction. However, repetitive acquisitions showed no detectable changes in the absorption spectra which we attribute to the weak intensity of the light source. A high pressure mercury lamp (200 W, Oriel) was used with 10 nm FWHM (full-width half maximum) band pass filters to switch the molecules from the open to the closed state and vice versa. Light beams with power densities of 0.094 mW/cm^2 for λ=546 nm were employed for ring opening, and 0.00354 mW/cm^2 for λ=313 nm to achieve ring closure. The power densities were measured (optical power meter Oriel 70260, Oriel, Stratford, USA) before and after the experiment for each temperature. In order to minimize artifacts due to diffusion the entire sample volume (1 cm^3) was irradiated. Temperature dependent measurements were performed between 115 K - 290 K, using liquid nitrogen cooled optical cryostat (Optistat, Oxford instruments). Isopentane solutions of both compounds, at a concentration of 6.07 x 10^{-5} mol/L for **36** and 7.94 x10^{-5} mol/L for **23** have been used.

5-Bromo-2,2'-bithiophene (12)

A solution of 2-bromothiophene (4.967 g, 24.92 mmol) in dry THF (5 ml) was added dropwise to Mg turnings (752 mg, 30.94 mmol) and a small I$_2$ crystal in dry THF (25 ml). When ca. 1 ml of the bromothiophene solution was added, the reaction started, and the mixture was kept under reflux during further addition. After complete addition, the mixture was stirred for 1h under reflux. The mixture was then transferred with a syringe to an

71

addition funnel and added slowly during 3 h to an ice-cooled mixture of 2,5-dibromothiophene (8.206 g, 33.91 mmol) and [1,1'-bis(diphenylphosphino)-ferrocene]dichloropalladium(II) ([PdCl$_2$(dppf)$_2$]; 250 mg, 0.306 mmol; 1 : 1 complex with CH$_2$Cl$_2$) in dry THF (50 ml). This mixture was stirred for 2h at 0° and for 16h at r.t. The solvent was evaporated and the residue suspended in AcOEt and washed with saturated aq. NaHCO$_3$ solution and brine. The aqueous layers were extracted with AcOEt and the organic layers dried (MgSO$_4$) and the solvents evaporated. Purification by flash chromatography (silicagel, hexanes) gave 4.229 g (57%) of **12**. Spectroscopic data were identical to those reported previously.[20]

1,2-Bis[5-(2,2'-bithiophen-5-yl)-2-methylthien-3-yl]cyclopentene (13)

To a solution of compound **1** (500 mg, 1.52 mmol) in THF (14 ml), kept under an inert N$_2$ atmosphere, *n*-BuLi (2.5 ml of 1.6 M solution in hexane, 4.00 mmol) was added. After 1h, B(OBu)$_3$ (1.2 ml, 4.60 mmol) was added and the mixture was stirred for 1h to produce a boronic ester intermediate. In a separate flask compound **12** (1.512 g, 6.16 mmol), Pd(PPh$_3$)$_4$ (202 mg, 0.173 mmol), THF (10 ml), 2M Na$_2$CO$_3$(aq.) (8 ml) and ethylene glycol (10 drops) were preheated to 80 ^{o}C and the boronic ester solution was added slowly. The reaction mixture was heated under reflux overnight, diluted with diethyl ether (100 ml) and washed with water (100 ml). The aqueous layer was washed with an additional volume of ether (100 ml) and the combined organic phases were dried over Na$_2$SO$_4$, filtered and concentrated in vacuum. Three subsequent precipitations (silicagel, chloroform/*n*-hexane) afforded compound **13** (500 mg, 56 %) as a solid. M.p. 227-232°C (dec.); ^{1}H NMR (300MHz, CDCl$_3$) δ 1.97 (s, 6H), 2.00 (m, 2H), 2.82 (t, *J* = 7.3 Hz, 4H), 6.89 (s, 2H), 6.95 (t, *J* = 4.0 Hz, 2H), 7.00-7.05 (m, 6H), 7.14 (d, *J* = 5.1 Hz, 2H), 7.20 (d, *J* = 5.1 Hz, 2H) ppm; ^{13}C NMR (75.4 MHz, CDCl$_3$): 14.5 (q), 22.8 (t), 29.3 (q), 38.4 (t), 123.5 (d), 123.8 (d), 124.6 (d), 125.1 (d), 125.4 (d),132.5 (s), 134.4 (s), 134.6 (s), 136.4 (s), 136.5 (d), 137.5 (s), 143.6 (s) ppm; MS (EI): 588 [M+]; HRMS calcd. for C$_{31}$H$_{24}$S$_6$ 588.923, found 588.922.

1,2-Bis[5-acetylsulfan-5'-yl-(2,2'-bithiophen-5-yl)-2-methylthieny-3-yl]cyclopentene (14) and 1-[5-acetylsulfan-5'-yl-(2,2'-bithiophen-5-yl)-2-methylthieny-3-yl]-2-[(2,2'-bithiophen-5-yl)-2-methylthieny-3-yl]cyclopentene (15)

Compound **13** (300 mg, 0.509 mmol) was dissolved in THF (15 ml) and the solution was cooled to -80 ^{o}C. To this solution was added dropwise *t*-BuLi (0.75 ml of 1.5 M solution in *n*-hexane, 1.122 mmol). After 2h, S$_8$ (32.7 mg, 1.02 mmol) dissolved in THF (3 ml) was added and the mixture was allowed to reach slowly room temperature. After 2h the reaction mixture was cooled to 0 ^{o}C and acetyl chloride (0.145 ml, 2.04 mmol) was added. After 3h the mixture was diluted with dichloromethane, washed with water and the organic phase dried (Na$_2$SO$_4$) and concentrated. Subsequent chromatography (silicagel, *n*-hexane /

72

dichloromethane 3:2) afforded compound **14** (150 mg, 40 %) and compound **15** (33 mg, 10 %) as viscous yellow oils. **14**: ^{1}H NMR (300MHz, CDCl$_3$) δ 1.99 (s, 6H), 2.08 (m, 2H), 2.42 (s, 6H), 2.83 (t, J = 7.3 Hz, 4H), 6.91 (s, 2H), 6.95 (d, J = 4.0 Hz, 2H), 7.03-7.06 (m, 4H) ppm; ^{13}C NMR (75.4 MHz, CDCl$_3$): δ 14.4 (q), 22.9 (t), 29.4 (q), 38.4 (t), 123.5 (d), 123.7 (d), 124.7 (d), 125.0 (d), 132.5 (s), 134.4 (s), 134.6 (s), 136.4 (s), 136.5 (d), 137.5 (s), 143.4 (s), 194.0 (s) ppm; MS (EI): 736 [M+]; HRMS calcd. for C$_{35}$H$_{28}$O$_2$S$_8$ 734.124, found 734.123. **15**: ^{1}H NMR (300MHz, CDCl$_3$) δ 1.98 (s, 6H), 2.07 (m, 2H), 2.42 (s, 3H), 2.82 (t, J = 7.3 Hz, 4H), 6.89 (s, 1H), 6.90 (d, 1H), 6.95 (d, J = 3.7 Hz, 2H), 7.00-7.02 (m, 1H), 7.03-7.06 (m, 3H), 7.10 (d, J = 4.0 Hz, 1H), 7.13-7.15 (m, 1H), 7.19 (m, 1H) ppm; ^{13}C NMR (75.4 MHz, CDCl$_3$): δ 14.4 (q), 23.0 (t), 29.5 (q), 38.4 (t), 123.5 (d), 123.5 (d), 123.8 (d), 124.2 (d), 124.3 (d), 124.5 (d), 124.8 (d), 125.4 (d), 127.8 (d), 132.5 (s), 132.8 (s), 134.3 (s), 134.5 (s), 134.6 (s), 134.7 (s), 135.5 (s), 136.4 (s), 136.5 (s), 136.6 (d), 137.2 (s), 137.6(s), 143.5 (s), 193.3 (s) ppm; MS (EI): 662 [M+]; HRMS calcd. for C$_{33}$H$_{26}$OS$_7$ 661.021, found 661.022.

1,2-Bis[5-(3-bromophenyl)-2-methylthien-3-yl]cyclopentene (16)

To a solution of compound **1** (500 mg, 1.52 mmol) in THF (14 ml), kept under an inert N$_2$ atmosphere, *n*-BuLi (2.5 mL of 1.6 M solution in *n*-hexane, 3.99 mmol) was added. After 1h, B(OBu)$_3$ (1.2 mL, 4.56 mmol) was added and the mixture was stirred for 1h to produce a boronic ester intermediate. In a separate flask compound 1,3-dibromobenzene (0.75 ml, 6.2 mmol), Pd(PPh$_3$)$_4$ (202 mg, 0.173 mmol), THF (10 ml), 2M Na$_2$CO$_3$(aq.) (8 ml) and ethylene glycol (10 drops) were preheated to 80 ^{o}C and the boronic ester solution was added slowly. The reaction mixture was heated under reflux overnight, diluted with diethyl ether (100 ml) and washed with water (100 ml). The aqueous layer was washed with an additional volume of ether (100 ml) and the combined organic phases were dried over Na$_2$SO$_4$ and concentrated. Purification by chromatography on silica gel (hexane) afforded compound **16** as a viscous oil (392 mg, 45 %). ^{1}H NMR (300MHz, CDCl$_3$) δ 1.99 (s, 6H), 2.09 (m, 2H), 2.84 (t, J = 7.3 Hz, 4H), 7.02 (s, 2H), 7.19-7.21 (m, 2H), 7.33-7.41 (m, 4H), 7.64 (s, 2H) ppm. ^{13}C NMR (75.4 MHz, CDCl$_3$): δ 14.4 (q), 23.0 (t), 38.4 (t), 122.9 (s), 123.9 (d), 124.8 (d), 128.2 (d), 129.7 (d), 130.3 (d), 134.7 (s), 135.4 (s), 136.5 (s), 136.8 (s) ppm; HRMS calcd. for C$_{27}$H$_{22}$S$_2$Br$_2$ 567.953, found 567.953.

1,2-Bis[5-(4-bromophenyl)-2-methylthien-3-yl]cyclopentene (17)

To a solution of compound **1** (500 mg, 1.52 mmol) in THF (14 ml), kept under an inert N$_2$ atmosphere, *n*-BuLi (2.5 ml of 1.6 M solution in *n*-hexane, 3.99 mmol) was added. After 1h, B(OBu)$_3$ (1.2 ml, 4.65 mmol) was added and the mixture was stirred for 1h to produce a boronic ester intermediate. In a separate flask 1,4-dibromobenzene (1.453 g, 6.16 mmol), Pd(PPh$_3$)$_4$ (202 mg, 0.173 mmol), THF (10 ml), 2M Na$_2$CO$_3$(aq.) (8 ml) and ethylene

73

glycol (10 drops) were preheated to 80 $^{\circ}$C and the boronic ester solution was added slowly. The reaction mixture was heated under reflux overnight, diluted with diethyl ether (100 ml) and washed with water (100 ml). The aqueous layer was extracted with an additional volume of ether (100 ml) and the combined organic phases were dried over Na_2SO_4 and concentrated. Purification by chromatography on silica gel (*n*-hexane) afforded compound **17** as a viscous oil (531 mg, 61 %). ^{1}H NMR (300 MHz, CDCl$_3$): δ 1.97 (s, 6H), 2.02-2.10 (m, 2 H), 2.81 (t, *J* = 7.5 Hz, 4H), 6.98 (s, 2H), 7.32 (d, *J* = 8.4 Hz, 4H), 7.42 (d, *J* = 8.4 Hz, 4H); ^{13}C NMR (75.4 MHz, CDCl$_3$): δ 14.4 (q), 23.0 (t), 38.4 (t), 124.4 (d), 126.8 (d), 131.8 (d), 133.4 (s), 133.6 (s), 134.7 (s), 135.0 (s), 136.8 (s), 138.4 (s) ppm; HRMS calcd. for $C_{27}H_{22}Br_2S_2$ 567.953, found 567.951.

1,2-Bis[5-(3-acetylsulfanylphenyl)-2-methylthien-3-yl]cyclopentene (18)

Compound **16** (200 mg, 0.351 mmol) was dissolved in THF (10 ml) and the solution was cooled to -80 $^{\circ}$C. To this solution was added dropwise *t*-BuLi (0.56 ml of 1.5 M solution in *n*-pentane, 0.841 mmol). After 2h, S$_8$ (22.5 mg, 0.702 mmol) dissolved in THF (3 ml) was added and the mixture was allowed to reach slowly room temperature. After 2h the reaction mixture was cooled to 0 $^{\circ}$C and acetyl chloride (0.099 ml, 1.404 mmol) was added. After 3h the mixture was diluted with dichloromethane, washed with water and the organic phase dried (Na$_2$SO$_4$) and concentrated. Purification by chromatography (*n*-hexane/dichloromethane 3:2) afforded compound **18** as a viscous oil (113 mg, 58 %). ^{1}H NMR (300MHz, CDCl$_3$) δ 1.98 (s, 6H), 2.08 (m, 2H), 2.42 (s, 6H), 2.84 (t, *J* = 7.3 Hz, 4H), 7.04 (s, 2H), 7.28 (d, *J* = 7.7 Hz, 2H), 7.38 (t, *J* = 7.7 Hz, 2H), 7.51-7.55 (m, 4H) ppm; ^{13}C NMR (75.4 MHz, CDCl$_3$) δ 14.4 (q), 23.0 (t), 30.2 (q), 37.5 (t), 124.6 (d), 124.1 (d), 128.5 (s), 129.5 (d), 131.0 (d), 132.7 (d), 134.7 (s), 135.2 (s), 135.6 (s), 136.8 (s), 138.4 (s), 193.8 (s) ppm; HRMS calcd. for $C_{31}H_{28}O_2S_4$ 560.097, found 560.096.

1,2-Bis[5-(4-acetylsulfanylphenyl)-2-methylthien-3-yl]cyclopentene (19)

Compound **16** (200 mg, 0.351 mmol) was dissolved in THF (10 ml) and the solution was cooled to -80 $^{\circ}$C. To this solution was added dropwise *t*-BuLi (0.56 ml of 1.5 M solution in pentane, 0.841 mmol). After 2h, S$_8$ (22.5 mg, 0.702 mmol) dissolved in THF (3 ml) was added and the mixture was allowed to reach slowly room temperature. After 2h the reaction mixture was cooled to 0 $^{\circ}$C and acetyl chloride (0.099 ml, 1.404 mmol) was added. After 3h the mixture was diluted with dichloromethane, washed with water and the organic phase dried (Na$_2$SO$_4$) and concentrated. Purification by chromatography (*n*-hexane/dichloromethane 3:2) afforded compound **18** as a viscous oil (101 mg, 52 %). ^{1}H NMR (500MHz, CDCl$_3$) δ 1.97 (s, 6H), 2.06 (m, 2H), 2.47 (s, 6H), 2.82 (t, *J* = 7.2 Hz, 4H), 6.97 (s, 2H), 7.20 (d, *J* = 8.4 Hz, 4H), 7.38 (d, *J* = 8.4 Hz, 4H) ppm; ^{13}C NMR (75.4 MHz, CDCl$_3$): δ 14.4 (q), 16.0 (q), 23.0 (t), 38.4 (t), 123.7 (d), 125.6 (d), 127.0 (d), 131.5 (s), 74

134.2 (s), 134.6 (s), 136.6 (s), 137.0 (s), 139.1 (s) ppm; MS (EI): 504 [M+]; HRMS calcd. for $C_{29}H_{28}S_4$: 504.108, found: 504.108.

1-(5-Chloro-2-methylthien-3-yl)-2-(2-methyl-5-phenylthien-3-yl)cyclopentene (20)

To a solution of compound **1** (2.25 g, 6.83 mmol) in THF (100 ml), kept under an inert N_2 atmosphere, *t*-BuLi (4.70 ml of 1.6 M solution in *n*-hexane, 7.51 mmol) was added. After 1h, $B(OBu)_3$ (2.77 ml, 10.3 mmol) was added and the mixture was stirred for 1h to produce a boronic ester intermediate. In a separate flask bromobenzene (2.86 ml, 13.66 mmol), $Pd(PPh_3)_4$ (0.237 g, 0.21 mmol), THF (23 ml), 2M Na_2CO_3(aq.) (18 ml) and ethylene glycol (20 drops) were preheated to 80 °C and the boronic ester solution was added slowly. The reaction mixture was heated under reflux overnight, diluted with diethyl ether (200 ml) and washed with water (200 ml). The aqueous layer was washed with an additional volume of ether (200 ml) and the combined organic phases were dried over Na_2SO_4 and concentrated. Purification by chromatography on silica gel (*n*-hexane) afforded compound **20** as a sticky oil (1.95 g, 77 %). ^{1}H NMR (300 MHz, CDCl$_3$): δ 1.94 (s, 3H), 2.05 (s, 3H), 2.08-2.16 (m, 2H), 2.78-2.89 (m, 4H), 6.68 (s, 1H), 7.05 (s, 1H), 7.30 (t, *J* = 7.0 Hz, 1H), 7.37-7.42 (m, 2H), 7.55 (d, *J* = 7.0 Hz, 2H) ppm; ^{13}C NMR (75.4 MHz, CDCl$_3$): δ 14.1 (q), 14.3 (q), 22.9 (t), 38.4 (t), 38.5 (t), 123.8 (d), 125.0 (s), 125.3 (d), 126.8 (d), 127.0 (d), 128.8 (d), 133.2 (s), 133.7 (s), 134.4 (s), 135.1 (s), 135.3 (s), 136.3 (s), 139.8 (s) ppm; MS (EI): 370 [M$^+$]; HRMS: calcd. for $C_{21}H_{19}S_2Cl$ 370.062, found 370.063.

1-[5-(3-Bromophenyl)-2-methylthien-3-yl]-2-(2-methyl-5-phenylthien-3-yl)cyclopentene (21)

To a solution of compound **20** (1 g, 2.70 mmol) in THF (35 ml), kept under an inert N_2 atmosphere, *t*-BuLi (2.13 ml of 1.5 M solution in *n*-pentane, 3.20 mmol) was added. After 1h, $B(OBu)_3$ (1.09 ml, 4.05 mmol) was added and the mixture was stirred for 1h to produce a boronic ester intermediate. In a separate flask 1,3-dibromobenzene (0.653 ml, 5.40 mmol), $Pd(PPh_3)_4$ (0.094 g, 0.081 mmol), THF (15 ml), (aq.) 2M Na_2CO_3 (10 ml) and ethylene glycol (15 drops) were preheated to 80 °C and the boronic ester solution was added slowly. The reaction mixture was heated under reflux overnight, diluted with diethyl ether (200 ml) and washed with water (200 ml). The aqueous layer was washed with an additional volume of ether (200 ml) and the combined organic phases were dried over Na_2SO_4 and concentrated. Subsequent chromatography on silica gel (*n*-hexane) afforded compound **21** as a viscous oil (0.88 g, 66 %). ^{1}H NMR (300 MHz, CDCl$_3$): δ 2.01 (s, 6H), 2.08-2.13 (m, 2H), 2.84-2.89 (m, 4H), 7.05 (s, 1H), 7.06 (s, 1H), 7.16-7.26 (m, 2H), 7.32-7.42 (m, 4H), 7.52 (d, *J* = 7.3 Hz, 2H), 7.66 (s, 1H) ppm; ^{13}C NMR (75.4, CDCl$_3$): δ 14.4 (q), 14.4 (q), 23.0 (t), 38.4 (t), 122.9 (s), 123.8 (d), 123.9 (d), 124.8 (d), 125.3 (d), 127.0

(d), 128.1 (d), 128.7 (d), 129.7 (d), 130.2 (d), 134.3 (s), 134.4 (s), 135.0 (s), 135.4 (s), 136.5 (s), 136.8 (s), 137.8 (s), 139.8 (s) ppm; HRMS: calcd. for $C_{27}H_{23}S_2Br$ 490.042, found 490.043.

1-[5-(4-Bromophenyl)-2-methylthien-3-yl]-2-(2-methyl-5-phenylthien-3-yl)cyclopentene (22)

To a solution of compound **20** (1 g, 2.70 mmol) in THF (35 ml), kept under an inert N_2 atmosphere, *t*-BuLi (2.13 ml of 1.5 M solution in *n*-pentane, 3.20 mmol) was added. After 1h, $B(OBu)_3$ (1.09 ml, 4.05 mmol) was added and the mixture was stirred for 1h to produce a boronic ester intermediate. In a separate flask 1-bromo-4-iodobenzene (1.53 g, 5.40 mmol), $Pd(PPh_3)_4$ (0.094 g, 0.081 mmol), THF (15 ml), (aq.) 2M Na_2CO_3 (10 ml) and ethylene glycol (15 drops) were preheated to 80 °C and the boronic ester solution was added slowly. The reaction mixture was heated under reflux overnight, diluted with diethyl ether (200 ml) and washed with water (200 ml). The aqueous layer was washed with an additional volume of ether (200 ml) and the combined organic phases were dried over Na_2SO_4 and concentrated. Purification by chromatography on silica gel (*n*-hexane) afforded compound **22** as a viscous oil (0.96 g, 72 %). [^1]H NMR (300 MHz, $CDCl_3$): δ 2.00 (s, 3H), 2.01 (s, 3H), 2.06-2.11 (m, 2H), 2.81-2.87 (m, 4H), 7.01 (s, 1H), 7.03 (s, 1H), 7.23-7.25 (m, 1H), 7.31-7.36 (m, 4H), 7.43-7.51 (m, 4H) ppm; [^13]C NMR (75.4, $CDCl_3$): δ 14.4 (q), 23.0 (t), 38.4 (t), 38.4 (t), 120.6 (s), 123.9 (d), 124.5 (d), 125.3 (d), 126.8 (d), 127.0 (d), 128.8 (d), 131.8 (d), 134.4 (s), 134.5 (s), 134.9 (s), 135.4 (s), 136.5 (s), 136.8 (s), 137.9 (s), 139.8 (s) ppm; HRMS: calcd. for $C_{27}H_{23}S_2Br$ 490.042, found 490.041.

1-[5-(3-Acetylsulfanylphenyl)-2-methylthien-3-yl]-2-(2-methyl-5-phenylthien-3-yl)cyclopentene (23)

Compound **21** (584 mg, 1.188 mmol) was dissolved in THF (25 ml) and the solution was cooled to -80 °C. To this solution was added dropwise *t*-BuLi (0.87 ml of 1.5 M solution in pentane, 1.307 mmol). After 2h, S_8 (38 mg, 1.188mmol) dissolved in THF (2 ml) was added and the mixture was allowed to reach slowly room temperature. After 2h the reaction mixture was cooled to 0 °C and acetyl chloride (0.17 ml, 2.376 mmol) was added. After 3h the mixture was diluted with dichloromethane, washed with water and the organic phase dried (Na_2SO_4) and concentrated. Purification by chromatography (*n*-hexane / dichloromethane 7:2) afforded compound **23** (301 mg, 52 %) as a viscous oil. [^1]H NMR (300 MHz, $CDCl_3$): δ 1.99 (s, 3H), 2.00 (s, 3H), 2.05-2.15 (m, 2H), 2.43 (s, 3H), 2.85 (t, *J* = 7.3 Hz, 4H), 7.04 (s, 1H), 7.06 (s, 1H), 7.20-7.40 (m, 5H), 7.48-7.56 (m, 4H) ppm; [^13]C NMR (75.4 MHz, $CDCl_3$): δ 14.4 (q), 23.0 (t), 30.2 (q), 38.5 (t), 123.9 (d), 124.7 (d), 125.3 (d), 126.3 (d), 126.9 (d), 128.5 (s), 128.8 (d), 129.5 (d), 131.0 (d), 132.7 (d), 134.4 (s),

134.5 (s), 134.9 (s), 135.2 (s), 135.7 (s), 136.6 (s), 136.8 (s), 138.3 (s), 139.7 (s), 193.8 (s) ppm; HRMS: calcd. for $C_{29}H_{26}OS_3$ 486.115, found 486.114.

1-[5-(4-Acetylsulfanylphenyl)-2-methylthien-3-yl]-2-(2-methyl-5-phenylthien-3-yl)cyclopentene (24)

Compound **22** (1.3 g, 2.64 mmol) was dissolved in THF (50 ml) and the solution was cooled to -80 ^{o}C. To this solution was added dropwise *t*-BuLi (1.94 ml of 1.5 M solution in pentane, 2.91 mmol). After 2h S_8 (0.085 g, 2.64 mmol) dissolved in THF (4 ml) was added and the mixture was allowed to reach slowly room temperature. After 2h the reaction mixture was cooled to 0 ^{o}C and acetyl chloride (0.38 ml, 5.28 mmol) was added. After 3h the mixture was diluted with dichloromethane, washed with water and the organic phase dried (Na_2SO_4) and concentrated. Purification by chromatography (*n*-hexane / dichloromethane 7:2) afforded compound **24** (0.67 g, 47 %) as a viscous oil. ^{1}H NMR (300 MHz, CDCl$_3$): δ 2.02 (s, 3H), 2.04 (s, 3H), 2.10-2.14 (m, 2H), 2.44 (s, 3H), 2.85-2.90 (m, 4H), 7.07 (s, 1H), 7.11 (s, 1H), 7.22-7.27 (m, 1H), 7.33-7.40 (m, 4H), 7.51-7.56 (m, 4H) ppm; ^{13}C NMR (75.4, CDCl$_3$): δ 14.4 (q), 14.5 (q), 23.0 (t), 30.1 (q), 38.4 (t), 38.5 (t), 123.9 (d), 124.9 (d), 125.3 (d), 125.8 (d), 125.9 (s), 126.9 (d), 128.7 (d), 134.3 (s), 134.4 (s), 134.8 (d), 134.9 (s), 135.4 (s), 135.6 (s), 136.5 (s), 136.9 (s), 138.5 (s), 139.7 (s), 194.1 (s) ppm; HRMS: calcd. for $C_{29}H_{26}OS_3$ 486.115, found 486.114.

4-Bromo-4'-tert-thiobutoxydiphenyl (27)

A solution of 4,4'-dibromodiphenyl (**25**) (5 g, 0.016 mol), *t*-butylthiol (1.8 ml, 0.016 mol), sodium *t*-butoxide (3 g, 0.032 mol) and Pd(PPh$_3$)$_4$ (0,56 g, 0.48 mmol) in *t*-butanol (200 ml) was heated at 65 ^{o}C under a nitrogen stream with stirring. After stirring for 4 h, the solvent was removed by rotary evaporation. From the residue the product was extracted into *n*-pentane. After washing with water, usual work-up and chromatography **27** (3.2 g, 64 %) was obtained as a white solid. M. p. 74-76 ^{o}C; ^{1}H NMR (400 MHz, CDCl$_3$): δ 1.32 (s, 9H), 7. 46 (d, *J* = 8.8 Hz, 2H), 7.51 (d, *J* = 8.8 Hz, 2H), 7.56-7.60 (m, 4H) ppm; ^{13}C NMR (75.4, CDCl$_3$): δ 31.0 (q), 39.5 (s), 99.8 (s), 126.9 (d), 128.7 (d), 132.0 (d), 137.9 (d), 138.5 (s), 139.1 (s), 141.7 (s) ppm; HRMS calcd. for $C_{16}H_{17}S_{Br}$ 320.023, found 320.024.

1,2-Bis[5-(5-(4'-(tert-butylthio)biphenyl-4-yl)thiophen-2-yl))-2-methylthien-3-yl]cyclopentene (28)

To a solution of compound **1** (200 mg, 0.607 mmol) in THF (7 ml), kept under an inert N_2 atmosphere, *n*-BuLi (0.95 ml of 1.6 M solution in *n*-hexane, 1.518 mmol) was added. After 1h, B(OBu)$_3$ (0.489 ml, 1.821 mmol) was added and the mixture was stirred for 1h to produce a boronic ester intermediate. In a separate flask **27** (390 mg, 1.214 mmol), Pd(PPh$_3$)$_4$ (70 mg, 0.061 mmol), THF (5 ml), 2M Na$_2$CO$_3$(aq.) (4 ml) and ethylene glycol

77

(5 drops) were preheated to 80 $^{\circ}$C and the boronic ester solution was added slowly. The reaction mixture was heated under reflux overnight, diluted with diethyl ether (50 ml) and washed with water (50 ml). The water layer was washed with an additional volume of ether (50 ml) and the combined organic phases were dried over Na_2SO_4 and concentrated. Purification by chromatography on silica gel (*n*-hexane) afforded compound **28** as a viscous oil (230 mg, 51 %). 1H NMR (300 MHz, CDCl$_3$): δ 1.33 (s, 18H), 2.03 (s, 6H), 2.13 (m, 2H), 2.83 (t, *J* = 7.3 Hz, 4H), 7.21 (s, 2H), 7.43 (d, *J* = 7.7 Hz, 4H), 7.57 (m, 8H), 7.62 (d, *J* = 7.7 Hz, 4H) ppm; ^{13}C NMR (75.4 MHz, CDCl$_3$): δ 14.5 (q), 23.0 (t), 31.0 (q), 39.5 (s) 38.5 (t), 99.8 (s), 124.3 (d), 125.7 (d), 126.8 (s), 127.5 (d), 134.0 (s), 134.7 (s), 134.8 (d), 134.9 (s), 136.8 (s), 138.5 (s), 139.1 (s), 141.7 (s) ppm; HRMS calcd. for $C_{47}H_{48}S_4$ 740.264, found 740.261.

1,2-Bis[5-(5-(4'-(acetylthio)biphenyl-4-yl)thiophen-2-yl)-2-methylthien-3-yl]cyclopentene (29)

To a solution of **28** (75 mg, 0.101 mmol) and 0.10 ml AcCl in 5 ml of CH_2Cl_2 under an inert atmosphere, BBr$_3$ (0.019 ml, 0.202 mmol) was added. The reaction mixture was stirred overnight after which the reaction mixture was diluted with diethyl ether (10 ml) and poured onto 5 g of ice. The phases were separated and the aqueous layer was extracted with an additional volume of ether (20 ml) and the combined organic phases were dried with Na_2SO_4 and concentrated. Purification by chromatography (*n*-pentane/dichloromethane 3:2) produced **29** (24 mg, 33%) as a transparent colorless oil. 1H NMR (300MHz, CDCl$_3$): δ 2.03 (s, 6H), 2.12 (m, 2H), 2.45 (s, 6H), 2.87 (t, *J* = 7.3 Hz, 4H), 7.10 (s, 2H), 7.47 (d, *J* = 7.7 Hz, 4H), 7.58 (m, 8H), 7.64 (d, *J* = 7.7 Hz, 4H) ppm; ^{13}C NMR (75.4 MHz, CDCl$_3$): δ 14.5 (q), 23.0 (t), 30.2 (q), 38.5 (t), 99.8 (s), 124.3 (d), 125.7 (d), 126.8 (s), 127.5 (d), 127.6 (d), 134.0 (s), 134.7 (s), 134.8 (d), 134.9 (s), 136.8 (s), 138.5 (s), 139.1 (s), 141.7 (s), 194.1 (s) ppm; HRMS calcd. for $C_{43}H_{36}O_2S_4$ 712.160, found 712.158.

1,2-Bis(2-methyl-5,2'-dithiophen-3-yl)perfluorocyclopentene (34)

A solution of **32** (2.5 g, 9.65 mmol) in dry ether (50 ml) was cooled to -80 $^{\circ}$C under a nitrogen atmosphere. *n*-Butyllithium (6.33 ml, 1.6 M solution in hexane, 10.13 mmol) was added and after 2h, octafluorocyclopentene (**33**) (0.643 ml, 4.83 mmol) was added. The reaction mixture was stirred for 2h at -80 $^{\circ}$C after which time the reaction was allowed to warm to ambient temperature. After an additional 2h, the reaction mixture was diluted with ether, washed with dilute hydrochloric acid (1 %), saturated aqueous sodium bicarbonate, and water, and extracted with ether (2 x 50 ml). The combined ether phases were then dried over Na_2SO_4, filtered and the solvent evaporated. Purification by chromatography (hexane) yielded solid compound **34** (1.1 g, 43%). Spectroscopic data were identical to those reported previously.[21]

78

1,2-Bis(5'-acetylsulfanyl-2-methyl-5,2'-dithiophen-3-yl)perfluorocyclopentene (35) and 1-(5'-Acetylsulfanyl-2-methyl-5,2'-dithiophen-3-yl)-2-(2-methyl-5,2'-dithiophen-3-yl)perfluorocyclopentene (36)

Compound **34** (1 g, 1.88 mmol) was dissolved in THF (20 ml) and the solution was cooled to -80 °C. To this solution was added dropwise t-BuLi (2.75 ml of a 1.5 M solution in *n*-pentane, 4.13 mmol). After 2h S_8 (0.120 g, 3.76 mmol) dissolved in THF (6 ml) was added and the mixture was allowed to reach slowly room temperature. After 2h the reaction mixture was cooled to 0 °C and acetyl chloride (0.53 ml, 7.52 mmol) was added. After 3h the mixture was diluted with dichloromethane, washed with water and the organic phase dried (Na_2SO_4) and concentrated. Subsequent chromatography (*n*-hexane / dichloromethane 3:2) afforded compound **35** (0.87 g, 68 %) as a main product and compound **36** (0.10 g, 9 %) as a minor product both as viscous oils. Compound **35**: ^{1}H NMR (300 MHz, CDCl$_3$): δ 1.95 (s, 6H), 2.44 (s, 6H), 7.05 (d, *J* = 3.7 Hz, 2H), 7.11 (d, *J* = 3.7 Hz, 2H), 7.15 (s, 2H) ppm; ^{13}C NMR (75 MHz, CDCl$_3$): δ 14.4 (q), 23.0 (t), 30.2 (q), 38.5 (t), 123.9 (d), 124.7 (d), 125.3 (d), 126.3 (d), 126.9 (d), 128.5 (s), 128.8 (d), 129.5 (d), 131.0 (d), 132.7 (d), 134.4 (s), 134.5 (s), 134.9 (s), 135.2 (s), 135.7 (s), 136.6 (s), 136.8 (s), 138.3 (s), 139.7 (s), 193.8 (s) ppm; HRMS: calcd. for $C_{27}H_{18}O_2S_6F_6$ 679.953, found 679.952. Compound **36**: ^{1}H NMR (400 MHz, CDCl$_3$): δ 1.95 (s, 3H), 1.96 (s, 3H), 2.43 (s, 3H), 7.02 (dd, *J* = 5.1 Hz, 3.3 Hz, 1H), 7.06 (d, *J* = 4.0 Hz, 1H), 7.10 (d, *J* = 4.0 Hz, 1H), 7.12-7.14 (m, 2H), 7.16 (s, 1H), 7.24 (dd, *J* = 5.1 Hz, 1.1 Hz, 1H) ppm; ^{13}C NMR (100 MHz, CDCl$_3$): δ 14.4 (q), 14.5 (q), 29.5 (t), 122.7 (d), 123.5 (d), 124.1 (d), 124.4 (d), 124.4 (s), 124.9 (d), 125.4 (s), 125.7 (s), 127.9 (d), 134.7 (s), 135.7 (s), 136.1 (s), 136.4 (d), 140.8 (s), 141.7 (s), 142.2 (s), 193.8 (s) ppm; HRMS: calcd. for $C_{25}H_{16}OS_5F_6$ 605.971, found 605.972.

tert-Butyl(3-iodobenzyloxy)dimethylsilane (38)

A mixture of 3-iodobenzyl alcohol (9.17 g, 39.2 mmol), TBDMSCl (7.1 g, 47 mmol), and imidazole (3.1 g, 47 mmol) was dissolved in CH_2Cl_2 (250 ml). The reaction mixture was stirred at room temperature for 2 h and then poured into H_2O. The organic layer was washed with H_2O (three times) and dried over $MgSO_4$ and the solvent removed in vacuo. The residue was filtered through a plug of silica gel to afford **38** as a clear oil (13.7 g, 100%). Spectroscopic data were identical to those reported previously.[22]

Ethoxytri-[3-tert-butyl-dimethylsilanyloxymethyl)phenyl]silane (39)

To a suspension of compound **38** (2 g, 5.74 mmol) in ether (30 ml) at -80 °C was added *n*-BuLi (3.59 ml, 5.74 mmol, 1.6 M in *n*-hexane) via a syringe. After the addition, the pale yellow slurry was stirred for 1 h and added via syringe to a precooled solution (-80 °C) of tetraethylorthosilicate (2.23 ml, 10.00 mmol) in ether (30 ml). The resulting clear solution

79

was stirred for 30 min at -78 °C and 3 h at room temperature. Subsequently, 1 N (aq.) HCl (5.74 ml, 5.74 mmol) was added. The organic layer was separated and washed with water (2x) and brine (1x). The aqueous solution was extracted with ether (2x). The combined organic fractions were dried over magnesium sulfate and filtered. Removal of the solvent in vacuo followed by flash chromatography (silicagel, n-hexane/CH_2Cl_2 1:1) gave **39** (0.80 g, 57% with respect to tetraethyl orthosilicate) as a clear oil. ^{1}H NMR (400 MHz, $CDCl_3$): δ 0.05 (s, 18H), 0.89 (s, 27H), 1.22 (t, J = 7.0 Hz, 3H), 3.84 (q, J = 7.0 Hz, 2H), 4.72 (s, 6H), 7.34 (t, J = 8.0 Hz, 3H), 7.40 (d, J = 8.0 Hz, 3H), 7.49 (d, J = 8.0 Hz, 3H), 7.54 (s, 3H) ppm; ^{13}C NMR (100 MHz, $CDCl_3$): δ -5.3 (q), 18.3 (s), 18.4 (q), 25.9 (q), 59.7 (t), 65.0 (t), 127.7 (d), 132.9 (d), 134.0 (d), 134.3 (s), 140.6 (s) ppm; HRMS: calcd. for $C_{41}H_{68}O_4Si_5$ 736.419, found 736.420.

1,2-Bis[5-(5-(tris(3-((tert-butyldimethylsilyloxy)methyl)phenyl)-silyl)-thiophen-2-yl)-2-methylthien-3-yl]cyclopentene (40)

An oven-dried 10 ml round-bottom flask was charged with **2** (46 mg, 0.109 mmol) and THF (3 ml). The solution was cooled to -80 °C. t-BuLi (0.16 ml, 1.5 M in pentane, 0.240 mmol) was added dropwise via a syringe. After the complete addition the reaction mixture was stirred at -78 °C for 2h. A precooled solution (-80 °C) of compound **39** (200 mg, 0.272 mmol) in THF (1 ml) was added dropwise via a syringe. The cooling bath was allowed to warm to room temperature overnight. The reaction mixture was poured into H_2O, and the mixture was extracted with CH_2Cl_2. The combined organic layer was dried over $MgSO_4$ and filtered, and the solvent was removed in vacuo. The residue was purified by column chromatography (n-hexane/CH_2Cl_2/t-butyl-methylether 8:2:0.025) to afford **40** (59 mg, 30%) as a slightly yellow clear oil. ^{1}H NMR (400 MHz, $CDCl_3$): δ 0.03 (s, 36H), 0.87 (s, 54H), 1.85 (s, 6H), 2.03 (m, 2H), 2.77 (t, J = 3.3 Hz, 4H), 4.71 (s, 12H), 6.95 (s, 2H), 7.13 (d, J = 7.4 Hz, 2H), 7.16 (d, J = 7.4 Hz, 2H), 7.35 (t, J = 7.4 Hz, 6H), 7.41 (d, J = 7.4 Hz, 6H), 7.48 (d, J = 7.4 Hz, 6H), 7.52 (s, 6H) ppm; ^{13}C NMR (100 MHz, $CDCl_3$): δ -5.3 (q), 18.3 (s), 18.4 (q), 25.9 (q), 59.7 (t), 65.0 (t), 124.4 (d), 124.9 (d), 127.7 (d), 130.5 (d), 131.7 (s), 132.4 (s), 132.9 (d), 134.1 (s), 134.3 (s), 134.4 (d), 134.7 (s), 135.5 (d), 136.3 (s), 137.2 (s), 140.6 (s), 145.1 (s) ppm; MS (ES): 1813.6 [M+Li]$^+$.

1,2-Bis[5-(5-(tris(3-(hydroxymethyl)phenyl)silyl)thiophen-2-yl)-thiophen-2-yl)-2-methylthien-3-yl]cyclopentene (41)

To the solution of **40** (58 mg, 0.032 mmol) in THF (10 ml) was added AcOH (0.015 ml, 0.257 mmol), followed by TBAF (1 M in THF, 0.257 ml, 0.257 mmol). The reaction mixture was stirred at room temperature for 28 h. The reaction mixture was poured into H_2O, and the mixture was extracted with EtOAc. The organic layer was washed with H_2O and brine, dried over $MgSO_4$, filtered and the solvent removed in vacuo. The residue was

80

purified by column chromatography (CH_2Cl_2/MeOH 20:1) to afford compound **41** (29 mg, 81%) as a clear oil. ^{1}H NMR (400 MHz, $CDCl_3$): δ 2.01 (s, 6H), 2.08 (m, 2H), 2.77 (t, *J* = 7.7 Hz, 4H), 4.60 (s, 6H), 5.30 (s, 12H), 6.84 (s, 2H), 7.10 (d, *J* = 3.6 Hz, 2H), 7.15 (d, *J* = 3.6 Hz, 2H), 7.36 (t, *J* = 7.0 Hz, 6H), 7.42 (d, *J* = 7.0 Hz, 6H), 7.51 (d, *J* = 7.0 Hz, 6H), 7.54 (s, 6H) ppm; ^{13}C NMR (100 MHz, $CDCl_3$): δ 14.4 (q), 29.7 (t), 38.1 (t), 65.2 (t), 124.4 (d), 125.4 (d), 128.2 (d), 128.9 (d), 131.8 (s), 132.4 (s), 134.0 (s), 134.5 (d), 134.7 (s), 135.5 (d), 136.4 (s), 139.2 (d), 140.3 (s), 145.1 (s) ppm; MS (ES): 1122.2 $[M+H]^+$.

1,2-Bis[5-(5-(tris(3-(acetylthiomethyl)phenyl)silyl)thiophen-2-yl)-2-methylthien-3-yl]cyclopentene (42)

To a solution of PPh_3 (0.642 g, 2.448 mmol) in THF (15 ml), cooled to 0 °C, was added diisopropyl azodicarboxylate (DIAD) (0.482 ml, 2.448 mmol). A white precipitate formed after stirring at 0 °C for 5 min. The mixture was stirred at 0 °C for an additional 30 min, and then a solution of compound **41** (0.152 g, 0.136 mmol) and thiolacetic acid (0.174 ml, 2.448 mmol) in THF (10 mL) was added dropwise. The reaction mixture became orange, then green, and finally brown during the addition. The flask that held **41** was rinsed with THF (2 x 5 ml), and the liquid was also added to the reaction mixture. The reaction mixture was stirred in an ice bath throughout the addition, and the ice bath was then allowed to warm to room temperature. After 18 h, the reaction mixture was poured into H_2O and extracted with EtOAc. The organic layer was washed with H_2O and brine, dried over $MgSO_4$, and filtered and the solvent removed in vacuo. The residue was purified by column chromatography on silica gel (*n*-hexane/EtOAc 2:1) to afford **42** (0.093 g, 47%) as a colorless viscous oil. ^{1}H NMR (400 MHz, $CDCl_3$): δ 1.89 (s, 6H), 2.02 (m, 2H), 2.33 (s, 18H), 2.79 (t, *J* = 8.4 Hz, 4H), 4.11 (s, 12H), 6.96 (s, 2H), 7.16 (m, 4H), 7.33 (t, *J* = 7.3 Hz, 6H), 7.39 (d, *J* = 7.3 Hz, 6H), 7.44 (d, *J* = 7.3 Hz, 6H), 7.50 (s, 6H) ppm; ^{13}C NMR (100 MHz, $CDCl_3$): δ 14.4 (q), 22.8 (q), 30.3 (t), 33.5 (t), 38.7 (t), 124.4 (d), 124.9 (d), 128.3 (d), 130.5 (d), 131.7 (s), 132.8 (s), 133.9 (s), 134.4 (s), 134.5 (s), 135.0 (d), 136.3 (d), 136.4 (s), 137.1 (s), 139.2 (d), 145.1 (s), 195.0 (s) ppm; MS (ES): 1476.3 $[M+Li]^+$.

3.7 References and Notes

[1] a) B. L. Feringa (Ed.), *Molecular Switches*, Wiley-VCH, Weinheim, **2001**; b) M. Irie, *Chem. Rev.* **2000**, *100*, 1685; c) H. Tian and S. Yang, *Chem. Soc. Rev.* **2004**, *33*, 85–97;

[2] D. Dulić, S. J. van der Molen, T. Kudernac, H. T. Jonkman, J. J. D. De Jong, T. N. Bowden, J. van Esch, B. L. Feringa, B. J. van Wees, *Phys. Rev. Lett.*, **2003**, *91*, 207402.

[3] S. J. van der Molen, H. van der Vegte, T. Kudernac, I. Amin, B. L. Feringa, B. J. van Wees, *Nanotechnology* **2006**, *17*, 310-314.

[4] a) L. N. Lucas, J. van Esch, R. M. Kellogg, B. L. Feringa, *Chem. Commun.* **1998**, 2313-2314; b) L. N. Lucas, J. J. D. de Jong, J. H. van Esch, R. M. Kellogg, B. L. Feringa, *Eur. J. Org. Chem.* **2003**, 155-166.

[5] L. N. Lucas, J. van Esch, R. M. Kellogg, B. L. Feringa, *Tetrahedron Lett.* **1999**, *40*, 1775-1778.

[6] M. Hanazawa, R. Sumiya, Y. Horikawa, M. Irie, *J. Chem. Soc., Chem. Commun.* **1992**, 206-207.

[7] a) M. Irie, T. Eriguchi, T. Takada, K. Uchida, *Tetrahedron*, **1997**, *53*, 12263-12271; b) K. Kuldová, K. Tsyganenko, A. Corval, H.P. Trommsdorff, A.T. Bens, C. Kryschi, *Synth. Met.* **2000**, *115*, 163-166.

[8] J. Reichert, H. B. Weber, M. Mayor, H. v. Löhneysen, *Appl. Phys. Lett.*, **2003**, *82*, 4137-4139.

[9] W. R. Browne, J. J. D. de Jong, T. Kudernac, M. Walko, L. N. Lucas, K. Uchida, J. H. van Esch, B. L. Feringa, *Chem. Eur. J.* **2005**, *11*, 6414-6429; W. R. Browne, J. J. D. de Jong, T. Kudernac, M. Walko, L. N. Lucas, K. Uchida, J. H. van Esch, B. L. Feringa, *Chem. Eur. J.* **2005**, *11*, 6430-6441.

[10] a) A. Blaszczyk, M. Elbing, M. Mayor, *Org. Biomol. Chem.* **2004**, *2*, 2722-2724; b) N. Stuhr-Hansen, J. B. Christensen, N. Harrit, T. Björnholm, *J. Org. Chem.* **2003**, *68*, 1275-1282.

[11] S. L. Gilat, S. H. Kawai, J. M. Lehn, *Chem. Eur. J.* **1995**, *5*, 275-284.

[12] S. M. Lindsay, *Faraday Discuss.* **2006**, *131*, 403-409.

[13] G. K. Ramachandran, T. J. Hopson, A. M. Rawlett, L. A. Nagahara, A. Primak, S. M. Lindsay, *Science* **2003**, *300*, 1413-1416.

[14] A. Peters, N. R. Branda, *Adv. Mater. Opt. Electron.* **2000**, *10*, 245-249.

[15] M. Irie, T. Lifka, K. Uchida, S. Kobatake, Y. Shindo, *Chem. Commun.* **1999**, 1487-1488.

[16] Both forms (open and closed) are photoactive when UV light is employed.

[17] J. Areephong, W. R. Browne, B. L. Feringa, *Org. Biomol. Chem.* **2007**, *5*, 1170-1174.

[18] At room temperature the photostationary state corresponds to more than 99 % of the switch in the closed form. At low temperatures the content of the closed form should not change, since ring closure is not affected, and ring opening is diminishing.

[19] a) M. Irie, T. Eriguchi, T. Takada, K. Uchida, *Tetrahedron*, **1997**, *53*, 12263-12271; b) K. Kuldová, K. Tsyganenko, A. Corval, H.P. Trommsdorff, A.T. Bens, C. Kryschi, *Synth. Met.* **2000**, *115*, 163-166.

[20] C. Strässler, N. E. Davis, E. T. Kool, *Helv. Chim. Acta* **1999**, *82*, 2160-2171.

[21] T. Saiko, M. Irie, T. Shimidzu, *J. Chem. Soc. Chem. Commun.* **1994**, 2123-2124.

[22] H. Jian, J. M. Tour, *J. Org. Chem.* **2003**, *68*, 5091-5103.

Chapter 4

Photo- and Electrochemical Properties of SAMs of Diarylethenes on Gold: Nanoparticles and Bulk Electrodes

This chapter deals with photochemical and electrochemical studies of self-assembled monolayers (SAMs) of diarylethenes on surfaces of gold nanoparticles and bulk gold electrodes. The photochemical properties of three structurally distinct diarylethenes self-assembled on the surface of gold nanoparticles are described first. These diarylethenes with their switching unit linked to the surface via a conjugated aromatic spacer show linker-dependent switching behavior. For the switch with the phenyl linker both photochemical ring opening and closure is observed while for the thienyl linker ring closure does not take place. Subsequently, the photochemical and electrochemical properties of SAMs of the three diarylethenes on bulk gold electrodes are reported. The photochemical and electrochemical switching between the open and closed forms was examined and found to be sensitive to the molecular structure of the switch. For the three diarylethenes, the electrochemical behavior with respect to electrochemical ring opening/closure is retained in the SAMs. In contrast, their photochemical properties resemble those of the SAMs on gold nanoparticles. The stability of the monolayers towards desorption following photochemical and electrochemical switching was examined through electrochemistry and X-ray photoelectron spectroscopy.[*]

4.1 Introduction

In Chapter 2, photoswitching of electrical conductivity by placing diarylethene based switches between the contacts of metal electrodes was demonstrated. Both, the Mechanically Controlled Break-Junction (MCBJ) experiments[1] and Scanning Tunneling Microscopy (STM) experiments[2] have revealed that when molecules **3** and **6** (see Chapter 2), respectively, are covalently connected to gold electrodes, they can be switched only from the closed to the open form. In contrast to the behavior of **3** and **6** in solution, the ring closure reaction is prohibited for molecules bound to gold surfaces. The lack of the ring closure reaction was attributed to the quenching of the excited state of the molecules with gold.[1] Density functional theory (DFT) calculations suggested that the quenching of the ring closure reaction may result from the alignment of Fermi-level of gold with the HOMO energy level of the open isomers. The deep lying HOMO level at a high metal density of states offers the opportunity for many possible electron transfer events, thus reducing the lifetime of the hole created after an excitation.[3] In order to overcome problems with quenching, several new diarylethene derivatives have been synthesized (see Chapter 3) bearing different spacer units. Once molecules are anchored onto gold electrodes these spacer units connecting the central photochromic unit with the terminal anchoring groups can influence the extent of electronic interactions of the switching unit with gold.

MCBJ and STM offer a unique opportunity to investigate single molecules. However, they are expensive and time consuming experiments and preparation of samples does not allow for fast screening of molecular properties. This prompted us to use a fast and reliable method to test the photochromic properties of molecules attached to a metal. The aim of the research described in this chapter is to explore the photochromic properties of diarylethenes self-assembled as monolayers on surfaces of gold nanoparticles[4] and bulk gold electrodes. These model systems may help us to better understand events happening at the molecule-metal interface of nanoelectrodes. It might hence fill the gap between solution-phase measurements and molecular device techniques that demand expensive and time consuming nanofabrications. Secondly, it is of great importance to investigate redox properties of self-assembled monolayers (SAMs) of diarylethenes formed on gold in order to explore how the redox properties are influenced by anchoring. Also it has been shown that cyclic voltammetry can be used as a read-out technique to follow photochromic interconversions of diarylethenes.[5]

4.2 SAMs of Diarylethenes on Gold Nanoparticles

4.2.1 Introduction to Gold Nanoparticles

Metal nanoparticles are fascinating objects of scientific research mainly due to their unique size-related properties. They occupy the intermediate region between dimensions of single atoms or small molecules and bulk matter. It has been predicted that nanoparticles in the diameter range of 1-10 nm would display electronic properties, reflecting the electronic band structure of the nanoparticles, owing to quantum-mechanical rules.[6] The important consequence is that in nanoparticles, there is a gap between the valence band and the conduction band, in contrast to bulk metals. The resulting physical properties are neither those of bulk metal nor those of molecular compounds, but they strongly depend on the particle size.[7]

Nanoparticles exhibit distinct optical properties. The most prominent feature is the surface plasmon excitation.[8] In gold, this gives rise to an intense transition in the visible region.[8] The sensitivity of the plasmon frequency to the environment of the nanoparticle, opens the way for application of such particles as sensors.[9]

Another important feature of nanoparticles is their high surface-to-volume ratio. Small particles have a large proportion of their atoms at the surface with a lower coordination number than bulk atoms. Bare nanoparticles are thus very unstable because of their extremely high surface reactivity. This inherent instability of nanoparticles, which results in their aggregation and subsequent precipitation from the dispersion, can be circumvented through surface-passivation by self-assembled monolayers (SAMs) of organic molecules (especially alkanethiols and amines).[10,11] By functionalizing SAMs, it is also possible to convey various additional useful properties to the particles, for example, specific packing and self-assembly, special optical and electrical properties, the recognition of chemical and biological molecules, etc.[12,13,14,15,16]

4.2.1.1 Standard Approaches Leading to Organic-Ligand Functionalized Gold Nanoparticles

In principle, ligand functionalized gold nanoparticles can be prepared using two general strategies;

1 Organic ligands encapsulating gold nanoparticles might be replaced by other organic ligands in exchange reactions.[17]

> 2 Nanoparticles might be grown by reduction of Au-salt in the presence of ligands.[18]

For the first approach the most commonly used strategy is based on citrate reduction of HAuCl$_4$ (*vide infra*) where the citrate acts as a reducing agent as well as a stabilizing ligand. If the second approach is employed it is usually referred as to the Brust-Schiffrin method (*vide infra*).

4.2.1.1.1 Citrate Reduction

Among the conventional methods of synthesis of gold nanoparticles by reduction of gold(III) derivatives, the most popular one for a long time has been that using citrate reduction of HAuCl$_4$ in water, which was introduced by Turkevitch in 1951.[19] It leads to nanoparticles of ca. 20 nm. In an early effort, reported in 1973,[20] to obtain nanoparticles of desired size (between 16 and 147 nm) via their controlled formation, a method was proposed where the ratio between the reducing/stabilizing agent (trisodium citrate) to the gold salt was varied. This method is often used even now when a rather loose shell of ligands is required around the gold core in order to prepare a precursor to valuable nanoparticle-based materials. More recently, a practical preparation of sodium 3-mercaptopropionate-stabilized gold nanoparticles was reported in which simultaneous addition of citrate salt and an amphiphile surfactant was adopted; the size could be controlled by varying the stabilizer/gold ratio.[21]

4.2.1.1.2 The Brust-Schiffrin Method

The stabilization of gold nanoparticles with alkanethiols was first reported in 1993 by Mulvaney and Giersig, who showed the possibility of using thiols of different chain lengths.[22] The Brust-Schiffrin method for gold nanoparticle synthesis, published in 1994,[18] has had a considerable impact on the overall field in less than a decade, because it allowed the facile synthesis of thermally stable and air-stable nanoparticles of reduced dispersity and controlled size for the first time (ranging in diameter between 1.5 and 5.2 nm). Indeed, these gold nanoparticles can be repeatedly isolated and redissolved in common organic solvents without irreversible aggregation or decomposition, and they can be easily handled and functionalized just as stable organic and molecular compounds. The technique of synthesis uses the thiol ligands that strongly bind gold due to the soft character of both Au and S.[18,23] In a two-phase reaction system, AuCl$_4^-$ is transferred from the aqueous phase to toluene using tetra-*n*-octylammonium bromide (TOAB) as the phase-transfer reagent and reduced by NaBH$_4$ forming nanoparticles that are weakly stabilized by tetra-*n*-

octylammonium bromide (Scheme 1). In the presence of thiols, tetra-*n*-octylammonium bromide is instantaneously replaced by thiol molecules (Scheme 1).
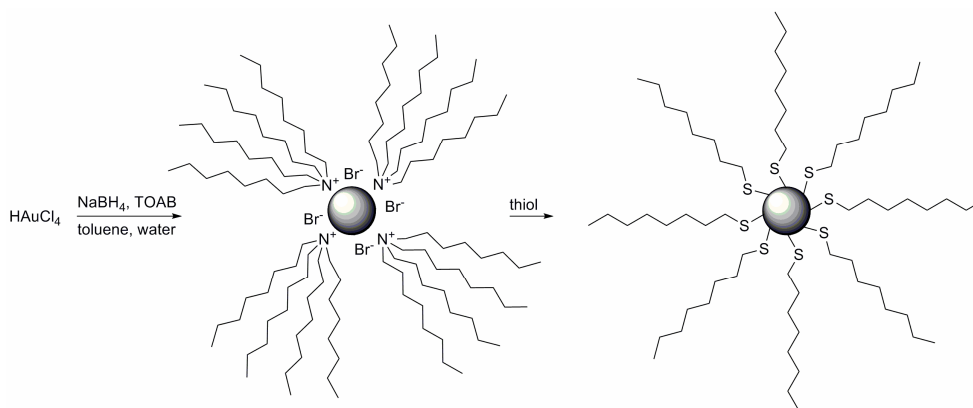
Scheme 1 *Formation of gold nanoparticles coated with organic shells by reduction of Au^{III} compounds in the presence of thiols.*

The transmission electron microscopy (TEM) images show that the diameters of gold nanoparticles prepared in such a way using dodecanethiol as a ligand are in the range 1-3 nm, with a maximum in the particle size distribution at 2.0-2.5 nm.[18] Subsequently, many publications appeared describing the use of the Brust-Schiffrin procedure for the synthesis of other stable gold nanoparticles of this kind that contained functional thiols.[24] It has been shown that the proportion thiol:AuCl$_4^-$ used in the synthesis controls the size of the gold nanoparticles[24] (for instance, a 1:6 ratio leads to a maximum average core diameter of 5.2 nm with a core diameter dispersity of ± 10%).

4.2.1.2 Characterization Techniques

The most common characterization technique is high-resolution transmission electron microscopy (HRTEM), which gives an image of the gold core of the AuNPs,[22,25] but the core dimensions can also be determined using scanning tunneling microscopy (STM), atomic force microscopy (AFM), small-angle X-ray scattering (SAXS),[24c,26] laser desorption ionization mass spectrometry (LDI-MS),[27] and X-ray diffraction.[28] A detailed high-resolution study of the nanoparticle shape using HRTEM revealed that the truncated cuboctahedron predominated, and that decahedra, dodecahedra and icosahedra were also present in the same preparation of alkanethiol-stabilized AuNPs.[10] The histogram providing the size distribution of these cores gives crucial information on the dispersity of the sample that is usually obtained from TEM pictures.[10] The mean diameter, *d*, of the cores allows

determination of the mean number of gold atoms, N_{Au}, in the cores:[10] $N_{Au} = 4\pi(d/2)^3/v_{Au}$. For instance, with $d = 2.06$ nm, $NAu = 269$.[29]

The UV-Vis and IR spectra provide an identification of the ligand that is also confirmed by ^{1}H NMR spectroscopy, except that the ligand atoms close to the core give broad signals.[24d,30] The NMR spectra are informative for the part of the ligand remote from the core. IR spectroscopy shows that, as in SAMs,[31] the thiolate ligands of gold nanoparticles adopt the all trans conformations, with 5-25% of gauche defects at both inner and terminal locations.[24c,30a]

4.2.2 Concept for Fast Screening of Photochromic Behavior of Diarylethenes Anchored on Gold Using Gold Nanoparticles

In this section, a study of photochromic properties of dithienylethene derivatives anchored to gold nanoparticles is reported, showing spacer-dependent uni- and bi-directional light induced switching. In particular, assembly of these molecules on gold nanoparticles (Scheme 2) might provide a useful model system mimicking molecule-gold electrode interactions. The reason why this approach is convenient for fast screening of different photochromic molecules is the solubility of nanoparticles in organic solvents and a relatively high ratio between anchored molecules and gold atoms. This enables easily accessible analytical tools to be employed (*vide supra*) such as absorption spectroscopy in order to study photochromic interconversions of the anchored diarylethenes on gold surfaces.
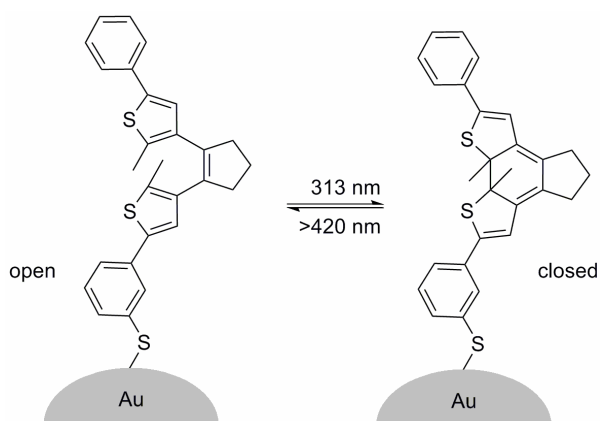
Scheme 2 *Schematic depiction of photoisomerization between the open and closed form of a diarylethene switch anchored on gold nanoparticles.*

90

In a recent paper dealing with the photochemistry of dithienylethenes attached to gold nanoparticles,[32] the photochromic unit was isolated from the metal core to some extent by an alkyl chain. The same held for related studies concerning other types of photoswitches.[33] In these cases electronic interactions between chromophores and metal cores were limited due to the spacing between them and the photochromic behavior was retained. However, if one wants to exploit photochromic switches and build up electronic devices, in order to make those molecular switching devices feasible, low on-state resistances (and high on-off ratios) are essential. This requires a certain level of communication between the metal electrodes and the switching unit. Such molecules have been described in Chapter 3. Consequently a photoswitching unit of these molecules interacts with a gold nanoparticle core and as a result of these interactions photochromic behavior might be modified or completely quenched (for the limitations of photochromic reactions of diarylethenes in the presence of bulk gold, see Chapter 2).

Among the compounds described in Chapter 3, **6**, **21** and **22** (Scheme 3) were chosen to study the photochromic behavior of diarylethenes on gold nanoparticles. Compounds **6**, **21** and **22,** with one acetyl-protected thiol group, are suitable candidates for functionalization of gold nanoparticles. When deprotected switch **6** is anchored to the flat surface of bulk gold, its photochromic reversibility is not preserved (for details see Chapter 2). This makes it an ideal candidate for comparing the effects of chromophore interactions with bulk surfaces *versus* nanoparticle surfaces. Furthermore, molecules **21** and **22** offer a possibility to test the effect of different positions of the anchoring group on the switching efficiency. The *meta* di-substituted phenyl spacer of **21** connects the central switching unit with the thioacetate group in a crossly conjugated fashion, whereas the *para* di-substituted phenyl of **22** acts as a linearly conjugated spacer.
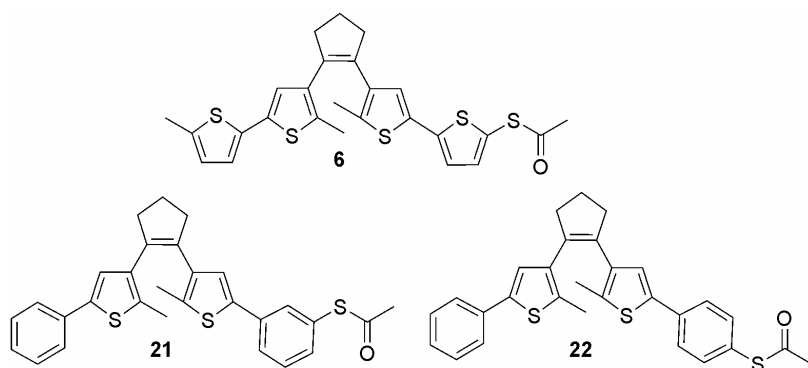

Scheme 3 *Molecular structures of dithienylethene molecular switches **6**, **21** and **22**.*

91

All three compounds **6**, **21** and **22** (for the synthesis and characterization, see Chapter 3) display typical photochromic behavior in solution. The initially colorless open isomers in toluene became colored when exposed to light with a wavelength of 313 nm (for more details on photochromic reactions in solution see Chapter 3). Similarly, the reverse process occurs upon irradiation with visible light (>420 nm) and the original open isomers are reformed, thus demonstrating the reversibility of the overall process.[34]

4.2.3 Synthesis of Diarylethene Functionalized Gold Nanoparticles

Monolayer-protected gold nanoparticles **Au-6o**, **Au-6c**, **Au-21o**, **Au-21c**, **Au-22o** and **Au-22c** were prepared by a modified Brust-Schiffrin's two-phase procedure[35] (Scheme 4). Acetyl- protected thiol groups of compounds **6**, **21**, **22** in both open and closed forms, were deprotected with ammonium hydroxide in THF under an inert atmosphere immediately before the nanoparticle preparation in order to avoid undesired oxidative dimerization. The preparation itself was performed in a mixture of toluene and water containing $HAuCl_4$, TOAB, deprotected thiol and $NaBH_4$. Purification of nanoparticle samples is essential since any traces of unbound switches could affect the photochemical experiments. Multiple precipitation or size-exclusion chromatography methods were employed to obtain a clean sample of nanoparticles free from thiols and TOAB. The purity of the nanoparticles was checked by ^1H NMR spectroscopy by monitoring the disappearance of the sharp adsorptions of the unbound switches. Although both methods lead to high purity, the multiple precipitation results in significant losses due to the partial solubility of the modified nanoparticles in appropriate solvents.
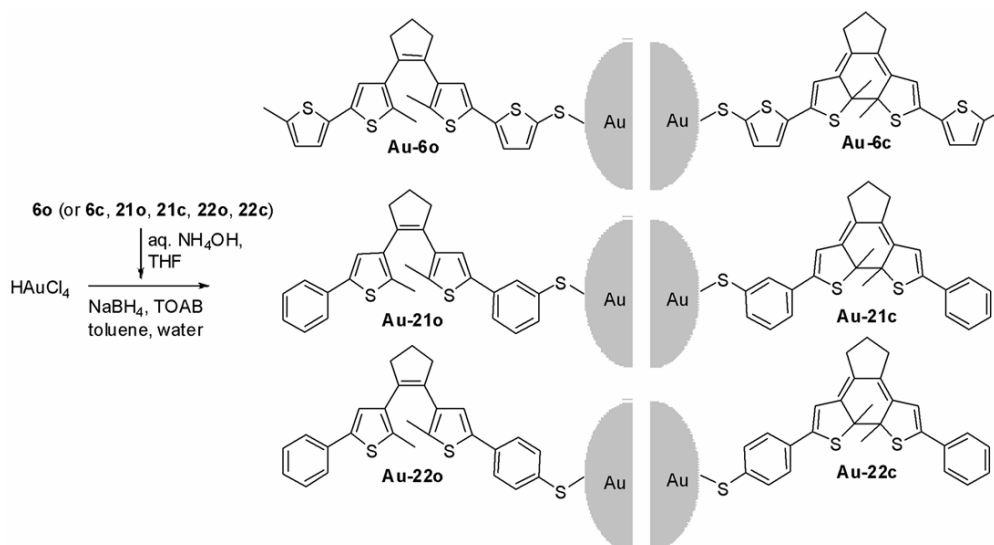
Scheme 4 *Synthesis of gold nanoparticles coated with a shell composed of the open and the closed forms of diarylethene photochromic switches by reduction of Au^{III}: the suffix o = open and c = closed form*

4.2.4 Transmission Electron Microscopy of Diarylethene Functionalized Gold Nanoparticles

Transmission electron microscopy was used to investigate the size of the functionalized gold nanoparticles. Samples for TEM experiments were prepared by dropcasting and blotting of a dilute dichloromethane solution on a carbon-coated Cu-grid. A typical micrograph of gold nanoparticles (**Au-6o**) (Figure 1) shows clearly the presence of small gold nanoparticles. The average diameter, established by TEM, was 2 nm. The size distribution is rather broad. The smallest size reaches a diameter of 0.6 nm and the largest nanoparticles have a diameter of 5 nm. Areas with a different distribution of nanoparticles can be observed within the same sample. In Figure 1a randomly distributed individual gold nanoparticles can be seen as well as small domains constituted of a few tens of nanoparticles. Besides individual molecules and small domains, large areas of organized nanoparticles are present within the same sample (Figure 1b). Hexagonal arrangement can be recognized although the variable size of nanoparticles induces packing defects. The average distance between two nanoparticle edges, as observed by TEM, is ~3.6 nm that is twice the size of compound **6**. This indicates the presence of the organic shell encapsulating nanoparticles.
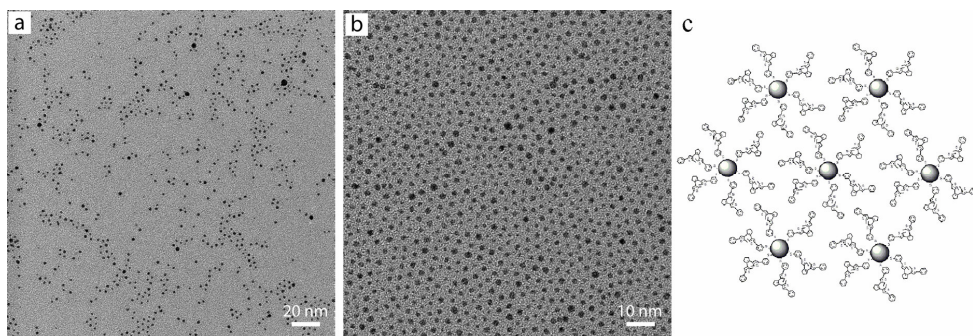
93

Figure 1 *a) and b) Representative TEM images of **Au-6o**, deposited on a carbon-coated Cu-grid film by drop-casting from a dilute toluene solution. An average size of gold nanoparticles is 2.0 nm. c) A schematic representation of the hexagonal arrangement of SAM modified Au nanoparticles.*

4.2.5 IR-Characterization of Organic Shell Encapsulating Nanoparticles

The nature of the organic shell encapsulating the nanoparticles was confirmed by reflectance FT-IR spectroscopy, showing similar spectral bands characteristics compared to those of unattached molecules (Figure 2). The absorption at 1710 cm^{-1} in the representative spectra of the open and closed forms of compound **21** (Figure 2a and 2c) was assigned to the C=0 stretching mode of the thioacetyl group. The absence of this absorption in the spectra of **Au-21o** and **Au-21c** (Figure 2b and 2d) is consistent with the loss of the acetyl group upon chemisorption on the gold nanoparticle surface. Instead of the absorptions at 1710 cm^{-1}, new absorptions with lower intensities are visible at 1730 cm^{-1}, which were previously obscured in unbound **21** by the more intense absorptions at 1710 cm^{-1}. These peaks are typical adsorption bands present in diarylethene switches.[36]
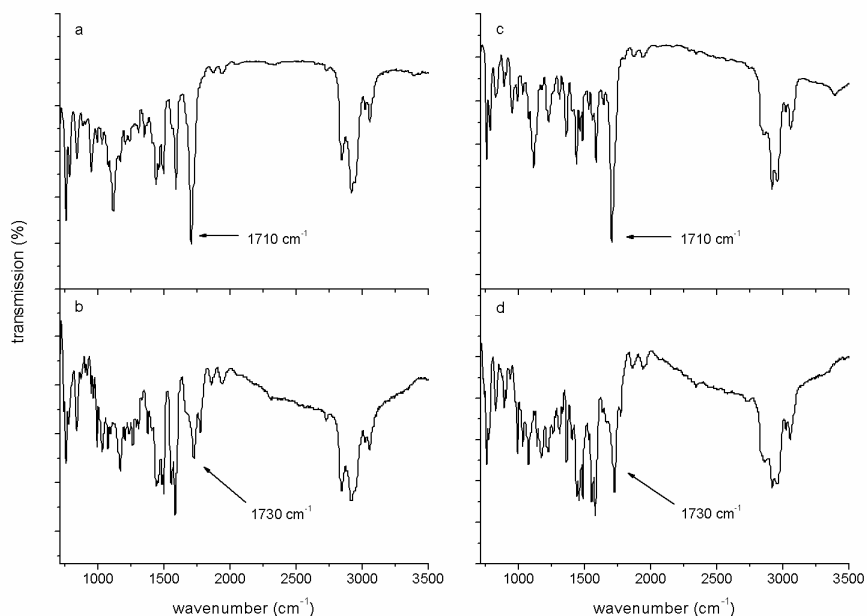
94

Figure 2 Representative FT-IR spectra of *21o* (a) and *Au-21o* (b). FT-IR spectra of *21c* (c) and *Au-21c* (d).

4.2.6 Photochromic Behavior of Surface Bound Diarylethenes on Gold Nanoparticles

Figure 3a shows absorption spectra of the **Au-21o** cluster in toluene (Scheme 4). Its absorption is a superposition of the spectral bands of the organic shell and a broad absorption of the gold nanoparticles, extending from the UV into the visible region. An additional absorption at 525 nm corresponds to the surface plasmon absorption which is typical for gold nanoparticles of 2 nm diameter in dimension.[37] Upon irradiation with light of 313 nm, the visible spectral band increases and a new maximum is found at 558 nm, indicating the formation of the closed isomer. Compared to the unbound molecules, the ring closure process is less efficient. The quantum yield[38] of this process was found to be 0.07, which should be compared to 0.4 for the unattached molecule (Table 1). Spectral characteristics and light-induced transformations of **Au-22o** are similar to those observed for **Au-21o** with the same quantum yield. The absorption profile of **Au-6o** resembles the absorption profiles of **Au-21o** and **Au-22o** with an UV absorption maximum at 336 nm. In

95

contrast to **Au-21o** and **Au-22o**, cluster **Au-6o** does not show any absorption changes upon irradiation with 313 nm light. The quantum yield (<<0.01, Table 1) reflects this observation. Further attempts to employ light with different wavelengths, ranging from 220 nm to wavelengths in the far visible region in order to overcome an unexpected inhibition of the photoreaction failed. This indicates that each excitation of the molecules, arising from light absorption, is effectively quenched by the presence of the gold core and does not lead to photoreaction.

*Figure 3 UV/Vis spectra of a) **Au-21o**, b) **Au-22o** and c) **Au-6o** measured in dry toluene before (—) and after (---) irradiation at 313 nm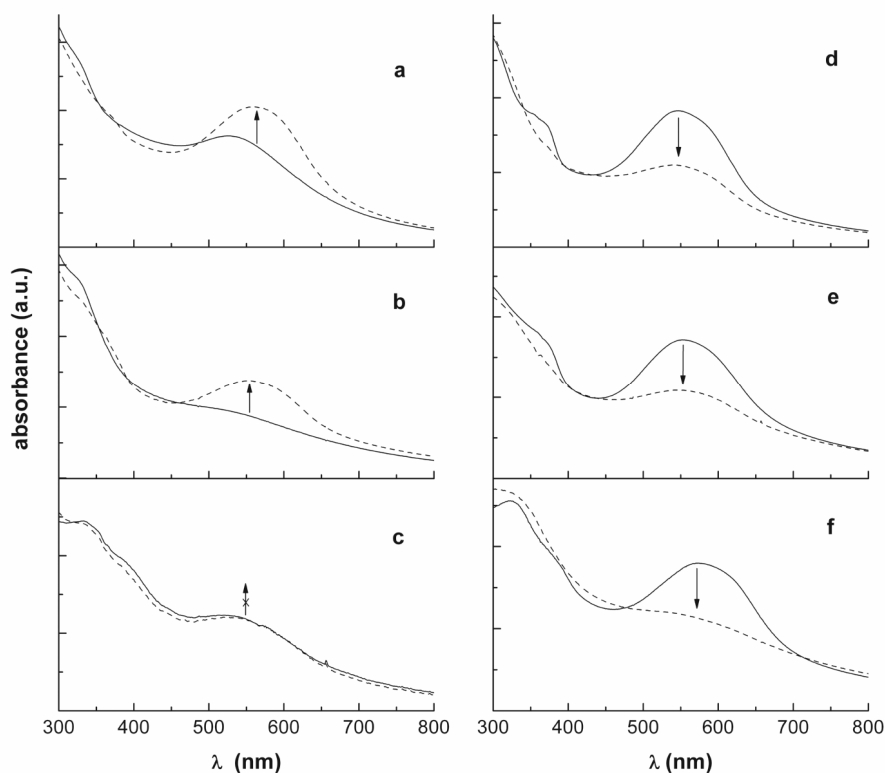. UV/Vis spectra of d) **Au-21c**, e) **Au-22c** and f) **Au-6c** measured in dry toluene before (—) and after (---) irradiation at >420 nm.*

In contrast to the ring closure process, ring opening does not vary going from the phenyl to the thiophene spacer. All three clusters **Au-21c**, **Au-22c** and **Au-6c** exhibit a decrease in

absorption around 560 nm (Figure 3), demonstrating that opening of the switching unit takes place.

Table 1 *Quantum yields of the ring closure reaction (excitation at 315 nm). The first column gives the relevant systems, the second the quantum yields of ring closure and the third the position of the maximum of the lowest-energy absorption band in the difference spectra.*

Compound	Quantum yield Φ (open $\rightarrow$ closed)	Maximum absorption λ_{max} (abs) [nm] closed form
21o	0.4 ± 0.1	536
22o	0.4 ± 0.1	540
6o	0.4 ± 0.1	560
Au-21o	0.07 ± 0.03	567
Au-22o	0.07 ± 0.03	567
Au-6o	$\ll 0.01$	-

Nevertheless, the efficiency of the ring-opening process is also slowed down compared to molecules in solution, just as was observed in the case of the ring closure of **Au-21o** and **Au-22o**. A number of factors probably contribute to this phenomenon including a reduced effective interaction with light due to the restricted motion in a packed monolayer and a deteriorated transparency of the medium due to the presence of light absorbing clusters. However, the most important contribution is presumably partial and, in the case of the **Au-6o** ring closure, complete quenching of the excited state. Quenching of the excited states of organic chromophores anchored to gold nanoparticles is well known and usually attributed to resonance energy transfer.[39] In energy transfer the efficiency of the process is related to the strength of the coupling between chromophores. This strength is determined by the proximity of energy states. As the HOMO-LUMO gap of **6o** is expected to be smaller, compare to that of the **21o** and **22o**,[40] we can reasonably assume that its LUMO lies closer to the lowest unoccupied states of gold nanoparticles, so that mixing is stronger. We suggest that this effect is at the origin of the differences in the observed switching quantum yields. More detailed studies of the quenching mechanism are currently under investigation. The fact that ring closure of **Au-21o** and **Au-22o** has the same quantum yield indicates that the effect of linear- versus cross-conjugated attachment does not play an important role in the switching efficiency on gold.

The observed photochromic behavior of compound **6** anchored on gold nanoparticles corresponds to its behavior on bulk flat gold surfaces (Chapter 2). More generally, it shows that monolayer-protected gold colloids form a convenient tool for fast screening of

properties of functional molecules grafted on gold surfaces. Subsequently, it might be anticipated that compound **21** and **22** retain their reversible photochromic behavior when anchored on bulk gold. This will be further explored for compound **21** in the following section 4.3 and Chapter 5.

4.3 SAMs of Diarylethenes on Bulk Gold Electrodes

4.3.1 Introduction

The electronic properties of redox active π-conjugated systems are of continuing interest[41] due to their potential application in the development of molecular based organic-electronic and -photonic devices.[42] Of particular interest in the latter area are photochemically active (photochromic) molecular systems,[43] such as spiropyran-,[44] diarylethene-[45] and azo-benzene-[46] based systems that exhibit readily accessible redox chemistry. The ability to harness the rich and, importantly, reversible photo- and redox-chemistry of molecular systems[47] requires that the functionality observed in solution is retained once immobilized on electroactive surfaces such as noble metals,[48] and semiconductor surfaces.[49]

A detailed understanding of 'hard/soft' interface phenomena using photo- and electro-active molecular switches is crucial to the development of molecular-based photonic devices.[2] It has been recently demonstrated that dithienylethene-based switches can be employed to form self-assembled monolayers (SAMs) on ITO glass, which enables both read and write/erase functions in a non-destructive manner.[49] Notably, the photo- and electrochemistry of the immobilized switches is comparable with that observed in solution. The effect of immobilization of similar dithienylethene photochromic switches on gold nanoparticles (see section 4.2), and Au-surfaces has shown that the metallic surface can influence the photochemical properties of the switches profoundly and is highly dependent on the nature of the linker group connecting the diarylethene switch to the surface. Employing optical spectroscopy it was demonstrate that compound **6o** shows inhibition of ring closure on gold nanoparticles, whilst the related compound **21o** showed photochemical ring opening and closure comparable to that observed in solution, albeit with a reduced photochemical efficiency. Furthermore Scanning Tunneling Microscopy (STM) has demonstrated reversible photo-induced switching of individual diarylethenes (**21**) immobilized as mixed monolayers (with alkylthiols) to a Au(111) surface[45c] (also see Chapter 5).

In this section, cyclic voltammetry and X-ray photoelectron spectroscopy (XPS) is employed to characterize the self-assembled monolayers (SAM) of dithienylethene (**6, 21**

and **36**, Scheme 5) switches on gold electrodes. Parameters of particular interest in this context are the surface coverage (Γ) of the diarylethene molecules, the stability of the monolayers with respect to both electrochemical and photochemical ring opening and closure reactions, and the influence of the spacer units, connecting central switching unit with anchoring thiol groups, on their photochemical reactivity; factors which may provide a deeper insight into the nature of the electronic interaction between the chemisorbed molecules and the gold surface.
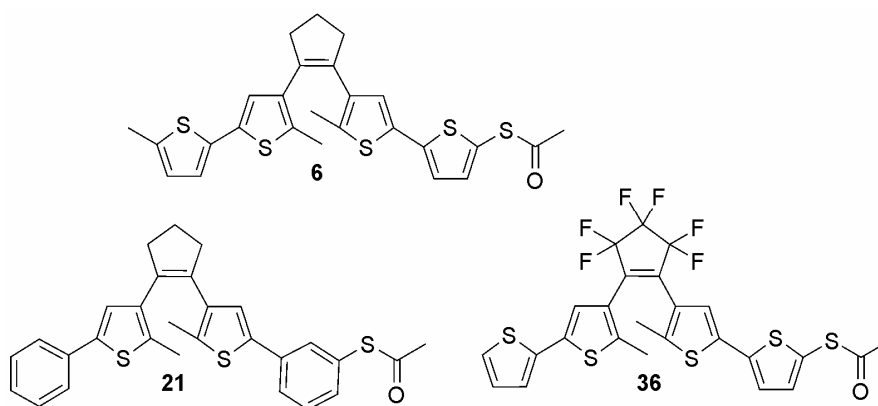
Scheme 5 *Molecular structures of dithienylethenes molecular switches **6**, **21** and **36**.*

All compounds **6o**, **21o** and **36o** convert readily to the closed states, i.e., **6c**, **21c** and **36c** respectively, upon irradiation in solution (toluene) with λ_{exc} 313 nm and revert to the open state upon irradiation with visible light (> 420 nm) (for more details, see Chapter 3).

4.3.2 Cyclic Voltammetry: Principles and Setups

Cyclic voltammetry[50] is a type of potentiodynamic electrochemical measurement. To obtain a cyclic voltammogram, the potential at an electrode is varied continuously at a steady rate and the change in current is measured with respect to the change in voltage. It is a specific type of voltammetry used for studying the redox properties of electroactive compounds in solution and interfacial structures.

Generally, when two electrodes are placed in an electrolyte solution and a voltage is applied, the electrolyte will conduct electricity. Lone electrons normally cannot pass through the electrolyte; instead, a heterogeneous electron transfer reaction occurs at the cathode consuming electrons from the cathode, and another heterogeneous electron transfer reaction occurs at the anode producing electrons to be taken up by the anode. As a result, a

negative charge cloud develops in the electrolyte around the cathode, and a positive charge develops around the anode. The ions in the electrolyte move to neutralize these charges so that the reactions can continue and the current can keep flowing. The electrolyte is employed so that ion migration of the redox active species is minimal as well as it makes the solution conductive.

In a cyclic voltammetry experiment, as in other controlled potential experiments, a potential is applied to the system, and the current (Faradaic + non-Faradaic current) response is measured (a Faradaic current is the current due to a redox reaction). The current response over a range of potentials (a potential window) is measured, starting at an initial value and varying the potential in a linear manner to a pre-defined limiting value i.e. the switching potential. At this potential the direction of the potential scan is reversed, and the same potential window is scanned in the opposite direction. This means that, for example, species formed by oxidation on the first (forward) scan can be reduced on the second (reverse) scan. This technique is commonly used, since it provides a fast and simple method for initial characterization of a redox-active system. In addition to providing an estimate of the redox potential, it can also provide information about the rate of heterogeneous electron transfer between the electrode and the analyte, and the stability of the analyte in different oxidation states (e.g., do they undergo subsequent chemical reactions)

For the majority of experiments the electroactive species is dissolved in a solution. The method uses a reference electrode, working electrode, and counter electrode (also called the secondary or auxiliary electrode). Electrolyte is usually added to ensure sufficient conductivity and prevent charge migration of the analyte double layer. The combination of the solvent, electrolyte and specific working electrode material determines the range of the potential.

The potential is measured between the reference electrode and the working electrode and the current is measured between the working electrode and the counter electrode. These data are then plotted as current (i) vs. potential (E) (Figure 4). The electroactive compound is initially present typically in the most stable oxidation state. The voltage scan starts at the open circuit potential (*i.e.* the potential where no current flows) and hence, there is only a non-Faradaic current response to solvent reorganization at the working electrode. As the voltage approaches the oxidation potential of the analyte E_p a Faradaic current begins to flow indicating that the molecule is being oxidized depending on the scan direction employed. The current continues to rise (exponentially). This is known as the kinetic region of the voltammogram. As the voltage increases, the rate of reaction also increases until a point is reached when the process becomes limited by the mass transfer of the analyte from the bulk to the electrode surface. The current then begins to fall and a peak is produced. As

100

the voltage sweep is reversed, the oxidized material that is in the vicinity of the electrode is reduced resulting in a reduction peak of similar magnitude. This reduction peak will usually have a similar shape to the oxidation peak. As a result, information about the redox potential and electrochemical reversibility of the analyte are obtained.
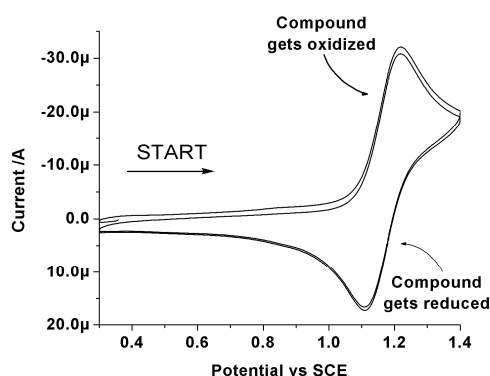

Figure 4 *A typical cyclic voltammogram.*

If the electronic transfer at the surface is fast and the current is limited by the diffusion of species to the electrode surface, then the current peak will be proportional to the square root of the scan rate.

The initial electrode potential (E_i) is set in a region where no reaction occurs. The potential is then scanned in the forward direction at a given scan rate (v) such that it can be determined at any given time t by the relationship;

$E(t) = E_i - v\,t$

All redox processes taking place during a potential sweep result in the appearance of current peaks. Assuming that the heterogeneous electron transfer reaction kinetics are very fast compared to the scan rate, the equilibrium involving the concentrations of reduced and oxidized species at the electrode surface will adjust rapidly according to the Nernst equation;

$E = E_o + RT/nF \ln C_O /C_R$

Where C_O and C_R represent the surface concentrations of oxidized and reduced species. If the system is diffusion controlled (the normal situation for cyclic voltammetry) then Fick's law of diffusion holds for both O and R. Under these conditions, the peak current (i_P) is given by the Randles Sevcik equation;

101

$$I_P = 2.69 \times 10^5 \, n^{3/2} \, A \, D_O^{1/2} \, v^{1/2} \, C_O$$

where A is the electrode area (cm^2), n is the number of electrons transferred, C_O is the concentration (mol.cm^{-3}) and v is the scan rate (volt/s).

The relationship for the reverse scan in the cyclic voltammogram is given by;

$$E = E_i - 2 \, v \, \lambda + v \, t$$

where λ is the time at which the potential is reversed. The shape of the reverse scan is therefore dependent on E_i (the switching potential) and the kinetics of the actual system under test.

4.3.2.1 Electrochemical cell and electrodes that can be used in cyclic voltammetry experiments

An electrochemical cell consists of at least two electrodes and one electrolyte solution. An electrode may be considered to be an interface at which the mechanism of charge transfer changes between electronic (movement of electrons) and ionic movement of ions. An electrolyte is a medium through which charge transfer can take place by the movement of ions.

In a cell used for electroanalytical measurements there are always three electrode functions. The first of the three electrodes is the working electrode. This is the electrode at which the electrochemical phenomena being investigated takes place. The second functional electrode is the reference electrode. This is the electrode whose potential is constant enough that it can be taken as the reference standard against which the potentials of the other electrodes present in the cell can be measured. The final functional electrode is the counter or auxiliary electrode, which serves as a source or sink for electrons so that a current can be passed from the external circuit through the cell. In general, neither its true potential nor current is ever measured or known.

4.3.2.1.1 Working electrodes

Noble metal indicator electrodes:

There are a number of noble metal electrodes currently available for voltammetric studies. In order of frequency of use, they are platinum, gold and silver followed occasionally by palladium, rhodium and iridium. Various polycrystalline forms including sheets, rods and wires are commercially available in high purity and the materials are readily machined into useful shapes. All of the noble metals have a low overpotential for hydrogen evolution. All of the noble metals adsorb hydrogen on their surfaces although gold does so to a lesser

102

extent. Palladium adsorbs hydrogen into the bulk metal in appreciable quantities and is not recommended for use as a cathode in protic solvents.

Carbon indicator electrodes

As an inert electrode material, carbon is useful for both oxidation and reduction in both aqueous and nonaqueous solutions. Only graphitic forms of carbon conduct and are therefore useful as electrode materials. Ordinary spectroscopic grade graphite rods can be used in which the surface area of the electrode does not need to be well defined. Other types of carbon electrode include the vitreous (glassy) carbon electrode and the carbon paste electrode.

4.3.2.1.2   Reference electrodes

The ideal reference electrode should posses the following properties: i) it should be reversible and obey the Nernst equation with respect to some species in the electrolyte, ii) its potential should be stable with time, its potential should return to the equilibrium potential after small currents are passed through the electrode, iii) if it is an electrode like the Ag/AgCl reference electrode, the solid phase must not be appreciably soluble in the electrolyte, iv) it should show low hysteresis with temperature cycling.

One of the most common reference electrodes is the KCl saturated calomel half cell (SCE). A simple form of this electrode can be assembled by adding to a tube, mercury metal, a small amount of solid mercury (II) chloride, several grams of solid KCl and some distilled water. Connection to the external measuring circuit can be made by using a fine platinum wire dipping into the mercury pool.

4.3.3 Cyclic Voltammetry and Electrochemical Switching of Diarylethenes in Solution

It has been recently shown that diarylethenes can undergo a ring closure or ring opening *via* electrochemical oxidation and subsequent reduction.[5c-e] The driving force for ring closure is stabilization of the monocation through (partial) delocalization of the charge on the second ring. Where the communication between the rings is poor the stabilization achieved does not compensate for the loss of ring stabilization (aromaticity), and hence ring opening of the monocation/dication of the closed form is favored.

The solution redox properties of compounds **6c**, **21c** and **36c** in both open and closed forms are detailed in Table 2. As expected for both **6o** and **21o** an irreversible oxidation process (Figure 5) is observed at ~1.0-1.1 V, which results in efficient ring closure to yield (on re-reduction) **6c** and **21c**, respectively. For **21c** and to a lesser extent **6c**, two resolved

103

reversible one-electron oxidation waves are observed at ~0.2-0.6 V. For **36o** an irreversible oxidation at 1.3 V is observed, which, in contrast to related hexafluorocyclopentene based switches,[5c,e] leads to partial cyclization to **36c**$^{2+}$ and (upon re-reduction) **36c**.

Table 2 *Electronic redox data of compounds* **6c**, **21c** *and* **36c**.

compound	$E_{p,a}$[a] vs SCE [V]	compound	$E_{1/2}$[a] vs SCE [V]
6Ho	0.985	**6Hc**	0.330, 0.395
21Ho	1.180	**21Hc**	0.405, 0.480
36Fo	1.310	**36Fc**	0.745, 0.805

[a] in CH_3CN/0.1 M $LiClO_4$
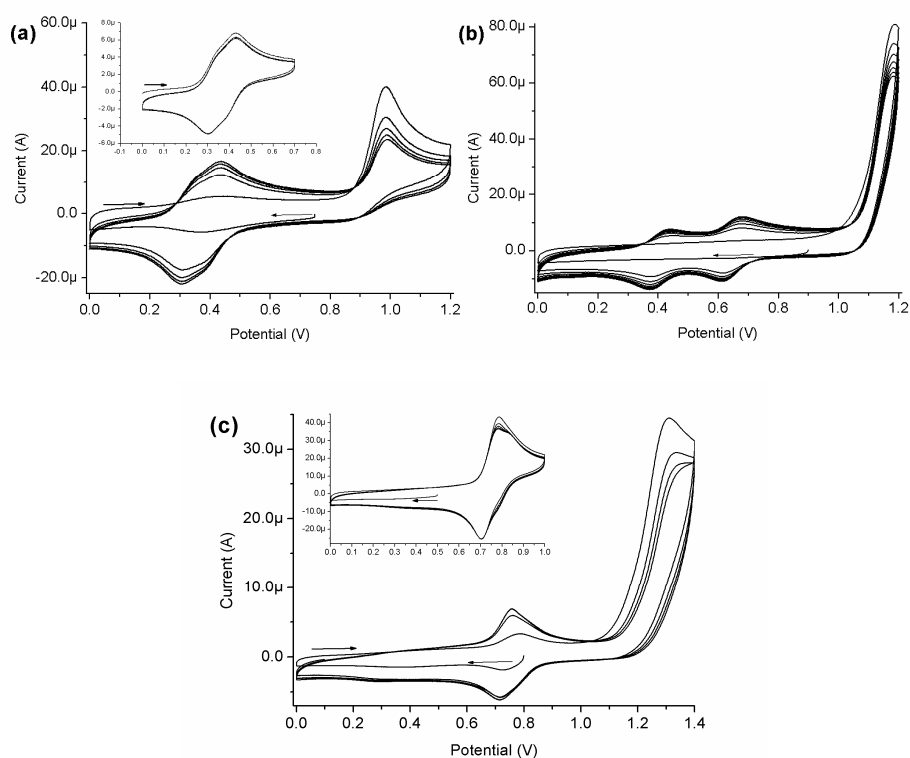
Figure 5 *Cyclic voltammetry in* CH_3CN/ *0.1 M* $LiClO_4$ *(vs SCE) of a)* **6o** *(0.5 V s*$^{-1}$ *inset:* **6c**, *0.1 V s*$^{-1}$*) b)* **21o** *(0.5 V s*$^{-1}$*) c)* **36o**, *0.1 V s*$^{-1}$*; inset:* **36c**, *0.5 V s*$^{-1}$*. Glassy carbon working electrode and platinum wire counter electrode.*

104

Overall the electrochemical properties of **6c**, **21c** and **36c** are in agreement with those observed for their symmetric analogues[5e] and the electrochemical relationships involved are outlined in Figure 6.
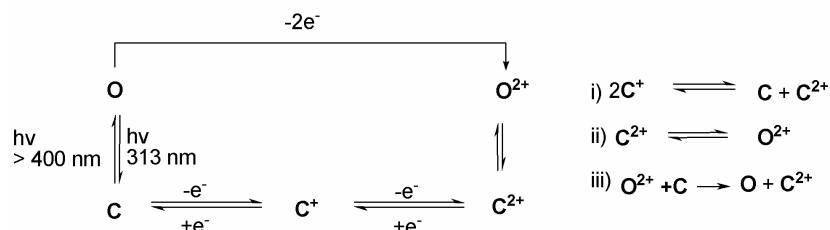

Figure 6 *Schematic diagram for electrochemical processes observed for diarylethene-based switches and reactions leading to electrochemical ring closure and ring opening i) disproportionation of C^+ to C and C^{2+}, ii) equilibrium between open (o) and closed (c) state of the dicationic switch and iii) oxidation of the closed form by the open dication. Arrows indicate chemical reversibility only.[5c,e]*

4.3.4 Electrochemically Driven Switching of 6o and 6c SAMs

Self-assembled monolayers of **6o** and **6c** were formed on both gold bead electrodes and on gold coated glass slide electrodes. The surface coverage was found to be independent of whether **6o** or **6c** was used in the formation of the SAM ($\Gamma = 0.7$ x 10^{-10} mol cm^{-2}) and as expected for a SAM the current varied linearly with scan rate. For SAMs of **6o** an irreversible oxidation is observed at ~1.0 V, which results in the formation of **6c**$^{2+}$ and upon re-reduction **6c** (Figure 6, Figure 7a and b). At low overpotentials for the oxidation of **6o** repetitive cyclic voltammetry results in ring closure with minimal oxidative damage to the underlying gold surface of the bead electrodes, i.e. the capacitance of the electrode is the same before and after ring closure (Figure 7c). Even at high scan rates loss of signal intensity for **6c** was observed upon repetitive cycling between 0.0 and 0.8 V. The loss in signal intensity (assigned to **6c**) is not due to desorption of the SAM but rather to very slow ring opening via the dicationic species (Figure 6). Indeed a complete recovery of the redox wave of **6c** is observed upon cycling between 0 and 1.4 V (vs SCE). Photolysis of **6o** SAMs with UV light did not result in the formation of the ring closed isomer **6c**, in stark contrast to the behavior observed for this compound in solution. Photolysis of **6c** SAMs with visible light (> 400 nm) controlled by repetitive cycling leads to the slow decrease of the signal intensity. However, this decrease of the signal intensity was assigned to decomposition of the SAMs by repetitive cycling. Weak photochemical activity of **6c** might still be present, however cannot be detected.
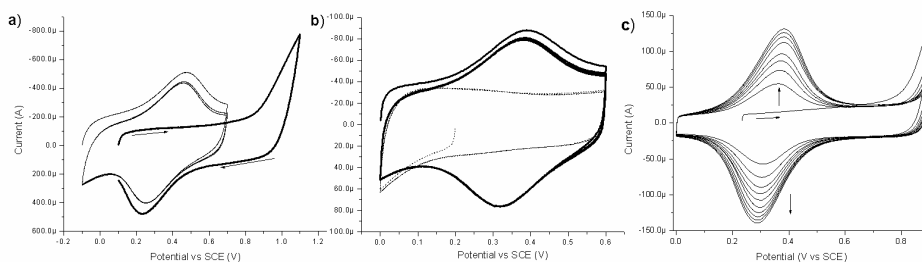
105

Figure 7 *Cyclic voltammetry of **6o** modified gold bead electrodes. a) Single cycle at 100 V s^{-1} for **6o** SAM on a gold bead electrode (thick line) and subsequent cyclic voltammetry between –0.1 and 0.70 V (thin line). b) Cyclic voltammetry (at 20 V s^{-1}) of **6o** modified gold bead electrode between 0.0 and 0.8 V before (thin line) and after (thick line) electrochemical ring closure. c) Repetitive cyclic voltammetry of a **6o** modified gold bead electrode between 0.0 and 0.90 V vs SCE at 1 V s^{-1}. Cyclic voltamograms are uncompensated for solution resistance.*

4.3.5 Electrochemical and Photochemical Opening of 36c SAMs.

Self-assembled monolayers of **36o** and **36c** where formed on both gold bead electrodes and on gold coated glass slide electrodes. The surface coverage of the gold bead **36c** SAMs ($\Gamma =$ 1.1 x 10^{-10} mol cm^{-2}) were found to be similar to those of **6o/6c**. The cyclic voltammetry and photochemistry observed on both substrates were essentially identical and the surface confinement of the redox process observed for **36c** on a gold bead electrode was verified by the linear current (I) dependence on scan rate (1-20 V s^{-1}) and comparison with the scan rate dependence of the non-Faradic current (i.e., the current at 0.2 V, Figure 8).
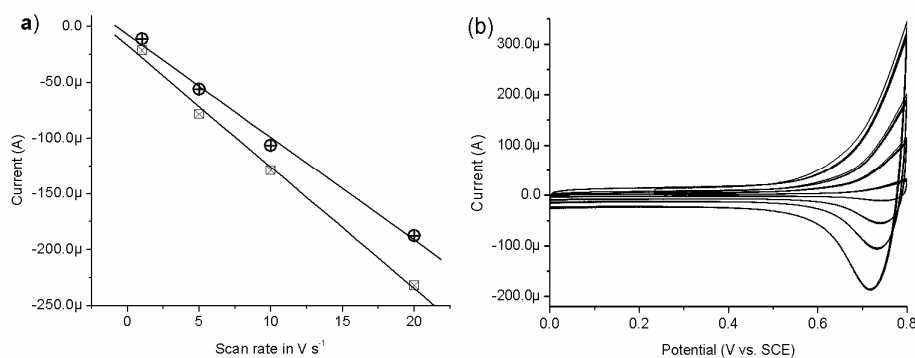
106

Figure 8 *a) Scan rate dependence of the non-Faradic (I ×10, at 0.2 V vs SCE, circles) and Faradic (0.75 V vs SCE, squares) currents of a **36c** SAM on a gold bead electrode, r^2 for linear fits > 0.99. b) Cyclic voltammetry of **36c** SAM on a gold bead electrode at 1, 5, 10 and 20 V s^{-1}.*

At high scan rates and low overpotentials (< 0.8 V vs. SCE) the redox response of **36c** was found to be stable[49] allowing for monitoring of the effect of irradiation on the **36c** modified electrodes by cyclic voltammetry (Figure 9). UV and visible irradiation of the surface of both the gold bead and gold coated glass slide electrodes shows minimal effect with no change to the surface capacitance or XPS spectra (*vide infra*, Figure 9). Irradiation of a **36c** SAM modified gold bead with visible light (> 400 nm) resulted in a steady depletion of the intensity of the redox wave at 0.8 V, Figure 9, due to photochemical ring opening to form **36o** (*vide infra*). On the other hand photolysis of **36o** SAMs with UV light did not result in the formation of the ring closed isomer **36c.**
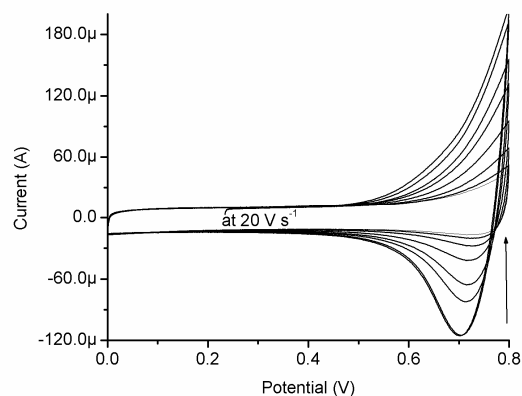
Figure 9 *Photolysis of a 36c SAM on a gold bead electrode with visible light (> 400 nm) monitored by cyclic voltammetry (each scan taken at 3 min time intervals).*

At lower scan rates (< 1 V s^{-1}) the intensity of the redox signal is reduced significantly over repeated cycling compared to that observed at high scan rates. At higher switching potentials, i.e. 0.9 or 1.0 V, a steady decrease in signal intensity is observed even at higher scan rates. Indeed, extended repetitive cycling at 1 V s^{-1} between 0.0 and 0.8 V results in a complete loss in signal intensity, as seen in Figure 10b. As for irradiation, however, the loss in signal is not due to desorption of the SAM. XPS analysis (*vide infra*) before and after visible irradiation and before and after slow repetitive cyclic voltammetry demonstrates that the sulfur-gold bond of the monolayer remains intact. Furthermore, cyclic voltammetry between 0 and 1.6 V indicates that in both cases the SAM has been converted from the closed form **36c** to the open form **36o** (Figure 11).
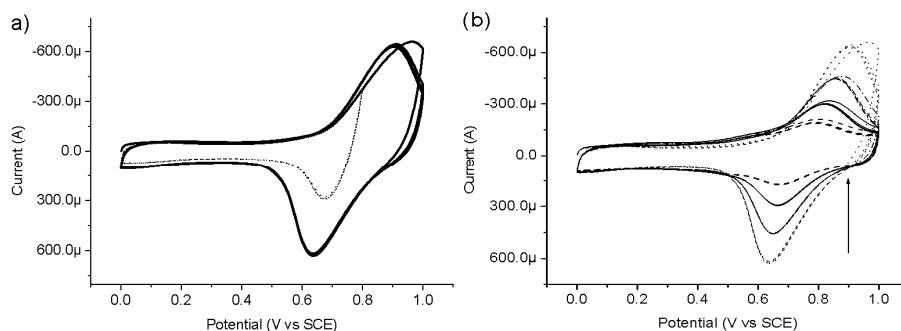
Figure 10 *Effect of switching potential and scan rate on the stability of the cyclic voltammetric response of a **36c** SAM on a gold bead electrode. a) Cyclic voltammetry of **36c** SAM modified gold bead electrode at 20 V s^{-1} between 0.0 and 0.8 V (dashed line) and 0.0 and 1.0 V (solid line). b) Cyclic voltammogram of a **36c** SAM at 20 V s^{-1} showing decrease in signal intensity after each set of 50 cycles at a scan rate of 1 V s^{-1}.*
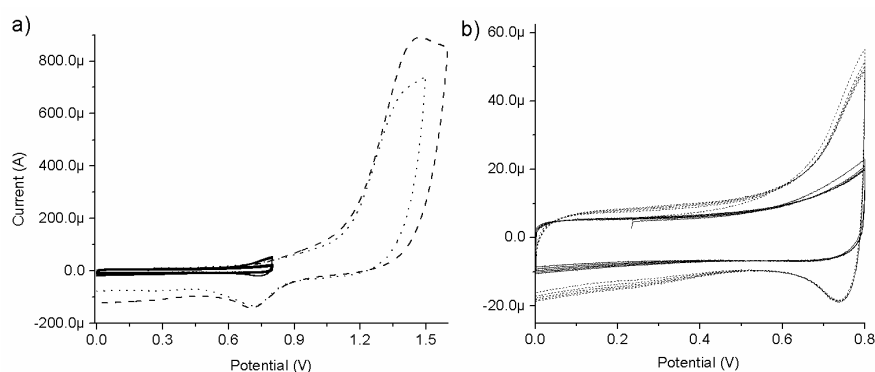

Figure 11 *a) Cyclic voltammetry of **36c** SAM modified gold bead electrode after visible irradiation (dashed) and a **36o** SAM modified electrode (dotted and solid) In CH$_3$CN/LiClO$_4$ 0.1 M vs SCE at 20 V s^{-1}. b) Cyclic voltammogram between 0.0 and 0.8 V before and after cyclic voltammetry of photochemically opened **36c** SAM between 0.0 and 1.6 V).*

As with cyclic voltammetry in solution (Figure 5), oxidation of the open form **36o**, leads to the formation of **36c** upon re-reduction. However, after a single cycle to 1.6 V, the recovery of the signal of **36c** is low indicating that ring closure is incomplete. The oxidation to 1.6 V results in some disturbance of the SAM (i.e. an increase in electrode capacitance), however

109

after ~10 min the cyclic voltammetric response between 0.0 and 0.8 V stabilized (Figure 12) and visible irradiation of the gold bead electrode to reopen the **36c** SAM could be repeated (Figure 12: inset). These results are in agreement with the behavior of this compound in solution. Overall oxidation of **36c** SAMs in the closed state leads to ring opening (e.g., **36c** → **36o**) as observed in solution.[5c,e] In principle there is an equilibrium between the open and closed dicationic species **36c**$^{2+}$ and **36o**$^{2+}$ (Figure 6), and oxidation of the open state SAM at a high scan rate leads to partial conversion of the SAM to the ring closed state. However, in solution the chemical stability of **36o**$^{2+}$ is poor and irreversible decomposition of **36o** is observed upon electrochemical oxidation.[5c,e] Hence although some electrochemically induced ring closure is observed, it is a minor process, due to the fact that the equilibrium between **36c**$^{2+}$ and **36o**$^{2+}$ favors the open dication and the reduction of the dicationic species must be carried out at a faster rate (i.e., at high scan rates) than decomposition of **36o**$^{2+}$ occurs.
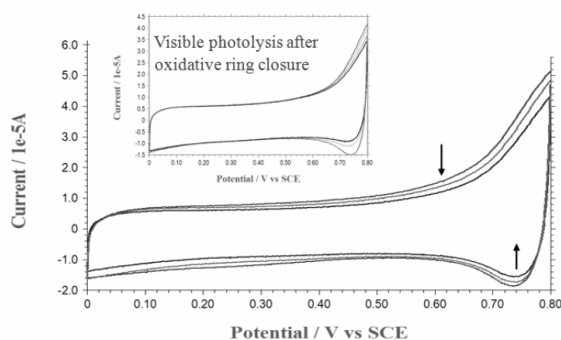

Figure 12 *Cyclic voltammetry of **36c** modified gold electrode after visible photolysis and subsequent electrochemical ring closure. Inset: visible photolysis of the electrochemically closed monolayer.*

4.3.5.1 *X-ray photoelectron spectroscopy (XPS)*

XPS measurements were performed on monolayers of **36o** and **36c** on gold coated glass slides to characterize the stability of the SAMs after oxidative cyclic voltammetry and photochemical ring opening. The corresponding XPS data are presented in Table 3.

110

Table 3 *XPS data for gold coated glass slide electrodes with self assembled monolayers of* ***36o***, ***36c*** *and a* ***36o*** *modified electrode after electrochemical ring closure*

compound	S 2p	S / F	S / Au
36o	163.8 (80.9 %)		
	162.5 (19.1 %)	69.6 %	30.4 %
36c	163.6 (79.0 %)		
	162.5 (21.0 %)	67.4 %	24.8 %
36o after oxdative cyclic voltammetry between 0.0 and 1.6 V (see Figure 10)	163.6 (77.7 %)		
	162.3 (22.3 %)	69.3 %	25.0 %

The carbon region of the XPS spectra (not shown) was not analyzed quantitatively due to the possibility of contamination in air. The S 2p core level region of both **36o** and **36c** shows two clear contributions, one where the S $2p_{3/2}$ is found at 162.5 eV and which is assigned to sulfur bound to gold,[51] and the other component with the S $2p_{3/2}$ peak at (163.7±0.1) eV, which is attributed to the thiophene sulfurs.[52] Signals at binding energies of 168.5 eV were not observed indicating that oxidized species of sulfur were not present in the sample.[53] Importantly, after electrochemical oxidation at 1.6 V (Figure 11) of **36o** SAMs, the S 2p core level region presents the same characteristics, highlighting the fact that degradation of the SAM is not significant during electrochemical switching of the molecules. Furthermore, the S/F ratio is not modified, which indicates that the chemical integrity of the molecules is preserved. The S/F value extracted from the spectra is slightly lower than the expected 80% value due to attenuation of S 2p photoelectrons.[54] Oxidation of **36o** SAMs does not modify the measured S/Au ratio substantially, indicating that the molecules do not desorb after application of such a potential sweep. Finally, analysis of the XPS spectra acquired after oxidative desorption of **36o** and **36c** SAMs did not show the presence of fluorine (a peak at 687.0 eV was not observed),[55] sulfur or oxidized sulfur on the gold substrate. This indicates that all molecules are desorbed by oxidation above 1.6 V over prolonged periods (30 s to 1 min at constant potential). Thus we can conclude that SAMs of diarylethene derivatives on gold are stable with respect to the electrochemical and photochemical ring opening and closing experiments described above, but can undergo desorption when oxidized for prolonged periods to the cationic state.

4.3.6 Electrochemical and photochemical switching of 21o and 21c SAMs.

The surface coverage of **21** on gold bead electrodes (Γ = 1.5 x 10^{-10} mol cm^{-2}, Figure 13) is as expected and compares well with that obtained for **6** and **36** SAMs. The linear dependence of current on scan rate confirms the surface confined nature of the redox

111

processes observed and the stability of the SAM of **21c** with regard to both ring opening and desorption was found to be excellent at scan rates above 1 V s^{-1} between 0 and 0.55 V (Figure 13).
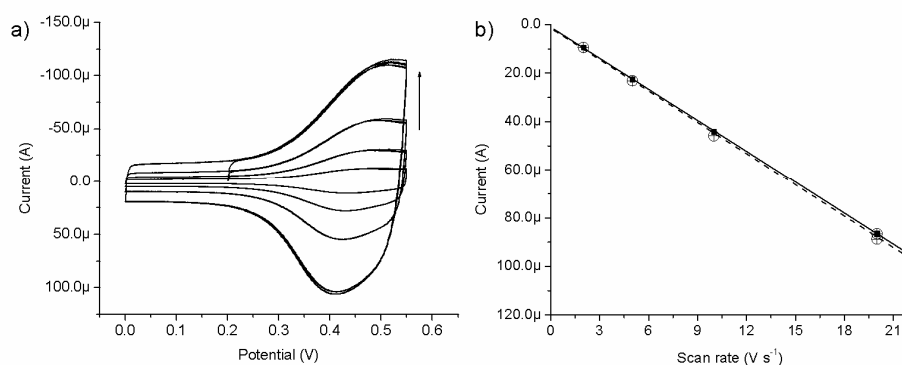

Figure 13 *Left: cyclic voltammetry of **21c** on a gold bead electrode at, 2, 5, 10 and 20 V s^{-1}. Right: current scan rate dependence of cathodic current at 0.1 (scaled by 5 for comparison) and 0.42 V.*

As observed in solution, electrochemical oxidation of **21o** results in the formation of **21c** (after re-reduction of **21c**$^{2+}$), Figure 14. Oxidation of a **21c** SAM to the dicationic state, although not resulting in immediate desorption, leads to loss in signal intensity (Figure 14). However, on gold the loss is sufficiently slow to allow for electrochemical ring opening of **21c** SAMs to be observed similar to that observed previously on ITO.[49]
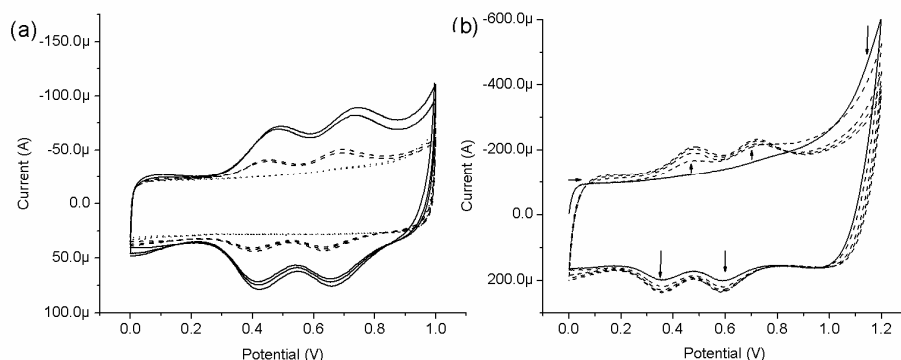
112

Figure 14 *a) Cyclic voltammetry (0.0-0.8V) of **21o** SAM on gold after irradiation at 312 nm (solid line), after subsequent electrochemical ring opening (by repetitive cycling between 0.0 and 0.9 V at 0.1 V s^{-1}) (dotted line) and closing (dashed line, closed by cycling, see Figure 13b); (b) electrochemical ring closure by cycling between 0.0 and 1.2 V at 100 V s^{-1}, Faradaic processes (i.e. due to **21c**) are not present on the first anodic scan (solid line) but appear on subsequent cycles (dashed line).*

The **21o** SAMs have been shown, by XPS, to be stable with respect to desorption, upon photochemical ring closure under ambient conditions.[45c] In contrast to both **6o** and **36o**, irradiation of **21o** modified gold beads with 312 nm light leads to the formation of **21c** (Figure 14a). The SAM on Au can be converted back to the **21o** state by irradiation with visible light (> 400 nm) (not shown) or by electrochemical ring opening.

4.3.7 Discussion

The surface coverage of the SAMs of the dithienylethene on gold lies in the range of 0.5-1.5 x 10^{-10} mol cm^{-2}, which is typical for molecules of this size.[56] For **6c**, **21c**, and **36c** the width at half height of the voltammetric waves is 160-220 mV, which is much broader than the ideal 90.6 mV for a one electron process, however, the linearity of the slope of i_p/v (using $i_p = n^2F^2\,vA\Gamma*/4RT$) confirms that both oxidation and reduction are of surfaced-immobilized species. For **21c** it is apparent that oxidation to the dicationic state involves two sequential one electron oxidation steps. For both **6c** and **36c** the single redox wave would indicate the possibility of a two-electron process being involved, however, in both cases two sequential one electron process are expected to take place by comparison with solution chemistry.[5c,e] The stability of the SAMs formed on gold bead and plate electrodes under extended electrochemical and photochemical conditions was found to be good, however, prolonged oxidation to the cationic forms resulted in desorption of the SAMs.

113

4.4 Conclusions

In conclusion, the photochromic behavior of three diarylethene switches directly linked to gold nanoparticles via an aromatic spacer has been investigated in section 4.2. Depending on the spacer uni- (compound **6**) or bi-directionality (compounds **21** and **22**) has been observed. This demonstrates that small changes in the molecular structure, leading to the variation of the alignment of HOMO/LUMO with the energy states of gold nanoparticles, can have an enormous impact on the overall photochemistry.

In section 4.3 the immobilization of the thiol-terminated dithienylethenes, in both the open and the closed form, as SAMs on gold plate and bead electrodes has been carried out for three structurally distinct examples. SAMs of compound **6** did not show any photoactivity whereas ring opening process is preserved for SAMs of **36** and SAMs of **21** show reversible photoactivity in both directions. It is apparent that the distance of a photoactive compound from the gold surface does not determine, to a first approximation, the magnitude of quenching of photochemical reactivity of the compounds by the surface since in all cases this distance is similar. The packing of all three compounds in the SAMs is similar, as observed from the measurements of capacitance, therefore the differences in observed photochemical activities are not due to the different packings. The differences in observed photochemical activities for different molecules should therefore depend mainly on the nature of the spacer employed (thienyl vs. *meta*-phenyl) but also the molecular structure itself (i.e., hexfluoro- vs. hexahydro-cyclopentene). Overall it may be concluded that in immobilizing photoactive molecular systems on gold does not, markedly, result in perturbation of the electrochemical properties of the compound. Indeed electrochemistry offers an excellent approach for not only characterizing and controlling photoactive SAMs, but allows for highly sensitive non-destructive readout of the molecular state of the SAM.

Both approaches, functionalized gold nanoparticles and electrochemical readout of the molecular state of photochromic compounds, offer a new route towards non-expensive and fast screening of photochemical properties of photoactive compounds anchored on gold surfaces. In the following chapter the next step will be taken towards single molecule switchable devices and light-induced single molecule switching will be examined employing compound **21** exhibiting reversible photochemical behavior on gold nanoparticles and bulk gold electrodes.

4.5 Experimental Section

General Remarks

See Chapter 2 for information on characterization, UV/Vis and IR spectroscopy and irradiation experiments performed in solutions.

Preparation of gold nanoparticles

The typical synthetic procedure is as follows: $HAuCl_4$ (135 mg, 0.343 mmol) in water (34 ml) was added to tetra-*n*-octylammonium bromide (375 mg, 0.686 mmol) in toluene (92 ml), and the mixture was vigorously stirred. The yellow aqueous solution became colorless, and the toluene phase turned orange. After 10 min, **6o** (167 mg, 0.343 mmol) (freshly deprotected with NH_4OH (0.84 ml of μ 25 % aq. solution) in THF (16 ml) stirred for 30 min and the solvent evaporated) in toluene (12 ml) was added and mixture was stirred for 10 min. A freshly prepared solution of $NaBH_4$ (129 mg, 3.34 mmol) in water (34 ml) was added to the vigorously stirred solution. The resulting mixture continued to be stirred overnight. The organic phase was then separated, evaporated and dried in vacuum for a day. The crude solid was dissolved in toluene (15 ml) and mixed with methanol (150 ml). The dark precipitate was filtered off and washed with methanol. Size-exclusion chromatography (sephadex LH-20, 1 m column, THF) gives **Au-6o** separated from remaining thiol and tetra-*n*-octylammonium bromide. The purity of nanoparticles was controlled by ^{1}H NMR spectroscopy by monitoring the disappearance of the sharp absorptions that can be attributed to unbound molecules present in solution.

Transmission Electron Microscopy

Electron microscopy investigations were carried out by Dr. C. van den Brom with a Philips CEM 120 transmission electron microscope, equipped with a LaB_6 filament. The microscope was operated at 120 kV. Images were acquired with a built-in Gatan 794 CCD-camera (1024 x 1024 pixels), controlled by Gatan Digital Micrograph v3.5 software.

All TEM samples were investigated using an amorphous carbon support-film of several nanometers thickness on a 3 mm 400 μm mesh copper grid. Amorphous carbon films were prepared by standard methods. The sample material was deposited by making a dilute solution in a dichloromethane, putting a droplet of about 0.05 ml on the film, rapidly followed by blotting of most liquid with filtration paper.

Reflectance FT-IR spectra

The IR spectroscopy measurements were performed on a Nicolet Nexus FT-IR apparatus. Small quantities of diarylethenes or diarylethene-modified gold nanoparticles were grinded together with the KBr and the final powder was equally spread on the sample holder.

Preparation of gold electrodes

Gold bead electrodes were prepared by beading gold wire (0.5 mm diameter and 99.995%) in a dihydrogen gas flame. After preparation, the electrodes were transferred immediately to a 0.5 mM ethanolic solution of the compound of interest and stored in the dark. After a minimum of 16 h the electrodes were removed and rinsed with ethanol and then with CH_3CN/0.1 M $LiClO_4$ prior to introduction into the electrochemical cell. Alternatively, the gold bead electrodes were cleaned electrochemically by repetitive cycling in 0.5 M H_2SO_4 between –0.2 and 1.45 V (vs SCE) until a stable cyclic voltammogram was obtained.

Flat gold macroelectrodes were prepared in a home-made vacuum deposition chamber. 200 nm of gold were evaporated onto glass coated with a chromium layer of 1 nm thickness as an adhesion promoter. After 30s annealing in a hydrogen flame, the samples were placed immediately in a 0.5 mM ethanolic solution of the compound of interest overnight, at room temperature and in the dark. After at least 16 h, the electrodes were rinsed with ethanol, dried under an argon stream and either introduced directly into a vacuum for XPS measurements or treated photo/electrochemically and then rewashed and dried prior XPS measurements.

X-ray photoelectron spectroscopy

XPS measurements were carried out by Dr. N. Katsonis using an X-PROBE Surface Science Laboratories photoelectron spectrometer equipped with a monochromatic Al Kα X-ray source (hν = 1486.6 eV). The energy resolution was set to 1.6 eV and the photoelectron take-off angle was 37°. The base pressure in the measurement chamber was better than 2 x 10^{-10} mbar. All binding energies were referenced to the Au $4f_{7/2}$ core level at 84.0 eV.[57] Spectral analysis included a linear background subtraction and peak separation using mixed Gaussian-Lorentzian functions in a least squares curve-fitting program (Winspec) developed in the LISE laboratory of the Facultes Universitaires Notre-Dame de la Paix, Namur, Belgium. The photoemission peak areas of each element, used to estimate the amount of each species on the surface, were normalized by the sensitivity factors of each element tabulated for the spectrometer used.

Electrochemistry

Electrochemical measurements were carried out on a Model 630B Electrochemical Workstation (CH Instruments) under the supervision of Dr. W. R. Browne. For solution analysis, analyte concentrations were typically 0.5 to 1 mM in anhydrous acetonitrile containing 0.1 M LiClO$_4$. Unless stated otherwise a Teflon shrouded glassy carbon working electrode (CH Instruments), a Pt wire auxiliary electrode and SCE reference electrode were employed in all measurements. Cyclic voltammograms were obtained at sweep rates between 10 mV s^{-1} to 100 V s^{-1}. For reversible processes the half-wave potential values are reported. Redox potentials are +/- 20 mV. Surface coverage (Γ/mol cm^{-2}) of the SAMs in the ring closed state were calculated from the current density of first or first and second oxidation wave. The area of the electrode was calculated from the AuO reduction wave obtained prior to monolayer deposition. Electrode capacitance was determined from the scan rate dependence of the non-Faradaic current (at least 300 mV lower potential than the least anodic oxidation process for a particular system) in 0.1 M LiClO$_4$ in acetonitrile. For a bare gold bead electrode the capacitance determined was 11.8 μF cm^{-2} and for a *n*-dodecanethiol modified bead electrode 1.6 μF cm^{-2}. Extended irradiation of either bare or *n*-dodecanethiol modified electrodes with 312 nm light for over 60 min did not result in a change in their capacitance. The capacitance of the SAM modified electrodes were typically 7-12 μF cm^{-2} for SAMs of **6o**, **36c** and **21c**.

Photochemistry

Irradiation of electrodes was carried out in the electrochemical cell and in air with UV light (312 nm) using a high pressure mercury/xenon lamp (200W, Oriel), and appropriate highpass or bandpass filters (Andover corporation) for visible irradiation. Samples were protected from heating during irradiation using a water filter. UV/Vis measurements were performed on a Hewlett-Packard HP 8453 diode array spectrophotometer.

4.6 References and Notes

[1] D. Dulic, S. J. van der Molen, T. Kudernac, H. T. Jonkman, J. J. D. de Jong, T. N. Bowden, J. van Esch, B. L. Feringa, B. J. van Wees, *Phys. Rev. Lett.* **2003**, *91*, 207402.

[2] S. J. van der Molen, H. van der Vegte, T. Kudernac, I. Amin, B. L. Feringa, B. J. van Wees, *Nanotechnology* **2006**, *17*, 310-314.

[3] a) J. Li, G. Speyer, O. F. Sankey, *Phys. Rev. Lett.* **2004**, *93*, 248302; b) M. Zhuang, M. Ernzerhof, *Phys. Rev. B* **2005**, *72*, 073104.

[4] a) M.-C. Daniel, D. Astruc, *Chem. Rev.* **2004**, *104*, 293-346; b) K. G. Thomas, P. V. Kamat, *Acc. Chem. Res.* **2003**, *36*, 888-898.

[5] a) S. H. Kawai, S. L. Gilat, R. Ponsinet, J.-M. Lehn, *Chem. Eur. J.* **1995**, *1*, 275–284; b) S. H. Kawai, S. L. Gilat, R. Ponsinet, J.-M. Lehn, *Chem. Eur. J.* **1995**, *1*, 285 –293; c) W. R. Browne, J. J. D. de Jong, T. Kudernac, M. Walko, L. N. Lucas, K. Uchida, J. H. van Esch, B. L. Feringa, *Chem. Eur. J.* **2005**, *11*, 6414-6429. d) A. Peters, N. R. Branda, *J. Am. Chem. Soc.* **2003**, *125*, 3404; e) W. R. Browne, J. J. D. de Jong, T. Kudernac, M. Walko, L. N. Lucas, K. Uchida, J. H. van Esch, B. L. Feringa, *Chem. Eur. J.* **2005**, *11*, 6430-6441.

[6] A. P. Alivisatos, *Science* **1996**, *271*, 933-937.

[7] M. Brust, C.J. Kiely, *Colloids Surf. A: Physicochem. Eng. Asp.* **2002**, *202*, 175-186.

[8] P. Mulvaney, *Langmuir* **1996**, *12*, 788-800.

[9] a) A. J. Haes, R. P. van Duyne, *J. Am. Chem. Soc.* **2002**, *124*, 10596-10604; b) D. C. Hone, A. H. Haines, D. A. Russell, *Langmuir* **2003**, *19*, 7141-7144.

[10] (a) M. Brust, M. Walker, D. Bethell, D. J. Schiffrin, R. Whyman, *J. Chem. Soc., Chem. Commun.* **1994**, 801-802. (b) M. Brust, J. Fink, D. Bethel, D. J. Schiffrin, C. J. Kiely, *J. Chem. Soc., Chem. Commun.* **1995**, 1655-1656.

[11] (a) C. S. Weisbecker, M. W. Merritt, G. M. Whitesides, *Langmuir*, **1996**, *12*, 3763-3772; (b) A. Manna, B. D. Kulkarni, K. Bondoypadhayay, K. Vijayamohanan, *Chem. Mater.* **1997**, *9*, 3032-3036; (c) F. Hide, B. J. Schwartz, M. Diaz-Garcia, A. J. Heeger, *Chem. Phys. Lett.* **1996**, *256*, 424-430; (d) L. Balogh, D. R. Swanson, R. Spindler, D. A. Tomalia, *Polym. Mater. Sci. Eng.* **1997**, *77*, 118-120; (e) M. Zhao, L. Sun, R. M. Crooks, *J. Am. Chem. Soc.* **1998**, *120*, 4877-4778; (f) S. Gomez, L. Erades, K. Philippot, B. Chaudret, V. Colliere, O. Balmes, J.-O. Bovin, *J. Chem. Soc., Chem. Commun.* **2001**, 1474-1475.

[12] (a) C. D. Bain, E. B. Troughton, Y.-T. Tao, J. Evall, G. M. Whitesides, R. G. Nuzzo, *J. Am. Chem. Soc.* **1989**, *111*, 321-335; (b) D. A. Hutt, G. J. Leggett, *Langmuir* **1997**, *13*, 2740-2748; (c) M. Sprik, E. Delamarche, B. Michel, U. Rothlisberger, M. L. Klein, H. Wolf, H. Ringsdorf, *Langmuir* **1994**, *10*, 4116-4130; d) X. Xu, N. L. Rosi, Y. Wang, F. Huo, C. A. Mirkin, *J. Am. Chem. Soc.* **2006**, *128*, 9286-9287, e) S. Koenig, V. Chechik, *Langmuir* **2006**, *22*, 5168-5173, f) R. Klajn, K. J. M. Bishop, M. Fialkowski, M. Paszewski, J. Campbell, T. P. Gray, B. A. Grzybowski, *Science* **2007**, *316*, 261-264.

[13] (a) K. Tamada, T. Ishida, W. Knoll, H. Fukushima, R. Colorado, Jr., M. Graupe, O. E. Shmakova, T. R. Lee, *Langmuir* **2001**, *17*, 1913-1921; (b) S. Frey, K. Heister, M. Zharnikov, M. Grunze, K. Tamada, R. Colorado, Jr., M. Graupe, O. E. Shmakova, T. R. Lee, *Israel J. Chem.* **2000**, *40*, 81-97; (c) C. A. Alves, M. D. Porter, *Langmuir* **1993**, *9*, 3507-3512; (d) C. E. D. Chidsey, D. N. Loiacono, *Langmuir* **1990**, *6*, 682-691; (e) Y. S. Shon, R. Colorado, C. T. Williams, C. D. Bain, T. R. Lee, *Langmuir* **2000**, *16*, 541-548;

(f) S. Lee, Y. S. Shon, R. Colorado, R. L. Guenard T. R. Lee, S. S. Perry, *Langmuir* **2000**, *16*, 2220-2224; (g) L. Duan, S. J. Garrett, *J. Phys. Chem. B* **2001**, *105*, 9812-9816.

[14] (a) K. Tamada, J. Nagasawa, F. Nakanishi, K. Abe, T. Ishida, M. Hara, W. Knoll, *Langmuir* **1998**, *14*, 3264-3271; (b) H. Wolf, H. Ringsdorf, E. Delamarche, T. Takami, H. Kang, B. Michel, Ch. Gerber, M. Jaschke, H. –J. Butt, E. Bamberg, *J. Phys. Chem.* **1995**, *99*, 7102-7107; (c) W. B. Caldwell, D. J. Campbell, K. Chen, B. R. Herr, C. A. Mirkin, A. Malik, M. K. Durbin, P. Dutta, K. G. Huang, *J. Am. Chem. Soc.* **1995**, *117*, 6071-6082; (d) R. Wang, T. Iyoda, L. Jiang, D. A. Tryk, K. Hashimoto, J. Fujishima, *Electroanal. Chem.* **1997**, *438*, 213-219; (e) A. N. Shipway, I. Willner, *Acc. Chem. Res.* **2001**, *34*, 421-432.

[15] (a) D. J. Revell, I. Chambrier, M. J. Cook, D. A. Russell, *J. Mater. Chem.* **2000**, *10*, 31; (b) H. Imahori, T. Hasobe, H. Yamada, Y. Nishimura, I. Yamazaki, S. Fukuzumi, *Langmuir* **2001**, *17*, 4925-4931; (c) T. Kondo, M. Yanagida, X. Q. Zhang, Uosaki, *Chem Lett.* **2000**, 964-965.

[16] (a) T. Neumann, W. Knoll, *Israel J. Chem.* **2001**, *41*, 69; (b) R. Georgiadis, K. P. Peterlinz, A. W. Peterson, *J. Am. Chem. Soc.* **2000**, *122*, 3166-3173; (c) K. E. Nelson, L. Gamble, L. S. Jung, M. S. Boeckl, E. Naeemi, S. L. Golledge, T. Sasaki, D. G. Castner, C. T. Campbell, P. S. Stayton, *Langmuir* **2001**, *17*, 2807-2816; (d) F. Hook, A. Ray, B. Norden, B. Kasemo, *Langmuir* **2001**, *17*, 8305-8312; (e) R. M. Nyquist, A. S. Eberhardt, L. A. Silks, Z. Li, X. Yang, B. I. Swanson, *Langmuir* **2000**, *16*, 1793-1800; (f) J. D. Faull, V. K. Gupta, *Langmuir* **2001**, *17*, 1470-1476; (g) F. Patolsky, E. Katz, A. Bardea, I. Willner, *Langmuir* **1999**, *15*, 3703-3706.

[17] a) M. J. Hostetler, A. C. Templeton, R. W. Murray, *Langmuir* **1999**, *15*, 3782-3789; b) R. L. Donkers, Y. Song, R. W. Murray, *Langmuir* **2004**, *20*, 4703-4707; c) G. Schmid, R. Pugin, J. –O. Malm, J. –O. Bovin, *Eur. J. Inorg. Chem.* **1999**, 2051-2055; d) L. O. Brown, J. E. Hutchinson, *J. Am. Chem. Soc.* **1997**, *119*, 12384-12385.

[18] M. Brust, M. Walker, D. Bethell, D. Schiffrin, R. Whyman, *J. Chem. Soc.-Chem. Commun.* **1994**, 801-802.

[19] J. Turkevitch, P. C. Stevenson, J. Hillier, *Discuss. Faraday Soc.* **1951**, *11*, 55-75.

[20] G. Frens, *Nature: Phys. Sci.* **1973**, *241*, 20-22.

[21] T. Yonezawa, T. Kunitake, *Colloids Surf. A: Physicochem. Eng. Asp.* **1999**, *149*, 193-199.

[22] M. Giersig, P. Mulvaney, *Langmuir* **1993**, *9*, 3408-3413.

[23] M. Brust, J. Fink, D. Bethel, D. J. Schiffrin, C. J. Kiely, *J. Chem. Soc., Chem. Commun.* **1995**, 1655-1656.

[24] (a) M. J. Hostetler, S. J. Green, J. J. Stokes R. W. Murray, *J. Am. Chem. Soc.* **1996**, *118*, 4212-4213; (b) R. S. Ingram, M. J. Hostetler, R. W. Murray, J. *Am. Chem. Soc.* **1997**, *119*, 9175-917;. c) A. C. Templeton, W. P. Wuelfing, R. W. Murray, *Acc. Chem. Res.*

119

2000, *33*, 27-36; d) A. C. Templeton, M. J. Hostetler, C. T. Kraft, R. W. Murray, *J. Am. Chem. Soc*. **1998**, *120*, 1906-1911; (e) M. J. Hostetler, A. C. Templeton, R. W. Murray, *Langmuir* **1999**, *15*, 3782-3789.

[25] M. Hasan, D. Bethell, M. Brust, *J. Am. Chem. Soc*. **2003**, *125*, 1132-1133.

[26] K. Nakamura, T. Kawabata, Y. Mori, *Powder Technol*. **2003**, *131*, 120-128.

[27] a) C. L. Cleveland, U. Landman, M. N. Shafigullin, P. M. Stephens, R. L. Whetten, *Z. Phys. D* **1997**, *40*, 503-508; b) C. Gutierrez-Wing, J. A. Ascencio, M. Pérez-Alvarez, M. Marin- Almazo, M. José-Yacamán, *J. Cluster Sci*. **1998**, *9*, 529-545.

[28] D. V. Leff, P. C. Ohara, J. R. Heath, W. M. Gelbart, *J. Phys. Chem*. **1995**, *99*, 7036-7041.

[29] A. Labande, J. Ruiz, D. Astruc, *J. Am. Chem. Soc*. **2002**, *124*, 1782-1789.

[30] a) A. Badia, L. Cuccia, L. Demers, F. Morin, R. B. Lennox, *J. Am. Chem. Soc*. **1997**, *119*, 2682-2692; b) A. Badia, L. Demers, L. Dickinson, F. G. Morin, R. B. Lennox, L. Reven, *J. Am. Chem. Soc*. **1997**, *119*, 11104-11105.

[31] A. Ulman, *Chem. Rev*. **1996**, *96*, 1533-1554.

[32] K. Matsuda, M. Ikeda, M. Irie, *Chem. Lett*. **2004**, *33*, 456-457.

[33] a) J. Zhang, J. K. Whitesell, M. A. Fox, *Chem. Mater*. **2001**, *13*, 2323-2331; b) A. Manna, P.-L. Chen, H. Akiyama, T.-X. Wei, K. Tamada, W. Knoll, *Chem. Mater*. **2003**, *15*, 20-28; c) J. Hu, J. Zhang, F. Liu, K. Kittredge, J. K. Whitesell, M. A. Fox, *J. Am. Chem. Soc*. **2001**, *123*, 1464-1470.

[34] The absence of absorption in the visible region for the open form, together with the fact that a ring-closure has typically a larger quantum yield allows high selectivity for a ring-closure (providing a photostationary state with undetectable amount of the open isomer as determined by proton NMR) and complete selectivity for ring-opening.

[35] T. Teranishi, S. Hasegawa, T. Shimizu, M. Miyake, *Adv. Mater*. **2001**, *13*, 1699-1701.

[36] a) K. Uchida, M. Saito, A. Murakami, S. Nakamura, M. Irie, *Adv. Mater*. **2003**, *15*, 121-125; b) J. J. D. de Jong, W. R. Browne, M. Walko, L. N. Lucas, L. J. Barrett, J. J. McGarvey, J. H. van Esch, B. L. Feringa, *Org. Biomol. Chem*. **2006**, *4*, 2387–2392.

[37] M. J. Hostetler, J. E. Wingate, C.-J. Zhong, J. E. Harris, R. W. Vachet, M. R. Clark, J. D. Londono, S. J. Green, J. J. Stokes, G. D. Wignall, G. L. Glish, M. D. Porter, N. D. Evans, R. W. Murray, *Langmuir* **1998**, *14*, 17-30.

[38] Details of the procedure used for quantum yield measurement can be found in P. R. Hania, R. Telesca, L. N. Lucas, A. Pugzlys, J. van Esch, B. L. Feringa, J. G. Snijders, K. Duppen, *J. Phys. Chem. A* **2002**, *106*, 8498.

[39] a) K. G. Thomas, P. V. Kamat, *Acc. Chem. Res*. **2003**, *36*, 888-898; b) E. Dulkeith, A. C. Morteani, T. Niedereichholz, T. A. Klar, J. Feldmann, S. A. Levi, F. C. J. M. van Veggel, D. N. Reinhoudt, M. Möller, D. I. Gittins, *Phys. Rev. Lett*. **2002**, *89*, 203002.

[40] J. Li, G. Speyer, O. F. Sankey, *Phys. Rev. Lett*. **2004**, *93*, 248302.

[41] (a) C. Joachim, J. K. Gmizewski, A. Aviram, *Nature* **2000**, *408*, 541-548; (b) R. L. Caroll, C. B. Gorman, *Angew. Chem. Int. Ed*. **2002**, *41*, 4378-4400.

[42] (a) A. H. Flood, E. W. Wong, J. F. Stoddart, *Chem. Phys*. **2006**, *324*, 280-290; (b) E. DeIonno, H. –R. Tseng, D. D. Harvey, J. F. Stoddart, J. R. Heath, *J. Phys. Chem. B*. **2006**, *110*, 7609-7612.

[43] (a) B. L. Feringa, *Molecular Switches*, Wiley-VCH, Weinheim, Germany, **2001**; (b) M. A. Ratner, J. Jortner, *Molecular Electronic*, Blackwell, Oxford, **1997**; (c) Y. Yokoyama, *Chem. Rev*. **2000**, *100*, 1717-1739; (d) B. L. Feringa, R. A. van Delden, N. Koumura E. M. Geertsema, *Chem. Rev*. **2000**, *100*, 1789-1816; (e) J.-P. Sauvage, *Molecular Machines and Motors*. Struc. Bond. **2001**, *vol. 99*; (f) F. M. Raymo, M. Tomasulo, *Chem. Soc. Rev*. **2005**, *34*, 327-333.

[44] (a) R. Baron, A. Onopriyenko, E. Katz, O. Lioubashevski, I. Willner, S. Wang, H. Tian, *Chem. Commun*. **2006**, 2147-2149; (b) I. Willner, E. Katz, *Angew. Chem., Int. Ed*. **2000**, *39*, 1180-1218; (c) G. Berkovic, V. Krongauz, V. Weis, *Chem. Rev*. **2000**, *100*, 1741-1753; (d) S. Giordani, M. A. Cejas, F. M. Raymo, *Tetrahedron* **2004**, *60*, 10973-100981; (e) M.-H. Yang, M. C. Biewer, *Tetrahedron. Lett*., **2005**, *46*, 349-351; (f) A. Doron, E. Katz, G. Tao, I. Willner, *Langmuir* **1997**, *13*, 1783-1790.

[45] (a) M. Irie, *Chem. Rev*. **2000**, *100*, 1685-1716; (b) H. Tian, S. Yang, *Chem. Soc. Rev*. **2004**, *33*, 85-97; (c) N. Katsonis, T. Kudernac, M. Walko, S. J. van der Molen, B. J. van Wees, B. L. Feringa, *Adv. Mater*. **2006**, *18*, 1397-1400.

[46] (a) Z. H. Liu, K. Hashimoto, A. Fujishima, *Nature* **1990**, *347*, 658-660; (b) N. Tamaoki, S. Yoshimura, T. Yamaoka, *Thin Solid Films* **1992**, *221*, 132-139; (c) A. Archut, F. Vogtle, L. De Cola, G. C. Azzellini, V. Balzani, P. S. Ramanujam, R. H. Berg, *Chem. Eur. J*. **1998**, *4*, 699-706; (d) J. M. Galvin, G. B. Schuster, *Supramol. Sci*. **1998**, *5*, 89-100.

[47] W. R. Browne, M. M. Pollard, B. de Lange, A. Meetsma, B. L. Feringa, *J. Am. Chem. Soc*. **2006**, *128*, 12412-12413.

[48] R. A. van Delden, M. K. J. ter Wiel, M. M. Pollard, J. Vicario, N. Koumura, B. L. Feringa, *Nature* **2005**, *437*, 1337-1340.

[49] J. Areephong, W. R. Browne, N. Katsonis, B. L. Feringa, *Chem. Commun*. **2006**, 3930-3932.

[50] D. T. Sawyer, A. Sobkowiak, J. L. Roberts, jr., Electrochemistry for Chemists, Wiley, New York, 1995.

[51] C. Fuxen, W. Azzam, R. Arnold, G. Witte, A. Terfort, C. Woll, *Langmuir* **2001**, *17*, 3689-3695.

[52] J. Noh, E. Ito, T. Araki, M. Hara, *Surf. Sci*. **2003**, *532*, 1116-1120.

121

[53] F. Cecchet, P. Rudolf, S. Rapino, M. Margotti, F. Paolucci, J. Baggerman, A. M. Brouwer, E. R. Kay, J. K. Y. Wong, D. A. Leigh, *J. Phys. Chem. B* **2004**, *108*, 15192-15199.

[54] P. E. Laibinis, C. D. Bain, G. M. Whitesides, *J. Phys. Chem*. **1991**, *95*, 7017-7021.

[55] C. A. Hacker, J. D. Batteas, J. C. Garno, M. Marquez, C. A. Richter, L. J. Richter, R. D. van Zee, C. D. Zangmeistr, *Langmuir* **2004**, *20*, 6195-6205.

[56] A. J. Bard, L. R. Faulkner, Electrochemical Methods, Fundamentals and applications, 2nd Ed., Wiley, New Jersey, **2001**.

[57] J. F. Moulder, W. F. Stickle, P. E. Sobol, K. D. Bomben, Handbook of Photoelectron Spectroscopy; Perkin-Elmer Corporation, Physical Electronics Division: Eden Prairie, MN, **1992**.

122

Chapter 5

Reversible Light-Induced Single Molecule Conductance Switching on Gold

In this chapter it is demonstrated that light-controlled reversible switching between two conductive states can be achieved for individual photochromic molecules bound chemically to a gold surface. Controlled opto-electronic switching which results in modulation of conductivity of single molecules linked to gold and inserted in an insulating matrix of alkanethiols is demonstrated by using Scanning Tunneling Microscopy (STM). Furthermore, optical spectroscopy of self-assembled monolayers of diarylethene photoswitches on a semi-transparent Au(111) surface shows the on-off states of the switch. The chemical analysis of the composition of monolayers using X-ray Photoelectron Spectroscopy (XPS) and the stability of monolayers upon irradiation is discussed.[*]

5.1 Introduction

In Chapter 4 reversible light-induced switching was demonstrated for monolayers of diarylethenes assembled on gold nanoparticles and macroscopic gold electrodes. However, one of the most important features of molecules that have potential applications in molecular electronics is to make use of single molecules that function as switches on metal surfaces. This requires the development of molecules, which can switch reversibly between two conductive states in response to an external trigger. Light is a attractive external stimulus for such switches because of ease of addressability, fast response times and compatibility with a wide range of condensed phases.[1] Opto-electronic switches offer a new functionality to molecular electronics provided that their switching properties are preserved when bound to a metal surface. Indeed interactions between molecules and substrate can considerably decrease the lifetime of the excited state of the molecules.[2] These aspects of hybrid metal-molecular systems were also addressed in Chapters 2 and 4.

Diarylethenes are promising synthetic photoswitchable molecules because of the outstanding fatigue-resistant light-induced reversible transformation between two isomers having different absorption spectra.[3] The difference in geometry and electronic structure between the two isomers, which is at the origin of the photochromism in various media,[4] has been exploited successfully to control reversibly other properties such as fluorescence intensity and wavelength,[5] electrochemical properties,[6] acid-base equilibriums,[7] magnetic[8] and self-assembly properties.[9] However, only a few attempts have been made to switch the conductance of surface-bound molecules by light.[10,11,12] Light-induced switching of conductance has been studied for individual diarylethenes linked to gold through a thiophene spacer but only one-way switching was observed (Chapter 2).[10,11] Theoretical studies predicted that the possibility to switch reversibly depends critically on the linker used[13,14] and the experiments with gold nanoparticles and gold macroscopic electrodes described in Chapter 4 confirm those predictions. Recently, photoisomerization was reported for diarylethenes with a benzyl linker connecting the central switching unit with the anchoring thiol group chemisorbed on gold.[12] It was also shown that a phenyl spacer can preserve the photochromic reactivity of a dimer in solution.[15] In this chapter, we present direct evidence of reversible switching of a diarylethene **23** grafted on Au(111), with the linker based on a *meta*-substituted phenyl group. Both ring closure and ring opening processes are observed for single molecules and a statistical analysis of numerous switching events confirms reversible behavior.

The two isomers of compound **23** which correspond to a closed and an open form of the molecule are shown in Figure 1. The π-conjugation extends over the entire molecule in the
124

closed form whereas it is restricted to each half in the open form. As a consequence, the closed form is expected to exhibit better electrical conductance than the open form. We will thus refer to them as the "ON" and the "OFF" states of the switch, respectively. The UV-Vis spectra (see Chapter 3 and 4) of this molecule in toluene show that the wavelengths that can be used for "ON" to "OFF" switching are $420 < \lambda < 650$ nm and $300 < \lambda < 350$ nm for the reverse operation.
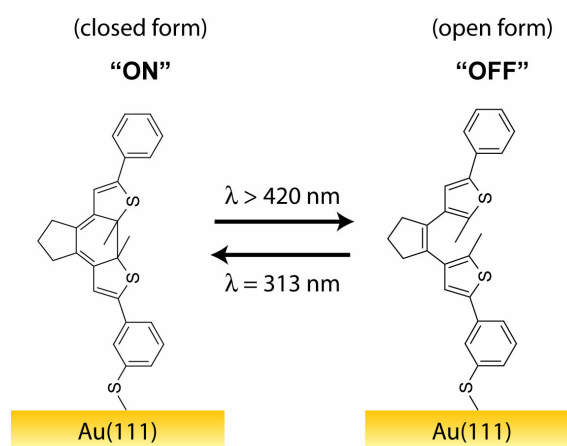

Figure 1 *Diarylethene switch **23** bound through a thiol bond to Au(111). The ring-closed form corresponds to the more conductive (conjugated) "ON" state (left) and the ring-open form corresponds to the less conductive (non-conjugated) "OFF" state (right). The "ON" state of this molecule is converted into the "OFF" state by UV light, and the "OFF" state returns to the "ON" state under visible light.*

In the following subsections two different experimental techniques demonstrating reversible light induced switching for molecule **23** bound to gold are discussed. First, optical spectroscopy is used to observe optical changes for a homogenous monolayer of compound **23**. This is followed by STM studies in order to demonstrate conductive changes upon light induced switching (for a short description of the STM technique see Chapter 6). Mixed monolayers are used to demonstrate switching events at the level of a single molecule.

5.2 Optical Switching of Homogeneous Monolayer on Gold

Coupling spectroscopic techniques to scanning probe microscopy requires the preparation of atomically flat and conductive, but also semi-transparent gold surfaces.[16] Earlier work has reported the use of semi-transparent Au(111) substrates, but to our knowledge preparative conditions employed did not allow formation of conductive layers.[12] In such case it is therefore difficult to compare directly the observed spectroscopic and scanning probe results, since such gold substrates are composed of small clusters of gold which possess discrete energy levels unlike bulk gold. Therefore, we prepared a conductive semi-transparent layer of 20 nm of Au(111) on mica (for details, see experimental section). Our substrates present flat terraces of Au(111) as shown by STM (Figure 2). The possibility of recording of STM pictures itself confirms that the semi-transparent gold substrate is conductive. Such gold substrate then allows to some extent transmission of light and can be used for spectroscopic characterization of adsorbed molecules.
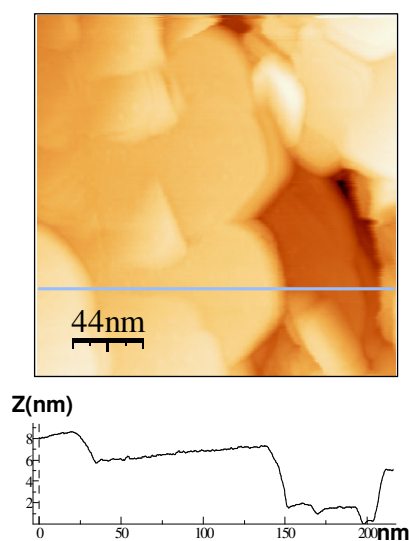
Figure 2 STM picture (218 x 218 nm^2) of a semi-transparent Au(111) surface of 20 nm thickness on mica in air. The cross-section, corresponding to the blue stripe on the STM picture, highlights the presence of atomically flat terraces.

Homogeneous monolayers of the closed form of compound **23** were formed on semi-transparent gold surfaces by self-assembly (for the synthesis of **23**, see Chapter 3). The anchoring of the molecule to the gold surface is ensured by a thiol anchor group. For

126

reasons of stability, the thiol group is protected by a thioacetate function which splits off spontaneously upon chemisorption.[17] In order to confirm attachment of a thiol anchoring group to gold, X-ray Photoelectron Spectroscopy was used.

5.2.1 XPS Characterization of Monolayers

Figure 3 shows the S 2p core level region for a self-assembled monolayer of the closed form of compound **23** on Au(111). For analysis of the data, each experimental spectrum is mathematically reconstructed with a minimum number of peaks consistent with the raw data and the molecular structure of **23**. Following this procedure, the analysis of the S 2p core level region reveals two contributions. The first peak for which S $2p_{3/2}$ is found at 161.8 eV is attributed to XPS spectra of thiols chemisorbed on the Au surface, indicating thiolate formation.[18] The main peak with the S $2p_{3/2}$ at 163.4 eV corresponds to the thiophene sulfur atoms.[19] In order to check the stability of the monolayer towards UV irradiation the same samples were exposed for 10 min to UV light (λ=313 nm). After irradiation oxidized sulfur species were not detected at binding energies in between 168.5 eV and 170 eV. Therefore, we can conclude that the self-assembled monolayer is stable, that gold-sulfur bond is preserved and that the layer has consequently not been destroyed upon UV irradiation.
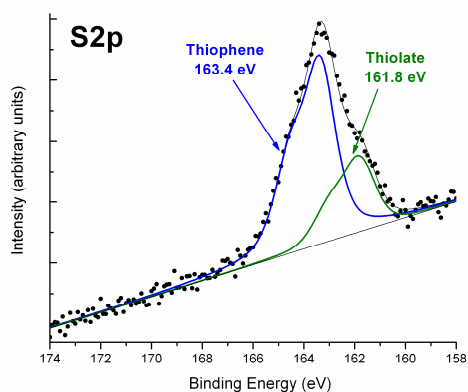

Figure 3 *Photoemission spectrum and fit of the S 2p core-level region for a homogeneous self-assembled monolayer of switches on Au(111).*

127

5.2.2 Optical Switching of Monolayer Monitored by UV-Vis Spectroscopy

The self-assembled monolayer (SAM) of the switches in the "ON" state (closed form) formed on semi-transparent Au(111) was subsequently used for UV-Vis spectroscopy experiment. The UV-Vis spectra of these SAMs were not directly informative because of the relatively low concentration of the molecules and the absorption due to the gold plasmon band. Hence, the following procedure was adopted: after self-assembly of the switches in the "ON" state, measurement of an initial spectrum (I_{ON}) is followed by 10 min irradiation using visible light to allow a photochemical ring opening. A second spectrum is recorded (I_{OFF}) and the cycle is completed by 5 min of UV irradiation. The differential spectrum I_{ON}-I_{OFF} reveals a broad absorption feature at λ_{max} = 540 nm (Figure 4). The position of the band corresponds to the λ_{max} of the differential absorption for the same switch **23** in solution. Consequently, we attribute the observed feature to the differential absorption signal of the "ON" to "OFF" for the switches on Au(111). A key factor that allows its assignment to the light-triggered molecular switching process is its reproducibility and reversibility through several switching cycles. Also, control experiments on self-assembled monolayers of *n*-dodecanethiol never produced any significant absorption in the UV-Vis spectrum. Over the three cycles presented in Figure 4, the system shows reversible switching without evidence of significant degradation or change in the switching properties. This experiment shows that collective structure-property relationships are preserved upon self-assembly of the switch on Au(111). The photochemical reaction of such switches in self-assembled monolayers is apparently not hampered by molecule-molecule interactions in accordance with the minor conformational change taking place during ring opening or ring closing of diarylethenes. These results are in agreement with the results that were discussed for SAMs of molecule **23** formed on gold nanoparticles and gold electrodes used in electrochemical experiments (Chapter 4).
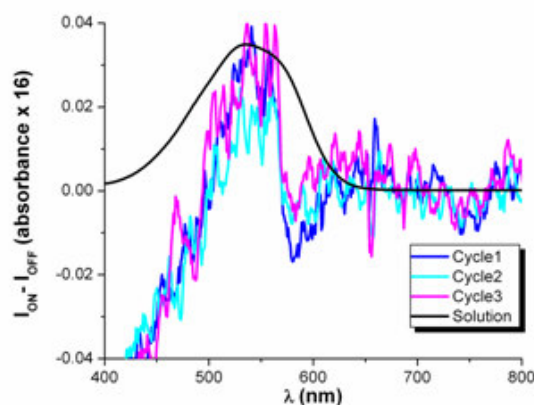
128

Figure 4 *Reversible conversion from "ON" to "OFF" states of the switch grafted on semi-transparent Au(111) as determined by UV-Vis absorption spectroscopy. The curves represent differential spectra of the "ON" state minus the "OFF" state. Black line: differential absorption for the molecule **23** in toluene. The observed peak corresponds to absorption in the visible range, which is used to switch from "ON" to "OFF". The spectrum has been normalized for comparison. Colored lines: differential absorption after three successive cycles of visible ($\lambda = 420$ nm) and UV ($\lambda = 313$ nm) irradiation of an initially "ON" form. The blue line corresponds to the first cycle, the red one to the third cycle. Typical irradiation times are 10 min for visible and 5 min for UV light.*

5.3 Conductance Switching of Single Molecules

A requirement for the development of molecular electronics is the ability to obtain precise atomic scale data under ambient conditions. Next, we show at the level of a single molecule that our molecular design avoids quenching from the gold surface and can be used as a prototype model for light-triggered single molecule electronic devices. Pioneering work has shown how two-dimensional isolation of molecules in host SAMs in combination with STM can be used to study the electronic properties of individual molecules.[20] We use an *n*-dodecanethiol monolayer as a matrix to isolate the switch molecules **23** (the same approach as in Chapter 2). STM measures a so-called apparent height which is a convolution of electronic and topographic characteristics. Consequently, it allows in-situ studies of conductance modification on isolated switches within a matrix of *n*-dodecanethiol.

129

5.3.1 STM Characterization of Mixed Monolayer

An STM image of the *n*-alkanethiol monolayer with switches inserted in the "on" state is shown in Figure 5. The switches appear as bright spots surrounded by domains of close-packed *n*-dodecanethiol molecules. The switches chemisorb preferentially on the etch-pits (dark circles) which are characteristic of these self-assembled monolayers,[21] on Au(111) step edges and boundaries between ordered domains of dodecanethiol. Though Figure 5 shows a large scale picture, molecular resolution of the alkanethiol lattice is already distinguishable under the aspect of preferential alignments (see also inset of Figure 5).
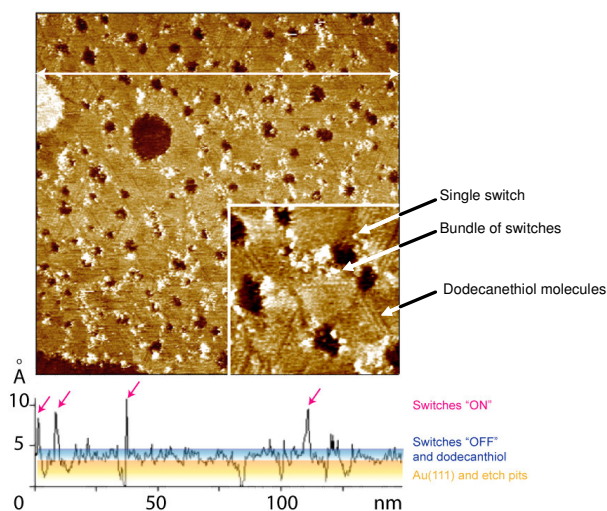
Figure 5 Scanning tunneling microscopy characterization of a mixed monolayer of the switches and dodecanethiol. (Upper part) The switches have been inserted by a replacement reaction with an n-dodecanethiol SAM on Au(111). Molecular resolution of the n-dodecanethiol matrix is distinguishable under the aspect of alignments. The bright spots correspond to inserted switches in the closed form. V_T=-0.811 V, i_T=8.7 pA. Insert: 30x30 nm^2 (Bottom part) cross-sectional profile of the STM picture along the double arrow.

Figure 5 (bottom part) also shows the cross-sectional profile along the arrow depicted in Figure 5 (upper part). The etch pits have a depth of ~0.3 nm, consistent with the theoretical value 0.28 nm.[21] The apparent height of dodecanethiol is ~0.1 nm, which is consistent with previous reports.[22] Under typical scanning conditions V_T = -800mV and i_T = 10pA the apparent height of switches in the "on" state is (0.60 ± 0.15) nm. The deviation from the mean value is relatively large but consistent with reported apparent heights of conductive nanowires.[23]

130

5.3.2 Observation and Switching of Single Molecule

Figure 6a (left panel) shows a zoomed in area of an STM picture where individual dodecanethiol molecules from the dodecanethiol lattice are distinguishable. On Figure 6a (right panel), the same domains of close-packed dodecanethiol molecules are visible. On this picture, a photochromic switch appears as a bright protrusion with the hight of 0.5 nm. The picture on right panel is obtained after irradiation of the sample shown in the left panel with UV light. This means that, as expected, the photochromic molecule switched from "OFF" to "ON" (or open to closed form). There is no distinctive difference between the apparent heights of dodecanethiol and switches in the "OFF" state (0.1 nm). The switch has the same apparent height as dodecanethiol, but the diameter of the corresponding spot is larger (~2.0 nm). This is the expected diameter for an inserted molecule and it is in accordance with previous observations on single molecules.[20] In the "ON" state, the apparent height of the bright spot is increased from 0.1 nm to 0.5 nm (similar results were obtained for compound **6**, Chapter 2). This is consistent with previous reports showing that the resistance of the "ON" isomer is in the MΩ range, whereas it is more than two orders of magnitude higher for the "OFF" form.[10,12] It can be concluded that the "ON" state of compound **23** is easily detectable whereas the "OFF" state cannot be directly distinguished from the *n*-dodecanethiol matrix.
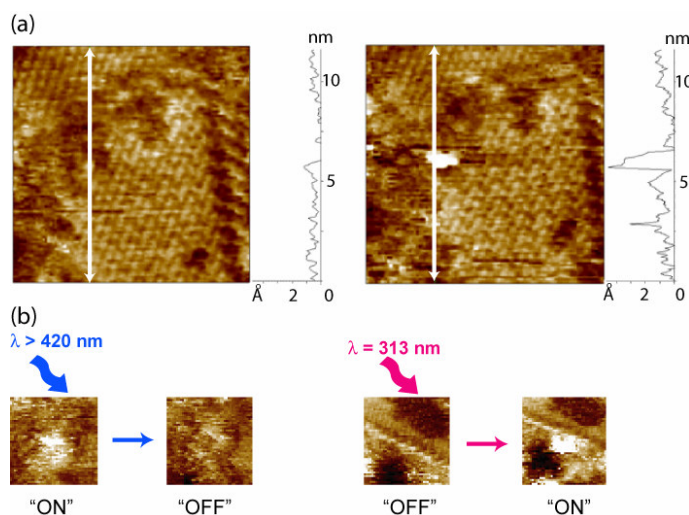

Figure 6 In-situ evidence of light-controlled switching of single molecules. (a) STM pictures registered in a time interval of ~3 min on the same area under UV (λ=313 nm) irradiation. The molecular resolution of the alkanethiol lattice is evidenced by the classical

131

√3x√3R30° structure on top left part of the picture and the c(4x2) superstructure on the bottom down part of the picture. The conductance modulation of the switches resulting from "OFF" to "ON" transition is visible (12x12 nm², V_T= -0.853 V, i_T=12 pA). The cross-sections show that the "OFF" form slightly protrudes from the monolayer with an apparent height of ~0.1 nm, whereas the "ON" form has an apparent height of ~0.5 nm. (b) Extracted frames displaying single molecules (8x8 nm²). The time interval between frames is 3 min. "ON" to "OFF" switching is observed during irradiation by visible light and the reverse process happens during UV irradiation.

In Figure 6b, switching in both directions for single molecules is demonstrated. Low contrast spots corresponding to "OFF" switches transform into bright spots under UV light, and reversibly, bright spots corresponding to "ON" forms become less conductive under irradiation by visible light.[24] The observed modifications in apparent heights could be due to an attenuation of the conductance of the molecules or a change in their physical height or a combination of both. However, the difference in molecular length between the open and closed forms is very small (0.1 nm). Consequently, we attribute the two different STM contrasts to two different conductive states of the switches. The apparent height difference is thus a signature for the two distinctive states of a single molecule.

5.3.3 Statistical Analysis of Multiple Single Molecule Switching Events

Using STM, we have established that many molecules switch back and forth under proper irradiation. This constitutes a strong indication that we succeeded in reversibly switching a photochromic molecule on gold. However, this does not constitute a sufficient proof to assign conductance switching to a light-induced phenomenon. Random conductance switching of individual thiol-derivatized conjugated wires surrounded by alkanethiols has been previously reported[20b] and attributed to fluctuations of the Au-S bond[25] or to tip-induced conformational modifications of the molecules.[23c] All these aspects of stochastic switching have been addressed in Chapter 2. In order to unequivocally demonstrate light-controlled switching, it is essential to use statistical analysis. In the following, this is demonstrated for a small number of isolated molecules.

For a sequence of measured STM pictures of a mixed monolayer of *n*-dodecanethiol and switches in the "ON" state, we use a routine to determine the number of molecules in the "ON" state, which present an apparent height over a fixed threshold of 0.40 nm (see experimental section). A curve displaying the number of molecules in the "ON" state as detected by STM during in-situ irradiation is given in Figure 7. After 30 min of scanning, irradiation of the switches with visible light is started (λ > 420 nm). The number of molecules in the "ON" state drops immediately and reaches a lower level after typically 20

132

min, with some fluctuations. After stabilization of this part of the curve, UV irradiation is started (λ = 313 nm) and the number of molecules in the "ON" state increases. While UV irradiation continues, a plateau is reached after the same characteristic time constant of 20 min. The correspondence between changes of irradiation and changes of the number of molecules in the "ON" state are strong indications of the occurrence of light-induced processes. The reversibility of the phenomenon indicates that the switch is not degraded. The establishment of plateaus is a characteristic of photoinduced isomerisation mechanisms for which equilibrium between two isomers is obtained. The time needed to reach such a photostationary state for the same switches in solution is 2 min. This difference of one order of magnitude between switching times in solution and on the surface is probably due to shortening of the lifetime of the excited state of the photochromic molecule by interaction with the metallic surface. The results of the experiments described in Chapter 2 and 4 as well as other studies of the photochemistry of monolayers on metal surfaces have shown that the excited states are partially quenched by the metal, and that the observed quantum yields of the photochemical reactions are lower than either in solution or in the solid state.[26] Also, a relatively low intensity reaches the sample in the STM setup. After repopulation of the "ON" state, the number of "ON" molecules is decreased by 10% compared to the initial situation. Presumably, this is due to the fact that the photostationary state for switches on Au(111) is modified by the presence of the metal surface. The fluctuations observed within each plateau may have different origins. The first one is the well-known random switching.[20b,25] Second, we do not exclude a possible influence of tip-induced switching between the "ON" and "OFF" states promoted by electrochemical changes in the molecule.[6,27] Nevertheless, the plateaus corresponding to "ON" and "OFF" states are clearly recognizable and show an "ON" to "OFF" ratio of 2.5. This ratio is comparable with electrochemically activated molecular switching systems on surfaces.[28] The fact that some "ON" state molecules cannot be switched to the "OFF" state is attributed to tilting of these molecules towards the surface, which quenches their excited state and thus prohibits light-induced switching. This indicates that the insertion matrix plays a critical role in the switching of the guest molecules.
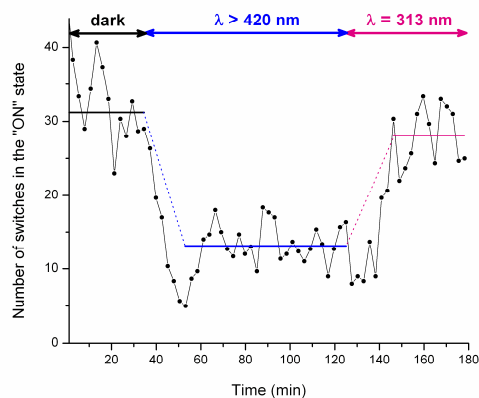
133

Figure 7 *Number of "ON" switches as a function of time for 60x60 nm^2 pictures. The pictures correspond to the series displayed in Figure 5. The plain horizontal lines correspond to mean values of the plateaus of the data. The dotted lines are guides to the eye.*

5.3.4   Comment on Possible Temperature Effects

Heating accompanies all other possible effects arising from absorption of light. In STM the most dramatic consequence of heating is thermal expansion of the tip, which affects the width of the tunneling gap. This effect is not important in the steady state with constant illumination, in which the STM feedback loop simply settles to a new equilibrium tip height.[29] We consequently exclude that the statistical phenomenon we observe could be a consequence of temperature. The broadening of the height distribution for the mixed switch-dodecanethiol monolayers during irradiation is illustrated by Figure 8. The broadening is more important when turning from the dark to visible irradiation. Nevertheless, this tendency is overcome by the light induced effects as the decrease of the number of molecules in the "ON" state was observed (Figure 8, right part). Therefore it can be concluded that the broadening does not affect the light-induced effects and for high apparent heights this tendency is overcome by the light-induced effects. The broadening of the height distribution is weaker when turning from visible to UV irradiation. This is consistent with the irradiation power provided by the lamp through the different filters.
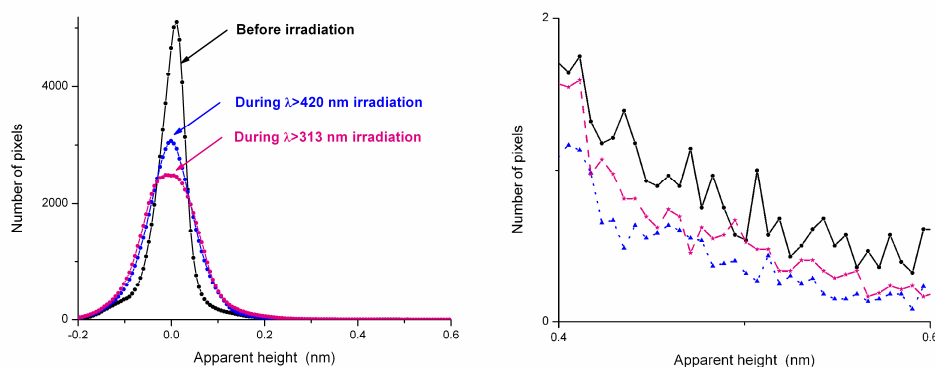
134

Figure 8 *Mean number of pixels for each apparent height of the STM pictures for three different sequences: in the dark, and during visible and UV irradiation. (Left) Global distribution of apparent heights. (Right) Zoom for apparent heights higher then 0.4 nm. Plain line: before irradiation. Dashed line: during UV irradiation. Dotted line: during irradiation by visible light.*

5.4 Conclusions

In summary, two independent experiments were used to demonstrate light-controlled reversible switching for *meta*-phenyl linked diarylethene molecule **23** on gold. This is drastically different from the behavior of the switch **6** described in Chapter 2, which has a thiophene linker. The UV-Vis spectroscopy experiments show that dynamic changes of molecules are detectable for as tiny amount as one monolayer. The structural stability of the molecular monolayer on gold and retention of the thiolate-gold bonding upon irradiation was confirmed by XPS.

The most important finding is that controlled single molecule switching of conductance has been achieved. Using STM it was possible to visualize single molecules and the molecular matrix. The subsequent statistical analysis of numerous single molecule switching events proves the light-induced origin of the switching phenomenon. Our results suggest that a single molecule could substitute bulk devices that are normally used to control conductance. To the best of our knowledge this is the first example of light-triggered fully reversible conductance switching for isolated molecules at ambient conditions. This is an important milestone in the field of molecular electronics. Potential future single-molecular

135

devices will be performing their actions at ambient conditions and not under ultra-high vacuum and at low temperatures for the sake of high cost requirements.

A few more challenges are about to be faced before a fully operating molecular device based on diarylethenes can be realized. It is essential to assemble large number of molecules in a controlled fashion in order to create large-scale, high-density circuits. Well-defined stable and reliable molecular junctions must be formed and each element of the device must be independently addressable. The so-called "crossbar" geometry, a periodic array of crossed wires with molecules sandwiched between electrodes, provides a promising architecture for molecular electronic circuitry[30] and might be a promising alternative to "wire up" diarylethene switches into a "real" molecular device.

5.5 Experimental Section

General Remarks

For general remarks see Chapter 2.

Preparation of substrates

Mica sheets were purchased from Pelco and heated for 16h at T = 375°C under a typical pressure of P = 3.3x10^{-7} mbar in a home-made vacuum deposition system. Gold was deposited on the hot substrate at a constant rate of 0.01 nms^{-1} to form semi-transparent (20 nm) Au(111) layers, and at a rate varying between 0.01 nms^{-1} and 0.1 nms^{-1} for 150 nm Au(111) layers. After deposition the substrates were kept at T = 375°C for 1h and subsequently the temperature was decreased to reach room temperature in approximately 5h.

Preparation of a solution of the "ON" form

A closed form of compound **23** (**23c** or "ON" state) was prepared by irradiation of a 4 mmolL^{-1} solution of an open form (**23o**) (for the synthesis and full characterization of **23** see Chapter 3) in toluene with ultraviolet light (313 nm). Photoisomerization was controlled by UV-Visible spectroscopy. The mixture obtained in the photostationary state was subjected to flash chromatography (*n*-hexane/dichloromethane 7:2) to give a pure closed form of **23**. All subsequent operations were handled in the dark to prevent back isomerization. ^{1}H NMR (300 MHz, CDCl$_3$): δ 1.86-1.96 (m, 2H), 2.03 (s, 6H), 2.45 (s, 3H), 2.43-2.53 (m, 4H), 6.42 (s, 1H), 6.43 (s, 1H), 7.29-7.43 (m, 5H), 7.52-7.58 (m, 4H) ppm.

136

Preparation of the monolayers

For optical spectroscopy and XPS, the substrates were immersed 12 h at room temperature in a 1 mmolL^{-1} solution of compound **23c** in ethanol. The sample were rinsed 3 times in ethanol and dried under argon flow to remove the solvent. For STM, the samples were prepared following a replacement procedure adapted from Donhauser *et al.*[23b] After 30 s flame-annealing in a hydrogen flame, Au(111) samples were placed in a 0.5 mmolL^{-1} solution of *n*-dodecanethiol (Acros, 98.5+%) in ethanol for 12 h at room temperature. The solution was then heated for 5 h at 333 K (60°C). After removal of the sample from the dodecanethiol solution it was rinsed 3 times with ethanol and immersed for 12 h at room temperature in a 0.5 mmol L^{-1} solution of compound **23c** ("ON" state) in ethanol. The acetyl-protecting group is spontaneously removed to allow grafting on gold, as confirmed by XPS spectra. Before the experiments the samples were rinsed three times in ethanol and dried under an argon flow to remove the solvent.

UV-visible Spectroscopy

Optical measurements were performed on a Hewlett-Packard HP 8453 diode-array spectrometer. In situ illuminations of the samples were carried out with a 200 W Hg lamp (LOT-Oriel). The samples were irradiated in situ. Illumination times were typically 10 min for visible irradiation (420 nm cut-off filter) and 5 min for UV light (313 nm band-pass filter). Each spectrum is the result of addition of 16 acquisitions.

X-ray Photoelectron Spectroscopy (XPS)

The XPS measurements were performed using an X-PROBE Surface Science Laboratories photoelectron spectrometer equipped with a monochromatic Al Kα X-ray source (hν=1486.6 eV). The energy resolution was set to 1.65 eV and the photoelectron take-off angle was 37°. The base pressure in the measurement chamber was 2x10^{-10} mbar. All binding energies were referenced to the Au $4f_{7/2}$ core level.[31] Spectral analysis included a linear background substraction and peak separation using mixed Gaussian-Lorentzian functions in a least squares curve-fitting program (Winspec) developed in the LISE laboratory of the Facultes Universitaires Notre-Dame de la Paix, Namur, Belgium. Three to five different points of each sample were examined. The presented spectrum is the sum of the scans taken at all points. The summing of the spectra was done to increase the spectral signal to noise ratio while minimizing the time the samples were exposed to the X-ray source. This should minimize the possibility of sample degradation by the incident X-rays or exciting photoelectrons.

137

Scanning Tunneling Microscopy (STM)

STM images were acquired in the constant current mode under ambient conditions in air. The experiments were performed with a Picoscan scanning tunneling microscope (molecular imaging). Tips were mechanically etched from a Pt-Ir wire (80-20) of 0.25 mm of diameter. The achievement of molecular resolution of the alkanethiol lattice demonstrates the quality of the tip which was used. The setting for tunneling current and voltage range from 10 to 50 pA and from -0.6 to -1.0 V. The presented pictures have been flattened by a routine procedure. No filtering procedure was used. Experiments required minimizing drift (i.e. to use a relatively low power of illumination), molecular resolution and scanning of flat areas (not more than one stepedge). In our setup, the typical drift evaluated by following the position of a stepedge or a defect over time is ~0.5 nm per min. This drift was partially compensated by controlled displacement of the scanning area. In-situ illumination was carried out with a 300 W Xenon lamp (LOT-Oriel) through an optical fiber. For irradiation with visible light, a $\lambda > 420$ nm cut-off filter was used. For irradiation with ultraviolet light, a $\lambda = 313$ nm band-pass filter was used.

Octave routine

An octave routine was used to treat the statistics of evolution of proportions of closed and open forms under irradiation (the software is available free of charge at www.octave.org). The image provided by the raw data is flattened by subtraction of the mean plane of the picture (Figure 9) which is calculated for each picture by the least squares method. After subtraction, the "zero" level corresponds to the maximum of the Gaussian peak for *n*-dodecanethiol apparent height. Then, all pixels under the threshold of 0.40 nm were attributed the value zero, whereas the others were attributed the value 1 (Figure 9).
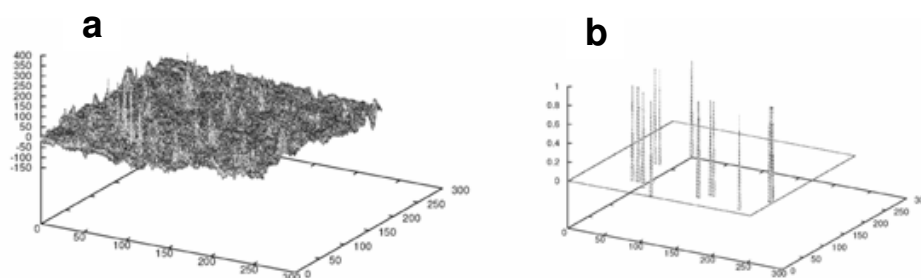

Figure 9 *Illustrations of the data treatment process for a 60x60 nm^2 STM picture. (a) After flattening of the raw picture (b) After thresholding of the flattened picture.*

138

The number of switches in the "on" state on each picture is then proportional to the sum of remaining pixels. Experimentally, we observe that for the ~1 nm bright spots corresponding to a single switch, the mean number of pixels overpassing the threshold is 3, so the number of pixels is transformed in a number of molecules by division. No other treatment than routine flattening has been applied to STM pictures before analysis. The resulting curve has been submitted to a simple three point smoothing.

5.6 References and Notes

[1] *Molecular Switches* (Ed.: B. L. Feringa), Wiley-VCH, Weinheim, Germany **2001**.

[2] R. R. Chance, A. Prock, R. Silbey, *Adv. Chem. Phys.* **1978**, *37*, 1-65.

[3] M. Irie, *Chem. Rev.* **2000**, *100*, 1683-1716.

[4] a) M. Irie, S. Kobatake, M. Horichi, *Science* **2001**, *291*, 1769-1772; b) S. H. Chen, H. M. P. Chen, Y. Geng, S. D. Jacobs, K. L. Marshall, T. N. Blanton, *Adv. Mater.* **2003**, *15*, 1061-1065; c) T. Yamaguchi, K. Nomiyama, M. Isayama, M. Irie, *Adv. Mater.* **2005**, *16*, 643-645; d) T. Kawai, Y. Nakashima, M. Irie, *Adv. Mater.* **2005**, *17*, 309-314.

[5] a) M. Irie, T. Fukaminato, T. Sasaki, N. Tamai, T. Kawai, *Nature* **2002**, *420*, 759-760; b) H. Tian, B. Chen, H. Tu, K. Mullen, *Adv. Mater.* **2002**, *14*, 918-923.

[6] a) W. R. Browne, J. J. D. de Jong, T. Kudernac, M. Walko, L. N. Lucas, K. Uchida, J. H. van Esch, B. L. Feringa, *Chem. Eur. J.* **2005**, *11*, 6414-6429. b) A. Peters, N. R. Branda, *J. Am. Chem. Soc.* **2003**, *125*, 3404-3405; c) W. R. Browne, J. J. D. de Jong, T. Kudernac, M. Walko, L. N. Lucas, K. Uchida, J. H. van Esch, B. L. Feringa, *Chem. Eur. J.* **2005**, *11*, 6430-6441; d) J. Areephong, W. R. Browne, N. Katsonis, B. L. Feringa, *Chem. Commun.*, **2006**, 3930-3932.

[7] S. J. Kawai, S. L. Gilat, J. M. Lehn, *Eur. J. Org. Chem.* **1999**, 2359-2366.

[8] K. Matsuda, M. Irie, *J. Am. Chem. Soc.* **2000**, *122*, 7195-7201.

[9] J. J. D. de Jong, L. N. Lucas, R. M. Kellogg, J. H. van Esch, B. L. Feringa, *Science* **2004**, *304*, 278-281.

[10] D. Dulic, S. J. van der Molen, T. Kudernac, H. T. Jonkman, J. J. D. de Jong, T. N. Bowden, J. van Esch, B. L. Feringa, B. J. van Wees, *Phys. Rev. Lett.* **2003**, *91*, 207402.

[11] S. J. van der Molen, H. van der Vegte, T. Kudernac, I. Amin, B. L. Feringa, B. J. vanWees, *Nanotechnology* **2006**, *17*, 310-314.

[12] J. He, F. Chen, P. A. Liddell, J. Andreasson, S. D. Straight, D. Gust, T. A. Moore, A. L. Moore, J. Li, O. F. Sankey, S. M. Lindsay., *Nanotechnology* **2005**, *16*, 695-702.

[13] J. Li, G. Speyer, O. F. Sankey, *Phys. Rev. Lett.* **2004**, *93*, 248302.

[14] M. Kondo, T. Tada, K. Yoshizawa, *Chem. Phys. Lett.* **2005**, *412*, 55-59.

[15] S. Kobatake, M. Irie, *Tetrahedron* **2003**, *59*, 8359-8364.

[16] M. Wanunu, A. Vaskevich, I. Rubinstein, *J. Am. Chem. Soc.* **2004**, *126*, 5569-5576.

[17] This is confirmed by the S 2p core level X-ray photoelectron spectroscopy (XPS) spectrum. The first peak for which S $2p_{3/2}$ is found at 161.8 eV indicates chemisorbed thiols. The main peak with the S $2p_{3/2}$ at 163.4 eV corresponds to the thiophene sulfur atoms.

[18] D. G. Castner, K. Hinds, D. W. Grainger, *Langmuir* **1996**, *12*, 5083-5086.

[19] H. Ahn, M. Kim, D. J. Sandman, J. E. Whitten, *Langmuir* **2003**, *19*, 5303-5310.

[20] a) L. A. Bumm, J. J. Arnold, M. T. Cygan, T. D. Dunbar, T. P. Burgin, L. Jones II, D. L. Allara, J. M. Tour, P. S. Weiss, *Science* **1996**, *271*, 1705-1707; b) M. T. Cygan, T. D. Dunbar, J. J. Arnold, L. A. Bumm, N. F. Shedlock, T. P. Burgin, L. Jones, D. L. Allara, J. M. Tour, P. S. Weiss, *J. Am. Chem. Soc.* **1998**, *120*, 2721-2732.

[21] G. E. Poirier, *Chem. Rev.* **1997**, *97*, 1117-1127.

[22] L. Muller-Meskamp, B. Lussen, S. Karthauser, R. Waser, *J. Phys. Chem. B* **2005**, *109*, 11424-11426.

[23] K. Moth-Poulsen, L. Patrone, N. Stuhr-Hansen, J. B. Christensen, J.-B. Bourgoin, T. Bjørnholm, *Nano Lett.* **2005**, *5*, 783-785; b) Z. J. Donhauser, B. A. Mantooth, K. F. Kelly, L. A. Bumm, J. D. Monnell, J. J. Stapleton, D. W. Price, A. M. Rawlett, D. L. Allara, J. M. Tour, P. S. Weiss, *Science* **2001,** *292*, 2303-2307; c) P. A. Lewis, C. E. Inman, Y. Yao, J. M. Tour, J. E. Hutchison, P. S. Weiss, *J. Am. Chem. Soc.* **2004**, *126*, 12214-12215.

[24] XPS excludes the possibility of desorption of the molecules, because after irradiation, no oxidized species of sulfur can be detected at binding energies between 168.5 and 170 eV.

[25] G. K. Ramachandran, T. J. Hopson, A. M. Rawlett, L. A. Nagahara, A. Primak, S. M. Lindsay, *Science* **2003**, *300*, 1413-1416.

[26] M. O. Wolf, M. A. Fox, *Langmuir* **1996**, *12*, 955-962.

[27] A. Peters, N. R. Branda, *Chem. Commun.* **2003**, 954-955.

[28] C. P. Collier, G. Mattersteig, E. W. Wong, Y. Luo, K. Beverly, J. Sampaio, F. M. Raymo, J. F. Stoddart, J. R. Heath, *Science* **2000**, *289*, 1172-1175.

[29] S. Grafstrom, *Appl. Phys. Rev.* **2002**, *91*, 1717-1753.

[30] a) J. E. Green, J. W. Choi, A. Boukai, Y. Bunimovich, E. Johnston-Halperin, E. DeIonno, Y. Luo, B. A. Sheriff, K. Xu, Y. S. Shin, H. –R. Tseng, J. F. Stoddart, J. R. Heath, *Nature*

140

2007, *445*, 414-417; b) H. B. Akkerman, P. W. M. Blom, D. M. de Leeuw, B. de Boer, *Nature* **2006**, *441*, 69-72.

[31] J. F. Moulder, W. F. Stickle, P. E. Sobol, K. D. Bomben, *Handbook of Photoelectron Spectroscopy*, Perkin-Elmer Corporation, Physical Electronics Division: Eden Prairie, MN, **1992**.

Chapter 6

Intermolecular Repulsion through Interfacial Attraction: Polymorphism in Self-Assembled Monolayers

A comparative study of the structure of molecular monolayers is reported, formed spontaneously at the interface between a series of atomically flat surfaces and a solution containing a Schiff-base derivative (PHB). Scanning tunneling microscopy (STM) at the liquid/solid interface shows that PHB forms well-ordered monolayers characterized by a columnar packing on all surfaces employed, including highly oriented pyrolytic graphite (HOPG), Au(111), MoS_2 and pentacontane-modified HOPG. Notably, a polymorphic monolayer is formed on Au(111), where in addition to the columnar arrangement, PHB molecules form dimeric structures also. It is shown that the formation of a dimeric 2D crystal on Au(111) is associated with a decrease in the surface density of the molecules. The decrease in surface density is ascribed to a strong interaction between PHB and the Au(111) surface, which induces partial charging of the aromatic moieties of PHB. These results suggest that polymorphism on Au(111) originates from molecule/surface attraction, which in turn induces molecule/molecule repulsion. They highlight the importance of considering molecule/molecule and molecule/substrate interactions both as independent and interdependent phenomena in understanding the mechanisms behind the formation of polymorphous 2D crystals on a surface.[*]

6.1 Introduction

Crystal polymorphism, which embodies the ability of molecules to form various packing arrangements displaying different physical and chemical characteristics, is of paramount importance in fields such as pharmacology, solid-state chemistry, and material science.[1] In particular, understanding which interactions drive the formation of 2D polymorphic crystals is a key to achieve control over nanofabrication methods, which utilize the bottom-up molecular approach to build organic devices. The interactions, which are involved in 2D self-assembly, on top of solid surfaces, are divided most commonly into molecule/molecule, and molecule/substrate interactions.[2] Recent studies have highlighted that slight modifications in these interactions can induce structural transformations in the self-assembled monolayer formed at the liquid/solid interface.[2,3,4,5,6,7] The parameters, which have been investigated include length and position of alkyl chains,[3] modification of the aromatic core,[4] physico-chemical properties of the solvent,[3,5] and addition of guest molecules.[6] Alternatively, the influence of substrates on the structure of self-assembled monolayers, in particular at the liquid/solid interface, has not been addressed systematically and was limited to a comparison of two substrates only.[7]

In addition to the strength of molecule/surface interactions, several factors are responsible for the structure of a 2D crystal formed on a given substrate. Geometric factors e.g., lattice constants of the substrate, can affect packing geometry,[8] generally because monolayers are formed so as to maximize commensuration.[9] However, this trend can be counterbalanced by the fact that high packing densities also favor energy gain by adsorption. Additionally, self-assembly is influenced by molecule/molecule interactions. The formation of less densely packed adlayers can be favored when intermolecular interactions, such as H-bonding[2,10] or electrostatic interactions between longitudinal dipolar moments of the molecules[2,11] dominate the self-assembly process. If molecule/molecule repulsion is too strong, self-assembled monolayers do not form at the liquid/solid interface, however, deposition of molecules in UHV results in the formation of individually stabilized nanostructures.[12] Identifying which of the aforementioned factors dominates the self-assembly process is challenging since, in the comparison of self-assembled monolayers on different substrates, several parameters are varied.

In this chapter, the effect of a systematic variation of substrate on the geometry of self-assembled monolayers formed at the liquid/solid interface is discussed. The polymorphism observed on Au(111) exclusively, is rationalized by consideration of the substrate-induced intermolecular interactions. The structures of the 2D crystals formed spontaneously at liquid/solid interfaces are rationalized, typically, on the basis of independent analysis of

144

molecule/molecule and molecule/substrate interactions, and on the interplay between these contributions.[2,13] However, molecule/molecule and molecule/substrate interactions are not independent, and hence here we show that molecule/substrate interactions can be used to tune molecule/molecule interactions. A range of substrates were employed to investigate the interdependence of these interactions: metallic Au(111), semi-metallic highly oriented pyrolytic graphite (HOPG), semiconducting MoS_2 and pentacontane-modified HOPG. Surface-adsorbate coupling is expected to vary between each of the substrates because they have different geometrical patterns, corrugations and electronic characteristics.

The molecule that is used is a Schiff-base derivative, 4-(*n*-dodecyloxy)-N-(4-*n*-dodecyl)-phenyl-2-hydroxybenzaldimine (PHB, Figure 1). Schiff bases can be considered as molecular switches because they undergo cis/trans photoisomerisation. The 2D molecular organization of simple alkylated Schiff bases has been reported on HOPG.[14] PHB constitutes a more complex photochromic molecular switch belonging to the sub-class of N-salicylideneanilines, which comprise hydroxy-substituted derivatives of Schiff bases (Figure 1). These compounds have attracted considerable attention recently due to their photochromic, thermochromic and aggregative properties and their ability to act as versatile metal-binding ligands.[15] The central unit of PHB, composed of aromatic cores, is functionalized by two alkyl chains with a length of 1.5 nm, incorporated to stabilize the monolayer.[16] The hydrogen of the hydroxyl group can interact with the adjacent nitrogen atom forming an intramolecular hydrogen bond or it can interact with another molecule in its proximity, thus creating an intermolecular hydrogen bond (Figure 1).

PHB monomer   PHB dimer
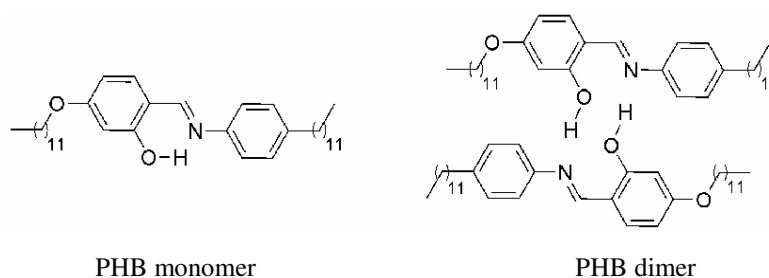
Figure 1 Structure of PHB monomer and dimer.

6.2 Scanning Tunneling Microscopy (STM) at the Liquid/Solid Interface

6.2.1 The Tunneling Effect, a Short Introduction

Let us consider an electron with an energy E which collides with a barrier of potential energy $V_0 > E$. Classical mechanics predict that the electron will not overcome the barrier. Alternatively, in quantum mechanics, the probability that this electron, which can be considered as a propagating wave, goes through the barrier of potential is not zero. Because everything happens as if the electron was using a tunnel to go through the barrier, this effect is known as the "tunneling effect". This effect was predicted early by quantum theory, but its first observation was not made until 1958 in p-n junctions of germanium.[17]

STM is based on the tunneling of electrons between two polarized electrodes, through an insulating medium such as vacuum, air or a carefully chosen liquid (Figure 2).[18] If we simplify the system by assuming that the two electrodes are made from the same metal, then the potential barrier that electrons have to overcome corresponds to the workfunction Φ of the metal, i.e. the energy which is necessary to take an electron from the metal. If the bias V applied between the two electrodes is small enough (eV $<< \Phi$), the barrier of potential has a trapezoidal shape and a simplified expression of the tunneling current can be given[19]:

$$I_{tunnel} = V \, e^{-2\kappa d} \quad \text{with} \quad \kappa \propto \sqrt{\Phi} \quad \text{and } d \text{ the distance between the two electrodes.}$$

This expression highlights that the tunneling current depends exponentially on the distance between the two involved electrodes, which means that its intensity is sensitive to this distance.

146
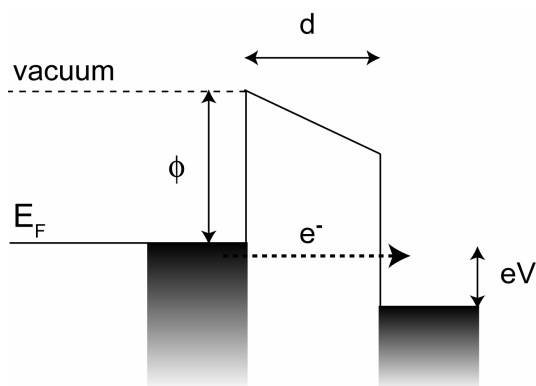
Figure 2 *Energy diagram for a tunneling junction polarized with a bias V. In this schematic representation, both electrodes have the same workfunction.*

In the configuration used for STM, the two electrodes which are used are a metallic tip and a conductive surface. Given a certain number of approximations Tersoff and Hamann have provided a more detailed expression of the tunneling current for this particular configuration.[20] In the expression they obtained it is of importance that the intensity of the tunneling current is directly proportional to the local density of states (DOS) of the tip and of the surface. Therefore, the variations of tunneling current on a surface cannot be interpreted strictly as topological variations, because they are directly related to the variations of DOS of the surface.

6.2.2 STM: the Experimental Setup

Basically, STM[21] consists in using a sharp tip in order to probe the surface of a conductive material (Figure 3), the tunneling current being localized between the apex of the tip and the planar conductive surface of the second electrode. By scanning the surface with the tip, it is thus possible to register the (amplified) variations of tunneling current, which are related to variations of topography and to spatial distribution of density of states. The main challenges in the implementation of such a concept lies in, first, the necessity to measure low intensities of tunneling current (typically lower than 50 pA), and, second, to control the displacement of the tip with nanoscale precision. These difficulties have been overcome by the development of ever more efficient preamplifiers and by the use of piezoelectric ceramics to displace the tip. In the work described hereafter, the STM was operated in "constant current" mode, where the tip scans the surface while a regulation loop imposes a setpoint value for the tunneling current. Therefore, the feedback loop readjusts the vertical position of the tip for each measuring point. These variations of height of the tip are the data which allows obtaining information about the structure of the conductive surface. In

147

particular, provided that the tunneling barrier has the same height everywhere, this allows mapping the repartition of electronic states of the surface. In STM images, the tip height variations are converted into coded colors in order to give a 2D representation.
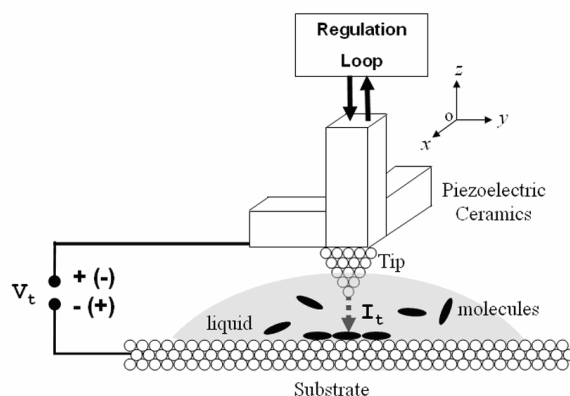

Figure 3 *Schematic description of a STM setup for experiments at liquid/solid interface.*

6.2.3 STM of Molecular Monolayers at the Liquid/Solid Interface

In the years following the birth of STM, the technique has been used mainly to study surfaces of metal or semiconductors,[22] which requires the use of ultra high vacuum (UHV) conditions because of the reactivity of these surfaces to atmospheric components. However, UHV experiments are quite expensive and time-consuming. Alternatively, it is possible to use STM under ambient conditions, in air or at the liquid/solid interface.[23] At the liquid/solid interface, the surface is scanned while the tip is immersed in an insulating liquid (Figure 3). These experimental conditions are well adapted to the study of molecular monolayers formed on conductive surfaces, because the liquid not only protects the tunneling gap from atmospheric impurities, but it can also be used as a solvent for the molecules to be studied. Upon deposition of a droplet of a solution on an atomically flat and conductive surface, the solubilized molecules are free to diffuse towards the surface and thus to form molecular monolayers by self-assembly. Since molecular monolayers are quite insulating, it is not strictly possible to study them directly by STM. What is registered by STM is in fact the DOS of a conductive surface modulated by the DOS of the adsorbed molecules. This conductive surface is also referred to as the substrate.

148

6.2.4   Description of the Solvent

The solvent should be commercially available, and apolar (and consequently hydrophobic) in order to avoid the creation of ion-mediated "leakage" currents between the tip and the surface. Moreover, it should not be too volatile over the timescale of the experiment. For the experiments described in this chapter n-tetradecane was used as a solvent, meeting these requirements.

6.2.5   Description of the Substrates

6.2.5.1   *Highly Oriented Pyrolytic Graphite (HOPG)*

Graphite occurs naturally but the graphite which is commonly used for research is a synthetic material called highly oriented pyrolytic graphite (HOPG). HOPG is composed of layers of carbon with hexagonal symmetry, called graphene sheets (Figure 4a). Because graphene sheets are held together by relatively weak van der Waals interactions, HOPG is easily cleavable, i.e. it is possible to dissociate graphene layers by use of scotch tape.[24] Freshly cleaved surfaces of graphite are composed by very large (typically a few hundreds of nanometers) and atomically flat terraces.
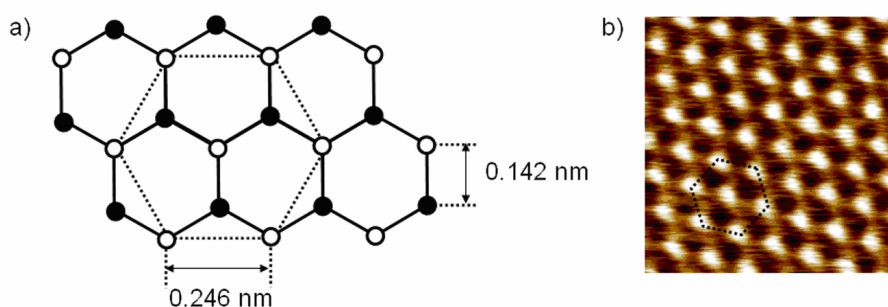
Figure 4 a) Structure of the cleaved surface of HOPG. Full circles represent the α atoms of the graphene sheet, which are placed on top of an underlying carbon atom. Open circles represent the β atoms. By using typical scanning conditions, usually only the β atoms are visible by STM. b) STM image (1.7x 1.7 nm^2) of HOPG with atomic resolution ($V_T = 180$ mV, $i_T = 46$ pA).

The structure of the cleaved surface of HOPG as observed by STM is a centered hexagonal (Figure 4b), whereas it should be a simple hexagonal (honeycomb structure, Figure 4a). Moreover, the distance observed between two bright spots on the STM image (0.246 nm) is

149

higher than the expected interatomic distance within a sheet of graphene (0.142 nm). This phenomenon is illustrative of the fact that STM does not provide a measure of geometrical structures but of electronic structures. In fact, this peculiar STM contrast is due to the fact that not all carbon atoms of a graphene sheet are equivalent. Due to a shift between adjacent graphene sheets some atoms are on top of an atom of the underlying sheet (α type), but some are not (β type). Consequently, with most scanning conditions, the β type atoms are generating a much brighter contrast and are thus the ones which are visible by STM.[25]

6.2.5.2 A Gold Substrate: Au(111)

Figure 5 shows typical STM images that can be obtained on the Au(111) surface. At large scale, the morphology of this substrate is characterized by triangular terraces which can reach areas of a few nm^2. These terraces are triangular because the stepedges delimitating them follow lines which are oriented at 120° with each other. These lines correspond to <110> directions of a (111) surface of gold,. The step edges have a height of 0.25 nm, which is close to the distance between two (111) crystallographic planes of gold. At medium scale, the typical feature of the Au(111) surface lies in its reconstruction lines, which correspond to relaxation of the surface atoms of gold.[26] Usually, these 22x√3 reconstruction lines follow a herringbone pattern. Observation of these lines is of crucial importance to ensure for cleanliness and quality of the prepared substrate. Atomic scale resolution is not possible to obtain by STM at the liquid/solid interface, but is achievable in ultra high vacuum, where it reveals the hexagonal centered structure shown on Figure 5c.
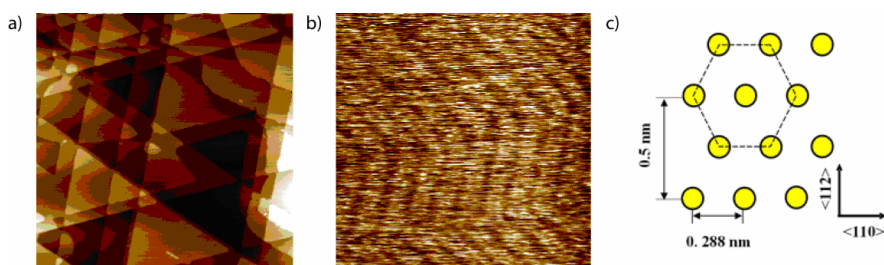
Figure 5 *Structure of Au(111). a) STM image (500x 500 nm^2) of Au(111) triangular terraces in air (V_T= -418 mV, i_T= 59 pA). b) STM image (78 x 78 nm^2) of Au(111) herringbone reconstruction in air (V_T= 630 mV, i_T= 30 pA). c) Schematic representation of the structure of the Au(111) surface. Each yellow dots represents one atom of gold.*

6.2.5.3 Molybdenum disulfide (MoS₂)

MoS$_2$ is a semi-conducting material found in nature as "molybdenite". It crystallizes with a layered structure shown in Figure 6a. Each layer is composed of sheets of molybdenum atoms sandwiched between sheets of sulphur atoms. As for HOPG, MoS$_2$ can be easily cleaved, but unlike HOPG this cleaving forms large 2D monocrystals. On the MoS$_2$ cleavage surface, sulfur atoms form a centered hexagonal network (similar to the network of Au(111)) with an interatomic distance of a = 0.316 nm.
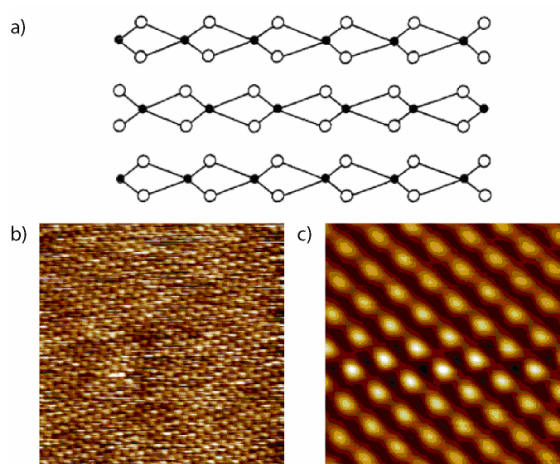
Figure 6 *Structure of the surface obtained by cleaving of MoS₂. a) The layered structure of MoS₂. Open circles represent sulfur atoms, the closed circles molybdenum atoms. b) STM image (7.7 x 7.7 nm²) of the MoS₂ surface in n-tetradecane, with atomic resolution (V_T = 400mV, i_T = 20 pA). c) Zoomed in area of the previous STM image (2.0 x 2.0 nm²), filtered by cross-correlation. This image shows a hexagonal network of bright spots corresponding to the location of the sulphur atoms.*

6.3 Synthesis of PHB

Schiff-base derivative PHB was prepared according to the Scheme 1 from known 4-*n*-dodecyloxy-2-hydroxybenzaldehyde[27] by reacting it with commercially available 4-*n*-dodecylaniline in ethanol with the presence of a catalytic amount of acetic acid. The resulting PHB was fully characterized by means of ^{1}H and ^{13}C NMR spectroscopy and mass spectroscopy (experimental section).

151
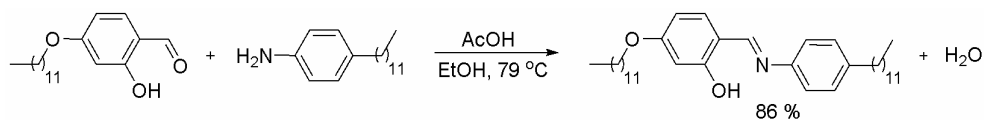
Scheme 1 *Synthesis of PHB.*

6.4 Columnar Packing on HOPG

Deposition of PHB from *n*-tetradecane onto highly ordered pyrolytic graphite (HOPG) leads to the formation of highly ordered self-assembled monolayers (Figure 7a). Within each domain, typically extending over a few hundreds of nanometers, STM images show regularly spaced bright columns separated by darker stripes, with an intercolumnar periodicity of a = 3.15 ± 0.05 nm. A mismatch between the columns is observed only rarely (Figure 7c). The relatively higher STM contrast is assigned to the two aromatic moieties of PHB (Figure 7b), whereas the lower contrast areas are assigned to the absorbed alkyl chains.[2] The intermolecular spacing within one bright column is b = 0.60 ± 0.01 nm. The regular spacing of the molecules within the columns suggests that intermolecular hydrogen bonding is not present between the molecular units.

152
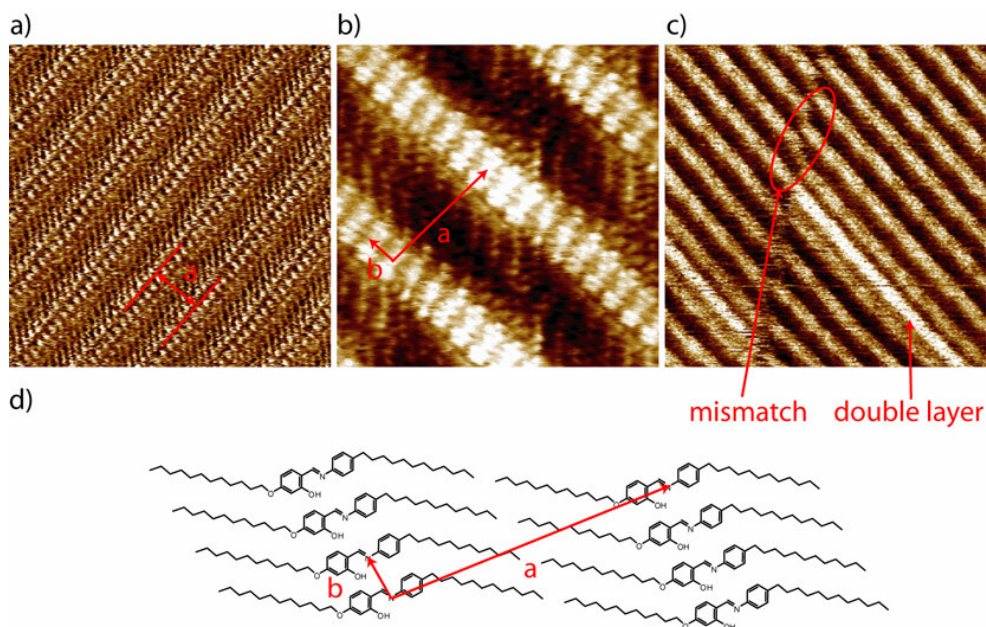
Figure 7 *a) STM image (20.1 x 20.1 nm^2) of a self-assembled monolayer of PHB on HOPG, V_T = 761 mV, i_T = 58 pA. b) High resolution STM image (7.2 x 7.2 nm^2) of PHB on HOPG, V_T = 374 mV, i_T = 9.2 pA. c) STM image (35.1 x 35.1 nm^2) of the monolayer of PHB on HOPG showing a "mismatch" between the columns within one domain, V_T = 827 mV, i_T = 32 pA. d) Schematic representation of the packing model proposed, and associated unit cell.*

Alkyl chains are aligned along one of the main <100> axes (determined by the direction of the periodicity of β atoms of HOPG, see Figure 4) of HOPG[28] and tilted by 46 ± 1° with respect to the main axis of the molecular columns. This tilt angle allows the chains to reach the well-known periodicity of densely packed alkanes on HOPG (~ 0.43 nm).[23] This implies that the self-assembly is dominated by alkyl chains through their 2D crystallization and their interaction with the surface. This is confirmed by the observation of inter-columnar spacing, which, instead of emulating the periodicity of the underlying substrate, is determined by the tilt and length of the alkyl tails.

6.5 Polymorphism on Au(111)

In order to compare the effects of different substrates on self-assembly, a solution of PHB in n-tetradecane was also deposited onto Au(111). As on HOPG, PHB molecules self-

153

assemble into parallel columns (Figure 8a,c). Within each column, the intermolecular spacing is the same as observed on HOPG. However, the angle between alkyl chains and the main columnar axis is $52 \pm 2°$, *i.e.* it is increased by $6°$ with respect to the angle observed on HOPG. Consequently, inter-columnar periodicity on Au (111) is increased up to 3.30 ± 0.05 nm. The tilt angle allows the alkyl chains to reach the well-known periodicity of densely packed alkanes on Au(111) (~0.48 nm)[29] and to align along the <110> axis,[28] which is known to be the favored direction of adsorption for alkanes on Au(111).[29] The mismatch between the periodicity of the Au(111) lattice and the inter-columnar and intermolecular periodicities of PHB molecules, indicates that alkyl chain adsorption is again the dominating factor determining the packing geometry. However, mismatches and other packing defects are observed more frequently on Au(111) than on HOPG. Typically, the columns are formed by less than a dozen molecules. The presence of these defects could be interpreted as the stronger adsorption of PHB molecules on Au(111) than on HOPG, which would render the repair of defects by either diffusion on the surface, or by desorption and subsequent re-adsorption from solution, energetically unfavorable. However, this hypothesis can be excluded as during scanning, we observed in real time the formation of a misfit dislocation within an ordered area (Figure 9), which suggests that the adsorption/desorption processes are sufficiently fast for the monolayer to reach thermodynamic equilibrium. Consequently, we conclude that the formation of defects on Au(111) is not a kinetically driven phenomenon.
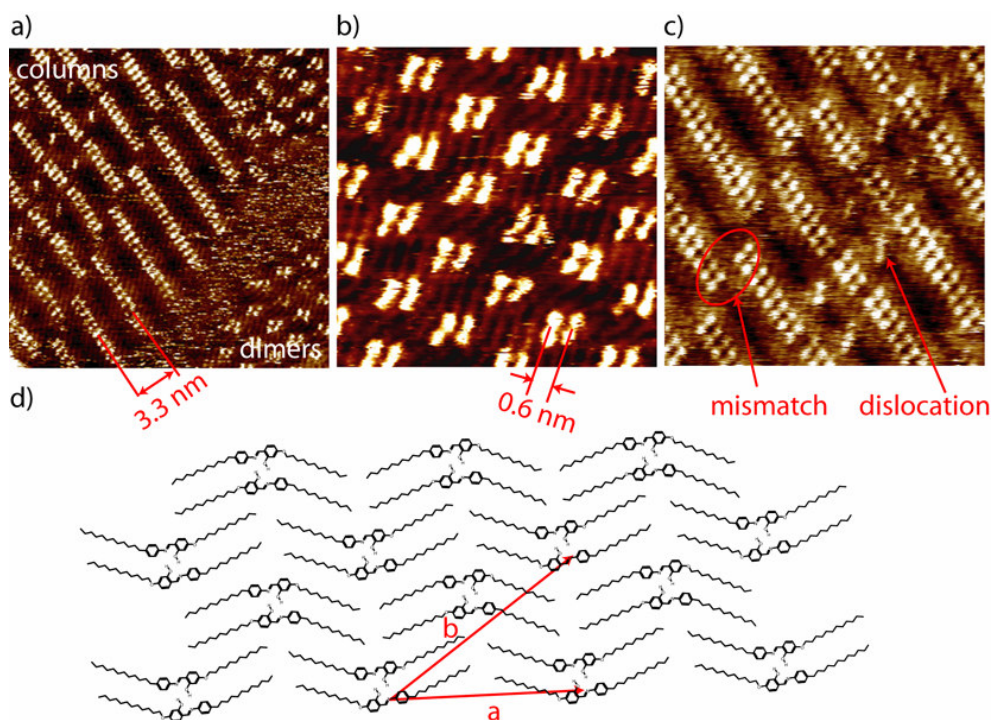
Figure 8 *a) STM image (24.7 x 24.7 nm^2) of the self-assembled monolayer of PHB on Au(111), V_T = -300 mV, i_T = 34 pA. b) High resolution STM image (9.3 x 9.3 nm^2) of PHB on Au(111) showing the area with molecules associated into the dimers, V_T = 340 mV, i_T = 37 pA. c) High resolution STM image (14.1 x 14.1 nm^2) of PHB on Au(111) showing the "mismatch" of the columns and the dislocations within one domain of columnar packing, V_T = 290 mV, i_T = 24 pA. d) Tentative model of PHB packing on Au(111) associated with areas of dimer formation. In this proposed model distances and angles fit the anticipated geometries.*

In addition to a columnar structure, a second type of packing of PHB was observed on Au(111), in which molecules associate into dimers and create a regular zig-zag pattern (Figure 8 a,b). Within a dimer, the intermolecular distance, 0.60 ± 0.02, nm is comparable to the intermolecular distance in the columnar structure. Despite this similar spacing between molecules, it is likely that the dimers are stabilized by hydrogen bonding (Figure 8d).[*] Alkyl chains adopt a *cis* orientation with respect to the central aromatic unit and align parallel to the <110> direction of Au(111). The distance between alkyl chains within a

---

[*] The hypothesis of the stabilization by intermolecular hydrogen bonding has to be further confirmed by molecular modeling calculations.

dimer 0.49 ± 0.02 nm is the same as the spacing between alkanes adsorbed on Au(111),[29] which means that they occupy optimal adsorption sites on the surface. The unit cell consists of four molecules and the average area per molecule is 2.40 ± 0.04 nm^2, which is 21% more than for columnar packing 1.98 ± 0.04 nm^2.
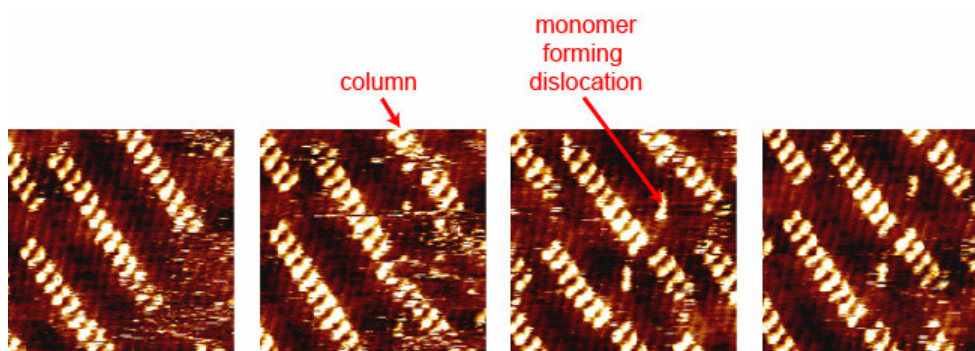

Figure 9 *Series of STM images (9.3 x 9.3 nm^2) highlighting the formation of a misfit dislocation in real time. The time scale of the measurement is 24 s per picture. V_T = - 300 mV, i_T = 37 pA*

6.6 Origin of Polymorphism on Au(111): Driving Force for Dimer Formation

It is noticeable that compared to columnar packing (Figure 8c), the dimeric structure formed on Au(111) (Figure 8b) shows an increase of average area per molecule of 21%. Throughout the STM measurements partial interconversions between columnar and dimeric structures were observed as can be seen in Figure 10 (dimer to column interconversion) and Figure 11 (column to dimer interconversion). Since the interconversion between both structures can be observed on the timescale of the STM measurements, we conclude that the activation energy of the interconversion is low and that adsorption energies are comparable for both structures. Consequently there must be an additional stabilizing effect in the dimer structure, which compensates for the loss in free energy associated with the lower density of packing. We propose that the formation of dimers on Au(111) is made possible by the presence of repulsive forces between the aromatic cores of PHB. Compared to (hypothetical dimers in) columnar packing, dimer packing allows additional stabilization because the equilibrium distance between dimers of PHB is increased: as dimers are separated from each other by insulating alkyl chains, destabilization through repulsion is minimized. Intermolecular hydrogen bonding is likely to contribute to the stabilization of dimers, however, since the spacing between the aromatic moieties within a dimer remains

156

unchanged with respect to the spacing between two molecules in columnar packing, it is unlikely that this factor would be sufficient to account for dimer formation.
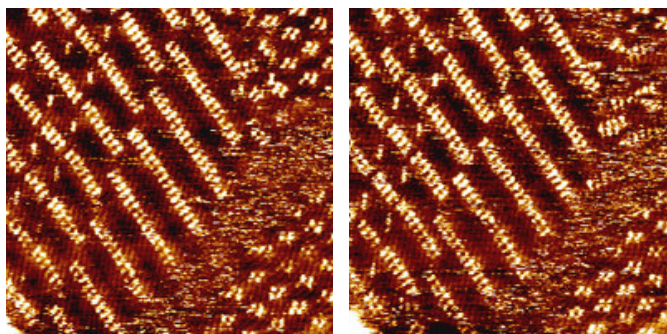

Figure 10 *Consecutive STM images of the same area (24.7 x 24.7 nm^2). During scanning, part of the dimer-packed area (top right part of the image) transforms into an area of columnar packing. V_T = - 300 mV, i_T = 34 pA.*
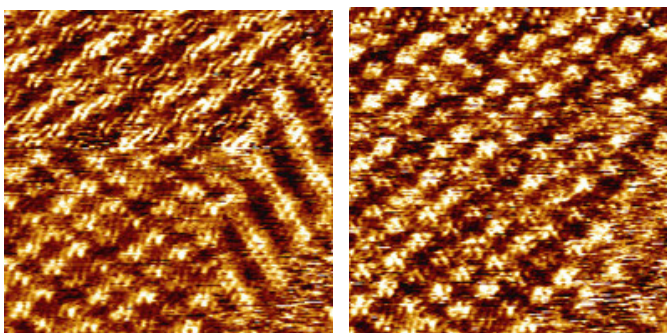

Figure 11 *Consecutive STM images of the same area (22.4 x 22.4 nm^2). During scanning, part of the columnar-packed area (right part of the image) is transformed into an area of dimer packing. V_T= 350 mV, i_T = 21 pA.*

In the light of these results we sought an explanation to account for the occurrence of repulsive forces and consequently for polymorphism within the self-assembled monolayer. We propose that molecule/molecule repulsive forces arise from molecule/substrate interactions, through either van der Waals or charge transfer interactions, or both of them.[*]

---

[*] In order to validate this hypothesis complementary experimental and theoretical investigations on interfacial dipole moments and possible charge transfer interactions are currently being conducted by means of XPS and UPS spectroscopies and molecular modeling calculations. Also see discussion below.

157

In physisorbed systems, attractive van der Waals interactions are present between the adsorbate and the substrate.[30] It is well known that when a molecule adsorbs on a substrate its permanent and induced dipolar moment create opposite image charges in the substrate. This leads to the formation of interfacial dipole moments, which are oriented perpendicularly to the surface.[31] Given that all interfacial dipoles are oriented in the same direction, lateral repulsive forces between dipoles increase the Gibbs free energy of the system. The strength of the induced dipole moment, and consequently of the repulsion, for different parts of the molecule interacting with the substrate, is a function of their polarizability. Since the polarizability of alkanes is low compared to that of aromatic compounds[32] we can assume that repulsions resulting from the induced dipole moment of the alkyl chains are negligible. This assumption is supported by the well-known formation of highly organized and densely packed adlayers of alkanes at different liquid/solid interfaces.[16,28,33]

However, it is likely that the intensity of induced surface dipoles formed through van der Waals interactions alone is not strong enough to explain polymorphism in PHB monolayers on Au(111). Calculations on the adsorption energy of cyanobiphenyl self-organized monolayers on MoS_2 have shown that neither the STM nor the XRD observations can be explained by dipolar and quadripolar interactions arising from the van der Waals interactions between molecule and substrate.[34] This suggests that in some cases the surface-induced intermolecular repulsion, and as a consequence the 2D crystal reorganization, arises from strong repulsive forces mainly created by partial charge transfer at the interface. Charge transfer between aromatic compounds and a conductive surface has been established recently with several techniques including photoemission spectroscopy,[35] reflectance absorption infrared spectroscopy,[36] scanning tunneling spectroscopy in UHV[37] or at the liquid/solid interface.[38] As a consequence, partially charged adsorbates of the same sign repel each other and increase the Gibbs free energy of system.

Whether charge transfer or van der Waals interactions are dominant features involved in the adsorption, both induce greater charging of the adsorbate on Au(111) than on HOPG. Therefore it is anticipated that stronger intermolecular repulsions between PHB molecules on Au(111) induce defects and strains within the columns of columnar packed structures and consequently increases the energy of the columnar lattice. This facilitates formation of the dimer lattice, which has a lower packing density and allows the aromatic units to be spaced further apart than in columnar packing. Both columnar and dimeric structure can thus coexist on Au(111) due to the similar energies unlike on HOPG where the columnar structure is more stable.

158

As discussed above, substrate-induced polymorphism can originate not only, as is shown, from substrate-induced intermolecular interactions, but also from simple geometric factors. In this particular case, the decreased surface density of the dimer packing on Au(111) could be due to the fact that the Au(111) lattice has a higher periodicity than the hexagonal HOPG lattice. However, these geometric factors do not play a significant role in the expansion of the molecular monolayer on Au(111) since the aromatic units of the molecules do not emulate the periodicity of the substrate, i.e. they show a low degree of commensuration with the substrate. STM experiments with PHB monolayers on other substrates, for example on MoS_2, on which the density of packing of alkanes has been shown previously to be the same as on Au(111),[33] and on pentacontane-(n-$C_{50}H_{102}$)-modified HOPG were carried out to exclude this possibility further.

6.7 Possible Influence of Geometrical Factors: Self-Assembly on MoS_2 and C50/HOPG

Deposition of PHB was performed on MoS_2 to exclude the influence of a modification in lattice periodicity and thereby to confirm the importance of the substrate-aromatic core interaction in the polymorphism observed on Au(111). Linear alkanes form self-organized monolayers on MoS_2 with an intermolecular distance of 0.48 ± 0.02 nm.[32] In contrast to HOPG and Au(111), the periodicities of adsorbed alkanes and of the substrate do not correspond on MoS_2: the periodicity of alkanes on MoS_2 mimics the spacing of alkanes in the bulk phase. This periodicity of packing for alkanes on MoS_2 is comparable to that reported on Au(111). Therefore, if only geometrical factors would be involved in the formation of bimorphic structures on Au(111) and assuming that 2D crystallization of alkyl tails is the prevailing factor of the self-assembly on MoS_2 as on Au(111), then a polymorphic monolayer with two different structures should be observed on MoS_2, as on Au(111). Since only columnar structures are observed on MoS_2 (*vide infra*), this experimental result supports that geometrical effects are not involved in polymorphism on Au(111).

Figure 12a shows a typical STM image of a self-organized monolayer of PHB on MoS_2. Within experimental uncertainty, the lattice constants are the same as those determined for self-organized monolayers on Au(111). The inter-columnar periodicity is 3.3 ± 0.1 nm and the intermolecular spacing within each column is 0.61 ± 0.02 nm. The separation between alkyl tails is 0.49 ± 0.02 nm and they adopt an angle of 53 ± 2° with respect to the columnar axis. The monolayer displays a low degree of commensurability and large uniform domains extending over a few hundreds of nanometers, free of mismatches or dislocations. Dimer

159

formation was never observed. This suggests that, in contrast to Au(111), strong intermolecular repulsive forces are absent. The semi-conducting nature of MoS_2 and hence the large energy gap between occupied and unoccupied states, limits the ability of MoS_2 to interact with orbitals of adsorbed molecules. Thus, PHB molecules cannot form charge transfer complexes on MoS_2 as readily as on Au(111).[39] We conclude that because charge transfer does not occur, the MoS_2 surface generates weaker adsorbate-surface interactions than those present on Au(111), and hence weaker intermolecular repulsion within the monolayer.
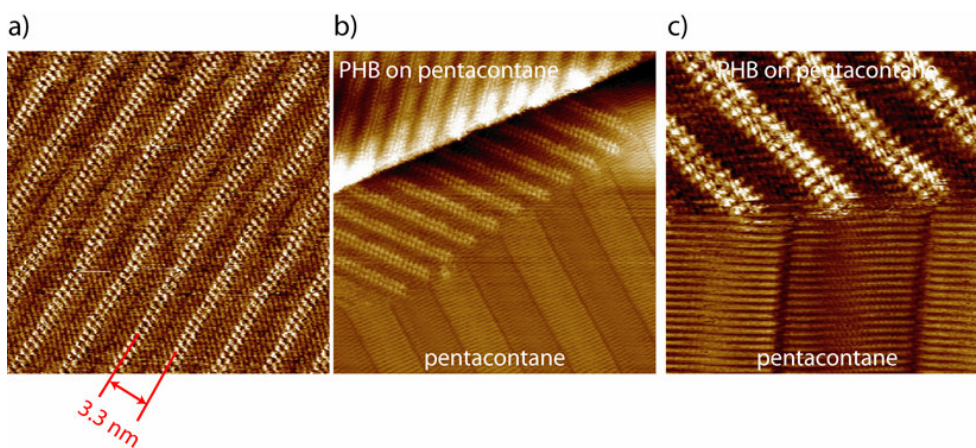
Figure 12 *a) STM image (27.2 x 27.2 nm^2) of the self-assembled monolayer of PHB on MoS_2, V_T = 2830 mV, i_T = 19 pA. b) STM image (43.8 x 43.8 nm^2) showing a growth of the domain composed of PHB on top of pentacontane-modified HOPG (n-$C_{50}H_{102}$/HOPG), V_T = 520 mV, i_T = 21 pA. c) High resolution STM image (15 x 15 nm^2) of the monolayer of PHB on (n-$C_{50}H_{102}$/HOPG), V_T = 520 mV, i_T = 21 pA.*

A second approach to elimination of charge transfer interactions is to employ buffer monolayers on top of which a self-assembled monolayer can be formed.[40] The buffer layer is typically composed of aliphatic alkanes[41] or functionalized alkanes[40,42] assembled on a surface, often HOPG. The buffer layer precludes electronic coupling of aromatic molecules with the substrate and hence limits charge transfer interactions. This strategy has been employed in the immobilization of phthalocyanines lacking the anchoring alkyl tails at the liquid/solid interface.[40] The immobilization was rationalized by reduction in charge transfer interactions between the aromatic molecules and HOPG.

In the present study a buffer layer composed of pentacontane (n-$C_{50}H_{102}$) was employed on HOPG, to study the self-assembly of PHB. Pentacontane is known to self-assemble on

160

HOPG by forming large domains of parallel lamellae[41] (Figure 12b, bottom part). Each lamella is composed of molecules oriented perpendicular to the lamellae direction and parallel to the <100> direction of the HOPG lattice. When PHB is deposited on pentacontane-modified HOPG (n-$C_{50}H_{102}$/HOPG) the domain formation is initiated primarily on step edges (Figure 12b). This suggests that molecule-substrate interactions are weak, decreasing the residence time of the molecule on the n-$C_{50}H_{102}$/HOPG surface and hence the probability of nucleation. High resolution STM images (Figure 12c) show that the alkyl tails of PHB are located in the troughs of the underlying pentacontane lamellae. Hence the formation of PHB columns is again expected to be driven by 2D crystallization of alkyl tails. As a consequence of the underlying buffer layer, whose geometry is directed by HOPG, the columnar structure has similar lattice characteristics as in case of the columns formed on bare HOPG. The inter-columnar periodicity is 3.15 ± 0.05 nm and the intermolecular spacing within each lamella is 0.60 ± 0.01 nm. The separation between alkyl tails is 0.42 ± 0.02 nm, as for simple alkanes on HOPG and they adopt an angle of $45 \pm 2°$ with the lamella axis. Neither defects within lamellae nor dimer formation were observed, indicating that intermolecular repulsion does not play as significant role as in the case of adsorption on Au(111) or HOPG.

6.8 Conclusions

In summary, this investigation indicates that in self-assembled monolayers, the 2D polymorphs that form spontaneously on a conductive Au(111) surface originate from surface-induced repulsion between aromatic units of the molecular building blocks. On Au(111), STM reveals two different packing types: a columnar packing, also observed on other surfaces including HOPG and MoS_2, and a dimer packing of lower density observed on Au(111) exclusively. We suggest that the presence of areas with dimer packing on Au(111) is due to a destabilization of the columnar packing in which partially charged aromatic units repel each other. This is likely to be a direct consequence of the ability of the substrate to form charge transfer interactions with the molecule, which, depending on the density and proximity of states, favors more conductive substrates. Further evidence of these strong intermolecular repulsions is found in the packing defects within the columnar packing. Such defects are observed frequently on Au(111), however, only rarely on HOPG, and never on MoS_2 or pentacontane-modified HOPG.

The demonstration that substrate-induced intermolecular repulsions can play a prominent role in 2D self-assembly highlights the fact that the effects of molecule/molecule and molecule/surface interactions on molecular packing cannot always be considered as independent phenomena. This also means that, in order to direct the self-assembly of

161

molecules into highly ordered patterns on a surface successfully, substrates must be chosen carefully.

Of particular note is the possibility of tuning the magnitude of intermolecular repulsive forces by varying the contribution of charge transfer between the substrate and adsorbed molecules and to reduce the strength of the interfacial dipole moment, which arises through physisorption of the molecules. By reducing the contribution of these effects, the need to employ strong intermolecular interactions such as coordination or hydrogen bonding, or the use of long alkyl spacer as stabilizing functional groups for monolayers at liquid/solid interface, can be reduced. In addition, it can be envisioned that when a mixture of two molecules is used to create a monolayer and one component acts as a donor forming a charge-transfer complex with the substrate and the other component as an acceptor, an evenly alternating monolayer composed of both components could be formed, which takes advantage of oppositely oriented interfacial dipoles. More generally, it is likely that by adjusting molecule/substrate interactions, intermolecular repulsion through interfacial attraction will provide an orthogonal approach to controlling the self-assembly process of monolayers.

6.9 Experimental Section

General Remarks

See Chapter 2 for details on synthetic methods and information on characterization of compounds.

Preparation of Substrates

Au(111) was prepared by evaporation of 99.99% gold, Umicore Materials AG, on freshly cleaved mica sheets, Ted Paella, Inc., at 10^{-7} mbar in a home-built evaporator in the Materials Science Centre, University of Groningen. The thickness of the gold layer was ~150 nm. Prior to formation of the self-assembled monolayer, reconstruction of the Au(111) surface was checked for by STM in *n*-tetradecane.

Highly oriented pyrolytic graphite (HOPG) was bought from Goodfellow and freshly cleaved prior to deposition of the molecules.

MoS_2 single crystals were provided by Dr. E. Lacaze, for which she is gratefully acknowledged. They were freshly cleaved before use.

Pentacontane-modified HOPG (n-$C_{50}H_{102}$/HOPG) was prepared by deposition of a warm droplet of saturated pentacontane (Fluka) solution in *n*-tetradecane (Aldrich), onto a freshly

162

cleaved surface of HOPG. The formation of the pentacontane monolayer was observed by STM. The excess of pentacontane was washed away with few droplets of tetradecane, before addition of the PHB monolayer.

Preparation of Samples

A solution of PHB in *n*-tetradecane (Aldrich) was sonicated for 5 min and heated at 40° for 20 min so as to form a saturated solution. A drop of the warm solution was applied to the prepared substrates and the STM tip was immersed into the solution for imaging.

Scanning Tunneling Microscopy (STM)

All experiments were performed at room temperature, using a PicoSPM (Molecular Imaging, Scientec), at the interface between the surface and tetradecane. Pt/Ir STM tips were prepared mechanically from Pt/Ir wire (80:20, diameter 0.25 mm, Goodfellow). The parameters of the unit cells were measured after drift effects were corrected with the Scanning Probe Image Processor (SPIP) software (Image Metrology ApS). However, the presented STM images contain raw data and are not subjected to any processing other than routine plane correction.

4-(Dodecyloxy)-N-(4-dodecyl)-phenyl-2-hydroxybenzaldimine (PHB)

The Schiff base derivative PHB was prepared by refluxing 2.34 g (7.65 mmol) of 4-dodecyloxy-2-hydroxybenzaldehyde with 2 g (7.65 mmol) of 4-dodecylaniline in absolute ethanol for 18 h, with a few drops of glacial acetic acid as the catalyst. The solvent was evaporated and the crude product was crystallized several times from hot absolute ethanol. Yield 86% (3.6 g). M. p. 102-103 °C; ^{1}H NMR (400 MHz, CDCl$_3$) δ 0.88 (t, 6H), 1.20-1.40 (m, 34H), 1.40-1.5 (m, 2H), 1.55-1.67 (m, 2H), 1.79 (quintet, *J*=7.7 Hz, 2H), 2.62 (t, 2H, *J*=7.7 Hz) 4.00 (t, *J*=6.6 Hz, 2H), 6.47 (d, *J*=8.3 Hz, 2H), 6.51 (s, 1H) 7.16-7.21 (m, 4H), 7.23 (d, 1H, *J*=8.3 Hz), 8.52 (s, 1H) ppm; ^{13}C NMR (100 MHz, CDCl$_3$) δ 14.1 (s), 22.7 (d), 26.0 (d), 29.1 (d), 29.2 (d), 29.3 (d), 29.5 (d), 29.6 (d), 29,6 (d), 29,7 (d), 31.5 (d), 31.9 (d), 35.5 (d), 68.2 (d), 101.5 (t), 107.5 (t), 120.7 (t), 129.3 (t), 133.3 (t), 141.4 (q), 145.8 (q), 160.5 (t), 163.4 (q), 164.0 (q) ppm; MS (EI): 549 [M+]; HRMS: calcd. for C$_{37}$H$_{59}$NO$_2$ 549.455, found 549.454.

6.10   References and Notes

[1] (a) I. Weissbuch, V. Y. Torbeev, L. Leiserowitz, M. Lahav, *Angew. Chem. Int. Ed.* **2005**, *44*, 3226-3229; (b) J. Bernstein, Polymorphism in Organic Crystals, Clarendon, Oxford, 2002.

² For recent reviews on STM investigations at the liquid-solid interface, see for example: (a) S. De Feyter, H. Uji-I, W. Mamdouh, A. Miura, J. Zhang, P. Jonkheijm, A. P. H. J. Schenning, E. W. Meijer, Z. Chen, F. Würthner, N. Schuurmans, J. van Esch, B. L. Feringa, A. E. Dulcey, V. Percec, F. C. De Schryver, *Int. J. Nanotechnology* **2006**, *3*, 462-479; (b) S. De Feyter, F. C. De Schryver, *Chem. Soc. Rev*. **2003**, *32*, 139-150; (c) S. De Feyter, F. C. De Schryver, *J. Phys. Chem. B* **2005**, *109*, 4290-4302; (d) P. Samorí, J. P. Rabe, *J Phys.: Condens. Matter* **2002**, *14*, 9955-9973; (e) L. C. Giancarlo, G. W. Flynn, *Acc. Chem. Res.* **2000**, *33*, 491-501; (f) L. –J. Wan, *Acc. Chem. Res*. **2006**, *39*, 334- 342; (g) D. M. Walba, F. Stevens, N. A. Clark, D. C. Parks, *Acc. Chem. Res*. **1996**, *29*, 591-597.

³ (a) K. Tahara, S. Furukawa, H. Uji-I, T. Uchino, T. Ichikawa, J. Zhang, W. Mamdouh, M. Sonoda, F. C. De Schryver, S. De Feyter, Y. Tobe, *J. Am. Chem. Soc*. **2006**, *128*, 16613-16625; (b) P. Wu, Q. Zeng, S. Xu, C. Wang, S. Yin, C. -L. Bai, *ChemPhysChem* **2001**, *2*, 750-754; (c) P. Zell, F. Mögele, U. Ziener, B. Rieger, *Chem. Eur. J*. **2006**, *12*, 3847-3857.

⁴ M. Palma, J. Levin, V. Lemaur, A. Liscio, V. Palermo, J. Cornil, Y. Geerts, M. Lehmann, P. Samori, *Adv. Mater*. **2006**, *24*, 3313-3317.

⁵ W. Mamdouh, H. Uji-I, J. S. Ladislaw, A. E. Dulcey, V. Percec, F. C. De Schryver, S. De Feyter, *J. Am. Chem. Soc*. **2006**, *128*, 317-325.

⁶ S. Furukawa, K. Tahara, F. C. De Schryver, M. Van der Auweraer, Y. Tobe, S. De Feyter, *Angew. Chem. Int. Ed*. **2007**, *46*, 2831-2834.

⁷ (a) K. Perronet, F. Charra, *Surf. Sci*. **2004**, *551*, 213-218; (b) N. Katsonis, A. Marchenko, D. Fichou, *Synth. Met*. **2004**, *147*, 73-77; (c) J. Gong, L. Wan, Q. Yuan, C. Bai, H. Jude, P. J. Stang, *Proc. Natl. Acad. Sci. U.S.A*. **2005**, *102*, 971-974; (d) N. Katsonis, J. Vicario, T. Kudernac, J. Visser, M. M. Pollard, B. L. Feringa, *J. Am. Chem. Soc*. **2006**, *128*, 15537-15541; (e) F. Lux, G. Lemercier, C. Andraud, G. Schull, F. Charra, *Langmuir* **2006**, *22*, 10874-10876.

⁸ For examples concerning n-alkanes, see: (a) A. J. Groszek, *Proc. R. Soc. A*. **1970**, *314*, 473-498; (b) O. Marchenko, J. Cousty, *Phys. Rev. Lett*. **2000**, *84*, 5363-5366.

⁹ E. Lacaze, R. Barois, *J. Phys. I France* **1997**, *7*, 1645-1664.

¹⁰ a) J. A. Theobald, N. S. Oxtoby, M. A. Phillips, N. R. Champness, P. H. Beton, *Nature* **2003**, *424*, 1029-1031; b) T. Yokoyama, S. Yokoyama, T. Kamikado, Y. Okuno, S. Mashiko, *Nature* **2001**, *413*, 619-621.

¹¹ a) G. Pawin, K. L. Wong, K. –Y. Kwon, L. Bartels, *Science* **2006**, *313*, 961-962; b) K. Wong, K. –Y. Kwon, B. V. Rao, A. Liu, L. Bartels, *J. Am. Chem. Soc*. **2004**, *126*, 7762-7763.

¹² J. Weckesser, A. De Vita, J. V. Barth, C. Cai, K. Kern, *Phys. Rev. Lett*. **2001**, *87*, 096101.

¹³ (a) A. Gesquiere, S. de Feyter, F. C. De Schryver, F. Schoonbeek, J. van Esch, R. M. Kellogg, B. L. Feringa, *Nano. Lett*. **2001**, *1*, 201-206; (b) M. Surin, P. Leclere, S. De

164

Feyter, M. M. S. Abdel-Mottaleb, F. C. De Schryver, O. Henze, W. J. Feast, R. Lazzaroni, *J. Phys. Chem. B.* **2006**, *110*, 7898-7908.

[14] Z. –C. Mu, J. –F. Kong, Y. Wang, G. –D. Yang, X. Zhang, *ChemPhysChem* **2004**, *5*, 202-206.

[15] (a) P. Guo, M. Liu, *Langmuir* **2005**, *21*, 3410-3412; (b) A. J. Gallant, M. J. MacLachlan, *Angew. Chem. Int. Ed.* **2003**, *42*, 5307-5310; (c) M. J. Ondrechen, J. M. Briggs, J. A. McCammon, *J. Am. Chem. Soc*. **2001**, *123*, 2830-2834; (d) E. Ito, H. Oji, T. Araki, K. Oichi, H. Ishii, Y. Ouchi, T. Ohta, N. Kosugi, Y. Maruyama, T. Naito, T. Inabe, K. Seki, *J. Am. Chem. Soc*. **1997**, *119*, 6336-6344.

[16] X. Qiu, C. Wang, Q. Zeng, B. Xu, S. Yin, H. Wang, S. Xu, C. Bai, *J. Am. Chem. Soc*. **2000**, *122*, 5550-5556.

[17] L. Esaki, *Phys. Rev*. **1958**, *109*, 603-604.

[18] "Scanning Tunneling Microscopy – From Birth to Adolescence", Nobel Lectures, Physics 1981-1990, Editor-in-Charge Tore Frängsmyr, Editor Gösta Ekspång, World Scientific Publishing Co., Singapore, **1993**.

[19] J.Simmons, *J. Appl. Phys*. **1963**, *34*, 1793-1803.

[20] J. Tersoff, D. R. Hamann, *Phys. Rev. Lett*. **1983**, *50*, 1998-2001.

[21] a) R. Wiesendanger, Scanning Probe Microscopy and Spectroscopy: Methods and Aplications, Gambridge University Press, 1998; b) C. Bai, Scanning Tunneling Microscopy and Its Applications, Springer-Verlag Berlin Heidelberg, 2000.

[22] G. Binnig, H. Rohrer, Ch. Gerber, E. Weibel, *Phys. Rev. Lett*. **1983**, *50*, 120-123.

[23] (a) J. P. Rabe, S. Buchholz, *Science* **1991**, *253*, 424-427; (b) G. C. McGonigal, R. H. Bernhardt, D. J. Thomson, *Appl. Phys. Lett*. **1990**, *57*, 28-30.

[24] S. -I. Park, C. F. Quate, *Appl. Phys. Lett*. **1986**, *48*, 112-114.

[25] A. Bryant, D. P. E. Smith, C. F. Quate, *Appl. Phys. Lett*. **1986**, *48*, 832-834; b) S. I. Park, C. F. Quate, *Appl. Phys. Lett*. **1986**, *48*, 112-114; c) D. Tomanek, S. G. Louie, H. J. Mamin, D. W. Abraham, R. E. Thomson, E. Ganz, J. Clarke, *Phys. Rev. B* **1987**, *35*, 7790-7793.

[26] J. V. Barth, H. Brune, G. Gertl, *Phys Rev B* **1990**, *42*, 9307-9317.

[27] K. Binnemans, Y. G. Galyametdinov, R. van Deun, D. W. Bruce, S. R. Collinson, A. P. Polishchuk, I. Bikchantaev, W. Haase, A. V. Prosvirin, L. Tinchurina, I. Litvinov, A. Gubajdullin, A. Rakhmatullin, K. Uytterhoeven, L. van Meervelt, *J. Am. Chem. Soc*. **2000**, *122*, 4335-4344.

[28] The orientation of the self-assembled monolayer with respect to HOPG was determined by imaging HOPG beneath the self-assembled monolayer. The orientation of PHB alkyl

chains with respect to Au(111) was determined by using the Au(111) reconstruction stripes which, under specific scanning conditions, can be distinguished under the self-assembled monolayer.

[29] (a) O. Marchenko, J. Cousty, *Phys. Rev. Lett*. **2000**, *84*, 5363-5366; (b) H. –M. Zhang, Z. Xie, B. –W. Mao, X. Xu, *Chem. Eur. J*. **2004**, *10*, 1415-1422; (c) A. Marchenko, S. Lukyanets, J. Cousty, *Phys. Rev. B* **2002**, *65*, 045414.

[30] K. W. Kolasinski, Surface Science: Foundations of Catalysis and Nanoscience; Wiley, Chichester, England, **2002**.

[31] S. M. Wetterer, D. J. Lavrich, T. Cummings, S. L. Bernasek, G. Scoles, *J. Phys. Chem. B*. **1998**, *102*, 9266-9275.

[32] E. V. Anslyn, D. A. Dougherty, Modern Physical Organic Chemistry, University Science Books, Sausalito, California, **2006**.

[33] S. Cincotti, J. P. Rabe, *Appl. Phys. Lett*. **1993**, *62*, 3531-3533.

[34] E. Lacaze, M. Alba, M. Goldmann, J. P. Michel, F. Rieutord, *Eur. J. Phys. B* **2004**, *39*, 261-272.

[35] H. Peisert, M. Knupfer, T. Schwieger, G. G. Fuentes, D. Olligs, J. Fink, Th. Schmidt, *J. Appl. Phys*. **2003**, *93*, 9683-9692.

[36] L. Scudiero, D. E. Barlow, K. W. Hipps, *J. Phys. Chem. B* **2002**, *106*, 996-1003.

[37] T. Nishino, T. Ito, Y. Umezawa, *Proc. Natl. Acad. Sci*. **2005**, *102*, 5659-5662.

[38] S. –B. Lei, K. Deng, D. –L. Yang, Q. –D. Zeng, C. Wang, *J. Phys. Chem. B* **2006**, *110*, 1256-1260.

[39] K. Iizumi, K. Ueno, K. Saiki, A. Koma, *Appl. Surf. Sci*. **2001**, *169-170*, 142-146.

[40] B. Xu, S. Yin, C. Wang, X. Qiu, Q. Zeng, C. Bai, *J. Phys. Chem. B* **2000**, *104*, 10502-10505.

[41] L. Piot, A. Marchenko, J. Wu, K. Müllen, D. Fichou, *J. Am. Chem. Soc*. **2005**, *127*, 16245-16250.

[42] (a) S. Lei, B. Xu, C. Wang, Q. Xu, L. Wan, C. Bai, *Jpn. J. Appl. Phys*. **2001**, *40*, 4273-4276; (b) S. -B. Lei, S. -X. Yia, C. Wang, L. -J. Wan, C. -L. Bai, *J. Phys. Chem. B* **2004**, *108*, 224-227; (c) S. Lei, C. Wang, L. Wan, C. Bai, *J. Phys. Chem. B* **2004**, *108*, 1173-1175.

Samenvatting

De ontwikkeling van elektronische apparatuur op nanometerschaal (miljardste meter), opgebouwd uit moleculaire componenten, is een grote uitdaging. Elektronica en informatiedragers met nanodimensies vereisen moleculaire bouwstenen, waarbij de omzetting tussen twee vormen van een molecuul extern aangestuurd moet kunnen worden. Moleculaire elektronica biedt veel mogelijkheden, aan de hand van moleculen die nieuwe operaties kunnen ondergaan die niet mogelijk zijn met conventionele halfgeleidertechnologie. Wellicht het meest elementaire deel van een moleculair apparaat is een molecuul dat geschakeld kan worden tussen twee toestanden van lage en hoge geleiding, wat wil zeggen dat deze aan- en uitgeschakeld kan worden.

Licht is een zeer aantrekkelijke vorm van externe aansturing voor zo'n schakel vanwege het aansturingsgemak, snelle responstijden en de compatibiliteit met gecondenseerde fasen. Optisch-elektronische schakelaars bieden nieuwe functionaliteit aan moleculaire elektronica, zolang de schakeleigenschappen behouden blijven als deze gebonden is aan een metaaloppervlak. Echter, interacties tussen de moleculen en een substraat kunnen de levensduur van de aangeslagen toestand van de moleculen zeer verkorten.

Fotochrome moleculaire schakelaars zijn verbindingen die reversibele lichtgeïnduceerde transformaties ondergaan tussen twee toestanden met duidelijk verschillende absorptiespectra (Schema 1). De twee isomeren hebben verschillende moleculaire geometrieën en fysische eigenschappen zoals hydrofobiciteit, redoxchemie etc. Het voordeel van fotochrome systemen ligt in hun aansturingsgemak, reversibiliteit en korte responstijden. Dit biedt de mogelijkheid om de locale en bulkeigenschappen van een moleculair systeem te veranderen aan de hand van bestraling. De veelzijdigheid van fotochrome moleculaire systemen heeft geleid tot hun toepassing in onder andere moleculaire geheugenapparatuur, moleculaire elektronica, *smart surfaces* en in de controle van supramoleculaire organisaties.

$$A \underset{\lambda_2}{\overset{\lambda_1}{\rightleftharpoons}} B$$
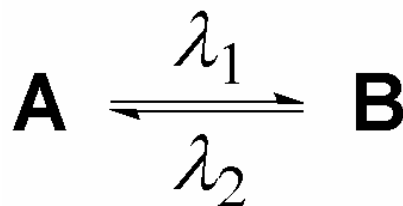
Schema 1 *Een optische moleculaire schakelaar die in twee verschillende vormen voorkomt, waarvan elk afzonderlijk beïnvloed kan worden met licht van specifieke golflengte.*

Vooral diarylethenen zijn veelbelovende lichtgeschakelde moleculen, vanwege de uitstekende reversibele stabiliteit van de lichtgeïnduceerde interconversie tussen de twee

isomere vormen. Deze twee vormen hebben elk verschillende eigenschappen voor ladingtransport. Zulke moleculen zijn goede kandidaten voor gebruik in moleculaire elektronica, waarbij moleculen gebonden zijn aan metalen contacten en waarbij door deze moleculen een elektrische stroom loopt (Schema 2).
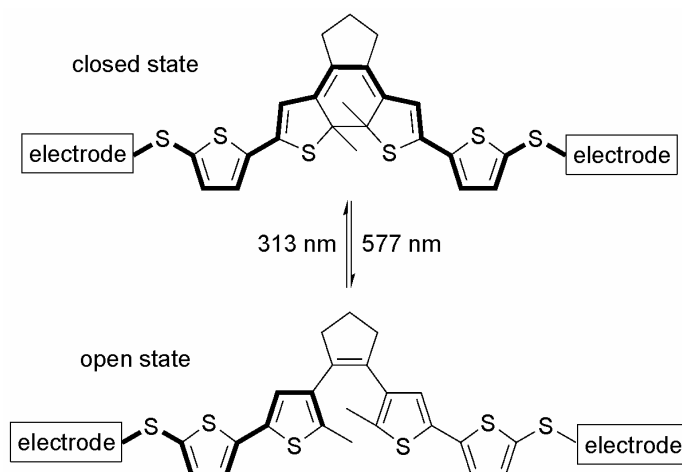

Schema 2 *Een fotochrome moleculaire schakelaar tussen twee elektroden in de gesloten en open toestand. Gedurende bestraling met 577 nm licht zal het molecuul van de gesloten naar de open vorm schakelen. Het molecuul kan teruggeschakeld worden naar de gesloten vorm door bestraling met UV licht van 313 nm.*

In dit proefschrift wordt de ontwikkeling beschreven van lichtgeschakelde elektronische moleculaire componenten gebaseerd op diarylethenen. In hoofdzaak draait het om fundamentele aspecten die opheldering vereisen voordat een volledig functionerend apparaat gemaakt kan worden. De speerpunten van dit onderzoek zijn: de synthese van de moleculaire componenten, fundamentele aspecten aangaande lichtgestimuleerde omzetting (bijvoorbeeld reversibiliteit, robuustheid, efficiëntie), de invloed van het verankeren van de moleculen aan een oppervlak op hun lichtgestuurde reactiviteit, de invloed die verschillende oppervlakken hebben op de ordening van moleculaire deeltjes en elektrische geleiding op moleculair niveau. Tenslotte wordt een antwoord gegeven op de vraag: kan stroomgeleiding geschakeld worden door één enkel molecuul?

De eerste poging tot lichtgeïnduceerde schakeling van geleiding via een enkel molecuul wordt behandeld in Hoofdstuk 2. Twee afzonderlijke technieken (MCBJ en STM) worden gebruikt om de veranderingen in de geleiding van individuele moleculen tijdens bestraling te volgen. De MCBJ sluit individuele diaryletheenmoleculen met geschikte

168

verankeringsgroepen in tussen twee elektroden. Metingen van de geleiding tonen een enorm verschil in de eigenschappen van ladingtransport tussen de gesloten en open vorm van het molecuul. Een schakelende geleiding van een individueel molecuul onder invloed van licht kan bestudeerd worden aan de hand van de weerstand. Echter, alleen de schakeling van de beter geleidende gesloten vorm naar de open vorm kan gevolgd worden. Dit is de belangrijkste beperking van de lichtgeïnduceerde schakeling van diaryletheenmoleculen wanneer deze door middel van chemisorptie aan goudoppervlakken zijn verankerd. Metingen met behulp van STM en MCBJ bevestigen het verschil in eigenschappen van ladingtransport van de verschillende isomeren van diarylethenen, evenals het irreversibele schakelgedrag van goudverankerde moleculen.

Hoofdstuk 3 behandelt de synthese van nieuwe diaryletheenderivaten die in staat zijn tot chemisorptie op goudoppervlakken. Verscheidene nieuwe derivaten zijn gemaakt met behulp van verschillende synthetische strategieën. Vervolgens zijn de fotochrome eigenschappen van de gesynthetiseerde moleculen bestudeerd in oplossing bij kamertemperatuur. Een typerende reversibele schakeling voor diarylethenen is waargenomen voor alle derivaten. Fotoschakelingsexperimenten bij lage temperaturen wijzen op een sterke temperatuursafhankelijkheid van het ringopeningsproces; daarentegen is de temperatuur van de ringsluiting onafhankelijk van de gemeten temperatuur (Schema 3). De onderdrukking van de fotochemische ringopening bij lage temperatuur wordt in detail behandeld, met de nadruk op de betrokken thermische activeringsbarrière. De sterke temperatuursafhankelijkheid van de ringopening impliceert dat de variatie in temperatuur gebruikt zou kunnen worden voor het beïnvloeden van het fotochrome schakelgedrag van diarylethenen.
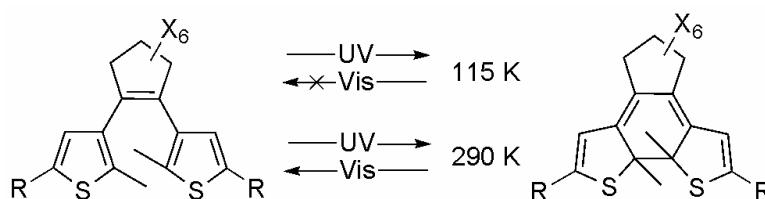
Schema 3 *Het ring openingsproces in diarylethenen wordt onderdrukt bij verlaging van de temperatuur; dit leidt tot de volledige afwezigheid van de fotoreactie onder een cut-off temperatuur. Daarentegen heeft het teruggaande ringsluitingsproces geen significante temperatuursafhankelijkheid boven 115 K. Reversibiliteit van het fotoproces kan dus bepaald worden via de temperatuur.*

Hoofdstuk 4 richt zich op de fotochrome eigenschappen van SAMs van diarylethenen op oppervlakken van gouden nanodeeltjes en bulk goudelektroden. Beide benaderingen lijken

169

belangrijke methoden om snel het schakelgedrag van de fotochrome moleculen te besturen. De belangrijkste conclusie is dat het schakelgedrag van de diarylethenen sterk beïnvloed wordt door de spacer, die de centrale schakeleenheid met het goudoppervlak verbindt. Afhankelijk van de spacer wordt uni- (thienyl spacer) of bidirectioneel (fenyl spacer) gedrag waargenomen. Even belangrijk is het onderzoek naar de redoxeigenschappen van de SAMs en de mogelijkheden voor niet-destructieve uitlezing.

Reversibele lichtgeïnduceerde schakeling van de geleiding van een individueel molecuul wordt beschreven in Hoofdstuk 5. Het molecuul, dat zijn fotochrome eigenschappen behoudt na chemisorptie op goud (Chapter 4), is bestudeerd aan de hand van STM. Een gemengde monolaag van het schakelmolecuul en dodecaanthiol wordt gevormd op een goudoppervlak dat als elektrode dient (Figuur 1). Een STM-tip wordt gebruikt als tweede elektrode terwijl deze het oppervlak scant. Bestraling van de fotochrome moleculen die geïnserteerd zijn in een isolerende matrix van alkaanthiolen, heeft een modulatie in de geleiding tot gevolg, die waar te nemen is als het verschil in hoogte van de tip. Schakeling in beide richtingen (van de open naar de gesloten vorm en omgekeerd) wordt waargenomen voor individuele moleculen. De reversibiliteit en de optische origine van dit fenomeen is bevestigd met behulp van statistische analyse van een groot aantal schakelhandelingen.
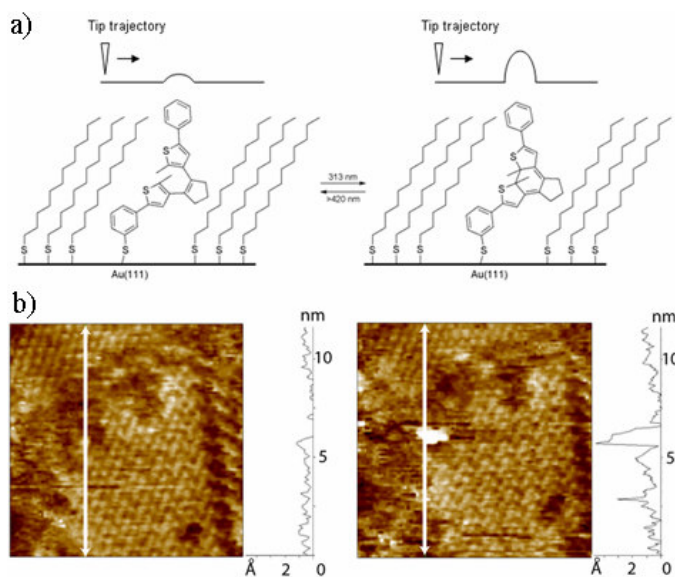
Figuur 1 *Karakterisatie van een gemengde monolaag van schakelaars en dodecaanthiol door middel van STM. a) Schema van het traject van een tip die over de geopende (links) en de gesloten (rechts) vorm van het molecuul beweegt. b) De hiermee corresponderende*

170

STM-beelden van een enkele schakelaar in de geopende (links) en de gesloten (rechts) vorm ingebed in een monolaag van dodecaanthiol op goud.

Tenslotte richt Hoofdstuk 6 zich op moleculaire monolagen die spontaan gevormd worden op het grensvlak van een atomair vlakke ondergrond en een oplossing van fotochrome moleculen gebaseerd op N-salicylideenaniline. Het effect van een systematische variatie in substraten op de geometrie van de SAMs wordt behandeld. Het polymorfe gedrag dat aanwezig is op Au(111) kan gerationaliseerd worden door de substraatgeïnduceerde intermoleculaire interacties in overweging te nemen. Dit suggereert dat een vereenvoudigd beeld van de gescheiden effecten van molecuul-molecuulinteracties en molecuul-substraatinteracties niet altijd genoeg is om de *self-assembly* eigenschappen van organische moleculen aan het grensvlak van de vloeibare en de vaste fase te beschrijven.

Zhrnutie

Nesmierna výzva súčasnej aplikovanej vedy je vývoj elektronických zariadení na úrovni niekoľkých nanometrov, použitím syntetických molekúl. Oblasť molekulárnej elektroniky ponúka enormný potenciál vďaka syntetickým molekulám, ktoré ponúkajú nové vlastnosti, absentujúce v súčasnej semikonduktorovej technológii. Základnou súčasťou molekulárnych zariadení sú molekuly, ktoré môžu byť "prepínané" medzi stavom s vyššou vodivosťou a nižšou vodivosťou, tzv. ON/OFF spínanie.

Svetlo je v tomto prípade vhodným externým stimulom pre tento typ zariadení, pretože sa vyznačuje jednoduchosťou použitia a rýchlosťou odpovede systému na daný stimul. Optoelektronické zariadenia preto ponúkajú nové možnosti a aplikácie pre molekulárnu elektroniku, za predpoladu že chemicky naviazané na kovových povrchoch nestrácajú svoju optoaktivitu. Pririodzene, interakcia medzi molekulami a povrchom, môže znížiť životnosť vzbudeného stavu daných molekúl a teda brániť ich fotoaktivite.

Fotochromické molekulové spínače patria do skupiny chemických zlúčenín, ktoré sú schopné obojstrannej fotoindukovanej transformácie medzi dvoma stabilnými stavmi (Schéma 1), pričom absorpčné spektrá sú zreteľne odlišné. Dve izomérne formy sa prejavujú rozdielnou molekulárnou geometriou a fyzikálnymi vlastnosťami ako napríklad rozdielnou hydrofobicitou, alebo rozdielnou redox chémiou. Veľkou výhodou fotochromických systémov je jednoduchá adresovateľnosť, reverzibílnosť a rýchla odpovede na daný stimul. To ponúka možnosť zmeniť nie len lokálne, ale aj makroskopické vlastnosti molekulárneho systému pomocou svetla. Samozrejme rôznorodá povaha fotochromických molekulárnych systémov ponúka ich využitie v molekulárnych pamäťových médiách, molekulárnej elektronike, inteligentných povrchoch, alebo pri kontrole supramolekulárnej organizácie a v mnohých iných oblastiach.
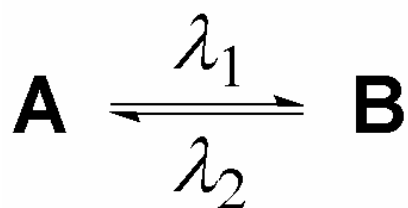
Schéma 1 *Optický molekulárny spínač môže existovať v dvoch rozdielnych formách, pričom každá z foriem môže byť selektívne získaná po ožiarení svetlom s rozdielnou vlnovou dĺžkou.*

Diaryletény sú zvlášť vhodné syntetické fotochromické molekuly, pretože sa vyznačujú vysokou odolnosťou voči neželaným vedľajším reakciám, zatiaľčo svetlom indukované transformácie medzi dvoma izomérnymi formami, vedú k rozdielnym elektrónovým

vlastnostiam. Tieto chemické molekuly sú obzvlášť vhodné pre využitie v molekulárnej elektronike. Umiestnené medzi dvoma kovovými elektródami sú schopné kontrolovať prenos elektrického náboja (Schéma 2).
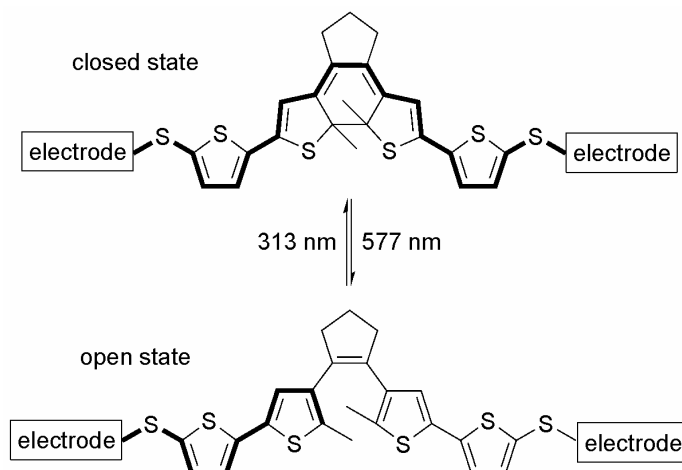

Schéma 2 *Fotochromický molekulárny spínač medzi dvoma elektródami vo svojej otvorenej (open state) a uzatvorenej (closed state) forme. Pri ožiarení svetlom o vlnovej dĺžke 577 nm, molekula prejde zo zatvorenej do otvorenej formy. Tá istá molekula môže byť prejsť z otvorenej do zatvorenej formy použitím svetla s vlnovou dĺžkou 313 nm.*

Tieto tézy pojednávajú o pokrok vo vývoji svetlom spínacích elektronických zariadení založených na diaryleténových fotochromických molekulách. Základným zreteľom bolo pochopenie fundamentálnych vlastností daných spínačov, vzhľadom na budúci možný vývoj funkčných zariadení založených na diaryleténoch. Základnými otázkami tohto výskumu boli: syntetická dostupnosť, následné fotochemické vlastnosti (reverzibilita, odolnosť voči únave), vplyv povrchu na ukotvenie molekuly na daný povrch a na reverzibilnosť spínacích procesov, efekt rôznych povrchov na "samo-organizáciu" molekúl, transport elektrického náboja cez molekulu, a najdôležitejšie; môžu byť electrické vlastnosti kontrolované jedinou molekulou?

Kapitola 2 popisuje kontrolu vodivostných vlastností založenú na svetelnom spínaní individuálnych molekúl. Dve nezávislé techniky (MCBJ a STM) boli použité na sledovanie zmien vodivosti jednotlivých molekúl počas ožarovania. MCBJ metóda umožňuje sledovať jednu molekulu umiestnenú medzi nano-elektródami. Merania vodivosti ukázali veľké zmeny kondaktivity medzi otvorenou a uzatvorenou formou molekuly. Zmeny vodivosti počas ožarovania boli merané pomocou zmeny odporu daného systému. Nevýhodou

systému je že iba spínanie z viac vodivej, zatvorenej formy do menej vodivej, otvorenej formy bolo možné, čo poukazuje na dôležité limity v používaní fotoaktívnych látkach naviazaných na kovových povrchoch. STM merania podporili MCBJ merania a potvrdili rozdiely medzi vlastnosťami transportu náboja v rozdielnych izomérnych formách diaryleténov a taktiež ireverzibilné vlastnosti spínania molekuly naviazanej na povrchu zlata.

Kapitola 3 sa zameriava na syntézu nových derivátov diaryleténov schopných chemického viazania sa na zlatých povrchoch. Niekoľko nových derivátov bolo pripravených pomocou rôznych syntetických stratégií. Následne fotochemické vlastnosti nových derivátov boli študované v roztokoch pri izbovej teplote. Charakteristické vratné spínanie, typické pre tento druh molekúl bolo dokázané pre všetky študované deriváty. Merania pri nízkych teplotách, ale poukázali na silnú závislosť procesu otvárania zatvorenej cyklickej formy diaryleténového spínača na teplote, pričom proces cyklizácie nie je teplotne závislý (Schéma 3). Obmedzenie tohto procesu je detailne diskutované a poukazuje na existenciu teplotnej aktivačnej bariéry.
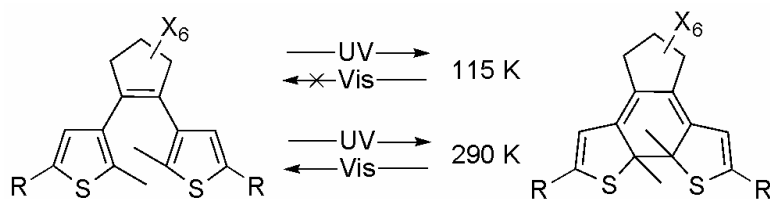
Schéma 3 *Proces cyklizácie pre diaryleténové spínače je blokovaný pri nízskych teplotách. Na druhej strane, opačný proces otvorenia cyklizovaného spínača je teplotne nezávyslý v meranom teplotnom rozsahu.*

Kapitola 4 sa zameriava na vlastnosti monovrstiev diaryleténov na zlatom povrchu, konkrétne na povrchu nanočastíc a taktiež na makroscopických zlatých elektródach. Oba prístupy poskytujú kľúčové metódy k rýchlemu odhadu spínacích vlastností fotochromických zlúčenín viazaných na povrchoch. Základný poznatok z týchto meraní je vysoká závislosť spínacích vlastností na charaktere reťazca spájajúceho cetrálnu spínaciu jednotku so zlatým povrchom. V závislosti na reťazci, bolo pozorované jednosmerné (pre tiofén), alebo dvojsmerné (pre benzén) spínanie.

Reverzibilná kontrola vodivosti, realizovaná použitím individuálnych fotochromických molekúl, je opísaná v kapitole 5. Molekuly ktoré si ponechávajú svoje vlastnosti aj po chemickom naviazaní na zlatý povrch boli študované pomocou STM. Zmiešaná monovrstva spínacích molekúl a dodekántiolu bola vytvorená na plochom zlatom povrchu

174

(Obrázok 1) slúžiacom ako elektróda. STM hrot (tip), skenujúci povrch, bol použitý ako druhá elektróda. Ožiarenie fotochromických spínačov, nachádzajúcich sa v alkentiolovom matrixe, má za následok zmeny vo vodivosti, čo sa odráža vo vzdialenosti STM hrotu od zlatého povrchu. Spínanie v oboch smeroch (z otvorenej formy do uzatvorenej formy a naopak) bolo potvrdené pre individuálne molekuly a reverzibilita a optická povaha tohto javu bola taktiež potvrdená štatistickou analýzou viacerých spínaní.
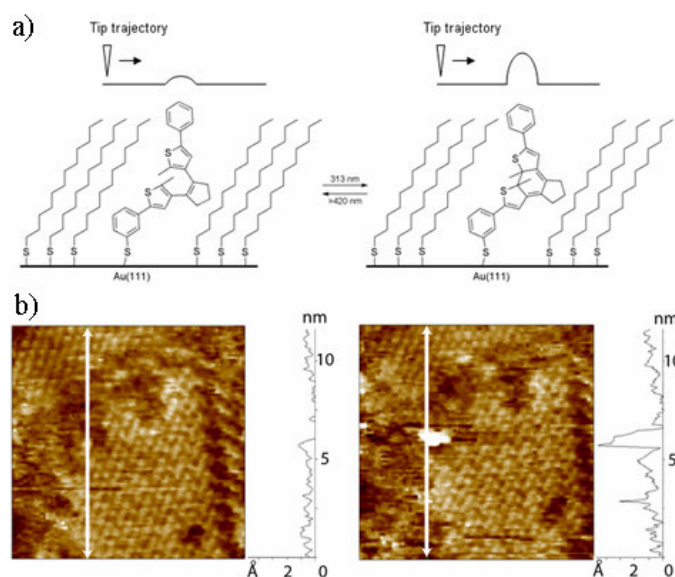
Obrázok 1 *STM charakteristika zmiešanej monovrstvy spínača a dodekántiolu. a) Schéma trajektórie tipu cez otvorenú (na ľavo) a zatvorenú (v pravo) formu. b) Zodpovedajúce STM obrázky jednotlivých spínačov v otvorenej (v ľavo) a zatvorenej (v pravo) forme inkorporovaných v dodekántiolovej monovrstve na zlatom povrchu.*

Spontánne formovanie molekulárnych monovrstiev, na rozhraní atomicky rovných povrchov a roztoku N-salicylidénanilínov, sú opísané v poslednej, šiestej kapitole. Efekt rôznych substrátov na geometriu monovrstvy bol systematicky skúmaný. Výskyt polymorfizmu na zlate Au (111) je racionalizovaný ako dôsledok intermolekulových repulzívnych síl, ktoré sú priamim dôsledkom interakcií molekúl so substrátom. Tento objav naznačuje že zjednodušené nazeranie na individuálne efekty interakcií medzi molekulami a interakcií medzi molekulou a substrátom nie su dostatočné na pochopenie procesov prebiehajúcich na kvapalnom a tuhom rozhraní.

Acknowledgements

It has been five years since I started the PhD period of my life which is about to end. This would not have been possible without the support that I have received from many directions. Quite a few people contributed to this either by direct scientific input into the conducted research or through friendship.

To start with, I would like to thank my promoters Professor Ben Feringa and Professor Bart van Wees. One important condition for a successful PhD thesis is a well founded research project. Therefore, I find myself lucky and grateful to both of you for what was "waiting" for me in Groningen before I even arrived. I am very happy to thank you, Ben, for giving me the opportunity to work in your group, and for the freedom and excellent working conditions that you create for your PhDs. Your enthusiasm and attitude often suppressed my skepticism and made me feel more confident about my research. Thank you, Bart, for those beautiful experiments done in your group which formed a solid basis for our joint research.

I would like to thank to the members of my reading committee, Professor Paul Blom, Professor Steven De Feyter and Professor Jan Engberts, for careful reading and approving my manuscript, interesting comments and critical remarks.

A special thank you goes to Dr. Diana Dulić, Dr. Sense Jan van der Molen, Henri van der Vegte, Ishan Amin, Marius Trouwborst and Eek Huisman for their substantial contribution to the single molecule experiments and their assistance to "understand" physics. Dr. Harry Jonkman is acknowledged for his calculations to support our findings. I would like to thank Dr. Diana Dulić and Dr. Audrius Pugžlys for their contribution to our colaborative work on low temperature photochromism. Albert Kiewiet is acknowledged for the mass spectroscopy measurements.

I thank Dr. Wesley Browne for his large contribution to the presented work. Thanks Wes for your help with various practical problems, CV measurements, scientific advice, discussions and "englishizing" (Tibor-style English) or "anglicizing" of my texts. If you need some help with Slovak translations, you can count on me. The same applies for Dr. Mike Pollard and Martin Walko. Thank you for your knowledge, your help with scientific problems and reading of my texts.

I would like to thank my two Paranymphs, Erik and Miki, not only for their help with the promotion but also for their unconditional friendship and all their peculiarities, which make the friendship richer.

With pleasure I thank all my lab-mates who helped to create a nice working ambiance, Robert (also acknowledged for the help with dutch translations), Lavinia, Frederic, Steve, Tatiana (also acknowledged for an ongoing scientific collaboration), Mahthild (also acknowledged for the help with dutch translations), Jetsuda, Gábor, Johan (also